A Probabilistic Approach to Understanding the Influence of Rainfall on Landscape Evolution

Eric Deal

Communauté
UNIVERSITÉ Grenoble Alpes

THÈSE

Pour obtenir le grade de

DOCTEUR DE LA COMMUNAUTÉ UNIVERSITÉ GRENOBLE ALPES

Spécialité : **Sciences de la Terre, de l'Univers et de l'Environnement**

Arrêté ministériel : 25 mai 2016

Présentée par

Eric Deal

Thèse dirigée par **Jean Braun**
et codirigée par **Anne-Catherine Favre**

préparée au sein de **l'Institut des Sciences de la Terre**
et de l'école doctorale **Terre Univers Environnement**

A Probabilistic Approach to Understanding the Influence of Rainfall on Landscape Evolution

Thèse soutenue publiquement le **2 Mars 2017**,
devant le jury composé de :

Peter van der Beek
Professeur, ISTerre, Université Grenoble Alpes, Grenoble, France, Président
Bodo Bookhagen
Professor, IEES, Universität Potsdam, Potsdam, Germany, Examinateur
Gianluca Botter
Professore Associato Confermato, ICEA, Università di Padova, Padova, Italy, Invité
Jean Braun
Professor und Sektionsleiter, Sektion 5.5, Deutsches Geoforschungszentrum, Potsdam, Germany, Directeur de thèse
Anne-Catherine Favre
Professeure, G-INP, ENSE^3, LTHE, Université Grenoble Alpes, Grenoble, France, Co-Directrice de thèse
Niels Hovius
Professor und Sektionsleiter, Sektion 5.1, Deutsches Geoforschungszentrum, Potsdam, Germany, Examinateur
Dimitri Lague
Directeur de Recherche CNRS, Université de Rennes 1, Rennes, France, Rapporteur
Taylor Perron
Associate Professor of Geology, EAPS, Massachusetts Institute of Technology, Cambridge, United States, Examinateur
Kelin Whipple

RÉSUMÉ

Dans cette thèse, j'aborde le problème du contrôle du climat sur l'évolution des reliefs. Plus spécifiquement, je travaille sur la relation entre la pluviosité et l'érosion fluviatile en utilisant une approche probabiliste. En premier lieu, je développe une méthodologie indépendante de la moyenne pour caractériser la variabilité de la pluviosité journalière. L'indépendance vis-à-vis de la moyenne permet une comparaison simple et objective de la variabilité de la pluviosité sous différents régimes climatiques. Elle se montre également utile pour intégrer le concept de variabilité de la pluviosité dans la théorie que je développe ensuite. J'applique cette approche à la chaine de montagnes Himalayenne en utilisant des données de pluviosité de hautes résolutions spatiale et temporelle et trouve qu'il existe des variations significatives de la variabilité de la pluviosité dans l'Himalaya. En prenant en compte la variabilité de la pluviosité en plus de la pluviosité moyenne, je trouve un lien entre pluviosité et érosion qui, d'un point de vue géomorphologique, diffère, de façon significative, de celui déduit de la seule pluviosité moyenne.

Ensuite, je développe une théorie d'érosion fluviatile du type 'puissance de flux' qui comprend une paramétrisation réaliste de la pluviosité et de l'hydrologie. Ceci est réalisé en intégrant un modèle hydrologique stochastique-mécaniste bien établi dans une formulation stochastique de la puissance de flux comprenant un seuil. La théorie hydrologique conduit à des expressions mathématiques pour la distribution et la variabilité du débit journalier en fonction des conditions climatiques qui sont valables pour la majorité des régimes de débit observés à la surface de la Terre. Les nouveaux paramètres qui en découlent ont une signification bien ancrée dans des théories climatique et hydrologique établies et se mesurent facilement. Cette approche nous permet de prédire comment le taux d'érosion fluviatile répond à des changements du forçage climatique. Je trouve ainsi que les processus hydrologiques peuvent avoir une influence significative sur l'efficacité érosive d'un forçage climatique donné. Cette approche peut également être utilisée comme fondement de nouveaux modèles d'évolution des reliefs qui prennent en compte des conditions aux limites climatique et hydrologique.

Une des principales conséquences d'intégrer l'hydrologie dans le modèle de puissance de flux est de révéler le double effet de la moyenne et de la variabilité du forçage climatique sur la réponse écohydrologique. Une corrélation négative existe entre la moyenne et la variabilité qui restreint grandement les réponses possibles d'un bassin versant à des changements climatiques. L'approche théorique que j'ai développée décrit également les relations qui relient la variabilité journalière à plusieurs paramètres écohydroclimatiques. Je trouve ainsi que l'index d'aridité, le temps de réponse du bassin versant, et l'épaisseur effective de sol sont les contrôles les plus importants sur la variabilité du débit. Ceci a d'importantes conséquences pour le rôle que jouent l'hydrologie et la végétation sur l'évolution des reliefs.

Finalement, je démontre que l'influence de la variabilité journalière du forçage climatique sur le taux d'érosion des rivières est principalement déterminée par l'existence et la valeur de seuils d'érosion. Je démontre que, quelques soient les détails du processus d'érosion considéré, c'est le rapport entre la valeur du seuil et la valeur moyenne

du forçage climatique qui détermine si la variabilité compte ou pas, et dans quel sens. Parmi de nombreuses autres applications, ces découvertes contribuent à l'élaboration d'un nouveau cadre permettant de comprendre et prédire la réponse de la surface de la Terre à des changements de la moyenne et de la variabilité de la pluviosité et du débit des rivières. La généralité de ces découvertes a d'importantes implications pour le reste des travaux présentés dans la thèse, ainsi que pour les travaux antécédents sur le rôle de la variabilité de la pluviosité et du débit sur l'efficacité érosive des rivières.

ABSTRACT

In this thesis, I address the problem of how climate drives landscape evolution. Specifically, I work on the relationship between rainfall and fluvial erosion using a probabilistic approach. First I develop a mean-independent methodology to characterize the variability of daily rainfall. The mean-independent nature allows for simple, objective comparison of rainfall variability in climatically different regions. It also proves useful for integrating the concept of rainfall variability into theory. I apply this method over the Himalayan orogen using high spatial and temporal resolution rainfall data sets and find significant variations in rainfall variability over the Himalayan orogen. By taking into account variability of rainfall in addition to mean rainfall rate, I find a pattern of rainfall that, from a geomorphological perspective, is significantly different from mean rainfall rate alone.

Next I develop a theory of stream power fluvial erosion that allows for realistically parameterized rainfall and hydrology. This is accomplished by integrating an established stochastic-mechanistic model of hydrology into a threshold-stochastic formulation of stream power. The hydrological theory provides equations for the daily streamflow distribution and variability as a function of climatic boundary conditions that are applicable across most of the observed range of streamflow regimes on Earth. The new parameters introduced are rooted firmly in established climatic and hydrological theory and are easily measured. This framework allows us to predict how fluvial erosion rates respond to changes in realistic rainfall forcing. I find that hydrological processes can have a significant influence on how erosive a particular climatic forcing will be. This framework can be used as a foundation for landscape evolution models that have realistic climatic and hydrological boundary conditions.

One of the main strengths of integrating hydrology into the stream power model is to reveal the dependence of both streamflow mean and variability on the climatic forcing and ecohydrological response. This negative correlation of the mean and variability vastly restricts the likely responses of a river basin to changing climate. The theoretical framework also describes the scaling of daily variability with several other ecohydroclimatic parameters. I find that the aridity index, the basin response time, and the effective soil depth are the most important controls on discharge variability. This has important implications for the role of hydrology and vegetation in landscape evolution.

Finally, I demonstrate that the influence of short-term climatic forcing variability on fluvial erosion rates is primarily determined by the existence and magnitude of erosional thresholds. I show that, irrespective of the details of the erosional process, it is the ratio between the threshold magnitude and the mean magnitude of climatic forcing that

determines whether variability matters or not and in which way. Among many other implications, these findings help provide a general framework to understand and predict the response of the Earth's surface to changes in mean and variability of rainfall and river discharge. The generality of this finding has important implications for the other work in this thesis, as well as previous work on role of rainfall and discharge variability on fluvial erosion.

PUBLICATIONS

Parts of the introduction are taken from a recent review by J. Braun and myself submitted to Tectonophysics for review in December 2016.
Citation: Braun, Jean and Eric Deal. "Links between climate and erosion at the Earth's surface: a review." *Tectonophysics*

Chapter 2 was submitted to Water Resources Research in November 2016 as it appears in this thesis, and and has received favourable reviews, with acceptance pending minor revisions.
Citation: Deal, Eric, Anne-Catherine Favre, and Jean Braun. "Rainfall variability in the Himalayan orogen and its relevance to landscape evolution." *Water Resources Research*

Chapter 3 was submitted to Journal of Geophysical Research: Earth Surface in July 2016 as it appears in this thesis, and has received favourable reviews, with acceptance pending moderate revisions.
Citation: Deal, Eric, Gianluca Botter, and Jean Braun. "Implications for the relationship between climate and landscape: including realistic climate and hydrology in a model of river incision" *Journal of Geophysical Research: Earth Surface*

ACKNOWLEDGEMENTS

I would like to thank my jury, Peter van der Beek, Bodo Bookhagen, Niels Hovius, Dimitri Lague, Taylor Perron, and Kelin Whipple for taking the time to read my thesis and attend my defense. An additional thank you to my 'rapporteurs' Kelin Whipple and Dimitri Lague. Thanks, also, to Dimitri, Bodo and Peter for formative discussions and encouragement early on.

Thanks to Christoff Andermann who aided me greatly in my foray into hydrology, and without whom, I would never have discovered the field of stochastic hydrology. Thanks to Jens Turowski for enriching my understanding of fluvial erosion over the course of many fascinating conversations. A very heartfelt thanks to Gianluca Botter for recognizing the significance when I mentioned the inverse gamma distribution in our fateful meeting at EGU in 2015 and welcoming me to Padova for an extraordinarily fruitful and stimulating collaboration. Thanks to Natalie Vögeli, Paul Wellington, Ellie Bakker and everyone else for creating a healthy and productive environment in ISTerre. Thanks to Joel Scheingross for invaluable guidance in the final months, the same for Jessica Stanley and Sam Wilson-Fletcher and the rest of section 5.5. Thanks to section 5.1 for being welcoming and always bringing the focus back to data. Thanks to Alex Bryk, Jesse Hahm, and Bill Dietrich for welcoming me into their group during my time at UC Berkeley. Also thanks to David Dralle, Sally Thompson, Marc Müller, and the rest of the ecohydrology research group at UC Berkeley for stimulating and helpful discussions during the same time.

Of course I would have been lost without the support and guidance of my advisors Anne-Catherine Favre and Jean Braun. Thank you Anne-Catherine for introducing me to the wonderful world of probability as well as the rigour that is expected in the field. An advantage to having your advisor go on sabbatical is that you are the only student, and receive proportionally more attention, something I took full advantage of. Thanks, Jean, for the countless hours spent discussing science, planning the next step, and keeping me on track. Finally, it goes almost without saying that I am incredibly thankful for the support and encouragement from my family and friends over the last three exciting years.

This work would have been possible without the financial support of the Marie Curie Initial Training Network (ITN) of investigating Tectonics Erosion Climate Couplings (iTECC), an inter-European research group.

For every complex problem there is an answer that is clear, simple, and wrong.

— H. L. Mencken

CONTENTS

1 INTRODUCTION 1
1.1 Climate and Erosion . . . 1
1.2 Short-term climate variability and long-term erosion rates . . . 3
1.3 State of the art . . . 5
1.3.1 Nonlinearity . . . 7
1.3.2 General conclusions of nonlinear models . . . 10
1.3.3 State dependency . . . 10
1.4 Summary . . . 13
1.4.1 Measurement techniques . . . 13
1.4.2 Realistic models . . . 14
1.4.3 General theory . . . 15
2 RAINFALL VARIABILITY IN THE HIMALAYAN OROGEN 17
2.1 Abstract . . . 17
2.2 Introduction . . . 17
2.3 Data and Methods . . . 19
2.3.1 Data . . . 19
2.3.2 Statistical model . . . 20
2.3.3 The applicability of the statistical model . . . 22
2.3.4 Data fitting techniques . . . 23
2.4 Results . . . 24
2.4.1 Spatial distribution of the gamma shape parameter . . . 24
2.4.2 Spatial distribution of mean wet day frequencies . . . 27
2.4.3 Spatial distribution of mean storm intensities . . . 27
2.4.4 Stationarity . . . 27
2.4.5 Correlations between intensity, frequency and shape parameter . . . 28
2.4.6 General along and across strike trends in variability . . . 29
2.5 Discussion . . . 32
2.5.1 Rainfall variability and erosion rates . . . 32
2.5.2 Relevance to the Himalayan orogen . . . 32
2.6 Conclusions . . . 36
2.7 Acknowledgements . . . 37
3 RAINFALL, HYDROLOGY AND FLUVIAL EROSION EFFICIENCY 39
3.1 Abstract . . . 39
3.2 Introduction . . . 39
3.3 The (eco)hydrological model . . . 42
3.3.1 Rainfall . . . 42
3.3.2 Soil moisture . . . 43
3.3.3 Catchment-scale water balance and the streamflow ratio . . . 44
3.3.4 Daily streamflow . . . 46
3.4 Integration of hydrology into the stream power incision model . . . 51
3.4.1 Channel hydraulics and distributions of daily erosion . . . 51
3.4.2 Mean long-term erosion rates as a function of climate and ecohydrology . . . 53
3.5 Results and Discussion . . . 55

3.5.1 Daily streamflow variability and longterm erosion rate 56
3.5.2 Hydrologic and climatic controls on streamflow 59
3.5.3 Ecohydrology, climate and erosion 64
3.5.4 Outstanding issues and limitations 68
3.5.5 Significance and Future work 70
3.6 Conclusions 70
3.7 Appendix A: Distribution of daily streamflow when $b = 2$ 71
3.8 Appendix B: Analytical approximations for C 72
3.9 Appendix C: Channel hydraulics 73
3.10 Appendix D: long-term erosion rate 74
3.10.1 pdf of daily erosion 74
3.10.2 long-term erosion rate 76
3.11 Appendix E: Importance of large floods 78
4 NEGATIVE CORRELATION BETWEEN MEAN AND VARIABILITY OF DISCHARGE 87
4.1 Abstract 87
4.2 Introduction 87
4.3 Section 1: Estimating distributions of discharge from hydrographs 88
4.3.1 Theory 90
4.3.2 Results and discussion 91
4.4 Section 2: Negative correlation of mean and variability 95
4.4.1 Coefficient of variability 95
4.4.2 Covariation of daily runoff variability and mean 98
4.5 Results and Discussion 99
4.5.1 Monte Carlo simulations 99
4.5.2 Empirical nonlinear dependence of variability on mean runoff . . 100
4.5.3 The effect of the basin response time 104
4.5.4 Understanding controls on discharge variability 105
4.5.5 Comparison to data 107
4.6 Conclusion 110
5 PROCESS INDEPENDENT INFLUENCE OF CLIMATIC VARIABILITY 113
5.1 Abstract 113
5.2 Introduction 113
5.3 Results and Discussion 114
5.4 Appendix A: Threshold stream power model 121
5.5 Appendix B: Derivation of tool and cover transport law 121
5.6 Appendix C: Monte Carlo Simulation Setup 122
Nomenclature 123

1 INTRODUCTION

1.1 CLIMATE AND EROSION

Perhaps the most easily observed mechanism linking surface processes to climate is the influence of rainfall and the subsequent surface runoff on erosion and sediment transport. Rainfall collects in low points on the landscape, forming streams and rivers. The flowing water exerts shear stress on hillslopes and river channels, driving sediment transport and fluvial erosion of the landscape. As river processes are, by definition, dependent on the river discharge, their efficiency has long been thought to be strongly modulated by rainfall (e.g. Gilbert, 1877). It is well documented, for example, that recent Quaternary glacial cycles have led to cycles of deposition and erosion in many non-glaciated river systems (e.g. Blum and Törnqvist, 2000; D'Arcy, Whittaker, and Roda-Boluda, 2016).

Fluvial erosion is not the only important process operating in landscapes, however, we focus on it exclusively in this thesis. There are good reasons for this. Though it is challenging to make simple, reductive statements about systems as complex as landscapes, there are good arguments to be made for the river incision being disproportionally important in forming landscapes. Rivers are the lowest points in landscapes, and as they incise, they steepen connected hillslopes and tributaries. In this way, incision by rivers can cause an erosive response that propagates throughout the river network as well as the hillslopes (e.g. DiBiase et al., 2010; Whipple, 2009; Whipple, Kirby, and Brocklehurst, 1999). In addition, much of the material that erodes, chemically or physically, from a landscape is ultimately transported away from tectonically active regions by the fluvial network. Theoretically the entire landscape can be slave to the behaviour of the river network, a concept which is commonly employed to justify the focus on fluvial erosion. In practice, this is likely an oversimplification. There are surely subtle, two-way interactions between hillslopes and river networks, such as the influence of hydrology discussed in chapter 3. For example, Singh, Reinhardt, and Foufoula-Georgiou, 2015 provide experimental evidence that hillslopes respond to climate before river channels. However, even if hillslopes are not simply responding to river channels, the importance of the river channel network as both an active agent of landscape evolution and a passive recorder of its history merits the close study it has received, and which is continued here.

The stream power model (Howard, 1994; Whipple and Tucker, 1999) is widely used to model fluvial incision in rapidly uplifting or steep regions, although its range of applicability and the value and meaning of its rate parameter and exponents are subject to ongoing research and debate (Beer and Turowski, 2015; Lague, 2014; Sklar and Dietrich, 2006). According to the stream power model, the long-term rate of erosion, $\langle E \rangle$, is directly proportional to slope, S, and contributing catchment area, A, used as a proxy for river discharge:

$$\langle E \rangle = KA^m S^n \tag{1}$$

Where the rate constant K and the exponents m and n are traditionally determined empirically. Several studies DiBiase and Whipple, (2011), Lague, (2014), Lague, Hov-

ius, and Davy, (2005), Snyder et al., (2003), and Tucker and Bras, (2000) have clearly demonstrated that the existence of an erosional threshold implies that K and n should also contain a dependence on discharge variability and, therefore, rainfall variability. Expanding this work, and exploring the influence of rainfall and rainfall variability on K is the focus of much of the work in this thesis.

According to the stream power model, one should observe a strong, positive correlation between precipitation rate and erosion efficiency. This link between climate and erosion is further supported by many modelling studies in which simple or complex representations of landform evolution have been subjected to a parametric study representing the effect(s) of the variability of the Earth's climate at a range of spatial and temporal scales (Armitage et al., 2013; Balen, Busschers, and Tucker, 2010b; Banwart, Berg, and Beerling, 2009; Bogaart et al., 2003; Bovy, Braun, and Demoulin, 2016; Collins, Bras, and Tucker, 2004; Coulthard and Macklin, 2001; Densmore, Allen, and Simpson, 2007; Fernandes and Dietrich, 1997; Godard et al., 2013; Hancock and Anderson, 2002; Pedersen and Egholm, 2014; Rinaldo et al., 1995; Roe, Montgomery, and Hallet, 2002; Roering et al., 2004; Simpson and Castelltort, 2012; Tucker and Bras, 2000; Tucker and Slingerland, 1997). It is clear from these models that climate should play a significant role in determining landscape form and rates of evolution. However, this has proved challenging to validate convincingly in real landscapes. Many studies have compared measured erosion rates to mean values of a number of potential direct or indirect climatic drivers of erosion such as mean precipitation amount or intensity, channel steepness, stream power, and vegetation density, but have struggled to find good correlations (e.g. Acosta et al., 2015; Bermudez, van der Beek, and Bernet, 2012; Godard et al., 2014; Olen, Bookhagen, and Strecker, 2016). However, such comparisons are potentially flawed, in that it is erosion efficiency, rather than erosion rate that should correlate with precipitation rate. In equilibrium landscapes, where the uplift rate is equalled everywhere by erosion rate, there is a decoupling between erosion rate and erosion efficiency, expressed in the morphology of the landscape.

Still, regional and global compilations show that more water falling on a landscape does not equal more erosion (e.g. Blanckenburg, 2005; Riebe et al., 2001a), which might be expected as a general, if noisy, trend if precipitation rate drives erosion efficiency. As suggested by many, the sensitivity of the erosional response to small changes in the climatic forcing and the dependence of the response on the recent history and antecedent conditions of the landscape demand a more sophisticated understanding of how climate drives erosion (Blum and Valastro, 1989; Lague, 2014; Leopold, 1951; Schumm, 1979; Tucker and Bras, 2000; Tucker and Slingerland, 1997; Webb and Walling, 1982; Wolman and Gerson, 1978; Wolman and Miller, 1960). For example, different river basins in different regions, or even in the same region but of different sizes have been observed to respond to similar changes in climate very differently (Blum and Valastro, 1989; Schumm, 1973). Complex depositional and erosional sequences have also been observed in response to simple, one way climatic changes. For example, a valley aggradation event caused by a climate-driven increase of sediment supply from hillslopes can be followed by incision due to a reduction of sediment input caused by exhaustion of erodible soil and regolith from these same hillslopes (Balen, Busschers, and Tucker, 2010a; Schumm, 1977; Tucker and Slingerland, 1997).

In support of the proposition that fluvial erosion efficiency and climate should be spatially correlated Thiede et al., (2004), for example, showed that in the southern Himalayas variations in erosion rate estimates from low-T thermochronology do not cor-

relate with tectonic structures. Surface processes, they argue, are more likely controlled by the very high monsoonal precipitations causing a simple altitudinal variations in observed erosion rates. More recent work (Ferrier, Huppert, and Perron, 2013) clearly demonstrated the almost linear dependence of bedrock incision rate on stream power and, consequently, precipitation rate using the large precipitation gradient across the flank of the Hawaiian island of Kaua'i.

In contrast Godard et al., (2014) evidenced a very large gradient in erosion rate across a region of uniform mean precipitation rate, based on a large compilation of cosmogenic isotopes along a transect in central Nepal. They concluded that the area has reached steady-state conditions between rock uplift and erosion. This study highlights the fact that evidence for climate control on erosion rate, in contrast to landscape form, must be sought in the transient response of erosional systems to a climate perturbation or change, rather than steady-state configurations under different climate/rainfall conditions, as suggested by Whipple, Kirby, and Brocklehurst, (1999).

Following this strategy, Bookhagen and Strecker, (2012) or Carretier et al., (2013) showed strong observational evidence that there is a spatial and temporal relation between current and past precipitation rates in the southern Central Andes and erosion rates as measured by cosmogenic isotope methods. More recently Carretier et al., (2015) postulated that the present-day spatial variability in erosion rate can only be explained by a transient response of the fluvial system to either climatic or tectonic change.

The evidence demonstrating the role climate plays in landscape evolution remains mixed. The importance of climate, and rainfall in particular, for erosion processes is so obvious that it has been a constant theme of geomorphology since at least Gilbert, (1877). Despite this, the relationship between rainfall and landscape evolution is complex enough that the role of climate remains debated (e.g. Burbank et al., 2003; Dadson et al., 2003; Ferrier, Huppert, and Perron, 2013; Godard et al., 2014; Reiners et al., 2003b; Thiede et al., 2004). The stream power model in particular has been successful in capturing widely observed features of real landscapes (e.g Kirby and Whipple, 2012; Lague, Hovius, and Davy, 2005; Willett et al., 2014; Wobus et al., 2006). However, it is known to ignore several key processes, such as sediment transport, hydrology, as well as spatially and temporally variable rainfall. Some key predictions of the stream power model, and related derivations have also been shown to be general properties of landscapes, not necessarily related to the stream power model (e.g. Kirchner, 1993; Schorghofer and Rothman, 2002, and chapter 5). Here we take the perspective that the judicious inclusion of key processes can lead to a better understanding of the relationship between climate and erosion, and therefore better match between theory and observations. The highly variable behaviour of climate, rainfall, and rivers over short timescales is one important source of complexity. As Lague, (2014) demonstrated, accounting for this temporal complexity, or short-term variability, leads to better prediction of several observations, such as the nonlinearity of the steady-state stream power model, the velocity of traveling knockpoints, and the scaling of steepness index with erosion rate.

1.2 SHORT-TERM CLIMATE VARIABILITY AND LONG-TERM EROSION RATES

Many of the concepts concerning short-term variability can be generalized and are similar across different landscapes and erosion processes. Because we discuss these general concepts we will use a general vocabulary. We refer often to an erosional sys-

tem, which is a portion of the landscape (hillslope, basin, river network, orogen, etc.) with a definable climatic forcing and erosional response. Both the climatic input and erosional output are defined by the processes in the system. For example, in a small river basin, the processes under consideration may be soil creep and landsliding on the hillslopes and sediment transport in the river system. In this case, the relevant climatic input would be precipitation and the erosional response would be the sediment flux on the hillslopes and in the river. Of interest will be both the erosional response to instantaneous climatic forcing, which in this case would be a single rainstorm, and the long-term erosional response due to many storms of different sizes over an extended period of time. In our river basin, the long-term erosional response is the long-term mean sediment flux out of the basin and the steady state form of the landscape. The climatic forcing is the range of storms the basin is subject to. It could be characterized by the mean annual precipitation rate, however, this may not be a useful or sufficient characterization to understand the long-term erosional response. The relevant characterization of climatic forcing from a geomorphological perspective is the goal of much of the thesis and the work that it builds upon, and will depend on the specific erosional processes under consideration. Also important are the conditions in the erosional system that determine, or at least influence, the manner in which the system responds to a particular instantaneous forcing. We refer to these relevant conditions collectively as the state of the system.

An example highlighting the importance of the system's state is given by Wolman and Miller, (1960) concerning bank erosion in a river. As they describe it, the bank erosion resulting from large storms is often greater during the winter months, even though the largest storms occur during the summer. This is because in the winter the riverbanks are often already wet due to generally damp conditions. As a result they are weaker and more easily eroded. Another example is the amount of bedrock incision during a flood event. The incision is sensitive to both the amount of sediment carried as bedload, which drives erosion by striking the bedrock (Sklar and Dietrich, 2004), and the amount of stationary sediment covering the bedrock and protecting it from erosion (Sklar and Dietrich, 2006). As a result, how much erosion that occurs for a certain size flood depends on the amount of sediment in the channel at the time of the flood (Turowski, 2012).

In both these examples the conditions of the system (bank wetness and sediment availability) determine the response to external forcing such as rainfall or river discharge. The same system can exhibit different responses to the same forcing depending on its state. The state can be characterized quite simply (the banks are wet or dry) or it can be more complex, as with sediment availability. In this case it is not just the amount of sediment that matters, but also the size distribution of particles, and even the manner that they are positioned. The sediment in a river channel is the result of several processes, including landsliding, previous floods bringing sediment from upstream and even the way the bedrock fractures into smaller particles. Therefore the state can represent a potentially complex evolution of the system from some point in the past and can be thought of as a history of the system. We refer to both the simple and complex cases as state dependency or a state dependent law.

Short-term variability can play an important role even in systems where the state is constant. Let us go back to river erosion and imagine for a moment a stretch of steep bedrock river overlain with a thin layer of gravel. We will say that these conditions are dominant, so the state is constant and not a concern. In order for erosion to occur,

the gravel must move across the bedrock. Two small, but similar magnitude floods, each only just able to mobilize the gravel layer would not result in much erosion of the bedrock. In contrast, a single flood with a magnitude twice the smaller ones will move more gravel with a higher velocity, and result in considerably more than twice as much erosion. If we imagine further that the rate of erosion increases disproportionally with the volume of river discharge, this effect will be magnified. The same volume of water can result in different amounts of erosion, based on the manner in which it is delivered to the erosional system. Because the threshold effectively introduces a nonlinearity into the relationship between climatic forcing and erosional response, we refer to the existence of either a nonlinearity or a threshold as either nonlinearity or a nonlinear law.

This example demonstrates that the mean annual discharge may not accurately capture the different effects of differently sized floods and will therefore be a poor predictor of the mean erosion rate if there is a threshold for erosion. The situation will be similar if the same forcing produces different erosional responses because of differences in the state of the system. This is the fundamental drive for taking variability into account. The result of both state dependency and nonlinearity is that the mean magnitude of climatic forcing will, in general, not be able to predict the mean magnitude of erosion, even if the correct erosion law is known. This is illustrated using a simple mathematical example. If x is a random variable, and we have a function $f(x) = x$ that is linear, then the mean of the function $\langle f(x) \rangle$ is equal to the function of the mean of x, $f(\langle x \rangle)$. However, if we have a different function $g(x) = x^2$, which is not linear, then in general $\langle g(x) \rangle \neq g(\langle x \rangle)$. In the first case, it is only necessary to know the mean of x and the form of f to calculate the mean of $f(x)$. However, when the function is nonlinear, one must also know the distribution of the sample of x. In an erosional system, this is equivalent to needing to know the full distribution of climatic forcing events applied to the erosional system. The variable nature of climatic forcing of all kinds is a feature that is consistently observed in many erosional systems.

1.3 STATE OF THE ART

Much of the early work on short-term variability was concerned with the state of the system (e.g. Anderson and Calver, 1977; Blum and Valastro, 1989; Newson, 1980; Wolman and Gerson, 1978) and the role of erosion thresholds (e.g. Schumm, 1979; Schumm, 1977; Wolman and Miller, 1960). However, taking into account state-dependency quantitatively is challenging, and most quantitative studies have focused on thresholds and nonlinearity. Climatically triggered erosion thresholds are common, and have been demonstrated or hypothesized to exist for many processes, including erosion and channel head initiation due to overland flow (e.g. Horton, 1945; Montgomery and Dietrich, 1992; Prosser and Dietrich, 1995), fluvial transport of bed-load sediment (e.g. Bagnold, 1980; Shields, 1936), fluvial erosion of bedrock channels (e.g. Baker and Kale, 1998; Howard, 1994), debris flows and shallow land sliding (e.g. Gabet et al., 2004; Guzzetti et al., 2008), as well as solifluction and soil creep (e.g. Matsuoka, 2001).

Leopold, (1951) made the convincing argument that due to a threshold for erosion, many hillslopes and rivers should only erode and transport sediment during large storms, because only then is the strength of flowing water sufficient to mobilize sediment. In light of this, he argued that the intensity of rainfall might be a better measure of the impact of climate on fluvial erosion than the mean annual rainfall amount.

This idea was supported by Chorley and Morgan, (1962), who arrived at a similar conclusion from a comparative study of two basins, and by Brakenridge, (1980), who hypothesized that increasing storm intensity is responsible for observed increases in erosion rate in the sedimentary record. Sugai, (1993) also illustrated the importance of rainfall intensity using river terrace data to show that the cycles of aggradation and erosion in the Usui river in Japan are due to the high frequency of typhoons during interglacial periods and their absence during glacial periods. Typhoons produce large storms capable of moving the largest sediment grains downstream. In their absence, these sediments accumulate. Using paleohydrological and paleoclimatic data from the US, Blum and Valastro, (1989) showed that the erosional response to climate change is complex and that it depends on the interaction of sediment transport dynamics and the discharge regime. They concluded that, in part due to the existence of thresholds, subtle changes in climate can have significant impacts on the fluvial regime and erosion rates.

In a landmark paper, Wolman and Miller, (1960) offered an in depth qualitative analysis of the potential role of short-term meteorological variability on landform evolution. They pointed out the importance of the history and ordering of meteorological forcing, stressing that the landform response to these forcings is likely controlled by several different processes occurring over different temporal and spatial scales. Although unable to quantitatively assess it, they emphasized how complex the landscape response to climate forcing can be, along with many others at the time (Beaty, 1963; Leopold, 1951; Schumm, 1973). Wolman and Miller, (1960) provided a framework to discuss and debate the role of meteorological and hydrological variability as well as the relative importance of extreme hydrological events on landscape form and evolution (Anderson and Calver, 1977; Andrews, 1980; Turowski, 2012; Webb and Walling, 1982; Wolman and Gerson, 1978). Wolman & Miller also make a distinction between geomorphic work and landform modification. Geomorphic work is an absolute measure of the effect of an event on the landscape, in contrast, landform modification is rather more nebulous. It is the idea that a large event can modify the landscape in a way that has an ongoing effect on the landscape long after it occurred, allowing for large events to potentially influence landscapes much more than would be suggested by the actual amount of geomorphic work accomplished.

Kirchner et al., (2001) demonstrated the variability inherent to erosional processes and the importance of extreme events by comparing erosion rates in the same region estimated over different periods of time. They argued that present day erosion rates do not match erosion rates integrated over longer periods of time because the long-term erosion rate is the result of punctuated erosion events, with much of the erosion (up to 90%) occurring during very rare events. In this conceptual framework, the integral over all possible erosion events does not converge very quickly; present day erosion rates do not integrate over a long enough period of time to capture these significant, but rare erosion events. The result is a positive bias in measured erosion rate with the period of integration - a sort of negative Sadler effect for measured erosion rates.

In direct contrast to this, Finnegan, Schumer, and Finnegan, (2014) provide evidence for a negative time bias that can exist over very long periods of time - up to millions of years. This implies the existence of very long, but rare erosion hiatuses, rather than large but rare erosion events. Gallen et al., (2015) describe a mechanism by which erosion rates derived from terrace dating can exhibit either a negative or a positive bias, (Finnegan, Schumer, and Finnegan, (2014) is based on terrace dating, but Kirchner

et al., (2001) is not). Finally, Ganti et al., (2016) puts forth a theory in which glacial erosion might exhibit a negative time bias, but measured fluvial erosion rates should not. Though it is actually about sedimentation and not erosion, Schumer and Jerolmack, (2009) discuss in depth the possibility of heavy tailed distributions of erosion intensity and hiatuses, and the opposite effects that each can have on the convergence of the integral over erosion events and the observed time bias of measured erosion rates. This ongoing debate highlights the importance of physically realistic models of climate and fluvial erosion that can provide insight into these vital problems.

1.3.1 *Nonlinearity*

The case of nonlinearity is considerably easier to tackle quantitatively, since one does not need to characterize the state of the system nor how it evolves through time. If the state of the erosional system is constant, modelling the impact of thresholds or nonlinearities on the relationship between a variable climatic forcing and the long-term erosional response is often straight forward, amounting to a nonlinear averaging of the distribution of instantaneous climatic forcing events. The major difficulties lie in finding a functional form of the relationship between instantaneous climatic forcing and erosional response for the process under consideration and finding the distribution of instantaneous climatic events. The modelling studies come in two flavours, at-a-station models that solve an equation describing the process at a point in space, and landscape scale models, which solve coupled equations for the entire landscape. At-a-station models are more common, and have provided the most useful insight to date. These insights have been largely confirmed by landscape scale models (e.g. Crave and Davy, 2001; Tucker and Bras, 2000)

Tucker and Bras, (2000) provide perhaps the first notable quantitative study in which they investigate the long-term impact of daily variability of rainfall on erosion rates. They study the impact of rainfall variability in the context of thresholds for surface runoff generation, sediment entrainment and bedrock erosion. Additionally they allow for nonlinear relationships between river discharge and sediment transport/bedrock erosion. They model both at-a-station dynamics and the full landscape. For at-a-station models they find that rainfall variability becomes more influential when thresholds are high enough that less than half of rainfall events cause erosion and when erosion increases more than linearly with discharge. They also find that erosion rates increase with increasing rainfall variability under the same conditions (more nonlinearity and higher thresholds). However, the erosion rate can decrease with increasing variability when thresholds are very small or when erosion rate increases less than linearly with increasing discharge. When modelling a 2D landscape, they are hampered by a lack of computational power, and they must make storms last years instead of days, impairing their ability to truly model short-term variability. They still expose their landscape to variable rainfall, and argue that if the system state is constant, extending storms for years does not change the end result. Taking this caveat into account, their at-a-station conclusions extend to the full landscape, with the subtle point that with the landscape in dynamic equilibrium (where the erosion rate is set by the uplift rate), it is the erosion efficiency (mm of erosion per mm of rainfall) rather than the erosion rate that increases with increasing variability. As a result, landscapes subject to higher variability rainfall exhibit gentler slopes and higher drainage density (because they assume thresholds to be relatively large).

A contemporary study to Tucker and Bras, (2000), Crave and Davy, (2001) also conduct a quantitative analysis into the impact of variable discharge on long-term erosion rates. They do not consider erosion thresholds, only nonlinearity between the climatic forcing (discharge) and erosion. Rather they focus on the establishment of the precipiton approach to landscape evolution modelling, a cellular automata method which allows them to take variability of discharge into account with minimal computational demands. They derive an inverse gamma distribution for discharge with a power law tail that is similar to that used in several later studies (DiBiase and Whipple, 2011; Lague, 2014; Lague, Hovius, and Davy, 2005; Molnar, 2001; Molnar et al., 2006). The resulting model is a full 2D landscape evolution model that delivers similar results to Tucker and Bras, (2000). Higher variability discharge generally leads to increased erosion efficiency, gentler landscapes and higher drainage densities.

Molnar, (2001) describe a similar analysis using a power law distribution for floods rather than an exponential one, but reach similar conclusions to Tucker and Bras, (2000). They also pointed out that due to the much observed negative correlation between the mean and variability of floods, a climate shift towards aridity could potentially increase variability enough to increase river incision rates. However, in a later study using empirical relationships between the mean and variability of discharge from the US, Molnar et al., (2006) conclude that this is only possible under specific conditions where a humid river basin with high erosion thresholds becomes more arid.

Snyder et al., (2003) applied the model developed by Tucker and Bras, (2000) and Tucker, (2004) using parameters constrained by observations. They show that accounting for short-term climatic variability and erosion leads to a nonlinear relationship between erosion rate and channel steepness index (a measure of the steepness of a river channel normalized for contributing area). Snyder et al., (2003) are careful to point that variability is not the only explanation for a nonlinear relationship between channel steepness and erosion rate. However, because channel steepness determines the overall elevation of a landscape, it has a potentially important influence of variability on the orogen scale. Many landscapes exhibit nonlinear relationships between erosion rate and channel steepness, which implies that meteorological variability plays an important role (DiBiase and Whipple, 2011; Lague, 2014; Ouimet, Whipple, and Granger, 2009).

Tucker, (2004) introduced an analytical solution for their models (including bedrock incision via the stream power model) which were obtained by using a slightly modified functional relationship between daily discharge and erosion. They demonstrated that erosion thresholds (which demand short-term variability be treated explicitly) have a major influence on landscape morphology and slope-area scaling as suggested by Snyder et al., (2003). They also reiterated the point made in Snyder et al., (2003) that channel steepness is expected to be a nonlinear function of erosion rate.

Lague, Hovius, and Davy, (2005) offer analytical solutions for the long-term erosion rate due to bedrock incision using the stream power model based on the same modification to the functional relationship between daily discharge and erosion used by Tucker, (2004). However, instead of using the Poisson model (exponential distribution of storm depths, durations and inter-arrival times), they use an inverse gamma distribution for daily discharge as derived by Crave and Davy, (2001), which has a power law tail for large storm magnitudes, and tends to match observed distributions of daily discharge better (DiBiase and Whipple, 2011; Lague, Hovius, and Davy, 2005). Despite using a different probability distribution for discharge, they draw nearly identical conclusions

about the influence of short-term variability and erosion thresholds on long-term erosion rates. Tucker and Bras, (2000) showed that the significance of short-term variability depends on the magnitude of the erosion thresholds. Lague, Hovius, and Davy, (2005) take this a step further, and use the distribution of daily discharge to estimate the return time of floods that exceed an erosion threshold of a given magnitude. Although the method they use to calculate flood return times is potentially flawed, they are still able to define different regimes based on the frequency of erosive floods. They show that when return times are short, short-term variability should not impact the channel steepness. They point out that, based on the observed frequency of erosion in rapidly eroding bedrock rivers (where their model assumptions are the most valid), variability should not have an large influence on the long river profile. However, they show that when return times are long, channel steepness should be a power law function of the long-term erosion rate with an exponent that depends on the short-term variability of discharge. This predicts that short-term variability will determine the scaling of channel steepness with long-term erosion rate. Short return times are associated with fast erosion rates or small erosion thresholds, and long return times are associated with slow erosion rates and large erosion thresholds, so these conclusions are in line with previous work. Finally, by defining variability simply with a single parameter that can easily be measured in real landscapes, they helped popularize the concept of short-term discharge variability. Their measure of variability (k) has been incorporated into several subsequent empirical studies (Carretier et al., 2013; DiBiase and Whipple, 2011; Rossi, Whipple, and Vivoni, 2016).

In an analysis similar to that of Snyder et al., (2003), DiBiase and Whipple, (2011) apply the models of Tucker, (2004) and Lague, Hovius, and Davy, (2005) (i.e., a Poisson model distribution and an inverse gamma distribution, respectively) to a case study in the San Gabriel Mountains. In this case, DiBiase and Whipple, (2011) show again that channel steepness scales as a power law of erosion rate in a real landscape. They find that Lague's model fits the observed scaling better than Tucker's. DiBiase and Whipple, (2011) clarified the conclusions of Lague, Hovius, and Davy, (2005) by defining three regimes based on the ratio of long-term erosion rate to erosion threshold. Regime one occurs when the ratio is small, implying that the erosion threshold is large or the erosion rate is small (or the return time of erosive events is long). It is in regime one that short-term discharge variability will be important in determining the channel steepness. It is also here that the erosion efficiency increases with increasing variability. Regime three occurs when the ratio of erosion rate to erosion threshold is large. This implies that erosion rates are high or that thresholds are very small. Here the discharge variability does not influence channel steepness and the erosion efficiency decreases with increasing variability. Regime two is a transitional regime between the other two regimes and exhibits a mixture of features of both regime one and three. These three regimes bring together the general results of all previous studies, describing how short-term discharge variability should theoretically control the scaling of channel steepness with erosion rate depending on the relative importance of the erosion thresholds. Their analysis clarifies points made earlier that variability matters when thresholds are large (Lague, Hovius, and Davy, 2005; Tucker, 2004; Tucker and Bras, 2000). By using an empirical relationship between the mean and short-term variability of discharge, DiBiase and Whipple, (2011) demonstrate that it is possible for rivers to become more erosive as they become more arid, in contrast to the conclusions of Molnar et al., (2006). At the very least, they show that is under a wide range of conditions, increasing the mean dis-

charge should not appreciably increase the long-term erosion rate due to the associated drop in discharge variability.

In a significant review of the state of the stream power model, Lague, (2014) focused on the importance of taking into account the variability of meteorological forcing and erosion thresholds. Lague, (2014) presented a large data set demonstrating that the steepness index - erosion rate relationship is a power law with an exponent less than one in many landscapes. This is possible evidence of the importance of variability and erosion thresholds. The review also emphasized that the observed nonlinearity of the stream power model calibrated to real landscapes can be instead described with a linear stream power model that allows for daily discharge variability. In addition, changes in the nonlinearity of the stream power model during transient adjustment of the landscape can also be explained by accounting for variability as well as dynamic river width. This all makes a powerful argument for the need to understand the stochastic nature of meteorological forcing and the role that erosion thresholds play.

1.3.2 *General conclusions of nonlinear models*

The studies described above make up a majority of the quantitative literature on the role of short-term climatic variability in determining long-term erosion rates. The uniformity of their conclusions is striking, and the three regimes proposed by DiBiase and Whipple, (2011) in response to Lague, Hovius, and Davy, (2005) provide a good framework for understanding the role of short-term discharge variability in real landscapes. Subsequent quantitative studies since Tucker and Bras, (2000) are important contributions that explore the problem more deeply from different perspectives and with different distributions of forcing and process laws. However, they do not find fundamentally different results from Tucker and Bras, (2000). The reason all these studies find such similar results is because the process law used does not have a significant influence on the role of variability and erosion thresholds.

Chapter 5 finds that there is a critical value for the erosion threshold, x_c, above which thresholds can be considered large. When the threshold is above this critical value variability is important, and higher variability increases erosion efficiency. When the threshold is smaller than the critical value, variability is less important, and erosion efficiency can either be increased or decreased by increasing variability. This critical value is reached when the threshold is not exceeded by a climatic event of mean magnitude. This critical threshold value is related to that found by Tucker and Bras, (2000) as well as the critical return time in Lague, Hovius, and Davy, (2005), but is relatively independent of the process law used. It can also be shown that the critical threshold value is the boundary between regime one and regime three as defined by DiBiase and Whipple, (2011).

1.3.3 *State dependency*

Chapter 5 shows that the role of variability and thresholds is process-law independent. However, in order to calculate absolute rates, rather than the qualitative effect of variability, the process law must be known. This is where the concept of state dependency becomes important. Data sets of instantaneous forcing and erosional response (e.g. Turowski, 2010) strongly suggest that the functional relationship between climatic forcing and erosional response for bed-load transport, and therefore fluvial erosion, cannot be

represented with one-to-one functions. The tools and cover model of fluvial erosion dictates that erosion rate is related to both the instantaneous discharge, as well as the state of the channel, in terms of hydraulic conditions and sediment supply (Sklar and Dietrich, 2004). This points to state-dependency as a major missing piece from the preceding studies. There is a good reason for this, state dependent models tend to be more challenging to construct and understand. While simple analytical solutions have been found that address nonlinearity and short-term variability in climatic forcing (Lague, 2014; Lague, Hovius, and Davy, 2005; Tucker, 2004, chapter 3), similar solutions are much less forthcoming in the case of state dependency.

State dependency has been discussed qualitatively more frequently than quantitatively, as mentioned previously. In particular, Schumm, (1973, 1979) consider something that they refer to as geomorphic thresholds. They cite several common examples of erosion thresholds, but consider how the state of the system evolves over time such that these thresholds are exceeded by an external forcing rather than how climatic events trigger the thresholds. In this way they bring together the concept of erosion thresholds and state dependency. They describes landscapes whose states are evolving towards erosion thresholds (e.g. steepening slopes due to uplift and thickening soils due to weathering) that are then triggered by large climatic events. Though the entire landscape responds to the instantaneous forcing, since different sections are in different states that depend on their histories, the response across the landscape is not uniform. They recognize the shortcomings of process based approaches that can connect instantaneous forcings and responses but are unable to take into account the history and evolution of the state of the landscape.

An early, and exceptional, quantitative treatment of state dependency can be found in Benda and Dunne, (1997a,b), which address state dependency in the context of short-term climatic variability in a series of studies modelling the evolution of the Oregon Coast range. By explicitly modelling the impact of climatic variability on the rates of soil accumulation, shallow land sliding and sediment transport using simple laws for each, they create a model with seemingly random response to climatic forcing at any particular time and place. The local landscape response to storms was heterogenous, depending heavily on the evolution of each part of the landscape up until that point, as a result the measured rates of different processes varied from place to place and time to time, even though the mean climatic forcing was constant. The state dependency aspect of the model arose naturally from a set of simple interacting laws. This demonstrates how a few simple processes characterizing the state of the system can lead to heterogenous responses to the same climatic forcing. Despite this complexity, they are able to draw general conclusions about what sort of conditions can be generally expected in certain parts of the landscape. In doing so they show how even in a landscape dominated by contingency, patterns emerge and can be understood. One issue with the study is that the model was constructed using very specific knowledge about the particular landscape carefully collected in the field. As a result it is difficult to generalize the results to other landscapes.

Two critical components of the work of Benda and Dunne, (1997a,b) were the role of vegetation in stabilizing slopes, and the episodic and unsteady delivery of sediment to the channel. These two controls on the state of the erosional system are frequent themes. Vegetation in particular is often used to create state dependent erosion models for hillslopes and small channels.

For example, Langbein and Schumm, (1958) show that vegetation is a state variable that controls the sediment yield for a given mean annual precipitation rate. Istanbulluoglu and Bras, (2006a) find the same relationship with a stochastic model of landscape evolution that explicitly models vegetation as a dynamic state variable. The vegetation influences the landscape by increasing the erosion threshold for fluvial erosion. However, vegetation is also destroyed by fluvial erosion. In this manner, the erosion rate at a point in the landscape is not only a function of the slope steepness and river discharge, but also the current state of vegetation at that point. This state reflects the history of plant growth, fluvial discharge and plant destruction. The resulting landscapes are visibly changed by the presence of vegetation at steady state, and the random temporal fluctuations are also changed in character by the influence of vegetation. In particular, the slope-area scaling is fundamentally changed, a result found in several similar studies (Collins, Bras, and Tucker, 2004; Istanbulluoglu and Bras, 2005).

Lague, (2010) analyze a model of sediment transport and bedrock erosion with state dependent sediment cover to understand the impact of cover and stochastic sediment flux in a stochastic-threshold context of fluvial erosion. This study is the most in line with the nonlinear law models in that it attempts to connect short-term variability to long-term erosion rates. It succeeds in deriving a functional description for the long-term erosion rate. It is notable that the long-term law is quite unrelated to the law describing instantaneous processes. The study also succeeds in conveying how quickly state dependent models become very complex, and the difficulty in upscaling process laws to geomorphic time if state dependency is to be taken into account.

In chapters 3 and 4, we take advantage of a theoretical framework that allows for a state-dependent hydrological response to rainfall. This framework, first derived in Rodriguez-Iturbe et al., (1999), is a rare case where state-dependancy can be accounted for in a set of analytical equations. The result is a powerful tool that has been a boon to the fields of ecology, hydrology, and now potentially, geomorphology. It can serve as an example of how state-dependent responses to climatic forcing can be included in theoretical treatments of fluvial erosion.

In order to make landscape evolution models more predictive and produce testable hypotheses on the interactions between climate, erosion and tectonics, it is important to unravel the complexity of the relationship between climate and erosion. This problem has been approached with some success with statistical methods that aim to understand the temporal complexity posed by meteorological variability (e.g Crave and Davy, 2001; DiBiase and Whipple, 2011; Huang and Niemann, 2006a; Lague, 2014; Lague, Hovius, and Davy, 2005; Molnar, 2001; Molnar et al., 2006; Rossi, Whipple, and Vivoni, 2016; Snyder et al., 2003; Tucker, 2004; Tucker and Bras, 2000). Focusing on erosion over meteorological timescales may seem far removed from tectonics, and its potential interactions with climate. However, it has been clearly shown, and in particular for fluvial processes crucial in linking climate with tectonics, that the impact of thresholds and meteorological variability must be taken into account in order to properly understand how climate drives erosion over long periods of time (DiBiase and Whipple, 2011; Lague, 2014; Lague, Hovius, and Davy, 2005; Snyder et al., 2003; Tucker, 2004; Tucker and Bras, 2000). Much of this work pertains to fluvial erosion, however, several aspects of this analysis are more generally applicable, with implications for other erosion processes.

These theories have mostly been developed considering the response of the landscape at a single point in space. When spatial dimensions are included, and full 2D

landscapes driven by stochastic meteorology are modeled, the result is far more complex. Different parts of the landscape respond to simple climate changes differently, leading to diachronous erosion and deposition events resulting from the temporal variability and spatial connectivity inherent in landscapes (Balen, Busschers, and Tucker, 2010a; Lague, 2010; Tucker and Slingerland, 1997). In these models, it is difficult to identify the causes of various effects, due to the significant role of history in determining how the landscape responds to a meteorological event (Benda and Dunne, 1997a,b). These modeling results match observations to the extent that they verify that landscape response to climate and tectonics is complicated and difficult to interpret (Blum and Valastro, 1989; Schumm, 1973). This helps to highlight the considerable temporal and spatial complexity involved in landscape evolution.

1.4 SUMMARY

When I arrived in Grenoble to start my PhD in January 2014, I was, by chance, alone for the first week in my advisor's office. He had told me the topic of my thesis should be related to climate, erosion and tectonics in the Himalaya, probably some modelling with the stream power model and some sort of climate model. By good fortune an excellent review on the stream power model had just come out (Lague, 2014), and it was the first paper I read. I spent the week undisturbed, learning the background and state-of-the-art of the stream power model. I had the impression going in that rainfall drives fluvial erosion. So I was surprised to see that it is discharge, not rainfall, that is represented in the equations. I could conceptualize integrating rainfall as a boundary condition in a landscape evolution model, but not discharge. I resolved to connect the two, and rewrite the stream power model in terms of rainfall without ignoring hydrology. The framework of Lague, Hovius, and Davy, (2005) and Tucker and Bras, (2000) seemed the perfect way to achieve this. The chapters that follow document this attempt, and as such represent a natural progression deeper into the problem of climatic variability and fluvial erosion.

1.4.1 *Measurement techniques*

I started with an analysis of the variability of daily rainfall in the Himalayan orogen. The choice to investigate meteorological and hydrological variability on daily timescales was a pragmatic choice. The investigation of variability often lends itself to a statistical treatment, and the ability to assume statistical independence between the events under investigation is a powerful tool. At a point, rainfall is often assumed to be independent on a daily timescale. This is also important in assuring independence between runoff-producing storms in the hydrological model set out in chapter 3. Clearly, considering daily rainfall and discharge rates will underestimate peak rates, which occur over a period of minutes or hours. A shorter timescale that more accurately captures the highest rates would be superior. However, this may break the assumption of independence, which is beyond the abilities of myself or the theories that I make use of. Further, data sets of rainfall or river discharge measurements are often given with a frequency of one measurement per day. The use of a daily timescale is a compromise between the demands of the problem and currently available theory and data. The problem of sub-daily variability remains for future work.

The Himalaya, with a dramatic rainfall gradient from south to north, as well as highly active erosion processes throughout the orogen, but a minimum of glacial erosion, is a natural laboratory to investigate the relationship between fluvial erosion and climate. However, in the end I realized that because of the consistent rainfall during the monsoon season, the rainfall, and in particular, fluvial discharge variability is exceptionally low in this region. This makes it less than ideal to study variability in particular, and after the study of rainfall, I did not pursue study in the region further. Regardless, valuable things were learned about rainfall variability.

This work prompted me to explore the fields of meteorology and probability. For guidance, I reached out to Anne-Catherine Favre. She introduced me to applied probability in the geosciences and was vital in ensuring the high quality of the work we did together. The most important outcome of chapter 2 was the development of a tool for comprehensively measuring rainfall variability. In the field of meteorology this is achieved by fitting a simple function to some form of the probability distribution of daily rainfall. Commonly, the function has a single parameter which influences its shape. This parameter then serves as a measure of variability. In chapter 2 we fit a gamma distribution to the observed frequency magnitude distribution of daily rainfall. In this case the shape parameter of the gamma distribution acts as a measure of variability in storm size. A second measure of variability is the frequency with which rainfall occurs, easily measured as the fraction between days with rainfall over total number of days. These two metrics of variability serve two purposes. First, they provide a mean-independent measure of variability that allows for accurate comparison from one data set or region to another. Second, in conjunction with the mean intensity of daily rainfall (mean of rainfall on days when it rains), these two metrics are sufficient to reconstruct the probability density function (pdf) of daily rainfall. This allows for calculation of any relevant metric, such as the P^{99} of daily rainfall, or the expected maximum annual storm size. These three numbers can also be used to construct a simple rainfall generator. The end result is a tool that can objectively measure variability, and provides a method for integration of rainfall variability into landscape evolution models.

In developing this tool, we tested several functions, such as the gamma function, the exponential function and the stretched exponential function. We found the gamma function worked best in the region we investigated, though that may not always be the case. We also tested several fitting techniques, including the method of moments, the maximum likelihood estimation method, the expectation maximization method and a hybrid of the maximum likelihood and expectation maximization methods. In the end, the maximum likelihood estimation (MLE) was superior because it performed reasonably well, and, critically, always returned physically reasonable parameter estimates. In addition, we could use the MLE method to estimate the statistical significance of the parameter estimation. The MLE method, a standard parameter estimation technique, works by finding a maximum on an n-dimensional surface that represents the likelihood of obtaining the observed sample given an assumed 'true' distribution (n = the number of parameters of 'true' distribution). The statistical significance of the parameter estimation is found using the Fisher information, which is an approximation of the second derivative of the likelihood surface (i.e. the curvature). When the curvature is large, the fit is considered significant.

Sensitivity tests predict that when the observed rainfall is gamma distributed, a sample size of several tens of measurements is large enough to obtain a good parameter

estimation. As a result, it is theoretically possible to measure variability during a single monsoon season. This tool has proved useful in understanding long-term rainfall patterns and erosion rates (chapter 2) and may also be useful in understanding seasonal rainfall and erosion patterns.

1.4.2 *Realistic models*

The purpose of measuring rainfall variability was to relate it to discharge variability, and understand the relationship between the two. This lead me into the field of hydrology, and a collaboration with Gianluca Botter. Chapters 3 and 4 are the result of our work together. In these chapters, we integrate a model of stochastic hydrology into a stream power model. The stochastic hydrology model describes the relationship between the probability distribution of daily rainfall and the probability distribution of daily discharge in a manner that is well suited for use in the current stochastic-threshold stream power theory. This work has been useful for understanding the response of stream power erosion to rainfall explicitly. It will be integral in the construction of a model of landscape evolution with realistic climatic forcing.

As a minimalist statistical model, the hydrological model is approximate. However, it has been well-studied, and often does well when tested empirically (e.g. Basso, Schirmer, and Botter, 2015; Ceola et al., 2010; Müller, Dralle, and Thompson, 2014). This work is also important in pointing to several specific controls on the relationship between rainfall and fluvial erosion. For example, the theory highlights evapotranspiration as an important control on discharge variability. Coincidentally, Rossi, Whipple, and Vivoni, (2016), without the guidance of this theory, demonstrate with a comprehensive data set, the importance of evapotranspiration for discharge variability and landscape evolution. Our work also points to the recession exponent b and the hydrologic timescale τ as important controls on fluvial erosion. These hydrological parameters, though well studied in the field of hydrology (e.g. Berghuijs et al., 2014; Bogaart, Lyon, and Dekker, 2016; Brutsaert and Nieber, 1977), have been ignored in landscape evolution.

Although the stochastic hydrology model of Botter et al., (2007, 2009) was already well suited for integration into the stochastic-threshold framework of Lague, (2014) and Lague, Hovius, and Davy, (2005), there was still work to bring the two theories together. The most important contributions that I personally made in this regard were, first, to rederive the theory from Lague, Hovius, and Davy, (2005) in a slightly different manner. Instead of taking an integral of daily discharge weighted by the erosional impact of each discharge magnitude, I first explicitly derive the distribution of daily erosion, and then integrate over it. This allows me to calculate separately the effect of events not exceeding the erosion threshold and the effect of the threshold on events that do exceed it. I made an effort to ensure the theoretical soundness of the derivation. The fact that I obtain the exact equations of Lague, Hovius, and Davy, (2005) when I make the same assumptions points to the soundness of both derivations. A second contribution I made was to verify the fact that the gamma distribution and the inverse gamma distribution were definitely the asymptotic solutions of the main pdf of discharge when the recession exponent, b is one and two respectively, and find the approximation for the normalization coefficient C for $b \neq 1, 2$ as presented in the appendix of chapter 3. In the course of this I also developed a robust code base for producing the cumulative density function, probability density function, survivor function, and random samples

for a wide range of b values, quickly and with high precision. Gianluca Botter and I plan to publish this code to allow others to take advantage of it. I made a third contribution by using the work of Dralle, Karst, and Thompson, (2015) as a justification to rewrite the pdf of daily discharge so that the shape parameter was constant for all values of b. This is the basis of the coefficient of variability that is critical to chapter 4. Botter et al., (2013) had already recognized the value of the coefficient of variability when $b = 1$, but this work helped to extend the concept to other values of b.

1.4.3 *General theory*

Throughout the course of my work, I read the literature concerning climatic variability and fluvial erosion carefully. In particular, I became familiar with the small collection of quantitative studies accounting for the nonlinearity in the erosional response to climatic forcing (Crave and Davy, 2001; DiBiase and Whipple, 2011; Huang and Niemann, 2006b; Lague, 2014; Lague, Hovius, and Davy, 2005; Molnar, 2001; Molnar et al., 2006; Snyder et al., 2003; Tucker, 2004; Tucker and Bras, 2000). It was striking how consistent the theoretical results were, despite the use of different probability distributions to describe climatic forcing and different erosion process laws. This lead me to develop a more general model to understand this consistency. The result is described in chapter 5. This chapter is useful in allowing the results from previous studies to be reinterpreted as general rather than specific. Their conclusion can be more widely applied as a general rule, to understand approximately the erosional response of fluvial systems to short-term climatic variability. This work also strengthens the results of the previous chapters. Even if there are significant inaccuracies in derived relationship between rainfall and fluvial erosion presented here and elsewhere (which there almost certainly are), the qualitative results and conclusions drawn from the work are more likely to be correct in light of chapter 5. Finally, it points to a better understanding of the fluvial erosion threshold, and controls on the threshold as a worthwhile endeavour.

2

RAINFALL VARIABILITY IN THE HIMALAYAN OROGEN

2.1 ABSTRACT

Over the last 15 years, it has been established that long-term fluvial erosion rates are sensitive not just to the mean annual river runoff, but also the short-term (daily) variability of runoff, with more erosion occurring in rivers characterized by high variability runoff. Though rainfall variability is not the only control on runoff variability, current research indicates that it at least partly determines runoff variability. This implies that high variability rainfall should increase or, at least, impact fluvial erosion rates. Further, fluvial erosion is not the only erosion process influenced by rainfall variability. Land sliding, for example, should also be more efficient under a high variability rainfall regime.

In light of this, we have characterized the variability of daily rainfall over the Himalayan orogen using high spatial and temporal resolution rainfall data sets. We find significant variations in rainfall variability over the Himalayan orogen. By taking into account variability of rainfall in addition to mean rainfall rate, we find a pattern of rainfall that, from a geomorphological perspective, is significantly different from mean rainfall rate alone. Though we cannot exclude the possibility that modern climate is not representative of past climate, the observed rainfall patterns are caused by conditions (high topography and the monsoon) that are thought to have existed for at least the last several million years. Using these findings we also demonstrate that short-term rainfall variability may help explain observed short and long-term erosion rates in the Himalayan orogen.

2.2 INTRODUCTION

Erosion rates are measured in years or thousands of years, in contrast, erosion events often occur over hours, taking place discretely and episodically until they sum in great numbers over extended periods of time to yield measured erosion rates. This is a common feature of geomorphic systems, where the average rates related to long-term landscape evolution are disconnected from the rapid processes we observe. Reconciling these two timescales with one another is key to understanding how climate and tectonics interact with each other and remains a formidable challenge.

The discrete and episodic nature of erosion events can often be directly attributed to the intermittent, variable nature of rainfall, one of the principle drivers of erosion. The vital role that rainfall plays in shaping landscapes is unquestioned; the vast majority of erosive processes require or are dramatically enhanced by the presence of water. Implicit in this comparison is the assumption that the details of rainfall, such as storm size and frequency, are unimportant, that more water yields more erosion. Many have concluded that the observed erosion rates are driven by uplift rates rather than climate (e.g. Burbank et al., 2003; Godard et al., 2014). This is expected if the Himalayas are in dynamic equilibrium (uplift rate $\approx$ erosion rate), which they are thought to be (Hodges, Hurtado, and Whipple, 2001). Still, the tectonic control on erosion rates should cause

the landscape morphology to adapt to the available climatic forcing - e.g. hillslopes will steepen where rainfall rates are low. The joint impact of climatic forcing and landscape form are taken into account by specific stream power, which estimates fluvial erosion rates as proportional to shear stress applied on the river bed. The shear stress is a function of river slope, river discharge and channel shape. Erosion rate can be increased with steeper channels, narrow channels, or higher river discharge. By taking into account slope steepness and channel width, the specific stream power should be a better match to the long-term erosion rates than rainfall rate. However, specific stream power also decreases across the topographic divide, albeit less rapidly than the mean rainfall rate (Burbank et al., 2003).

This leads to several possible conclusions: 1) current theories are mistaken and climate is not important in determining erosion rates, or 2) climate is important but the modern climate is a poor representation of the past climate that produced the observed erosion rates, or finally, 3) climate is important and the modern climate is representative but mean rainfall rates and specific stream power based on mean discharge rates do not accurately characterize the active erosion processes, and are therefore a poor predictor of erosion rates.

It is not possible to rule out that the modern climate is a poor representation of past climate. However, the current climatic regime results from moisture laden air brought by the Indian monsoon colliding with high relief topography (the southern edge of the Tibetan plateau) (Bookhagen and Burbank, 2006). Both the plateau and the Indian monsoon are estimated to have existed in their current form for the last 8 million years (Zhisheng et al., 2001). This implies that the current climate should be roughly representative of climatic forcing in the region over the last few million years, and lends credence to the idea that the Himalayan orogen is in dynamic equilibrium. Assuming modern climate to be representative, we show that the observed erosion rates can be consistent with modern climate if key erosion processes active in the orogen, such as fluvial erosion and landsliding, do not depend solely on the mean rainfall rate, but are also sensitive to the variability of forcing. This is accomplished by characterizing the variability of daily rainfall in the Himalayan orogen using high resolution gridded data sets.

There are several established methods for characterizing the daily variability of rainfall. Extreme rainfall analyses describe the most intense days of rainfall, their frequency of occurrence and magnitude. This has obvious value to human society, and has been applied to the Himalayan orogen (e.g. Joshi et al., 2014; Bharti et al., 2016), where intense monsoon storms can cause significant economic damage (Thayyen et al., 2013). Here, we are not attempting an extreme value assessment of daily rainfall. Theoretical work accounting for erosion thresholds and nonlinearities argues that it is not just extreme events that are potentially significant, but also the distribution of moderate magnitude events (e.g. annual maximum storm or even smaller, depending on the erosion threshold) (Wolman and Miller, 1960; Tucker and Bras, 2000; Snyder et al., 2003; Tucker, 2004; Lague, Hovius, and Davy, 2005; Lague, 2014). Also, we do not wish to estimate future rainfall statistics, but rather to characterize the observed distribution of daily rainfall, and do so as succinctly as possible. Characterizing variability by fitting a function to some empirical form of the distribution of daily rainfall is another established technique. Whether the function is fit to the empirical frequency distribution (e.g. May, 2004b; Suhaila et al., 2011), the normalized rainfall curve (e.g. Burgueño et al., 2010), or the concentration index (e.g. Martin-Vide, 2004; Caloiero, 2014; Jiang,

Wang, and Cao, 2016) the result is the same: the actual form of the distribution of daily rainfall variability is summarized by a function with just a few parameters. In order to keep in line with previous work on the importance of climatic variability on long-term landscape evolution (Tucker and Bras, 2000; Tucker, 2004; Lague, Hovius, and Davy, 2005; Rossi, Whipple, and Vivoni, 2016), we fit a mixture of gamma distributions to the empirical frequency distribution of daily rainfall.

In this study we make use of two high spatial and temporal resolution gridded rainfall data sets. Several studies have characterized the daily variability of rainfall using high spatial resolution gridded data sets (e.g. Burgueño et al., 2010; Jiang, Wang, and Cao, 2016), however, not over the Himalayan orogen. Several others describe the distribution of Indian rainfall using similar methods to those employed in this study (Mooley, 1973; May, 2004a; May, 2004b). However, they make use of data sets with low spatial resolution and tend to focus on rainfall patterns across the Indian subcontinent rather than the orogen. Prakash, Mitra, and Pai, (2015) compute the coefficient of variation of monsoon rainfall, which is closely related to daily variability, using TMPA and other high resolution gridded data sets, however by restricting the analysis to India, they leave out much of the Himalayan orogen. Finally, there are several studies comparing the frequency-magnitude distribution of daily rainfall to erosion patterns in the Himalayas (e.g. Craddock et al., 2007; Bookhagen and Burbank, 2010; Wulf, Bookhagen, and Scherler, 2010; Wulf, Bookhagen, and Scherler, 2012). However, these studies do so only from the perspective of extreme events and often only on the scale of individual valleys. The previous studies of daily variability of Indian and Himalayan rainfall are useful to to corroborate our results where the different data sets overlap. However, they do not allow for a careful assessment of daily variability over the entire Himalayan orogen, which is the goal of this study.

First, in section 2.1, we describe the gridded data sets that we use in our analysis (APHRODITE and TMPA) (section 2.1) followed by the statistical model of rainfall that we use in section 2.2, and the methods applied to fit the model to the data in section 2.3. Then we show the model parameter estimates obtained and compare the two rainfall data sets in section 3. Finally, in section 4, we discuss the pattern of rainfall variability in the Himalayan orogen and the implications for measured erosion rates.

2.3 DATA AND METHODS

2.3.1 *Data*

In recent years several rainfall data sets spanning the entire Himalayan orogen have become available, ranging from moderate to high temporal and spatial resolution. We use two, described below, that are known to perform well in the Himalayan orogen (Andermann, Bonnet, and Gloaguen, 2011).

2.3.1.1 *APHRODITE*

Asian rainfall Highly Resolved Observational Data Integration Towards Evaluation of Water Resources, Monsoon Asia, Version 11 - APHRO_MA_025deg_V1101R2 (referred to here as APHRODITE) is a distance weighted interpolation of daily rainfall depths from between 5,000 and 12,000 ground based stations (depending on the time period) spread throughout Asia over the period from 1951 to 2007. It is made available by the Research Institute for Humanity and Nature (RIHN) Japan and the Meteorological Re-

search Institute of Japan Meteorological Agency (MRI/JMA). The data set has a spatial resolution of 0.25° x 0.25°, and a temporal resolution of one day (Yatagai et al., 2012). Despite making use of an orographic correction algorithm, there are concerns with the accuracy of the data set due to the relatively small number of stations it is interpolated from in the orogen. Particularly outside of Nepal and north of the main topographic divide. Andermann, Bonnet, and Gloaguen, (2011) tested the accuracy of this data set in the Himalayan orogen and found it to be good relative to other large scale rainfall data sets available in the region. However, their analysis is potentially problematic because APHRODITE incorporates nearly all available station data, making it difficult to find independent station time series against which to test the accuracy of APHRODITE.

2.3.1.2 *TMPA*

Tropical Rainfall Measuring Mission (TRMM) Multisatellite Precipitation Analysis (TMPA) - 3B42 V7 (TMPA) is a remotely sensed, gauge-adjusted, precipitation data set composed of measurements from several space borne instruments (Huffman et al., 2007) covering the globe from 50°N to 50°S and spanning from the beginning of 1998 to mid 2015 available at 3 hour, daily and monthly resolution. The data set integrates infrared and microwave observations from multiple satellites as well as ground based gauge data (Prakash, Mitra, and Pai, 2015). We use the daily version of the product from 1998 to the end of 2013.

TMPA is known to have difficulties properly estimating the magnitude of rainfall in complex, steep terrain, though the new version V7 has improved in this regard (Bharti et al., 2016). Bharti et al., (2016) also find that TMPA V7 does a good job estimating the frequency of large storms, but has difficulty accurately measuring their magnitude, commonly overestimating the storm magnitude below 3000 m and underestimating above 3000 m. In general it is also known to overestimate rainfall magnitudes in the Indian subcontinent (e.g. Prakash et al., 2015). Despite these shortcomings TMPA outperforms all other available multisatellite products in the region (Prakash et al., 2014).

2.3.1.3 *Quality of the data sets*

While recognizing that both gridded data sets have potential issues, they are also the best currently available with a daily resolution (Andermann, Bonnet, and Gloaguen, 2011; Prakash et al., 2014). In addition their respective weaknesses and strengths are complementary. APHRODITE is interpolated from accurate ground data, but suffers from a lack of stations. TMPA consists of measurements with a very high spatial resolution, but suffers from a lack of accuracy in the orogen. To mitigate the potential weaknesses of these data sets, we restrict our interpretations to features observed in both data sets and on a scale larger than the scale of the data set resolution.

2.3.2 *Statistical model*

We define here the distribution of daily rainfall intensity to be the distribution of daily rainfall depths on days with rainfall exceeding 0.5 mm (wet days). The mean of this statistical distribution is referred to as the mean daily rainfall intensity (α). The mean rainfall rate including days with less than 0.5 mm of rainfall (wet days and dry days) is referred as the daily rainfall amount ($\mathbb{E}[P]$). The relationship between the two means is

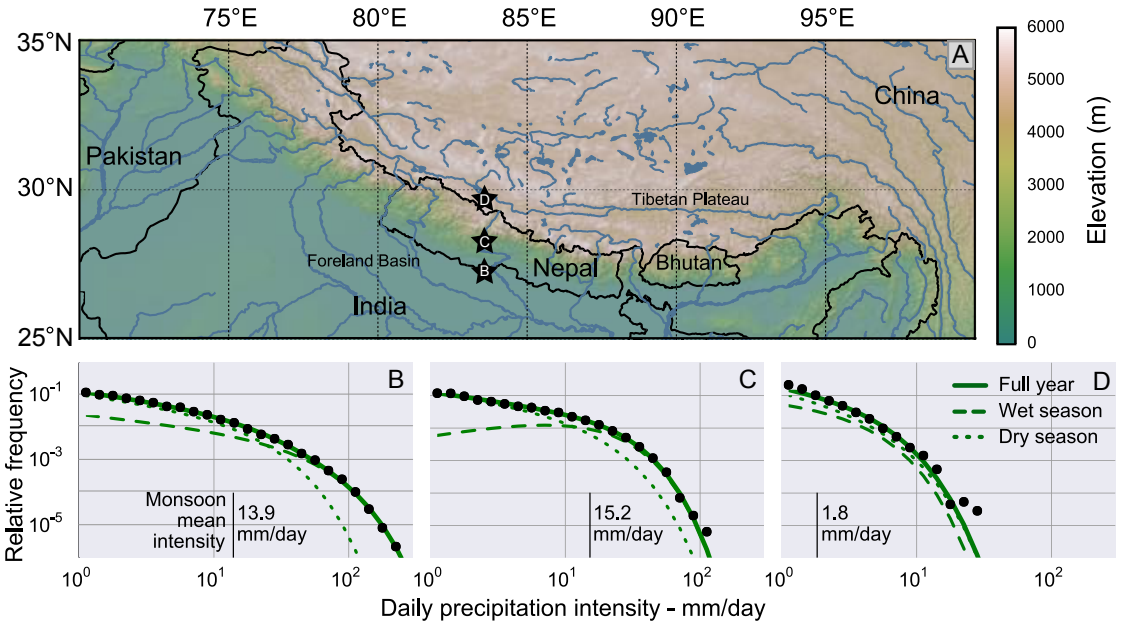

Figure 1: Map of the region of interest. Shown in b), c) and d) are examples of fitting the empirical distribution (black points). The plots correspond to the three black stars in a). The full pdf is shown as a solid line, the monsoon season pdf as a dashed line, and the dry season as a dash-dotted line. Note the fundamental change in shape of the monsoon pdf from b) the southern band of high magnitude rainfall to c) the northern band, and d) the Tibetan plateau. The approximate location of the topographic divide is shown by the smoothed 3,000, 4,000 and 5,000 meter contour lines.

controlled by the ratio of wet days to the total number of days (λ) such that $\mathbb{E}[P] = \lambda\alpha$. We refer to λ as the mean wet day frequency.

In order to describe the distribution of daily rainfall intensity (ignoring days with less than 0.50 mm of precipitation) we use a pdf that can be fit to the empirical distribution. We searched for a model that is both simple (only a few, physically interpretable parameters) and flexible (it can fit well the empirical distribution over a wide range of climates). With only two parameters, the gamma distribution can fit the empirical distribution from markedly different climates. It also has a long history of application in modelling daily rainfall in general (e.g. Eagleson, 1978; Srikanthan and McMahon, 2001, and references therein), and in the Indian monsoon region specifically [e.g. Mooley, 1973; Stephenson et al., 1999, and references therein; May, 2004b, and references therein; May, 2004a; Mueller and Thompson, 2013].

Due to the marked difference in daily rainfall intensity between the monsoon season and the dry season, we follow Mueller and Thompson, (2013) and model the two seasons separately, so that the annual distribution is a mixture of distributions composed of one gamma distribution for the wet season and a second for the dry season, each weighted by the relative length of the associated season as shown in figure 1. The resulting pdf, $f_P(p)$, has seven parameters - two daily rainfall intensity distributions with three parameters each and the length of the wet season.

$$f_P(p) = (1 - T_w)\, f_d + T_w\, f_w, \tag{2}$$

where T_w is the length of the wet season divided by 365, f_w is the daily rainfall intensity distribution for the wet season and f_d for the dry season. The distribution for the wet season is,

$$f_w(p) = (1 - \lambda_w)\,\delta(p) + \lambda_w\, g(\beta_w, \kappa_w, p), \tag{3}$$

where $\delta(p)$ is the delta dirac function and $g(\beta_w, \kappa_w, p)$ is the gamma distribution,

$$g(\beta_w, \kappa_w, p) = \frac{\beta_w^{\kappa_w}}{\Gamma(\kappa_w)} p^{\kappa_w - 1} e^{-\beta_w p}, \tag{4}$$

where $\Gamma(\cdot)$ is the gamma function, β_w is the rate parameter, and κ_w is the shape parameter. The first term of equation 3 describes an atom of probability that the daily rainfall intensity is zero. The theoretical mean of the gamma distribution can be expressed as $\mathbb{E}[x] = \kappa_w/\beta_w$, which can be interpreted as the wet season mean rainfall intensity α_w.

The dry season daily rainfall intensity distribution has the identical form, where all parameters are subscripted with d instead of w. Because we are interested in the ability of the rainfall to drive erosion, we will focus exclusively on the wet season rainfall since it delivers a majority of the annual rainfall in much of the Himalayan orogen. All future references to the parameters of the gamma distribution refer to those from the wet season distribution.

In this model, the daily variability is described by two different parameters: the mean wet day frequency λ and the shape parameter κ. The first describes the likelihood of observing rainfall on a given day, with a lower likelihood of rain implying higher daily variability. This is very similar to how daily rainfall variability is quantified by Tucker and Bras, (2000) or Rossi, Whipple, and Vivoni, (2016). The second describes the variability of daily rainfall magnitude on days that have rainfall, with lower values implying higher variability in daily rainfall magnitude. Figure 2 shows how λ and κ separately effect the shape of the rainfall pdf. Knowing λ, κ and α gives detailed information about the probability structure of daily rainfall for a given season. This allows for the computation of how often and by how much various geomorphic thresholds are expected to be exceeded in different climates.

There are several other distributions that are commonly used for wet day rainfall, such as the stretched exponential distributions (e.g. Rossi, Whipple, and Vivoni, 2016), and we do not claim any strong theoretical reasons for using the gamma distribution over others. We make use of it because it fits the empirical distributions over the wide range of climates found in the Himalayan orogen, though it is probable that other distributions could do so as well.

2.3.3 *The applicability of the statistical model*

We can use the statistical model to predict the average maximum annual storm. We obtain this from the mean of the probability distribution of the maximum annual storm magnitude. This is equivalent to the probability of exceeding a given storm size p over the course of a year, which is the joint probability of exceeding p on each day of the year. Rainfall is assumed to be independent from day to day, so $F_{max}(p)$ is the probability to exceed a storm size of p on a given day raised to the power n_a, where n_a is the number of rainy days per year. Therefore, $F_{max}(p) = \Pr[x \geqslant p]^{n_a} = F_P(p)^{n_a}$, where $F_P(p) = \Gamma(\kappa, \beta p)$ is the cumulative distribution function of the gamma distribution and $\Gamma(\cdot,\cdot)$ is the regularized upper incomplete gamma function. We assume that the

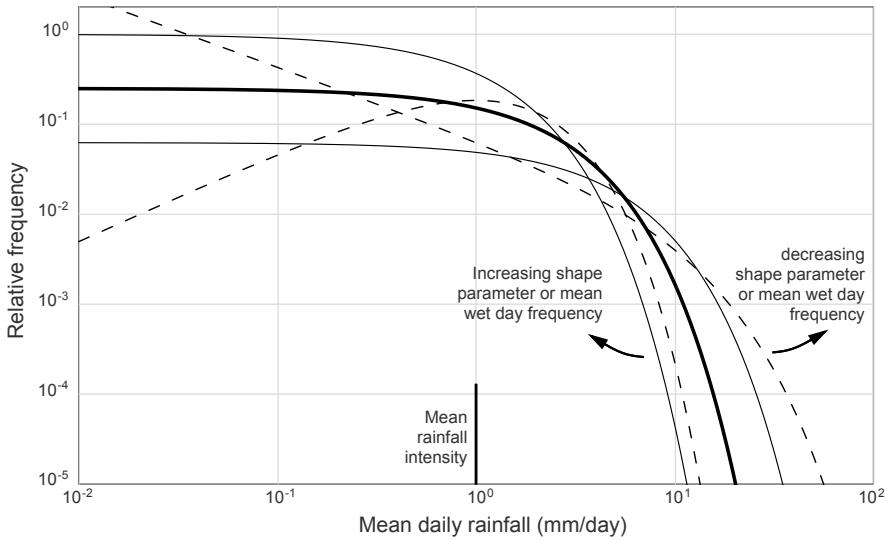

Figure 2: The thick line shows an example of a seasonal distribution with a shape parameter of 1 and a mean wet day frequency of 0.5. The thin solid lines show the effect of increasing or decreasing the mean wet day frequency λ to 1 and 0.25 respectively. The thin dashed lines show the effect of increasing and decreasing the shape parameter κ across much of the observed range from 2 to 0.2. When either λ or κ are decreased, the magnitude of storms for low relative frequencies (e.g. $< 10^{-2}$) increases though the total amount of rainfall does not.

monsoon season will always contribute the largest storm of the year, so the average maximum annual storm is $P_{max} = \mathbb{E}[\Gamma(\kappa_w, \beta_w p)^{n_w}]$, where $n_w = \lambda_w T_w \cdot 365$ is the mean number of rainy days in the monsoon season.

2.3.4 *Data fitting techniques*

We estimate the model parameters described in section 2.2 for the distribution of daily rainfall at each node in both gridded data sets. To obtain estimates of the model parameters we first created seasonal distributions by fitting a step function to the annual time series using the technique of Mueller and Thompson, (2013). The fitting of the step function is a simple method that provides an average start and end date for the wet season at each grid point. The results we obtain agree well with other assessments of the onset of the monsoon (Wang, 2002). The seasonal mean wet day frequency was computed as the ratio of the number of days with more than 0.5 mm of rainfall to the total number of days in each season. We used maximum likelihood estimation to find the seasonal shape and rate parameters (figure 3).

To assess the significance of our parameter estimation for the shape parameter and the rate parameter we used the Fisher information to estimate the standard error (figure 4a-d). While useful, this only informs us about how probable the estimated parameters are under the assumption that the sample is gamma distributed. It does not inform us about how well the chosen gamma distribution fit the data; the best fitting gamma distribution may still fit poorly. To establish objectively the quality of the fit to observed daily rainfall distributions we calculated the coefficient of determination, r^2, of a linear regression of the theoretical quantiles against the observed quantiles (figure 4e and f). The closer r^2 is to one, the better the fit. To be conservative, we reject all fits where $r^2 < 0.90$.

2.4 RESULTS

The three estimated parameters, mean intensity, mean frequency, and wet day variability ($\widehat{\alpha}$, $\widehat{\lambda}$, and $\widehat{\kappa}$ respectively) are shown in figure 3. Other aspects of the data analysis are shown in figure 4. The relative standard error for both the shape parameter and the mean rainfall intensity is shown in figure 4a-d. The standard error tends to be lower ($< 5\%$) for the APHRODITE data because the sample size is larger. However, it is still quite low for the TMPA data set, with most estimates having less than 10% relative standard error. Figure 4e and f show the r^2 value of the quantile-quantile fits. We note that the goodness of fit is for the most part above the 0.9 threshold we chose, though there are some poor fits on the Tibetan plateau, particularly in the west. Rejected fits are shown in figure 3 as shaded regions. Also shown in figure 4 is the length of the monsoon season as computed by fitting a step function to the annual rainfall time series, and the number of monsoon season wet day samples in each data set (figure 4g-l). The abrupt change in the length of the monsoon season in the western edge of the Himalayan orogen (34°N, 75°E) is associated with the breakdown of the dry season/-monsoon season model due to the influence of significant winter rainfall. This results in a poor fit of the statistical model to empirical rainfall distributions and the low r^2 values in the region.

2.4.1 *Spatial distribution of the gamma shape parameter*

As discussed previously, the variability of daily rainfall is described by both the shape parameter and the mean wet day frequency. We find in this case that the range in the shape parameter is more significant than the range in the wet day frequency. Overall, the observed range of gamma shape parameter is between 0.1 and 4, with the majority of the values falling between 0.2 and 2. The range from 0.1 to 4 represents nearly an order of magnitude change in the size of the 99^{th} percentile storm for a given mean rainfall amount. This means that there is a significant and important change in the variability of daily rainfall across the Himalayan orogen.

The spatial distribution of the gamma shape parameter, shown in 3a and b, are qualitatively similar for both data sets across the Himalayan arc, though the range of values is smaller in the TMPA data set. The TMPA data set also exhibits higher wet day variability in western India, the southwestern edge of the Tibetan plateau and Pakistan. This may be due to the fact that the very low magnitude and frequency of rainfall in these areas allows them to be disproportionally affected by measurement errors.

Although the previous studies that measure the gamma shape parameter in a comparable manner do not focus on Himalayan rainfall and have a much coarser resolution, the general trends in shape parameters match well between all studies. May, (2004b) and May, (2004a) show large shape parameters along the Himalayan mountain front and May, (2004a) and Mooley, (1973) also show small shape parameters in northwestern India and Pakistan, all observations which match our estimates well. More specifically, the magnitudes of the measured shape parameters from this study are very similar to May, (2004b) and in particular, the reanalysis data set from May, (2004a).

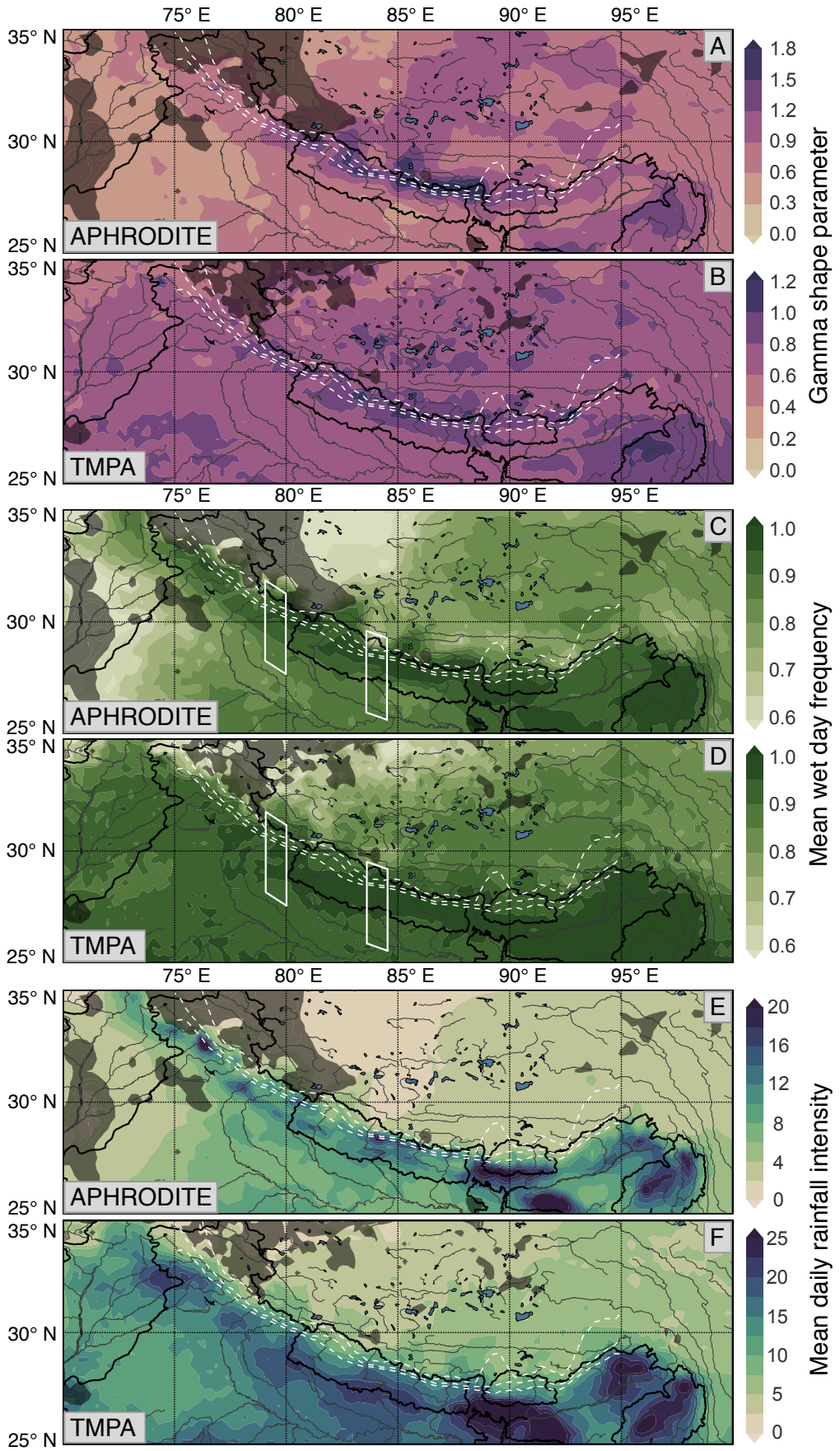

Figure 3: Gamma shape parameter (a and b), mean wet day frequency (c and d), and mean daily intensity (e and f) for both APHRODITE and TMPA. The cross sections in figure 7 are shown in white in c and d.

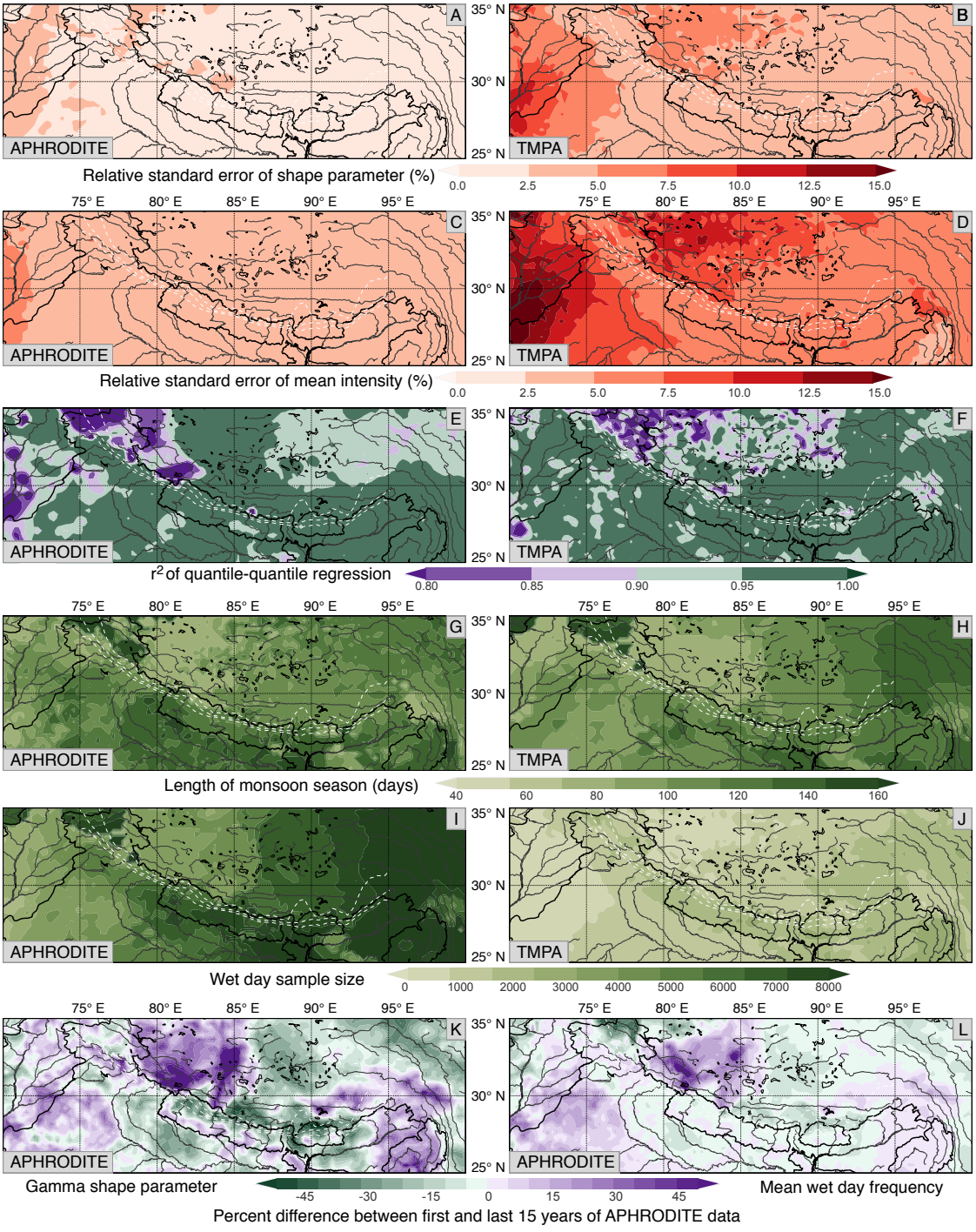

Figure 4: Relative standard error for the shape parameter estimate (a and b), relative standard error for mean daily intensity (c and d), coefficient of determination (e and f), estimate length of monsoon season (g and h) and data set sample size (i and j) for both APHRODITE and TMPA. Panels k and l show the percent difference between the first and last 15 years of the APHRODITE data set for the shape parameter and mean wet day frequency respectively.

2.4.2 *Spatial distribution of mean wet day frequencies*

The pattern of mean wet day frequencies, seen in figure 3c and d is broadly similar between the two data sets, though there are notable differences in the far western reaches of the range. The TMPA data set has in general higher wet day frequencies, though the frequencies are high overall in both data sets during the monsoon. The TMPA data set may exhibit higher frequencies because it is an areal measurement rather than a point measurement (Del Jesus, Rinaldo, and Rodríguez-Iturbe, 2015). In both data sets frequencies are much higher closer to the bay of Bengal, the source of moisture for monsoonal rainfall, and fall off westward in the foreland basin. In contrast, wet day frequencies remain high for several thousand kilometres along the Himalayan mountain front where high relief has been shown to drive frequent rainfall (Bookhagen and Burbank, 2006). Overall the estimated monsoon intensities and frequencies match well with previous analyses using large ground station data sets (Stephenson et al., 1999; May, 2004a; May, 2004b), and high spatial resolution remotely sensed data sets (Bookhagen and Burbank, 2006, 2010).

2.4.3 *Spatial distribution of mean storm intensities*

The mean rainfall intensities for the two data sets (figure 3e and f) again have similar general trends, exhibiting high mean rainfall along the Himalayan mountain front. They also both measure low rainfall in the Tibetan plateau and Pakistan. However, TMPA has higher magnitudes of daily rainfall intensity in general (note the different scale bars). The APHRODITE intensities are in agreement with estimates of intensity from three other studies, two using ground station data (Stephenson et al., 1999; May, 2004b) (four and 89 years long respectively), and a third using a reanalysis data set (May, 2004a). The TMPA intensities agree well with intensities measured by GPCP, another satellite data set (May, 2004a).

2.4.4 *Stationarity*

Malik, Bookhagen, and Mucha, (2016) demonstrate secular nonstationarity in daily rainfall in the Indian subcontinent. The main data set that they rely on for their analysis is derived from the same source as the APHRODITE data set we use here. Though their analysis of long-term trends is considerably more sophisticated, it is not surprising that we also find similar trends. Figure 4k and l, show the difference in the shape parameter and the mean wet day frequency between the first 15 years (κ_F, λ_F) and the last 15 years (κ_L, λ_L) of the APHRODITE data set such that $\text{diff}(\kappa) = (\kappa_F - \kappa_L)/\kappa_L$ and $\text{diff}(\lambda) = (\lambda_F - \lambda_L)/\lambda_L$. There is a notable decrease in both the shape parameter and mean wet day frequency towards the present in the western Tibetan plateau (increase in variability), though this largely corresponds to regions where the statistical model we use does not work well, and therefore may be suspect. There is also a significant increase in the shape parameter in northern Nepal and Bhutan and moderate decrease in the shape parameter in southern Nepal. This implies that the pattern we observe in Nepal of a band of low variability in the north has increased in strength towards the present. The changes in variability implied by the observed shift in the mean wet day frequency and shape parameter match the changes in the distribution of rainfall across quantiles observed by Malik, Bookhagen, and Mucha, (2016). Though the number and

distribution of stations from which the APHRODITE data are interpolated from has changed over the decades, and this may be partly responsible for the observed nonstationarity. Regardless, the main spatial trends in rainfall variability which we discuss in this study are observed in throughout the APHRODITE data set, even if their magnitudes shift, as well as in the TMPA data. One perspective is that the nonstationarity can be viewed as part of the variability, and we do not find it problematic that we implicitly include it in our measurement of daily variability. We are interested in the patterns of daily variability over periods of hundreds to thousands of years, which encompasses variation in measures of daily variability such as the shape parameter and mean wet day frequency which undoubtably occur over decades and centuries. Ideally we would have data sets spanning these timescales, but given the dearth of such data, we make do with 50 years.

2.4.5 *Correlations between intensity, frequency and shape parameter*

There is a strong negative correlation between the mean rainfall intensity and variability as measured by the frequency and the shape parameter. This is not surprising, because the shape parameter is related to the mean storm intensity via the scale parameter ($\alpha = \kappa/\beta$), and the mean wet day frequency is related to the mean rainfall intensity via the mean daily rainfall amount ($\mathbb{E}[P] = \alpha\lambda$). Further the negative correlation between mean rainfall intensity and variability has been observed before (Tucker, 2004). These negative correlations are shown in figure 5. We have only shown the results from the TRMM data. The trends for the APHRODITE data are even stronger (steeper slopes and higher r^2 values) however, because the data is interpolated, there is the risk the observed correlations result in part from the interpolation.

Figure 5a shows the negative correlation between the mean rainfall intensity and one minus the mean wet day frequency. This reflects a negative correlation between intensity and variability. We have separated the data by elevation, and it can be seen that the trend between frequency and intensity is the same for different elevations. We can collapse the data by normalizing both the intensity and the frequency for each elevation range by the mean value for that elevation range as seen in figure 5b. The result is a nondimensional relationship between the mean intensity and mean wet day frequency that is valid at all elevations in the Himalayan orogen of the form $1-\lambda \propto \alpha^{c_1}$. Although there is a positive correlation between the shape factor and mean intensity (5c), this still reflects a negative correlation between intensity and variability because increasing the shape parameter reduces the variability. We can also collapse this trend by normalizing the mean intensity (5d), giving $\kappa \propto \alpha^{c_2}$. Notably, the slope between all elevations are similar with the exception of elevations below 500 m, which includes much of the foreland basin and exhibits a weak relationship between mean intensity and variability. Given that both the shape parameter and the wet day frequency are strongly correlated with the mean intensity, it is not surprising that they are correlated with one another as well. Figure 5e shows a negative correlation between one minus the frequency and the shape parameter which reflects a positive correlation between both measures of variability. Again we can collapse the trends by normalizing the mean wet day frequency by the mean of the mean wet day frequency for each elevation range (5f). This yields a relationship between the shape parameter and the mean wet day frequency of the form $\kappa \propto (1-\lambda)^{c_3}$.

These empirical relationships can potentially be used to relate the variability and intensity of rainfall to the mean annual rainfall amount at different elevations in a landscape evolution model of a monsoon dominated orogen. This is useful because it allows for the distribution of daily rainfall to be reconstructed with an estimate of the mean annual rainfall and estimates for the slopes (c_2) of the trends between intensity and variability.

2.4.6 *General along and across strike trends in variability*

We observe large scale trends in the shape parameter and mean wet day frequency both across and along the east-west strike of the orogen. These trends are shown in figure 6a-d, separated by elevation. Again, we show only the TRMM data, for the same reasons as before. The APHRODITE data show the same trends, with the difference that the variation in the shape parameter is much larger and the mean wet day frequencies somewhat lower. Along strike from east to west both the shape parameters (6a) and the mean wet day frequencies (6c) increase at all elevations above 500 m. Below 500 m, both the shape parameter and the mean wet day frequency are relatively constant. At moderate and high elevations (500 to 4500 m) the shape parameter reaches peak values at around 85°E, after which it decreases again, but even at these elevations, the shape parameters in the east are still larger than in the west. Because increases in either the mean wet day frequency or the shape parameter imply a decrease in rainfall variability, it can be seen that the variability is highest in the west and decreases significantly to the east with a low in variability at around 85°E. Similar trends exist across strike. At all elevations both shape parameter and mean wet day frequency decrease to the north (6b and d respectively). Therefore, in general the variability of daily rainfall during the monsoon is lowest in the east and the south of the orogen, and increases both northwards and westwards. This reflects the pattern of rainfall mean and intensity, which is unsurprising, given the strong correlation between daily intensity and both the shape parameter and mean wet day frequency.

The mean rainfall amount and intensity decrease towards the west from the source of moisture, the bay of Bengal, in the east. However, because of the increasing rainfall variability at elevations above 500 m (as shown by both the frequency and shape parameter), the magnitude of the average maximum annual daily rainfall is nearly constant at those elevations (6e). At elevations above 4500 m, the magnitude of the average maximum annual daily rainfall increases towards the west from a minimum at around 83°E. Wulf, Bookhagen, and Scherler, (2016) found a bias in the TMPA data that causes rainfall to be overestimated in the dry, high relief regions in the west of the orogen. This bias could potentially cause the trend seen here. However, the APHRODITE data, which will not be influenced by this bias, exhibits the same trend. In fact, in the APHRODITE data, the average maximum annual daily rainfall magnitude increases slightly for all elevations above 500 m rather than remaining constant.

Figure 6 g and h show the standard deviation of the maximum annual daily rainfall as a percent of the maximum annual daily rainfall. It is relatively constant from east to west, perhaps increasing slightly in the west, however from south to north it can be seen to increase modestly. This means that in the orogen interior, storms with return times longer than a year can be larger with respect to the mean rainfall intensity than in the south, reflecting the higher variability in the north and highlighting that big storms are likely to be very significant in the relatively dry orogen interior.

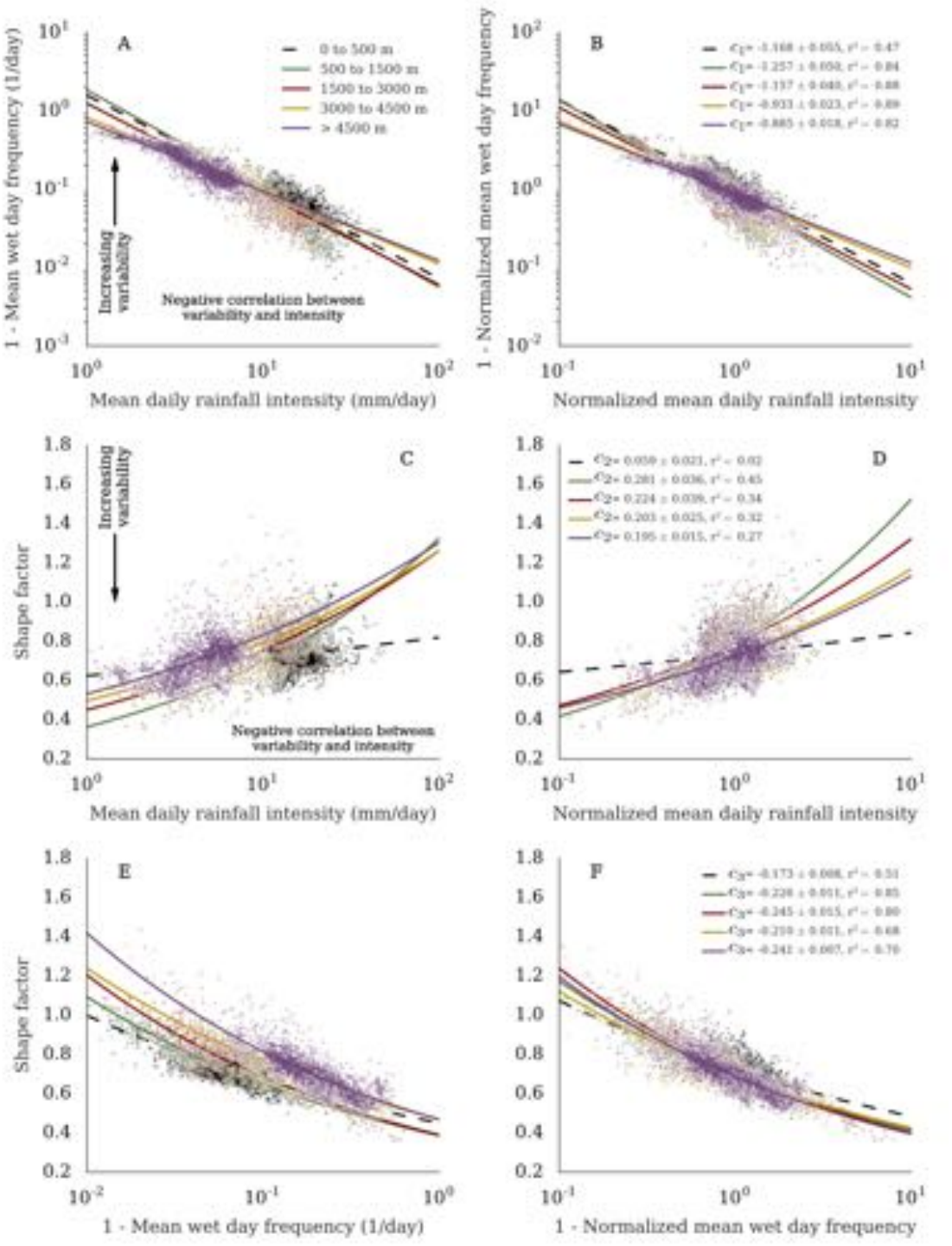

Figure 5: For the TMPA data set, a shows correlations between the mean wet day frequency and the mean rainfall intensity with trends fit to the data sorted by elevation. b shows the same, except the mean intensity and mean wet day frequency have been normalized by the mean value for each elevation range, collapsing the trends (normalized frequency - $(1-\lambda)/(1-\lambda_o)$ where λ_o is the mean value for each elevation range). Panel c shows the correlation between the shape factor and the mean intensity, which can be again collapsed by normalizing the mean intensity as in b (shown in d). Panels e and f show the same for the shape factor and the mean wet day frequency. In f, the mean wet day frequency has been normalized as in b.

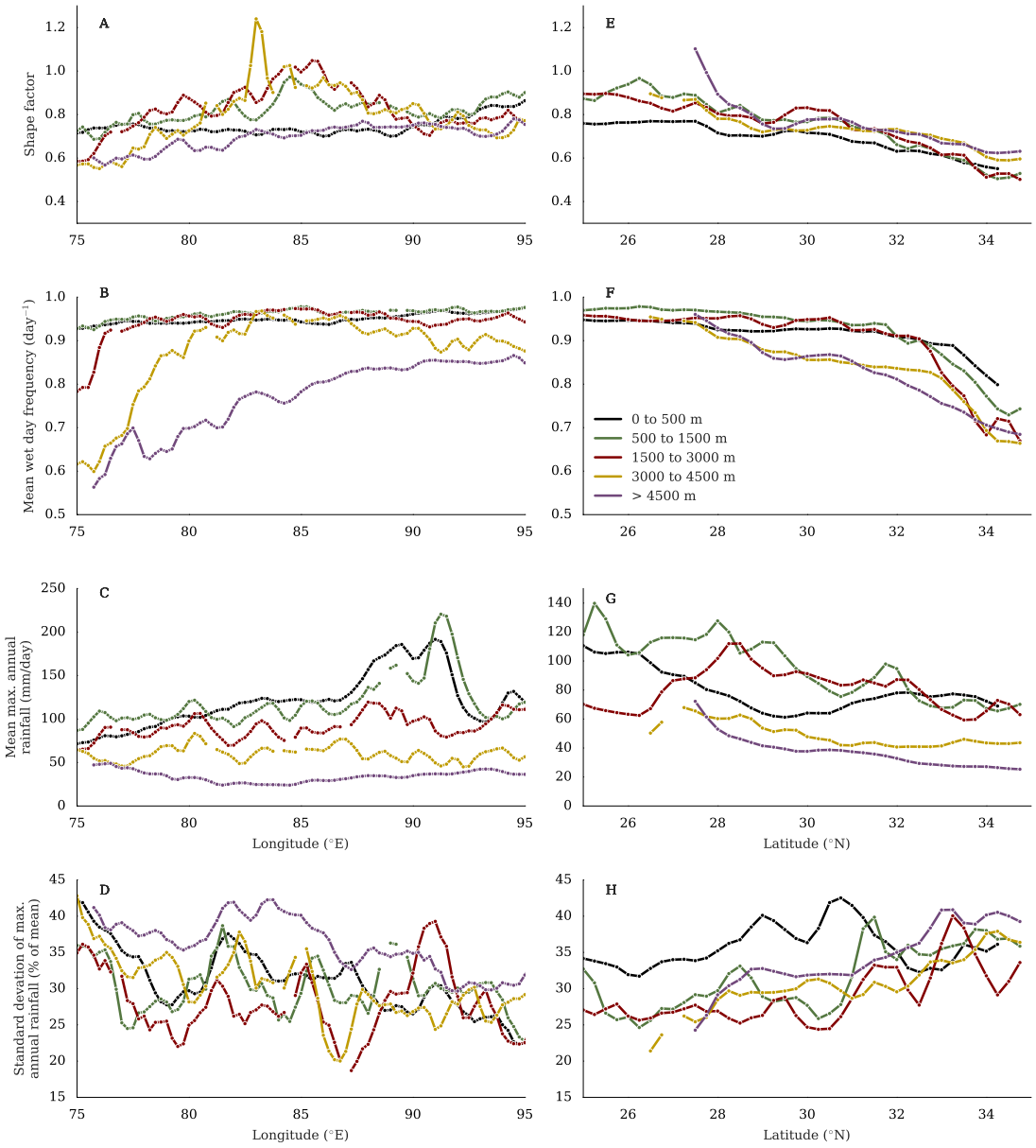

Figure 6: The average trends in the TMPA data along strike of the orogen from 75°E to 95°E of, a, the shape parameter, b, the mean wet day frequency, c, the mean maximum annual daily rainfall, and d, the standard deviation of the max. annual daily rainfall. Panels e-f show the same respectively from 25°N to 35°N. Data has been smoothed by taking the running mean with a window size of 3 (averaging across one point on either side of each data point). For d the window size was increased to 5.

2.5 DISCUSSION

2.5.1 *Rainfall variability and erosion rates*

The relative importance and impact of the intensity and variability of daily rainfall will depend on the details of the erosion regime in question, with emphasis on the kind and magnitude of erosion threshold or nonlinearity considered. For an erosion threshold associated with a minimum storm size or a nonlinearity which disproportionally weights larger storms, higher variability rainfall will lead to higher erosion rates. This is thought to be the case for erosion occurring in mountainous bedrock rivers (Tucker and Bras, 2000; Snyder et al., 2003; Tucker, 2004; Lague, Hovius, and Davy, 2005; DiBiase and Whipple, 2011). River erosion is far from the only erosion process occurring in the Himalayan orogen, but it is generally considered to be one of the most significant in active orogens (e.g. Molnar, 2001; Whipple, 2004), especially considering the minor influence of glaciers and glacial erosion in central Nepal. Due to the complexity of hydrological processes, it is challenging to link daily rainfall distributions to daily streamflow distributions. Empirical work investigating the drivers of daily streamflow find a number environmental controls, including the evapotranspiration rate and aridity index (Rossi, Whipple, and Vivoni, 2016). Importantly, they find a positive correlation between the wet day frequency and streamflow variability, and to a lesser extent between rainfall variability (i.e. the shape parameter) and streamflow variability. Using numerical simulations, another study found that the shape parameter of daily rainfall could have a significant impact on streamflow variability (Müller, Dralle, and Thompson, 2014), and a third theoretical study predicts that the mean wet day frequency should be an important control on the streamflow variability [Deal et al. submitted].

These results are not particularly surprising. It is intuitive that a river catchment with high variability rainfall (i.e. larger storms for a given mean rainfall rate) will experience larger floods than a river catchment with low variability rainfall. In light of these studies it seems likely that higher variability rainfall will lead to higher river erosion rates.

2.5.2 *Relevance to the Himalayan orogen*

One of the more striking features of the spatial distribution of the shape parameter and the wet day frequency in figure 3 is the 1000 km long arc along the crest of the Himalayan orogen, particularly strong in Nepal. This band appears in both data sets, and corresponds with the northern most of the two bands of high magnitude rainfall described by Anders et al., (2006) and Bookhagen and Burbank, (2006). The large shape parameter and high wet day frequency imply that the northern band of high magnitude rainfall is characterized by low variability rainfall. In contrast, the southern band possesses moderate to high variability along its length. Therefore the two bands of rainfall, while similar in mean intensity of daily rainfall, overall rainfall amount, and topographic setting, differ greatly in the frequency and magnitude of rainfall during the monsoon. This is supported by Bookhagen and Burbank, (2010) who use both the frequency of lightning strikes (a feature of extreme rainfall events) and the intensity of rainfall during extreme events to characterize the magnitude of extreme events and

find a maximum of extreme events along the front of the Himalayan arc, over the southern rainfall band.

2.5.2.1 *Patterns of variability and long-term erosion rates*

The band of low rainfall variability may help to explain the inconsistency between measured long-term erosion rates and rainfall rates in the region. Burbank et al., (2003) and Thiede and Ehlers, (2013) showed that in central Nepal, erosion rates increase north of the band of high magnitude rainfall. It can be seen that mean erosion rate increases even as the mean rainfall rate decreases. Erosion rates peak close to the topographic divide, well north of the highest mean rainfall rates. If the region is in dynamic equilibrium, we expect the erosion rate to be set by the uplift rate rather than climate. However, the specific stream power should still reflect the erosion rate. In this region the specific stream power still decreases northward (albeit more slowly that rainfall) (Burbank et al., 2003). This implies that steeper slopes and narrower channels can make up only partially for the decreasing rainfall. Increasing rainfall variability may explain the rest of the discrepancy between erosion rates and rainfall rates. Figure 7a shows a representative cross section over the topographic divide in this region. The rainfall variability increases rapidly as the mean rainfall rate decreases across the topographic divide, as demonstrated by the observed decrease in the shape parameter and mean wet day frequency. The observed increase in rainfall variability, in conjuction with narrowing channels and steepening slopes, is consistent with a peak erosion rate on the topographic divide despite significantly decreasing mean rainfall rate. As further support for this, both steeper slopes and higher rainfall variability are expected to enhance other important erosion processes, such as landsliding (Gabet et al., 2004).

Increasing rainfall variability means that while the total amount of rainfall decreases sharply across the topographic divide, the size of large storms will decreases more slowly. The solid yellow line in figure 7a and b show the average maximum annual storm size, and it can be seen that it does not track with the mean daily rainfall rate, and does decrease more slowly across the divide. More than that, the east-west striking band of very low variability associated with the northern band of high rainfall results in the large storms in this region being exceptionally small given the high rainfall rate. The ratio of the mean maximum annual storm to the mean daily rainfall rate can be used as another measure of rainfall variability. Shown as the solid red line in figure 7, we see that it is consistent with the measured changes in the shape parameter and mean wet day frequency. It is very low over the northern band of high magnitude rainfall, and highest over the Tibetan plateau. Figure 7c and d show another representative cross section further to the west near the end of the arc of low variability. The same pattern holds for this cross section as well, with increasing variability across the topographic divide, reflected both in the ratio of the maximum annual storm to the daily mean rainfall as well as the shape parameter and wet day frequency. In this cross section, the rise in topography from south to north is gentler, as are the gradients in the erosion rate, mean daily rainfall, mean wet day frequency and the shape parameter.

We put forth the idea of rainfall variability resolving the inconsistency between long-term erosion rate and rainfall rate only as a possibility. The theoretical arguments provide a basis for this theory, and the APHRODITE data support it. However, the way that rainfall drives erosion rates across the landscape is not perfectly understood, so we must restrict ourselves to a qualitative assessment of the patterns of rainfall variability and mean. It is not clear how to asses whether the magnitude of increase in variability

is sufficient to offset the magnitude of decrease in mean rainfall. Additionally, the TMPA data (7b and d) only broadly match the pattern observed in the APHRODITE data set (7a and c). The rise in variability observed in the TMPA data occurs further north than in the APHRODITE data, and is not coincident with the peak in the erosion rate. Further, the TMPA data do not resolve the northern rainfall maximum, making it more difficult to compare the peak in erosion to rainfall. Due to this, in the Nepal swath (7b) the TMPA data do not support the theory that increasing rainfall variability offsets decreasing rainfall mean (though they do in swath 7d). Additionally the elevation is an important parameter in the interpolation scheme of the APHRODITE data, making swath profiles with the APHRODITE data suspect.

One point in support of the theory comes from a data set derived from the TMPA 2B31 data that has much higher spatial resolution that the ones we used here Bookhagen and Burbank, 2006; Bookhagen, 2010; Bookhagen and Burbank, 2010; Olen, Bookhagen, and Strecker, 2016. While we do not have access to the data directly and cannot compute the shape parameter, mean frequency and mean intensity, the data agrees well with our results here. The TMPA derived data resolve the northern peak in rainfall magnitude and, as far as we can tell, low in variability in a very similar location to the APHRODITE data. This lends support to the APHRODITE data. So, while we find the data presented here is suggestive that rainfall variability may be a key parameter influencing the erosion efficiency of rainfall in the Himalayan orogen, we conclude that better data, which may become available in the future, is necessary to confirm or refute this hypothesis.

2.5.2.2 *Patterns of variability and short-term erosion rates*

Olen, Bookhagen, and Strecker, (2016) conducted an analysis of the empirical relationships between vegetation density, precipitation rates and short-term denudation rates in the Himalayan orogen. They find a strikingly clear negative correlation between vegetation density and the variability of measured denudation rates within a single basin. The lower the vegetation density, the higher the variation in measured denudation rates. They point out the logic in this; vegetation tends to stabilize soils, increasing the resistance to erosion. Basins with low vegetation density should be more vulnerable to substantial surface erosion during large rainstorms than those with high vegetation density. The erosion caused by large rainstorms will likely not be evenly distributed across the basin for a variety of reasons including localized high intensity rainfall, non-uniformly distributed vegetation, and different antecedent conditions on different hillslopes. This will lead to more episodic, localized erosion events, and consequently, more variation in denudation rates measured within a single basin or region.

It is also logical that rainfall variability would influence this trend by increasing the size and frequency of large storms in regions with high rainfall variability relative to those with low variability. Olen, Bookhagen, and Strecker, (2016) therefore also compare rainfall variability to denudation variability and vegetation density. However, while they observe vegetation density to increase and denudation variability to decrease from west to east along the strike of the orogen, they find rainfall variability trends in the opposite sense, increasing from west to east. This doesn't match the decrease in denudation variability from west to east, so they conclude that the influence of increasingly dense vegetation towards the east is so strong as to erase any effects of increasing rainfall variability on denudation variability.

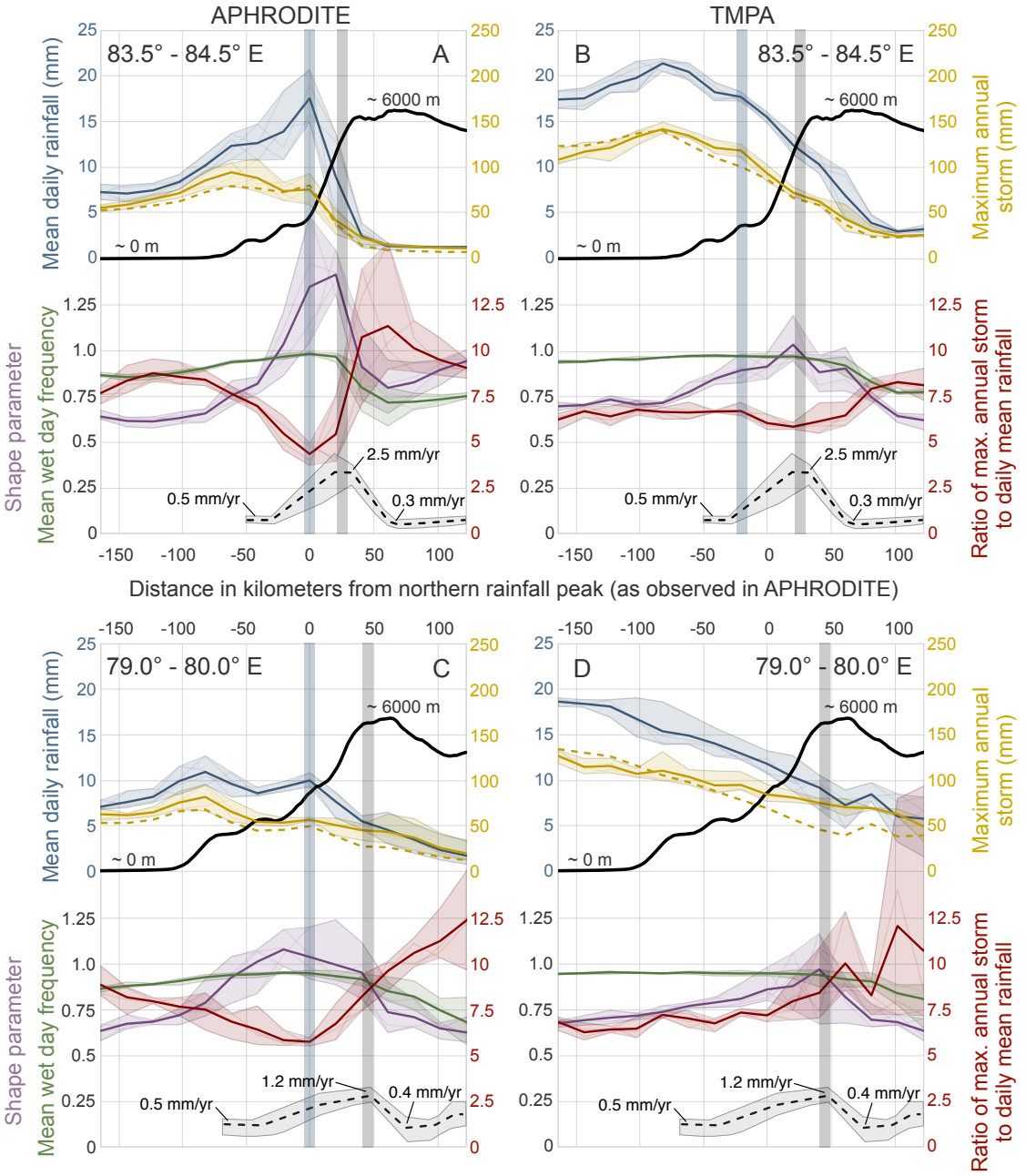

Figure 7: Representative cross sections orthogonal to the strike of the orogen showing the patterns of daily rainfall mean and variability across the topographic divide. Cross sections are aligned relative to the location of the northern rainfall peak. The lines show the average value across the section, and the shaded regions show the range. The mean daily rainfall rate is shown in blue, the mean maximum annual storm is shown in solid yellow, the estimated maximum annual storm is shown in dashed yellow, the ratio of the daily mean to the annual max. storm is shown in red, the gamma shape parameter is shown in purple and the mean wet day frequency is shown in green. Estimated erosion rates over the last 2 million years obtained from a 1D inversion of thermochronological data taken from Thiede and Ehlers, (2013) are are shown with the dashed black line. Average maximum topography shown as solid black line.

While we agree completely with their explanation of how vegetation density and rainfall variability are likely to influence the variation in measured denudation rates, we find that rainfall variability increases along strike from east to west rather than west to east. Olen, Bookhagen, and Strecker, (2016) use the number of times per year that extreme events occur as a measure of variability. Extreme events are defined by them as events above the 90th percentile. Since, by definition, extreme events consist of 10% of observed events, the number of extreme events is more a reflection of the mean wet day frequency than anything else. Although the data sets are not directly comparable because they analyze annual rainfall, and we only consider monsoon rainfall, the spatial pattern of mean wet day frequencies during the monsoon match the number of extreme events per year quite well.

The issue with using the number of events above the 90th percentile as a measure of daily rainfall variability is that there is not a standard relationship between the magnitude of the 90th percentile event and the mean rainfall intensity. This is in fact determined by the shape parameter of the distribution and varies from region to region. Figure 8 shows the mean magnitude of events above the 90th percentile as a function of the shape parameter. As gamma falls below one, the average magnitude of extreme events approaches ten times the mean rainfall intensity, but above one, it is only about 2-3 times the mean. Therefore, right where they find the most frequent extreme events, in central Nepal, is where those extreme events will be the smallest. This is an important point, because from the perspective of geomorphology it is not just the frequency of big storms that is important, but also their magnitude. The shape parameter and mean wet day frequency can be used to measure the magnitude of these big storms relative to the mean rainfall intensity in an unbiased way that allows for comparison between regions with significantly different mean rainfall intensities (such as central Nepal and the Tibetan plateau).

As figure 6 shows, these measures of variability point to an increase in varability from the east to the west and from the south to the north of the orogen. This is more consistent with the patterns of denudation variability and vegetation density observed by Olen, Bookhagen, and Strecker, (2016). Moving along the orogen from east to west, the mean annual rainfall drops, as does the mean rainfall intensity and the vegetation density. At the same time the variability of rainfall and the variability in denudation increase. As figure 6c shows, the maximum annual storm magnitude does not change along strike for most elevations, because of increasing rainfall variability. As a result, large storms become more extreme relative the mean rainfall intensity. It is unsurprising that the most episodic erosion is observed in the west. However, whether the denudation variability increases to the west because of increasingly significant large storms, or because of decreasing vegetation density or both is less clear.

2.6 CONCLUSIONS

In this study we have made a careful characterization of the distribution of rainfall in the Himalayan orogen. We find a consistent pattern appearing with the gamma shape parameter, mean wet day frequency and mean rainfall intensity in many places along the Himalayan arc, particularly in Nepal. We observe moderate rainfall variability in the foreland basin up to and including the southern band of high magnitude rainfall. This is where the biggest storms are taking place during the monsoon as the moist air coming from the bay of Bengal collides with the first rapid rise in topography and relief

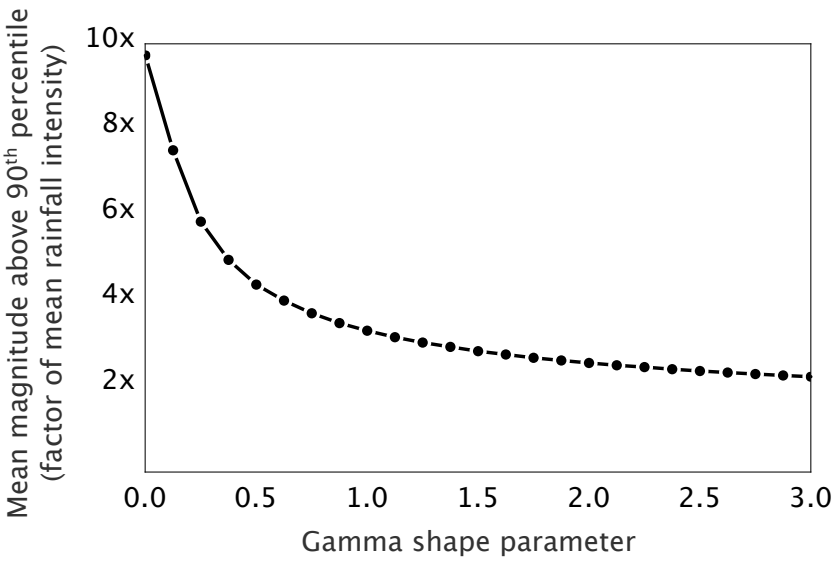

Figure 8: The change in the mean magnitude of daily rainfall above the 90th percentile as a function of the shape parameter. When the shape parameter is less than 0.5, the average intensity of storms above the 90th percentile is 5 to 10 times the mean rainfall intensity. For shape parameters above one, the it is only about two times the mean rainfall intensity.

(Bookhagen and Burbank, 2006). Although a significant amount of moisture makes it past the initial mountain front to collide with the second steep rise in topography and relief near the topographic divide and form the northern band of high magnitude rainfall, the storms there are not as intense. Instead a more frequent, more moderate rainfall regime is observed. This is reflected in the rainfall variability which begins to drop rapidly starting at the southern band moving north, and reaches a low right at or directly north of the northern band. Further into the orogen from the northern band, mean rainfall amount decreases rapidly while variability increases due to both the mean wet day frequency and the shape parameter. In general the plateau directly behind the mountains possesses moderate to high rainfall variability. Similarly, while the mean monsoonal rainfall amount and intensity decrease along strike from east to west, the rainfall variability increases. As a result, the magnitude of moderate to large storms remains constant along the strike of the orogen above 500 m elevation. These two trends point to monsoonal rainfall having a larger geomorphic impact in the north and the west of the orogen than the mean rainfall intensity and amount suggest. This demonstrates the potential importance of rainfall variability in understanding the relationship between erosion and climate.

2.7 ACKNOWLEDGEMENTS

The APHRODITE and TMPA data sets used in this study are freely available at
http://www.chikyu.ac.jp/precip/index.html and
http://TMPA.gsfc.nasa.gov/data_dir/data.html respectively.

3

RAINFALL, HYDROLOGY AND FLUVIAL EROSION EFFICIENCY

3.1 ABSTRACT

As a result of the postulated influence of climate on landscape morphology and tectonic deformation rates, the erosional response of mountainous bedrock rivers to changes in climatic forcing has been the subject of intense research. However, due to the challenges in upscaling daily climatic forcing to geological time, physically realistic models describing how rainfall drives fluvial erosion are lacking. We derive a theoretical framework for long-term fluvial erosion rates driven by realistic climate by integrating an established stochastic-mechanistic model of hydrology into a threshold-stochastic formulation of stream power. The hydrological theory provides equations for the daily streamflow distribution and variability as a function of climatic boundary conditions that are applicable across most of the observed range of streamflow regimes on Earth. The new parameters introduced are rooted firmly in established climatic and hydrological theory and are easily measured. We predict how fluvial erosion rates respond to changes in realistic climatic forcing, observing an anti-correlation between streamflow mean and variability, peak erosion rates for moderate climatic conditions, and an insensitivity to increasing mean streamflow above a certain point in many cases. We find that hydrological processes can have a significant influence on how erosive a particular climatic forcing will be. Based on the generally unaccounted for role of hydrology, we conclude that the failure to find a clear dependence of long-term erosion rates on rainfall rates or steepness indices does not exclude the possibility that climate is an important control on erosion rates and landscape evolution.

3.2 INTRODUCTION

Rivers play an important role in shaping Earth's surface, especially in high relief, mountain environments; they have become a major focus of research in quantitative geomorphology (e.g. Whipple, Kirby, and Brocklehurst, 1999; Whipple, 2009; Tucker and Hancock, 2010b), because they are one of the main links between climate and erosion. (e.g. Whipple and Tucker, 1999; Tucker and Bras, 2000; Crave and Davy, 2001; Burbank et al., 2003; DiBiase et al., 2010; DiBiase and Whipple, 2011; Lague, 2014). Mountainous bedrock rivers control landscape evolution in unglaciated mountain environments by steepening hill slopes through bedrock incision and transporting the resulting debris away. In doing so, they not only set the relief structure of a mountain, but also communicate tectonic signals throughout the landscape (Whipple, Kirby, and Brocklehurst, 1999; Whipple, 2009). All of this is accomplished ultimately by the ability of flowing water to transport sediment. Therefore it is natural to conclude that climate, or more specifically, rainfall plays an important role in landscape evolution as the main source of river water. Gilbert, (1877) pointed this out more than 140 years ago. In the intervening time there have been a myriad of theoretical models postulating, and sometimes demonstrating, that climate should play an integral part in determining the form and rate of change of Earth's surface. Some consider climate specifically in the context of a

landscape dominated by fluvial erosion (e.g. Beaumont, Fullsack, and Hamilton, 1992; Whipple, Kirby, and Brocklehurst, 1999; Roe, Montgomery, and Hallet, 2002), and others in a more general sense (e.g. Dahlen and Suppe, 1988; Willett, 1999; Whipple and Meade, 2006).

Despite theoretical predictions and the obvious influence of rainfall on erosion processes at the local scale, many studies attempting to relate mean rainfall rates or stream power to erosion rates struggle to find a functional relationship across a range of spatial and temporal scales (e.g. Riebe et al., 2001b; Burbank et al., 2003; Blanckenburg, 2005; Bermudez, van der Beek, and Bernet, 2012; Godard et al., 2014; Acosta et al., 2015). However, a few studies that carefully consider factors that may obscur the relationship between rainfall and erosion rates find a clearer relationship (e.g. Moon et al., 2011; Ferrier, Huppert, and Perron, 2013). This suggests that when the major confounding factors can be tightly controlled, a relationship between climate and erosion is likely to emerge. In a fluvially dominated landscape, a non-comprehensive list of these factors includes spatially varying rock type and uplift rate, the nature of the dominant erosion process(es), erosion thresholds, the intensity and frequency of big storms, the type amount and influence of vegetation, sediment supply and transport dynamics, channel form, as well as perhaps other as yet unidentified factors. In order to implement a landscape evolution model that incorporates realistic climatic forcing, these confounding factors must be elucidated and accounted, and their potential effect on erosional efficiency must be quantified.

Understanding the specifics of how climate controls fluvial erosion is a key part of understanding how the tectonic history is encoded in a landscape (Whipple, 2009), and could potentially influence the interpretation of sedimentary records (e.g. Armitage et al., 2011). The pace of erosion set by the balance between climatic and tectonic forcing in a landscape also has implications for the rate of weathering, CO_2 draw down and carbon burial that can effect the global climate (e.g. Raymo and Ruddiman, 1992; Galy et al., 2007). Therefore, in order to untangle the past and future joint evolution of the lithosphere, atmosphere and hydrosphere, it is critical to understand the role of climate, especially the effect of a changing climate, on landscape evolution.

A major difficulty with understanding the impact of climate is the large disparity in timescales. Rainfall rates are measured over hours or days, landscape evolution over millennia (Tucker and Bras, 2000). Another major difficulty with understanding the impact of climate on erosion processes is the ecological and hydrological response to climatic forcing, which is complex and time dependent, and can have unexpected results (Istanbulluoglu, 2009). It is a challenge to establish geomorphic transport laws that capture the net effects of this complexity over the relevant ranges of spatial and temporal scales in a quantifiable way. Initial attempts used a parameterized effective streamflow that was assumed to capture the average effect of sediment laden water flowing over bedrock (Wolman and Miller, 1960; Beaumont, Fullsack, and Hamilton, 1992; Tucker and Slingerland, 1994). It has since been shown that this does not work well in detachment limited rivers due to the existence of erosion thresholds and potential nonlinearities between streamflow and erosion (Tucker and Bras, 2000; Snyder et al., 2003; Lague, Hovius, and Davy, 2005). An erosion threshold represents the existence of a minimum forcing, usually shear stress, that is required before erosion takes place. The effect of an erosion threshold has been investigated for overland flow on vegetated slopes (Horton, 1945), channel initiation (e.g. Dietrich et al., 1993; Prosser and Dietrich, 1995), sediment entrainment in rivers (e.g. Wolman and Miller, 1960),

and fluvial erosion of gravel bed and bedrock rivers (e.g Tucker and Bras, 2000; Lague, Hovius, and Davy, 2005; Beer and Turowski, 2015).

Stochastic methods are well suited to the task of understanding the long-term effect of nonlinear time and state dependent processes operating over short timescales, and thus ideal for problems such as these. Pioneering efforts by Tucker and Bras, (2000), Crave and Davy, (2001) and Lague, Hovius, and Davy, (2005) using stochastic rainfall forcing and/or the full distribution of streamflow quantitatively established the advantages of using a threshold-stochastic approach rather than a constant streamflow one. They established a theoretical basis for streamflow variability, a concept long considered important (e.g. Wolman and Miller, 1960), permanently changed the perspective on bedrock river erosion and set the stage for other important work to follow (e.g. Molnar, 2001; Snyder et al., 2003; Collins, Bras, and Tucker, 2004; Tucker, 2004; Istanbulluoglu and Bras, 2005, 2006b; Molnar et al., 2006; DiBiase and Whipple, 2011; Carretier et al., 2013; Lague, 2014; Phillips and Jerolmack, 2016; Rossi, Whipple, and Vivoni, 2016).

However, one of the key features missing from these original works is a realistic description of hydrology. Tucker and Bras, (2000), Crave and Davy, (2001) and Tucker, (2004) use a very simplified model for hydrology which is only applicable in very small catchments. Lague, Hovius, and Davy, (2005) use a distribution of daily streamflow known to result from natural hydrological systems, but do not include any model for hydrology itself. A few other studies include stochastic rainfall forcing in conjunction with a hydrological model, but many use a simplified model for hydrology similar to Tucker and Bras, (2000) (e.g. Collins, Bras, and Tucker, 2004; Istanbulluoglu and Bras, 2006b). Ijjász-Vásquez, Bras, and Moglen, (1992) develop a clever way to integrate stochastic rainfall into a hydrological and landscape evolution model, but the hydrological model used is a constant streamflow one. Huang and Niemann, (2006b, 2008) present a landscape evolution model with a sophisticated hydrological model. However, the hydrological model requires very short time steps that make the model slow to run (runtimes measured in weeks).

It would be acceptable to ignore hydrology if it had only second order influence on the distribution of daily streamflow. However, this is not the case. Hydrological and ecological processes have first order importance in determining the fluvial response to a particular climatic forcing (Rodriguez-Iturbe, 2000; Huang and Niemann, 2008; Istanbulluoglu, 2009). For example, they are often responsible for producing heavy tailed daily streamflow distributions from light tailed daily rainfall distributions (Basso, Schirmer, and Botter, 2015; Rossi, Whipple, and Vivoni, 2016), which has important implications for fluvial erosion. Therefore, in order to build a landscape evolution model with realistic climatic forcing, hydrology and to some extent ecology must be accounted for. However, realism and accuracy must be balanced with computational efficiency. A landscape evolution model that requires time steps on the order of hours or days to keep track of ecological and hydrological processes will be prohibitively slow when the timescales of interest are millions of years.

To that end, we have integrated a stochastic-mechanistic model of hydrology (Botter et al., 2007, 2009) which has been demonstrated to work well across a range of landscapes and climates (e.g. Botter et al., 2010; Ceola et al., 2010; Schaefli, Rinaldo, and Botter, 2013; Basso, Schirmer, and Botter, 2015; Doulatyari et al., 2015) into the threshold-stochastic stream power formulation of Lague, Hovius, and Davy, (2005). By using a stochastic approach, we develop analytical solutions that describe the net effect

of daily climatic, hydrological and ecological processes over long periods. In this way, key thresholds and nonlinearities can be accounted for with a minimum loss of efficiency. We used the hydrological theory, which incorporates water related ecological processes, to establish equations for the daily streamflow distribution and streamflow variability that are applicable across most of the observed range of streamflow regimes on Earth. The model shows how the distributions of daily streamflow arise from the climatic and ecohydrological (hydrology plus water related ecological processes) conditions in a river basin. The new climatic and ecohydrological parameters introduced are rooted firmly in established hydrological theories and can be measured from hydrographs and weather station data.

Our equations for the daily streamflow distribution eliminate the problem of choosing which probability distribution function (pdf) to use (e.g. exponential or power law tail) (DiBiase and Whipple, 2011; Rossi, Whipple, and Vivoni, 2016) and unite previous geomorphological theory on stochastic-threshold stream power erosion into a single framework. We also describe a general coefficient of daily streamflow variability with a firm physical basis and provide a theoretical foundation for the long observed negative correlation between mean daily streamflow magnitude and variability. Using the coefficient of variability and the negative correlation between streamflow mean and variability we reproduce previous work on the role of the mean and variability in setting the long-term erosion rate (Tucker and Bras, 2000; Tucker, 2004; Lague, Hovius, and Davy, 2005; DiBiase and Whipple, 2011), but in a more general framework and related it explicitly to the climatic forcing and ecohydrological setting. We found that ecohydrological processes (water storage in the soil layer and evapotranspiration) and the fundamental hydrological response time of river basins can have a significant influence on how erosive a particular climatic forcing will be. Combined with the already established role of streamflow variability in determining the erosiveness of a river, the work we present here leads to the prediction that care must be taken to evidence trends between mean rainfall rates or mean streamflow rates and long-term erosion rates due to the complexity of the ecohydrological and fluvial response to climatic forcing.

3.3 THE (ECO)HYDROLOGICAL MODEL

The fluvial erosion model presented in this work is an extension of the physically based stochastic hydrology and soil moisture model laid out in Botter et al., (2007) and Botter et al., (2009). In the following sections we briefly go over the key aspects of the stochastic hydrology model and then describe our extension to fluvial erosion.

3.3.1 *Rainfall*

Daily rainfall is modelled after Rodriguez-Iturbe et al., 1999 as a marked poisson process of rate λ [T^{-1}]. The sub-daily temporal structure of individual storms is not considered. The depths of daily rainfall are considered to be independent and identically distributed random variables, p, described by an exponential pdf,

$$f_P(p) = \frac{1}{\alpha} e^{-p/\alpha}, \tag{5}$$

where α is the specific mean daily rainfall amount on days with rainfall - i.e., the volume of rainfall divided by the catchment area [L] - from now on referred to as

the mean storm depth. We follow this practice for all variables which are measured as volumes integrated over a river catchment. It is worth noting, however, that the specific storm depth, α, is not necessarily the same as the mean storm depth that would be measured at a point. There are often scaling effects that can cause the point-scale value and the catchment-scale specific value to differ. In the case of rainfall, for α to be equal to the point-scale storm depth requires uniform rainfall across the catchment, which is usually not the case. Thus, in general, and for the majority of parameters discussed in this work, the point-scale value and the catchment-scale specific value will differ. The rate of the poisson process λ can be interpreted as the mean frequency with which rainfall occurs, thus we refer to it as the mean storm frequency. The specific mean daily rainfall rate is the product of the mean storm depth and the mean storm frequency, $\bar{p} = \alpha\lambda$ (Rodriguez-Iturbe, Cox, and Isham, 1987).

There are some potential issues with using the exponential distribution to represent daily rainfall depths, which we address at the end of the discussion. Regardless, the exponential distribution for daily rainfall depths has been applied with great success in hydrology and ecohydrology, particularly for the characterization of daily soil moisture and streamflow dynamics (e.g. Milly, 1993; Rodriguez-Iturbe et al., 1999; Laio et al., 2001; Porporato, Daly, and Rodriguez-Iturbe, 2004; Settin et al., 2007; Botter et al., 2010; Ceola et al., 2010; Tamea et al., 2010; Müller, Dralle, and Thompson, 2014; Park et al., 2014; Basso, Schirmer, and Botter, 2015; Doulatyari et al., 2015).

3.3.2 *Soil moisture*

Soil moisture has come to be recognized as a vital ecological and hydrological feature of river basins (Rodriguez-Iturbe, 2000), influencing the river response to storm events (Rodríguez-Iturbe et al., 2006). The processes involved in determining the daily soil moisture state are numerous and complex, including rainfall, evapotranspiration, surface runoff and runon, subsurface flow, and leakage to deeper water reservoirs.

After Botter et al., (2007), we model the effect of these processes on daily streamflow with a physics based model of soil moisture first developed by Rodriguez-Iturbe et al., (1999). For simplicity, we refer to the hydrologically active layer, or the layer of soil that is affected by rainfall and evapotranspiration processes at a daily timescale as the soil layer. The soil layer acts as a reservoir that is filled by random rainfall inputs. Each rainfall event of depth p replenishes the soil layer which has capacity $n_s Z_r$ (where n_s is soil porosity and Z_r the active or rooting depth) until a critical threshold $s = s_1$ is reached, after which the soil layer is saturated, and any additional rainfall recharges the catchment-scale excess water storage and eventually becomes streamflow. In between rainfall events, the soil moisture is reduced by evapotranspiration, which is considered to be nonexistent below the wilting point $s = s_w$ and increases linearly with increasing soil moisture up to a maximum rate of E_{max}. E_{max} depends on available energy for vaporization as well as the abundance and kind of vegetation present. Since the soil moisture can only range from s_w to s_1, the dynamic soil moisture capacity is $s_o = (s_1 - s_w) n_s Z_r$. For a more in depth description, see the Laio et al., (2001) or Porporato, Daly, and Rodriguez-Iturbe, (2004).

This model captures one of the key roles of ecohydrology in determining daily streamflow, which is that the soil layer acts as a buffer to incoming rainfall, and allows for the intervention of ecological processes in the form of evapotranspiration. The presence of a soil moisture threshold that needs to be exceeded before significant

runoff and infiltration processes occur means that the buffer effect is more dramatic for small storms than large storms. This reduces the frequency of streamflow producing storms (referred to from now on as effective storms) relative to the frequency of rainfall events, which in turn reduces the mean streamflow rate relative to the mean rainfall rate. Calculating the mean frequency of effective storms is challenging because the storm depth required to exceed the soil moisture threshold depends on the antecedent soil moisture state, which is time dependent. It has been shown by Porporato, Daly, and Rodriguez-Iturbe, (2004) to be $\omega\lambda$ where ω is a nondimensional filtering factor that is a complex function of ecohydrology and climate,

$$\omega = \frac{\phi\, h_s^{h_s/\phi} e^{-h_s}}{h_s \Gamma(h_s/\phi)\gamma(h_s/\phi, h_s)} \tag{6}$$

where $\Gamma(\cdot)$ is the gamma function, $\gamma(\cdot,\cdot)$ is the regularized lower incomplete gamma function, ϕ is the aridity index and h_s is the effective soil depth. The effective soil depth is the dynamic soil layer water storage capacity divided by the average storm depth, $h_s = s_o/\alpha$ and the aridity index is the ratio of the potential evapotranspiration rate to the mean rainfall rate ($\phi = ET_{max}/\bar{p}$). We refer to ω as the streamflow ratio.

In the following sections, the effects of the soil layer (storage and evapotranspiration) on incoming rainfall are captured by ω. The relevant parameters of the soil moisture model are the dynamic soil storage, s_o, and the maximum evapotranspiration rate, ET_{max}, which express the influence of the soil layer conditions on the streamflow ratio. Despite its simplicity and low dimensionality, this minimalist mechanistic-stochastic model has seen wide application and success in predicting probability distributions of catchment-scale daily soil moisture and streamflow (e.g. Laio et al., 2001; Porporato et al., 2002; Porporato, Daly, and Rodriguez-Iturbe, 2004; Rodríguez-Iturbe et al., 2006; Settin et al., 2007; Doulatyari et al., 2015; Feng, Porporato, and Rodriguez-Iturbe, 2015).

3.3.3 *Catchment-scale water balance and the streamflow ratio*

Here we consider a simplified mean catchment-scale water balance at steady state that can be written as,

$$\frac{\langle ET \rangle}{\langle P \rangle} + \frac{\langle Q \rangle}{\langle P \rangle} = 1 \tag{7}$$

where $\langle P \rangle = \bar{p}A$ is the mean rainfall rate (A is catchment area), $\langle ET \rangle$ is the mean loss to evapotranspiration, and $\langle Q \rangle$ is the mean drainage rate to the catchment-scale storage caused when the soil moisture threshold is exceeded. The fraction of rainfall lost directly to the atmosphere as evapotranspiration does not contribute to streamflow, whereas the fraction of water drained to the catchment-scale storage must leave the catchment as streamflow. Therefore $\langle Q \rangle$ also represents the mean daily streamflow. $\langle Q \rangle$ is the product of the mean frequency of effective storms, $\omega\lambda$ and the mean storm depth. Therefore, the fraction of incoming rainfall that is partitioned into streamflow is described by ω,

$$\frac{\langle Q \rangle}{\langle P \rangle} = \frac{\alpha\omega\lambda A}{\alpha\lambda A} = \omega, \tag{8}$$

and the specific mean daily streamflow is simply,

$$\mu = \alpha\omega\lambda = \omega\bar{p}. \tag{9}$$

As seen in equation 6, the streamflow ratio is controlled by the effective soil depth and the aridity index, two nondimensional numbers that describe the interaction of climate and ecohydrology. The effective soil depth is a measure of how easily a single storm can saturate the soil layer. When h_s is small, the average storm can easily saturate the soil, putting the catchment into the thin soil regime. When h_s is large, the soil is saturated only by big, rare storms, and the catchment is in the thick soil regime.

The aridity index is a measure of the drying power of a catchment. The larger ϕ is the larger the losses to evapotranspiration relative to the volume of incoming rainfall. Although there is always a probability for a storm to occur while the soil layer is still wet from a previous storm, the larger that ϕ is the more unlikely this is to occur because the soil layer dries rapidly. We refer to the case where ϕ is greater than one as the dry soil regime. When ϕ is less than one, the opposite is true; rainfall onto a wet soil layer will be common and the catchment is in the wet soil regime. A storm is more likely to exceed the soil moisture threshold and produce streamflow if the soil layer is already wet. Therefore the aridity index influences the ability of a storm to drive streamflow, which has implications for the partitioning of incoming rainfall.

These two numbers, ϕ and h_s, define four different soil moisture regimes that are determined by climate and catchment soil properties as shown in figure 9. When ϕ is greater than one, the catchment is in the dry soil regime, and the main control on ω, the streamflow ratio, is the effective soil depth. This divides the dry soil regime further into the thick dry soil regime and the thin dry soil regime, depending on whether h_s is less than or greater than one. When $h_s > 1$, the catchment is in the thick dry soil regime, ω is very small, and the transformation of rainfall to streamflow is dramatically impacted by ecohydrology. The effectively thick dry soil layer acts as a buffer on incoming storms, absorbing small to moderate storms, and releasing the water from these storms back to the atmosphere through evapotranspiration. As a result both the mean streamflow μ and the effective storm frequency are strongly reduced. When $h_s < 1$ the impact on the mean streamflow and storm frequency are less dramatic because moderate and even small storms can saturate the soil layer, and the role of evapotranspiration is downplayed due to the small soil moisture storage capacity.

When ϕ is less than one, the catchment is in the wet soil regime. As before, the wet soil regime is further impacted by the effective soil depth. When $h_s > 1$ the catchment is in the thick wet soil regime and the main control on the streamflow ratio ω is the aridity index ϕ. Although the soil layer is effectively thick, the slow drying rate means that storms will often occur over wet antecedent conditions. This means that even small storms normally incapable of saturating the soil layer may push an already wet soil layer over the threshold and produce a streamflow event. For this reason the thick wet soil layer can behave similarly to the thin dry soil layer, though the important control is ϕ rather than h_s. When ϕ and h_s are both less than one the catchment is in the thin wet soil regime and the highest transmission rates of rainfall to streamflow occur. Most storms are able to saturate the soil layer and produce a streamflow event, and both ϕ and h_s are important in setting the streamflow ratio.

3.3.4 *Daily streamflow*

3.3.4.1 *Streamflow variability*

The hydrological model makes the common assumption that excess storage in the catchment (W) is released as river streamflow (q) according to a power law relationship

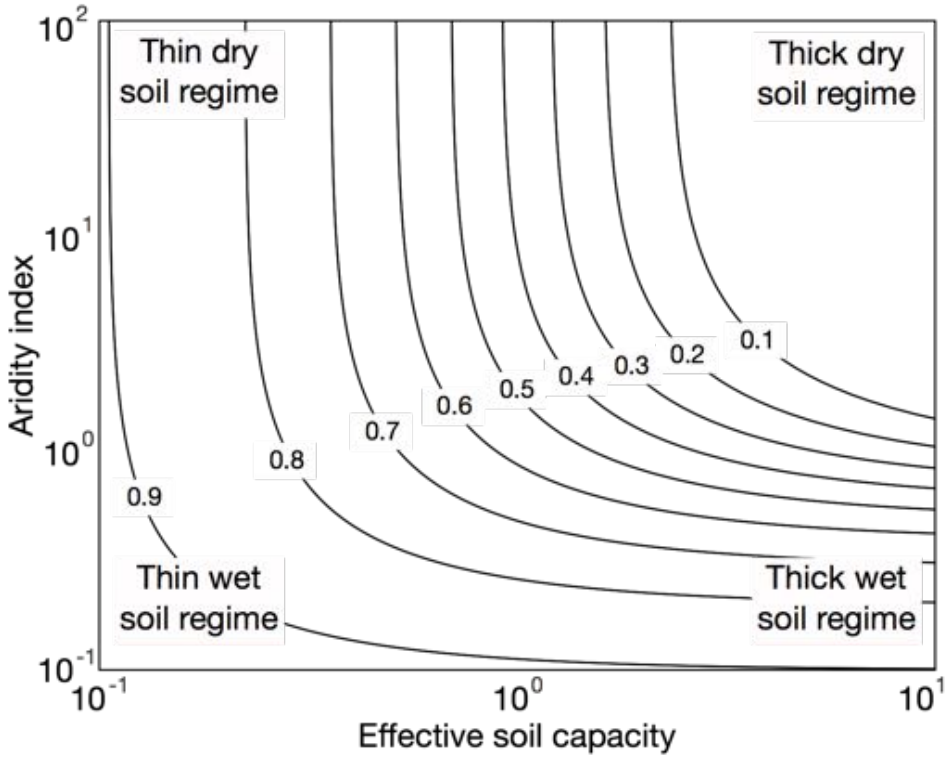

Figure 9: The four water balance soil regimes. The contours denote the value of the streamflow ratio ω as a function of the aridity index ϕ and the effective soil capacity h_s.

($q = cW^d$) e.g. Botter et al., 2009; Kirchner, 2009; Basso et al., 2015. This results in the time rate change of streamflow being governed by,

$$\frac{dq}{dt} = -aq^b + \xi_r, \tag{10}$$

where q is the (specific) daily streamflow, ξ_r is the stochastic effective rainfall forcing, and a and b are the recession coefficient and the recession exponent, respectively. Botter et al., (2007) show that the effective rainfall forcing ξ_r can be well approximated by a poisson process with the same distribution of depths as rainfall, but a lower rate that is modulated by the streamflow ratio, such that the rate is equal to the effective storm frequency ($\omega\lambda$).

It has been shown that the variability of streamflow is important for long-term landscape evolution e.g. Tucker and Bras, 2000; Tucker, 2004; Lague, Hovius, and Davy, 2005; DiBiase and Whipple, 2011; Lague, 2014. Therefore we are not only interested in how the mean daily streamflow arises out of climatic forcing and ecohydrological response, but also the variability of daily streamflow. Daily streamflow variability refers how often and by how much the daily streamflow strays from the mean, and can be measured in many ways. In the context of landscape evolution we are concerned in particular with the frequency and magnitude of streamflow events significantly larger than the mean - floods. In distributions of daily streamflow, this manifests itself in the shape of the right hand tail of the distribution, which can be described as being light or heavy. When the tail is heavy, the probability of observing very large floods is higher than when the tail is light. If the tail follows an exponential form it is considered light, if it instead follows a power law form, it is considered heavy. The nature of the tail can easily be observed in a log-log plot of the probability density function or probability of

exceedence (one minus the cumulative density function). In what is a slight abuse of the terminology, we refer subsequently to the tail heaviness as a measure of the daily streamflow variability. The heavier the tail, the more variable the daily streamflow is. Figure 33 shows two hydrographs and their associated pdfs, including a log-log inset to show the heaviness of the tail. The hydrograph in 33a is from a river with high variability, and the hydrograph in 33b from one with low variability. This can be seen from the hydrograph directly, as well as in the heaviness of the tail of the distributions.

If we idealize hydrographs as being made up of storm impulses followed by streamflow recessions that last until the next impulse we can understand the controls on the variability of daily streamflow. In this idealized case, the variability is controlled by the time it takes for the river basin to relax from its initial excited state directly after a storm impulse and by the frequency of those storm impulses. If a river basin relaxes quickly relative to the time between storms then the recessions will be long, spanning a large range of daily streamflows. The river will spend some time well above the mean and a lot of time well below the mean, such as in figure 33a. If, in contrast, the relaxation time is slow and the storm impulses frequent, there will be few long recessions. The daily streamflow magnitude will hover more closely around the mean, leading to low streamflow variability as in figure 33b.

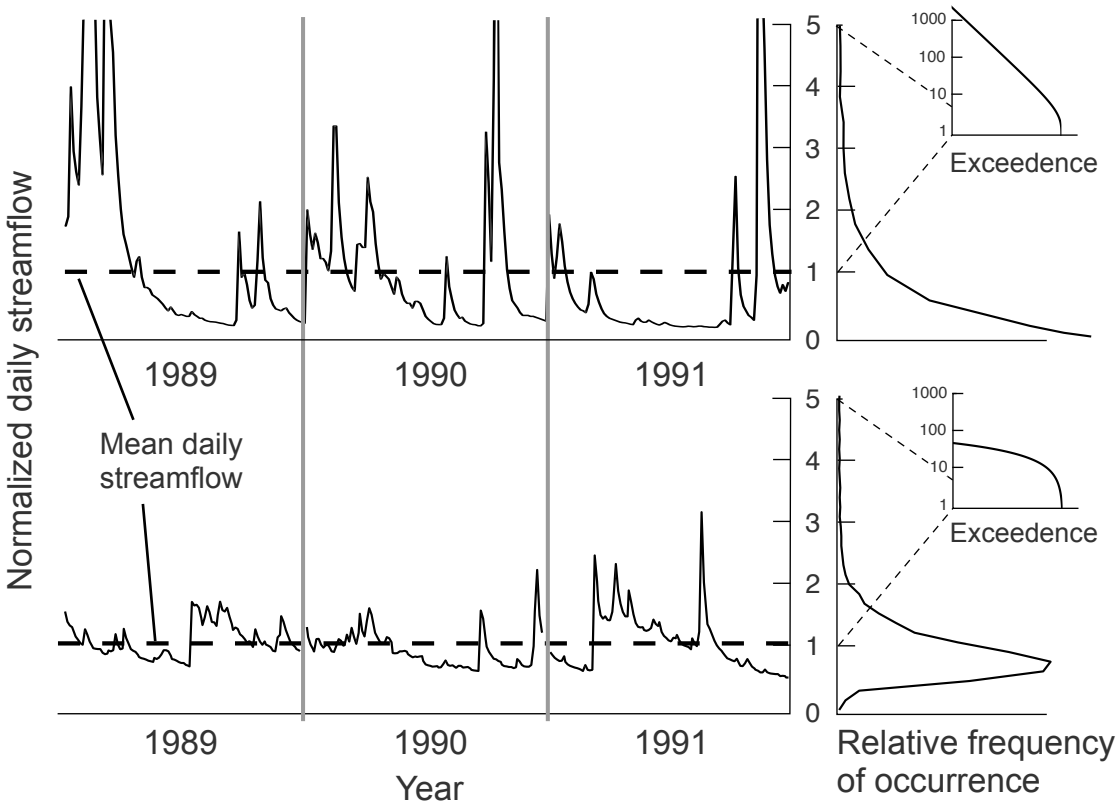

Figure 10: Figure adapted from Botter et al. 2013. Streamflow time series from a high variability river (a) and a low variability river (b) are shown along with the associated distributions. The high variability in (a) can be attributed to the fast recessions which can discharge the large storm impulses before the next storm.

3.3.4.2 *The recession exponent*

In this model we will assume that the first control on daily streamflow variability, the mean time between storms, is described by the mean effective storm frequency ($\tau_{storm} = 1/\omega\lambda$). Therefore in order to fully determine the streamflow variability it is only necessary to understand what controls the rate of the streamflow recession. Within the framework of equation 10, the recession exponent b determines in part the response of a river basin to a single storm impulse by dictating the shape of the recession curve. When b is one, the recession follows a decreasing exponential function of time. When b is greater than one, the response of the basin to an impulse is more dramatic, with a faster drop from the initial high streamflow state to a slower decay at very low streamflows. This means that for higher values of b, the peak of the storm impulse is larger relative to the mean. This leads to a heavier tailed distribution of daily streamflow.

While there are some theories as to precisely what determines b in a river basin (e.g. Rupp and Selker, 2006; Harman, Sivapalan, and Kumar, 2009; Biswal and Marani, 2010), there is not yet a general consensus (Harman, Sivapalan, and Kumar, 2009; Chen and Krajewski, 2016). Empirical data sets show that it is likely influenced by climate (Berghuijs et al., 2014), ecohydrology (Szilagyi, Gribovszki, and Kalicz, 2007), land use (Bogaart, Lyon, and Dekker, 2016) and basin geology/geomorphology (Tague and Grant, 2004). For now we consider b to be an externally defined parameter. Despite uncertainties due to different approaches used for fitting b (Chen and Krajewski, 2016), empirical distributions from bulk analysis (rather than individual recessions) point to values which mostly fall between 0.5 and 2.5, with values above 3.5 rare (Ye et al., 2014; Berghuijs, Hartmann, and Woods, 2016; Bogaart, Lyon, and Dekker, 2016), an example of this is shown in figure 11.

3.3.4.3 *Characteristic response time*

The recession exponent b is only part of what determines the streamflow recession. River basins with the same value of b can still exhibit different recession times. This is because there exists a characteristic timescale for the catchment's hydrological response to a storm impulse independent of the shape of the recession set by b. This timescale captures important catchment wide hydrological features such as catchment morphology and aspect ratio, average hydrological pathway length and conductivity, etc. (Botter et al., 2013). Here we refer to this timescale as τ. If, for a given value of b, the mean time τ_{storm} between effective storms is small compared to the characteristic time τ associated with the time for a storm pulse to leave the basin, the supply of water to the river will be relatively consistent, and the daily streamflow will stay close to the mean daily streamflow. This will yield a streamflow regime with low variability. On the other hand if the time it takes for the river basin to drain a storm pulse is small relative to the effective interstorm period, then the river streamflow will often be well below the mean, with infrequent but significant deviations well above the mean. This will yield a streamflow regime with high variability.

To take this into account we define the coefficient of daily streamflow variability ν. It is a nondimensional ratio of the timescale of the hydrological response to the effective interstorm period, and is known to be a robust description of the streamflow variability in the case $b = 1$ (Botter et al., 2013). Here we extend it to all values of b.

$$\nu = \frac{\tau_{storm}}{\tau} = (\omega\lambda\tau)^{-1}. \tag{11}$$

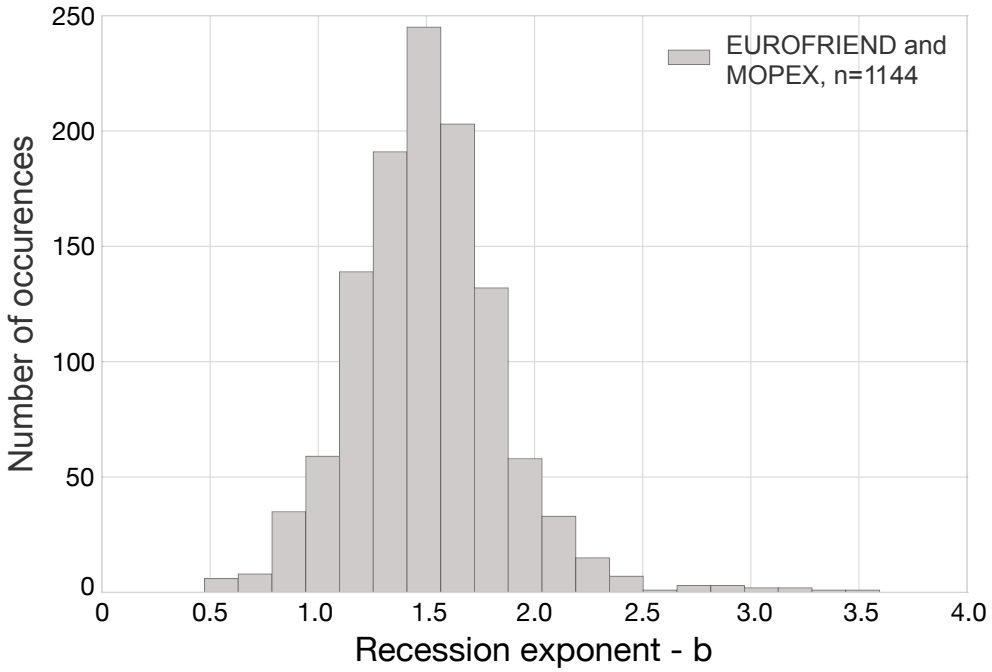

Figure 11: Observed distribution of b from 1144 rivers, 725 in Europe (Berghuijs, Hartmann, and Woods, 2016) and 419 in the US [Berghuijs, personal communication]. The values of b are well distributed around 1.5, with the majority falling between 1 and 2.

We are left then with defining a formal measure of the characteristic response time τ. We can extract this timescale from the recession coefficient a. Dralle, Karst, and Thompson, (2015) point out that due to the scaleless nature of the power law describing streamflow recessions (equation 10), a will exhibit an artificial correlation with b. They show that there exists a decorrelated recession coefficient $\hat{a}$ such that $\hat{a} = aq_o^{b-1}$, where q_o is a scaling factor that is basin specific. Here we use the mean daily streamflow μ as a proxy for q_o. Though not perfect, there is some preliminary evidence that this is not a poor choice [Berguijs, personal communication] and (Dralle, Karst, and Thompson, 2015). This defines a new recession coefficient $\hat{a}$ with units of $[T^{-1}]$. The characteristic timescale for the streamflow recession is then defined as $\tau = 1/\hat{a}$.

3.3.4.4 *Distributions of daily streamflow*

Given the known probability distributions of the magnitudes of climatic forcing (rainfall) and antecedent conditions (soil moisture state) as well as the hydrological response (as parameterized by b, ν and μ and described by equation 10) for a given catchment, we can now derive the probability distribution of the magnitudes of daily streamflow. Depending on the value of b, this leads us to three different solutions for the distribution of daily streamflow in terms of ecohydroclimatic parameters. For the case $b = 1$, (Botter et al., 2007) showed that the streamflow distribution is a gamma distribution with shape parameter k and scale parameter k/μ shown here in nondimensional form,

$$f_{Q_*}(q_*) = \frac{k^k}{\Gamma(k)} q_*^{k-1} \exp[-kq_*], \tag{12}$$

where $q_* = q/\mu$ is the nondimensional daily streamflow, and $k = \omega\lambda\tau$ contains the climatic and ecohydrological parameters. For the second solution we present a newly derived distribution of streamflow for the case $b = 2$ that is an inverse gamma distribution with shape parameter $k+1$ and scale parameter $k\mu$ (derivation in appendix A),

$$f_{Q_*}(q_*) = \frac{k^k}{\Gamma(k)} q_*^{-k-2} \exp\left[-kq_*^{-1}\right] \tag{13}$$

This distribution has a power law tail, meaning that it has a much heavier tail relative to the gamma distribution found for $b = 1$. The general solution for the case that $b \neq 1, 2$ is (Botter et al., 2009),

$$f_{Q_*}(q_*) = C\, q_*^{-b} \exp\left[-k\left(\frac{q_*^{2-b}}{2-b} - \frac{q_*^{1-b}}{1-b}\right)\right] \tag{14}$$

where C is a normalizing constant such that $\int_0^\infty f_{Q_*}(q_*)dq_* = 1$. An analytical solution for C is impossible, though some analytical approximations exist (see appendix B). In equation 14 there is an atom of probability, p_o, that $q = 0$ for $0 < b < 1$ (Botter et al., 2009).

$$p_o = C\frac{k}{\mu^{1-b}}\delta(q^*) \tag{15}$$

Equation 14 is undefined at $b = 1, 2$. However, it can be shown numerically that the limit of equation 14 as it approaches $b = 1$ is equation 12 and the limit as it approaches $b = 2$ is equation 13. Further, for $1 < b < 2$ equation 14 exhibits probabilities of extreme events between that of the analytical solutions for $b = 1$ and $b = 2$, as shown in figure 12. This allows us to obtain the distribution of streamflow across the observed range of b. It is worth noting that equation 13 is identical to the inverse gamma used in Lague, Hovius, and Davy, (2005). The range of solutions for different values of b leads to a resolution of the issue of which distribution to use to best represent daily streamflow. Depending on the value of b, the distribution of streamflow ranges from exponential (light tailed) to power law tailed (heavy tailed), and heavier.

In all three of the above solutions, the climatic and ecohydrological variables are contained in $k = \omega\lambda\tau$. This happens to be one over the coefficient of variability defined earlier. Therefore, equations 12-14 show that the heaviness of the tail of the distribution of daily streamflow is controlled by the shape and timescale of the recession (b, τ) and the time between effective storms (τ_{storm}). In geomorphology literature, k has often been referred to as the daily streamflow variability. However this is confusing, because low values of k describe high variability, and vice versa. Therefore, to enhance clarity we use the coefficient of variability ν instead of k. When ν is large, so is the daily streamflow variability.

The recession exponent b determines the underlying distribution type (gamma, inverse gamma, or something in between). However, the variability parameter determines the precise form of the tail of the streamflow distribution. Figure 12 plots distributions of daily streamflow as calculated by equations 12-14 for different values of b. The shaded regions surrounding the distributions for $b = 1$ (black line) and $b = 2$ (blue line) show the effect of changing the coefficient of variability ν from 0.5 to 2.

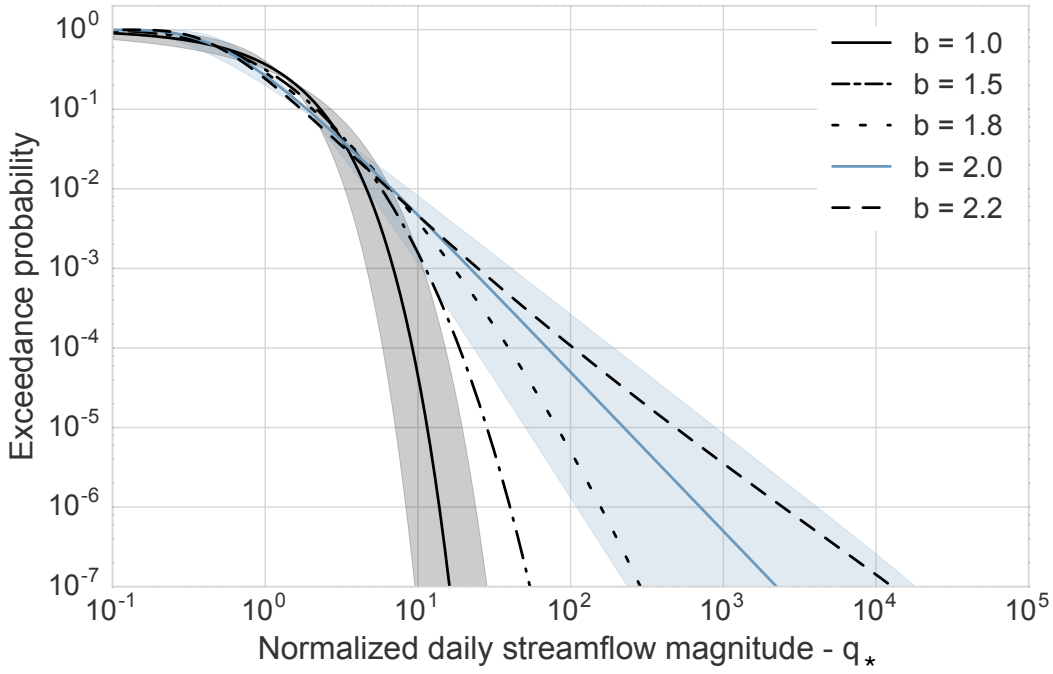

Figure 12: Shown are the distributions of streamflow for constant ecohydrological and climatic conditions where only the recession coefficient has been changed. All lines correspond to a variability parameter of 1, and the shaded regions show the effect of changing the variability parameter from 0.5 to 2.0 for $b = 1$ and $b = 2$.

3.3.4.5 *Daily streamflow mean and variability*

Both the daily streamflow mean and variability depend on the effective storm frequency $\omega\lambda$. This leads to a spurious correlation (or in this case anticorrelation) between the two parameters (Pearson, 1896),

$$\nu = \frac{\alpha}{\tau}\mu^{-1} \tag{16}$$

The spurious correlation is referred to as such in order to make clear that one parameter does not control the other, but rather reflects the dependence of both on a common control (the effective storm frequency). This helps explain the long observed anticorrelation between μ and ν (Molnar et al., 2006; Lague, 2014; Rossi, Whipple, and Vivoni, 2016). Figure 13 uses this anticorrelation to support the common observation that dry river basins have high daily streamflow variability. For a given set of ecohydrological conditions (here b is arbitrarily set to 1.4), we computed three streamflow distributions, shown in figure 13b, corresponding to three mean rainfall frequencies (0.9, 0.4, and 0.1), shown in figure 13a. As the mean rainfall frequency decreases, the effective storm frequency decreases which, in turn, causes a decrease in the mean streamflow and an increase in the coefficient of streamflow variability. The effect is that the frequency of moderate events is much lower in the dry basin, while the frequency of large floods is more comparable between basins.

Hydrological systems are very complex, and there are other factors, besides mutual dependence on the effective storm frequency, that influence the relationship between streamflow mean and variability. However, this simple framework provides a useful

way to think about climate, streamflow mean and variability that is important in moderate sized catchments.

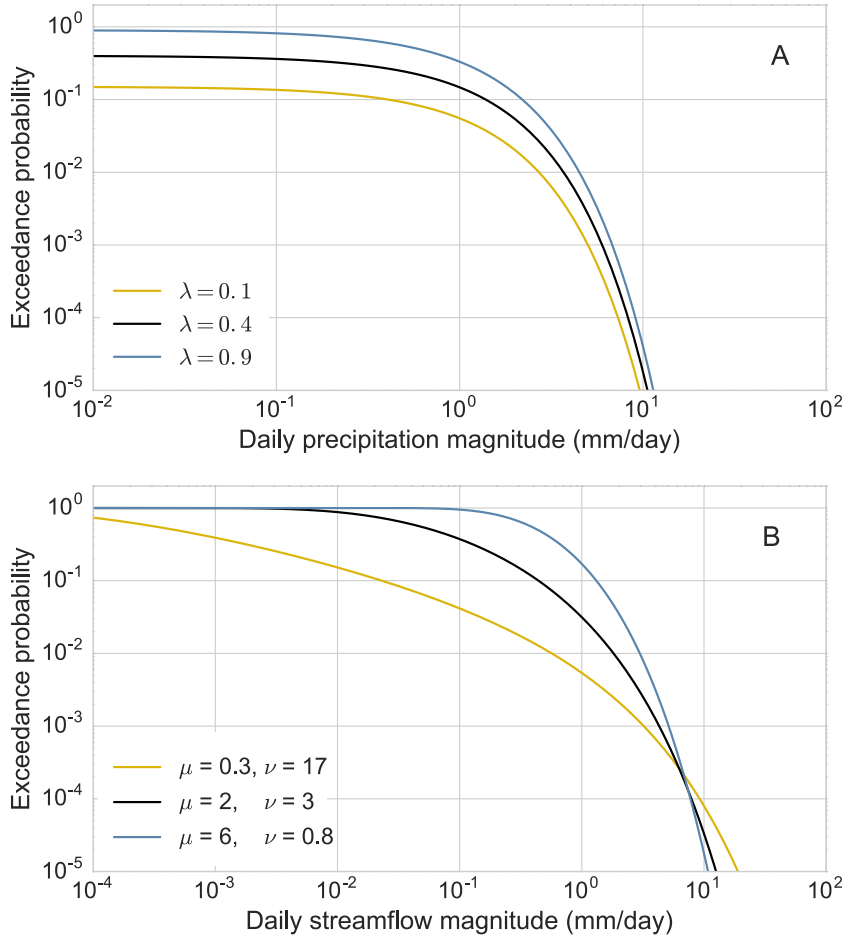

Figure 13: Changing the storm frequency λ while keeping the ecohydrological conditions constant demonstrates the covariation of μ and ν. Panel (a) shows three different daily rainfall distributions with different rainfall frequencies (λ). The resulting streamflow distributions in panel (b) range from classically arid (yellow line), with low mean and high variability to classically humid (blue line), with high mean and low variability.

3.4 INTEGRATION OF HYDROLOGY INTO THE STREAM POWER INCISION MODEL

3.4.1 *Channel hydraulics and distributions of daily erosion*

In detachment limited rivers incising into bedrock, the erosion rate is commonly modelled as a power law of excess shear stress (e.g. Howard, 1994; Lague, Hovius, and Davy, 2005; DiBiase and Whipple, 2011) of the form,

$$\varepsilon = k_e(\tau_s^c - \tau_c^c), \quad \tau_s > \tau_c, \tag{17}$$

where ε is the vertical incision into the riverbed with units of $[LT^{-1}]$, τ_s is the basal shear stress, τ_c is the critical shear stress for erosion to occur, k_e is an erosional efficiency constant, and c an exponent reflecting the dominant erosion process (Whipple,

Hancock, and Anderson, 2000). In order to relate streamflow to shear stress, it is necessary to know the channel cross-sectional profile and roughness. To obtain this we make common assumptions about channel width and depth as a function of mean streamflow and daily streamflow (e.g. Lague, Hovius, and Davy, 2005; DiBiase and Whipple, 2011). For more details see appendix C. This results in the following expression for the daily incision as a function of daily streamflow, mean daily streamflow and channel slope,

$$\varepsilon = K\langle Q\rangle^{m} S^{n} q_*^{\gamma} - \Psi, \quad q > q_c \tag{18}$$

where K is a complex erodibility coefficient that is a function of channel hydraulics and lithology but not climate, q_* is the daily streamflow, $\langle Q\rangle$ is the mean daily catchment integrated streamflow ($\langle Q\rangle = \mu A$), S is the river slope and Ψ is the threshold for erosion. The exponents m, n, and γ are determined by the channel form and hydraulics. The exponent n determines the relative importance of the river slope. The exponent m is related to the bankfull width of the channel, and how this increases with increasing $\langle Q\rangle$ downstream. In contrast the exponent γ describes in part the shape of the cross sectional channel profile. This determines how the channel width at a given location on the river changes with the daily variations in streamflow and therefore controls the sensitivity of the daily erosion rate to streamflow variability. When $\gamma > 1$ shear stress τ_s increases disproportionately to daily streamflow, and large floods will be more important in determining the long-term erosion rate than when $\gamma \leqslant 1$.

We can use this relationship between daily erosion rate and daily streamflow to rewrite the distribution of streamflow in terms of daily erosion rate. For the case $b = 1$ (derivation in appendix D),

$$f_E(\varepsilon) = \frac{(\varepsilon+\Psi)^{1/\nu\gamma-1}}{\Gamma_\varepsilon \gamma(\varepsilon_o \nu^{\gamma})^{1/\nu\gamma}} \exp\left[-\left(\frac{\varepsilon+\Psi}{\varepsilon_o \nu^{\gamma}}\right)^{1/\gamma}\right] \tag{19}$$

where $\Gamma_\varepsilon = \Gamma(1/\nu)[\Gamma(1/\nu, q_{c*}/\nu) - \Gamma(1/\nu, q_{m*}/\nu)]$ is a normalizing constant that takes into account the fact that the distribution of erosion only exists for streamflows above q_{c*}, the critical streamflow, and below q_{m*}, the maximum streamflow we expect to see over the time period of observation. We define $\varepsilon_o = K\langle Q\rangle^{m} S^{n}$ as the reference erosion rate; it is the erosion rate we would see in the absence of any stochastic variations in streamflow or erosion threshold effects ($q_* = 1$, $\Psi = 0$).

For $b = 2$ (derivation in appendix D),

$$f_E(\varepsilon) = \frac{(\varepsilon+\Psi)^{-(1/\nu+1)/\gamma-1}}{\Gamma_\varepsilon \gamma(\varepsilon_o \nu^{-\gamma})^{-(1/\nu+1)/\gamma}} \exp\left[-\left(\frac{\varepsilon+\Psi}{\varepsilon_o \nu^{-\gamma}}\right)^{-1/\gamma}\right] \tag{20}$$

where $\Gamma_\varepsilon = \Gamma(1/\nu+1)[\Gamma(1/\nu+1, 1/\nu q_{m*}) - \Gamma(1/\nu+1, 1/\nu q_{c*}]$ is a slightly different normalizing constant that serves the same role as in the case $b = 1$.

In the case $b \neq 1, 2$ (derivation in appendix D),

$$f_E(\varepsilon) = C_\varepsilon \frac{(\varepsilon+\Psi)^{(1-b)/\gamma-1}}{\varepsilon_o^{(1-b)/\gamma}} \exp\left[-\frac{1}{\nu}\left(\frac{(\varepsilon+\Psi)^{(2-b)/\gamma}}{(2-b)\varepsilon_o^{(2-b)/\gamma}} - \frac{(\varepsilon+\Psi)^{(1-b)/\gamma}}{(1-b)\varepsilon_o^{(1-b)/\gamma}}\right)\right] \tag{21}$$

where C_ε is a normalizing constant such that $\int_0^{\varepsilon_m} f_E(\varepsilon)d\varepsilon = 1$. In the above expressions, we see that the pdf of daily erosion can be expressed as a function of geomorphic (K, S, m, n, γ, Ψ) and ecohydrological (b, ν, μ) parameters.

Figure 14 shows the distributions of daily erosion corresponding to the distributions of daily streamflow in figure 12. The effect of changing the coefficient of variability ν is shown as shaded regions for $b = 1$ and $b = 2$. It's influence is slightly different due to the significant probability to have days with no erosion at all.

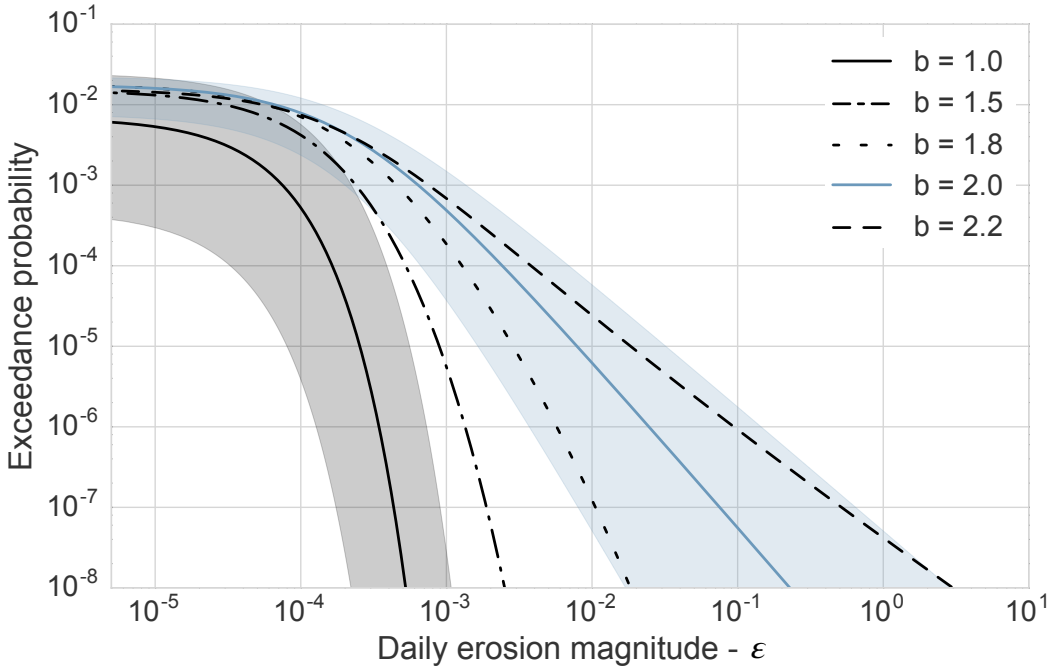

Figure 14: Distributions of daily erosion associated with the distributions of streamflow from figure 12. For all distributions the ecohydrological and climatic conditions are held constant, $\nu = 1$ and $\gamma = 1$. The shaded regions show the effect of changing the variability parameter from 0.5 to 2.0 for $b = 1$ and $b = 2$.

3.4.2 *Mean long-term erosion rates as a function of climate and ecohydrology*

To obtain the mean erosion rate we can integrate over the distribution of daily erosion from $\varepsilon(q_c) = 0$ to $\varepsilon(q_m) = \varepsilon_m$. This yields the mean erosion intensity $\bar{E}$, but does not take into account the days on which no erosion occurs. To account for that we must calculate the fraction of the days when there was erosion. This amounts to the probability that the daily streamflow is equal to or greater than the critical streamflow q_{c*}, $Pr[q_* \geqslant q_c]*$, taking into account that the distribution has already been truncated at $q_* = q_{m*}$. This can be thought of as the frequency with which the threshold q_{c*} is exceeded, therefore we refer to it as the threshold term and label it λ_ε.

$$\lambda_\varepsilon = Pr[q_* \geqslant q_{c*}] = \int_{q_{c*}}^{\infty} f^t_{Q_*}(q_*)dq_* = \begin{cases} \frac{\Gamma(1/\nu, q_{c*}/\nu) - \Gamma(1/\nu, q_{m*}/\nu)}{1 - \Gamma(1/\nu, q_{m*}/\nu)} & ; b = 1 \\ \frac{\Gamma(1/\nu+1, 1/\nu q_{m*}) - \Gamma(1/\nu+1, 1/\nu q_{c*})}{\Gamma(1/\nu+1, 1/\nu q_{m*})} & ; b = 2 \end{cases} \tag{22}$$

where the superscripted t on the distribution of streamflow denotes the fact that it has been truncated at q_{m*} and renormalized such that the $Pr[q_* < q_{m*}] = 1$. The mean

long-term erosion rate is the product of the mean erosion intensity and the fraction of days that have erosion,

$$\langle E \rangle = \lambda_\varepsilon \bar{E} \tag{23}$$

where,

$$\bar{E} = \int_0^{\varepsilon_m} \varepsilon \, f_E(\varepsilon) d\varepsilon \tag{24}$$

We make a point to calculate the mean erosion rate $\langle E \rangle$ and the mean erosion intensity $\bar{E}$ separately so that we can differentiate between rivers with low frequency, high impact erosion events and rivers with high frequency, low impact erosion events. These may both have similar mean erosion rates, but will have very different mean erosion intensities and erosion frequencies.

The integral in 24 can be solved analytically (derivation in appendix D) in the cases $b = 1$ or 2 yielding,

$$\bar{E} = \psi \, \varepsilon_o \tag{25}$$

$$\psi = \begin{cases} \frac{\Gamma(1/\nu+\gamma)}{\Gamma(1/\nu)\nu^{-\gamma}} \left(\frac{\Gamma(1/\nu+\gamma, q_{c*}/\nu) - \Gamma(1/\nu+\gamma, q_{m*}/\nu)}{\Gamma(1/\nu, q_{c*}/\nu) - \Gamma(1/\nu, q_{m*}/\nu)} \right) - q_{c*}^{\gamma} & ; b = 1 \\ \frac{\Gamma(1/\nu+1-\gamma)}{\Gamma(1/\nu)\nu^{\gamma-1}} \left(\frac{\Gamma(1/\nu+1-\gamma, 1/\nu \, q_{m*}) - \Gamma(1/\nu+1-\gamma, 1/\nu \, q_{c*})}{\Gamma(1/\nu+1, 1/\nu \, q_{m*}) - \Gamma(1/\nu+1, 1/\nu \, q_{c*})} \right) - q_{c*}^{\gamma} & ; b = 2 \end{cases} \tag{26}$$

The new term ψ quantifies the impact of stochastic streamflow events above the erosion threshold accounting for their relative frequency of occurrence and erosive power. It is mainly a function of q_{c*} and ν. We refer to this term as the stochastic term. In the general case that $b \neq 1$ or 2, we can solve for λ_ε and ψ numerically.

This brings us to the new form of the stochastic-threshold stream power incision model,

$$\langle E \rangle = \lambda_\varepsilon \psi \, K \langle Q \rangle^m S^n \tag{27}$$

where $\langle Q \rangle = \mu A$. The terms λ_ε and ψ are both functions of the ecohydroclimatic conditions of the catchment with analytical solutions in the cases $b = 1$ or 2. As q_{m*} becomes very large and q_{c*} becomes much smaller than the mean daily streamflow, λ_ε tends to one because there are no threshold effects, and ψ becomes a function of only the streamflow variability ν and the exponent of the erosion rate γ. In the case $\gamma = 1$ (erosion rate increases linearly with streamflow), ψ becomes one as well, and the erosion rate is simply the reference constant streamflow erosion rate ε_o.

3.5 RESULTS AND DISCUSSION

The hydrological model creates a framework where only the daily mean and variability of streamflow (μ and ν) and the recession exponent b are needed to fully specify the distribution of daily streamflow, and to relate that distribution back to the climatic and ecohydrological conditions giving rise to it. This allows us to unite the work of Tucker and Bras, (2000) with the work of Crave and Davy, (2001) and Lague, Hovius, and Davy, (2005). These workers established two different theoretical bases of stochastic climatic forcing in landscape evolution that have been used in several

subsequent studies (Snyder et al., 2003; Collins, Bras, and Tucker, 2004; Tucker, 2004; Istanbulluoglu and Bras, 2005, 2006b; Molnar et al., 2006; DiBiase and Whipple, 2011; Carretier et al., 2013; Lague, 2014; Rossi, Whipple, and Vivoni, 2016). Tucker and Bras, 2000 and Tucker, (2004) consider the effect of realistic stochastic climate forcing but neglect hydrology, arriving at a light tailed exponential distribution for streamflow and representing the variability of climate through the one over the storm frequency ($1/\lambda$). In contrast, Lague, Hovius, and Davy, (2005) consider hydrology directly, using a heavy tailed distribution for streamflow commonly observed in nature and representing climatic variability with the shape parameter of their heavy tailed distribution (k). However they do this at the expense of the connection to realistic climatic forcing, as they cannot cast their distribution in terms of rainfall. Within the framework presented here, a light tailed distribution of streamflow and a solution for the longterm erosion rate very similar to Tucker, (2004, eq. 33) is recovered when $b = 1$. When $b = 2$, the streamflow distribution is heavy tailed, and the solution for the longterm erosion rate is equivalent to Lague, Hovius, and Davy, (2005, eq. 17). Furthermore, the different concepts of climatic variability can be reconciled in this framework with the variability parameter $\nu = 1/k = (\omega\lambda\tau)^{-1}$, which is equivalent to one over Lague's variability (k), and a linear function of Tucker's variability ($1/\lambda$), revealing that the two forms of variability are related to each other, and adequately captured by ν.

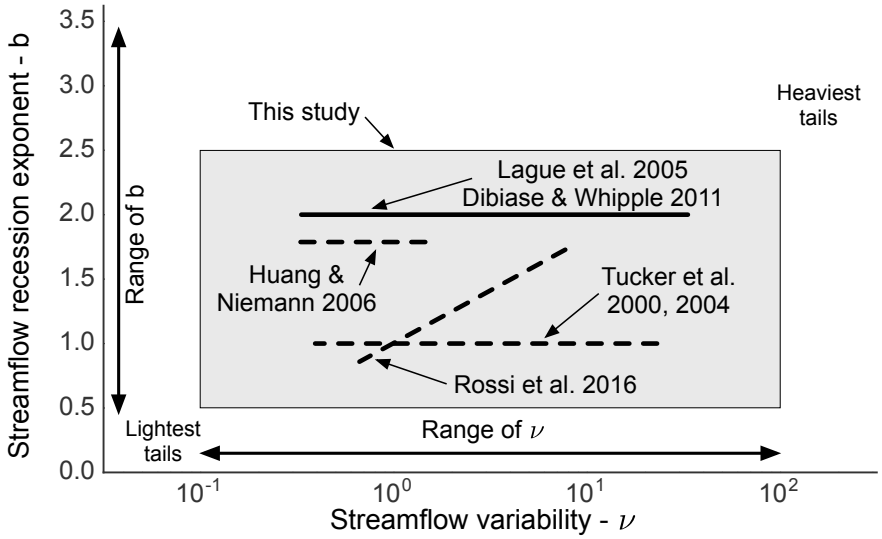

Figure 15: The hydrological parameter space covered in this study compared to previous studies on the effect of streamflow variability on fluvial erosion. Some of the other studies can only be approximately represented in the parameter space presented here, these are shown with dashed lines. The arrows show the observed natural ranges of b and ν.

The hydrological model allows us to model how the mean and variability of streamflow respond to changes in the climatic and hydrological boundary conditions. In turn, the influence that streamflow mean and variability have on stream power erosion has been clearly investigated in previous studies (e.g. Lague, Hovius, and Davy, 2005; Lague, 2014) and is well understood. As a result, the coefficient of streamflow variability ν and the mean streamflow μ provide a useful way to understand the effect of ecohydrology and climate on longterm fluvial erosion rates. In the following we first briefly review the impact of the streamflow variability on the longterm ero-

sion rate. Then we discuss climatic and hydrological controls on streamflow mean and variability. We finish with some examples of how climatic and hydrological conditions can influence fluvial erosion rates and the development of steady state river profiles. Throughout the entire following discussion we assume that the erodibility coefficient K and the stream power exponents are constant ($n = 1$ and $m = 0.5$). The effect that changes in these parameters have is already well understood (e.g. Whipple and Tucker, 1999).

3.5.1 *Daily streamflow variability and longterm erosion rate*

We briefly explore here how longterm erosion rates vary as a function of streamflow variability, finding results similar to Tucker, (2004), Lague, Hovius, and Davy, (2005) and DiBiase and Whipple, (2011). However, in contrast to previous studies, we present the analysis for a range of values of b, exploring how tail-heaviness influences the results. We use the normalized longterm erosion rate as a measure of the erosion efficiency, which highlights the influence of the variability of daily streamflow and the erosion threshold. The normalized longterm erosion rate is defined as the longterm erosion rate $\langle E \rangle$ divided by the constant streamflow reference erosion rate ε_o.

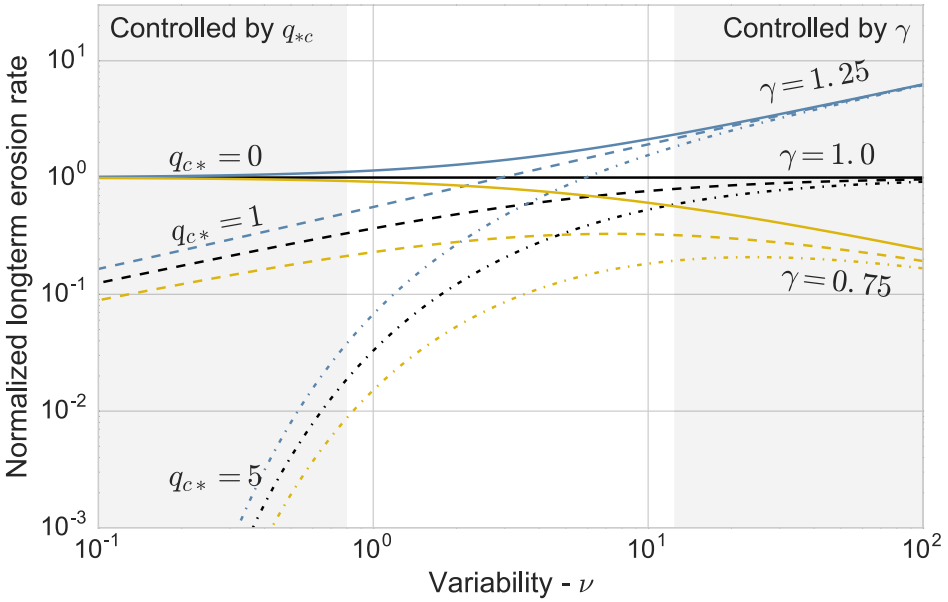

Figure 16: At low streamflow variability the erosion threshold q_{c*} controls the erosion rate, with the erosion rate decreasing progressively as the erosion threshold is increased. At high streamflow variability, the erosion nonlinearity γ becomes the dominant control, and the erosion rate increases as γ increases. The trend is the similar for $1 \leqslant b \leqslant 2.5$.

When the coefficient of variability is large, the normalized erosion rate is controlled by the at-a-station nonlinearity, γ (see figure 16). The normalized erosion rate increases with increasing variability when $\gamma > 1$ because of the strengthened influence of large floods and decreases with increasing variability when $\gamma < 1$ because of the weakened influence of large floods. In contrast, when the coefficient of variability is small, the erosion rate is controlled by the threshold streamflow q_{c*}. The normalized erosion

rate decreases with increasingly high thresholds at low variability, regardless of the value of γ. These results are consistent for $1 \leqslant b \leqslant 2.5$, and are in line with previous work (Tucker and Bras, 2000; Lague, Hovius, and Davy, 2005). This suggests that for a wide range of conditions, the erosion threshold will be a dominant factor in setting the longterm erosion rate for $\nu \leqslant 1$.

3.5.1.1 *Tail heaviness*

Larger values of b imply more nonlinear discharge recessions, which leads to heavier tailed distributions of discharge. The rare discharge events associated with heavier tailed distributions are larger than distributions with smaller values of b. This is similar to distributions with larger coefficients of variability. As a result, increasing b leads to an increased sensitivity to γ when the coefficient of variability is large and a lowered sensitivity to the erosion threshold when the coefficient of variability is small (see figure 17).

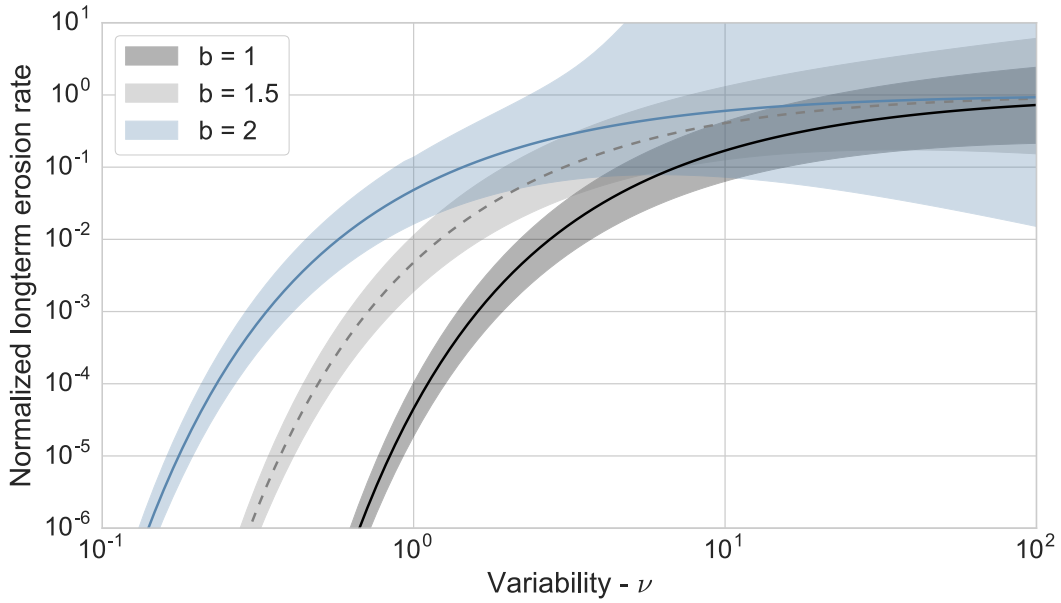

Figure 17: The effect of the coefficient of variability on the normalized erosion rate for different values of b. The solid lines represent $\gamma = 1$, and the shaded region shows the range from $0.75 \leqslant \gamma \leqslant 1.25$. The erosion threshold $q_{c*} = 5$, maximum discharge $q_{m*} = \infty$. As b increases, the sensitivity to q_{c*} decreases and the sensitivity to γ increases.

Though the hydrological and climatic controls on the coefficient of variability are consistent across the range of b, the effect that changes in the coefficient of variability has on the erosion rate will differ for different values of b. One consequence of this is that if b and ν covary, the response to increasing variability will be compounded by increasing tail heaviness, and will be more significant than would be predicted for a constant b value.

3.5.1.2 *The importance of maximum streamflow for power law tailed streamflow distributions*

For heavy tailed distributions ($b \geqslant 2$), the longterm mean erosion rate does not necessarily converge to a constant value, even for long observation periods. Instead the

measured longterm erosion rate will fluctuate continuously over time. However, if there exists a physical upper limit on the magnitude of daily streamflow q_{m*}, the erosion rate will converge to a mean value once the observation period is long enough to have a good probability of including q_{m*}. Thus the existence of maximum streamflow has a significant impact on the longterm erosion rate, especially when $b \geqslant 2$ and $\gamma \geqslant 1$. Despite the critical role of the maximum streamflow, the precise value of q_{m*} is not important in determining the longterm mean erosion rate. This was also noted by Lague, Hovius, and Davy, (2005) who showed that, except for nonlinear regimes ($\nu > 1$ and $\gamma > 1$) the value of q_{m*} was not significant.

3.5.1.3 *Peak in erosion frequency as a function of variability*

It is possible to use the distribution of streamflow to estimate the return time of extreme events simply by calculating the probability of observing an event larger than a chosen extreme event threshold magnitude. However, this implicitly assumes that the individual daily floods are unrelated to one another, an assumption which is known to be poor for daily streamflow, where storms can cause floods spanning several days. This means that the estimated return time resulting from such an analysis is a minimum estimate, the actual return times are likely to be longer. A more rigorous assessment of return times requires a treatment of extreme value theory that is beyond the scope of this work.

That said, we can still use the above approach to get a rough estimate of how the importance of extreme events changes with ν and q_{c*}. To measure the importance of extreme events we calculate the daily streamflow magnitude above which 50% of erosion occurs (referred to as q_{50*}). When q_{50*} is large, it implies that very large events accomplish 50% of the total erosion, and therefore extreme erosion events are important. We have arbitrarily selected q_{50*}, other values could be used (derivation in appendix E). We would expect that as variability increases, the importance of extreme erosion events would go up. Figure 18a shows the magnitude of q_{50*}, demonstrating that it indeed increases with increasing variability for a range of values of b, q_{c*} and q_{m*}. The increase is stemmed by imposing a maximum streamflow, which reduces the importance of extreme events.

A high value for q_{50*} implies that extreme erosion events are important. However, it does not say anything about the frequency of these large erosion events. If erosion events themselves are rare due to low variability or a high erosion threshold then even common erosion events will require large, rare streamflow events. We can calculate the fraction of streamflow events responsible for the upper 50% of erosion (ε_{50*}). This takes into account the effect of both q_{50*} and the erosion frequency λ_ε and is shown in figure 18b. Unexpectedly, figure 18b shows that the frequency of ε_{50*} is very low at low variability, with a peak at moderate variabilities. This is due to the fact that all erosion events are caused by extreme streamflow events at very low streamflow variabilities. This predicts counter-intuitively that infrequent erosion events will be important for low and high variability rivers, while moderate variability rivers will be driven by frequent erosion events.

3.5.2 *Hydrologic and climatic controls on streamflow*

Neither the climate nor the ecohydrology of a river basin alone dictates the resulting streamflow distribution, but rather the interaction between the two. This means that

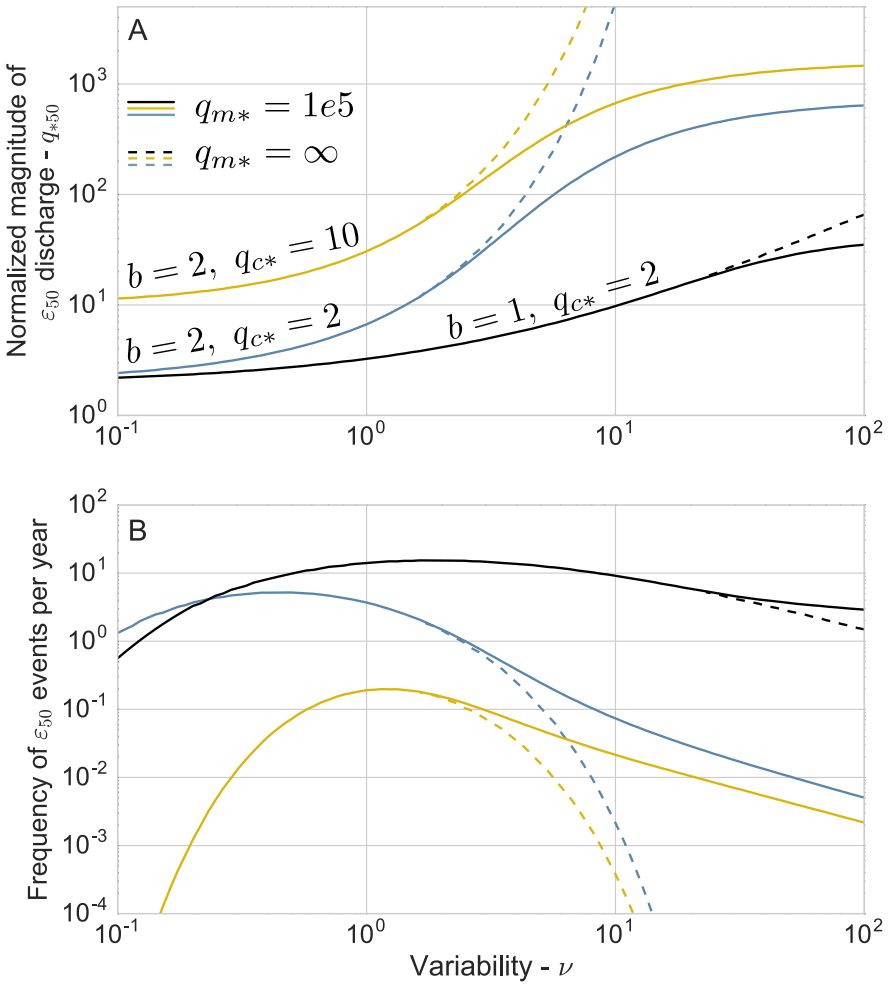

Figure 18: Panel (a) shows the streamflow above which 50% of erosion is accomplished as a function of variability for a range of q_{c*}, q_{m*} and b. Panel (b) shows the frequency of erosion events associated with the upper 50% of total erosion. The colors and linestyles correspond to panel (a).

the same climate can give rise to different fluvial responses depending on the ecohydrological regime, leading to the conclusion that the erosional response to a given climate cannot be predicted without taking into account the ecohydrology of a river basin, among other things.

The manner in which ecohydrology modulates climate to yield the streamflow regime (described by μ, ν and b) is not straightforward. Ecohydrology effects both the total amount of water transmitted through the hydrological system to the river as well as the frequency of effective storms (storms significant enough to produce streamflow), and consequently the streamflow variability. In some cases ecohydrology acts as a strong filter of incoming rainfall, fundamentally altering the statistics of incoming rainfall. In other cases it can be less important as a filter, leaving the statistics of rainfall relatively intact as they are transmitted through the basin to become the statistics of streamflow.

3.5.2.1 *Mean streamflow*

The ecohydrological conditions in a river basin have a major influence on the mean streamflow by controlling which proportion of the incoming rainfall enters the fluvial

system (expressed by the streamflow ratio ω), and which proportion of rainfall leaves the catchment as vapor due to evapotranspiration. Through this influence the ecohydrological regime in a catchment can dictate the longterm erosion rate by reducing the fraction of rainfall that goes to streamflow.

Considering the form of the mean, $\mu = \alpha\omega\lambda$, and the fact that $\omega \leqslant 1$ it is clear that taking ecohydrology into account will always reduce the estimation of the mean streamflow. The reduction of the mean streamflow due to ecohydrology can be significant, with arid catchments approaching 100% loss of incoming rainfall to evapotranspiration (Budyko, 1974). Two basins with similar mean rainfall rates, but very different effective soil depths or aridity indices, e.g. as a result of different soil depths or evapotranspiration rates, can have significant differences in the fraction of rainfall that is partitioned into streamflow, with the catchment that has low evapotranspiration rates and thin soils having higher streamflow. We can see this by increasing the mean storm intensity while holding ecohydrological conditions constant, which changes the effective soil thickness and the aridity index (figure 19). When the mean storm size is large compared to the soil capacity, the soil layer is easily saturated, and most storms produce runoff events. In this case the intensity and frequency of rainfall are closely correlated with the mean and frequency of streamflow events, and the streamflow ratio is close to one. As the storm size decreases, the effective soil depth increases, and the soil layer is saturated only by increasingly infrequent, large storms. This results in fewer runoff events, as larger fractions of each storm are stored in as soil moisture, resulting in proportionally more water from each storm lost to evapotranspiration, a larger aridity index, and a reduced mean streamflow magnitude. An interesting consequence of this is that the mean streamflow may be significantly influenced by factors other than the mean rainfall in a river basin, including temperature, insolation, slope aspect, soil depth and porosity, and vegetation type and cover.

The partitioning of rainfall into streamflow and evapotranspiration can also respond nonlinearly to changes in rainfall intensity or frequency, such that changes in mean rainfall rate have a disproportionate effect on mean streamflow (figure 19). Additionally, mean streamflow will respond differently to a change in mean rainfall intensity than it does to a change in mean rainfall frequency, even if the change to mean rainfall rate is the same in both cases. This is because the rainfall intensity and frequency have different influences on the effective soil thickness and aridity index (figure 20.)

All else constant, the erosion rate will be less sensitive to changes in river slope when the mean daily streamflow is lower. This means that catchments in the thick and/or dry soil regimes will require steeper riverbed slopes to achieve the same erosion rate compared to catchments with effectively thinner, wetter soils but with the same mean rainfall rate. To the extent that vegetation is correlated with thicker soils and higher evapotranspiration rates (leading to the dry thick soil regime), highly vegetated catchments could experience slower erosion for the same steepness not only because of the vegetation's ability to stabilize slopes, but also because of its role in reducing the erosiveness of the rivers by a (potentially significant) reduction in the mean daily streamflow relative to the incoming mean rainfall. Similarly, arid catchments are expected to use each millimeter of rainfall less efficiently for erosion due to more significant losses to atmospheric fluxes. However, this may be obfuscated by other differences such as the erosion threshold or streamflow variability that are also expected to vary systematically between catchments in different ecohydrological regimes.

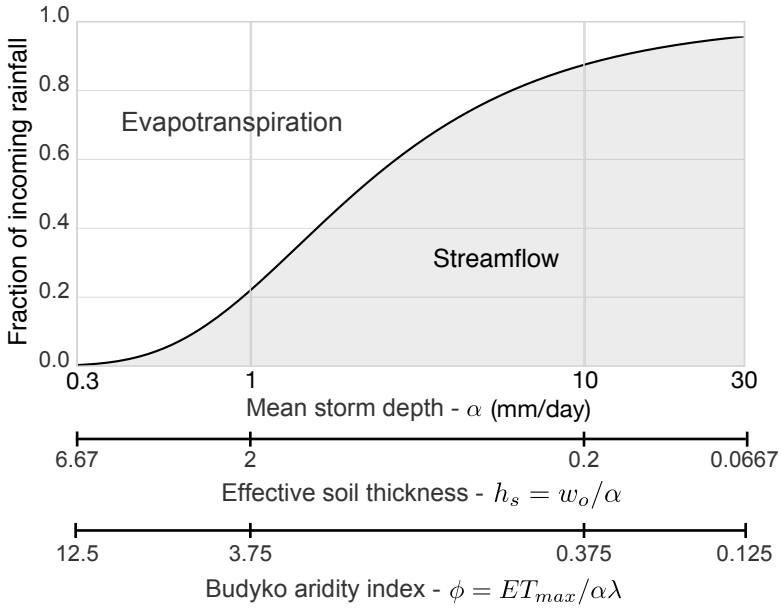

Figure 19: The interaction of climatic and ecohydrological conditions (expressed as h_s and ϕ) is what determines the water partitioning in a catchment. The ecohydrological conditions are held constant (PET = 0.5 cm/day, λ = 0.4, soil capacity $n_s Z_r(s_1 - s_w)$ = 2 cm) while the mean storm intensity is varied (0.2 cm $< \alpha <$ 20 cm). The result is that the relative importance of ecohydrology changes across the range of storm depths, with the fraction of rainfall lost to evapotranspiration and interception decreasing significantly with increasing storm depth.

3.5.2.2 *Streamflow variability*

The retention of rainfall in the soil layer, and its release back into the atmosphere via evapotranspiration does not only reduce the mean streamflow, but also causes a shift in the statistics of runoff events relative to rainfall. This is because small and moderate rainstorms are more affected by the buffering effect of the soil layer than larger rainstorms. This is why the water balance term, ω, that describes the partitioning of water into fluvial and atmospheric fluxes appears in the equations for both the mean and variability of streamflow. This aspect of the hydrological model is well supported by the study of the environmental controls on streamflow variability in several hundred river basins in the US and Puerto Rico (Rossi, Whipple, and Vivoni, 2016). This study finds that the increase in streamflow variability associated with increasing basin aridity can be understood as a decrease in the frequency of moderate streamflow events (events with a frequency of 0.2-2 years) relative to rare streamflow events (event frequency $>$ 20 years). Additionally, the study finds that the basin aridity index, ϕ, evapotranspiration rate, ET_{rat}, and the rainfall frequency, λ, are the best predictors of streamflow variability in rainfall dominated catchments (<10% precipitation as snow). Finally, study finds that mean and variability of daily rainfall intensity are not predictors of streamflow variability, suggesting that these are not important controls.

These findings match well with the environmental controls on the coefficient of streamflow variability described by the model as well as the conceptual description of how thin, thick, wet, or dry soil regimes drive the runoff ratio, and consequently streamflow variability. Equation 11 predicts that the coefficient of variability is controlled by the hydrological response time, the mean rainfall frequency, and the runoff ratio, which is a function of the effective soil thickness and the aridity index (ν =

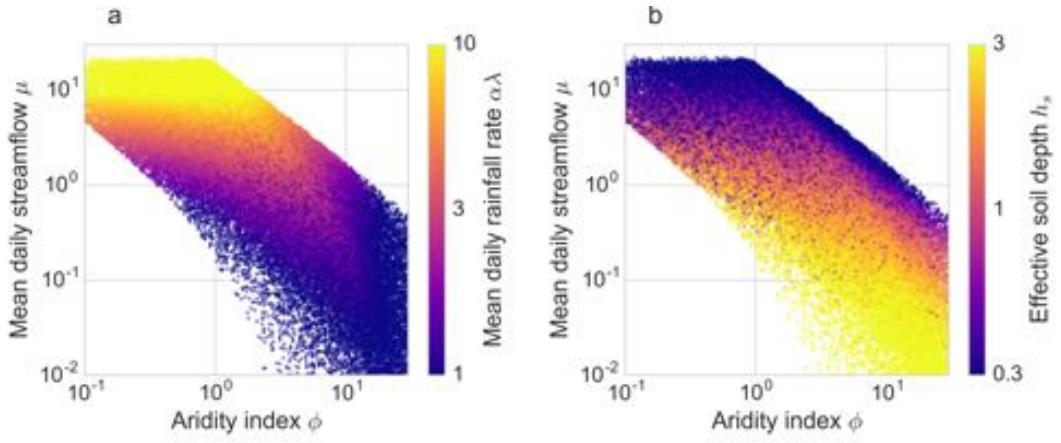

Figure 20: Monte Carlo simulations of the mean daily streamflow ratio for a wide range of hydrological and climatic boundary conditions (for more information see chapter 4). Panel (a) the mean daily rainfall rate is an important control on mean streamflow rate, particularly in humid basins ($\phi < 1$) with thin effective soils (thin, wet soils). Panel (b) through their influence on the runoff ratio (ω), the aridity index and effective soil thickness are also important controls on mean streamflow (as explained in section 3.3.3).

$[\omega(h_s, \phi)\lambda\tau]^{-1}$). Rossi, Whipple, and Vivoni, (2016) do not assess the relationship between soil moisture storage capacity or hydrological response time and streamflow variability, but the relationships they find between aridity index and streamflow variability as well as mean rainfall frequency and streamflow variability are well captured by this model.

Using Monte Carlo techniques we can probe the controls on streamflow variability predicted by the model over a wide range of climatic and ecohydrological conditions (see figure 21). When the aridity index is less than one (energy limited conditions), the variability is mostly controlled by the hydrological response time. When the aridity index is larger than one (water limited conditions), streamflow variability is predominantly controlled by the effective soil depth, h_s. The control of the effective soil depth reflects both the importance of soil moisture storage capacity and mean rainfall intensity. The fact that Rossi, Whipple, and Vivoni, (2016) find mean rainfall intensity to be a poor predictor of streamflow variability may imply that the model overemphasizes the role of the effective soil depth. Across a wide range of climatic and ecohydrological conditions, streamflow variability is predicted to be higher under more arid conditions. This matches the observation from Rossi, Whipple, and Vivoni, (2016) that evapotranspiration and rainfall frequency are good predictors of streamflow variability (because the aridity index is a function of the potential evapotranspiration rate and, indirectly, mean rainfall frequency).

3.5.3 *Ecohydrology, climate and erosion*

3.5.3.1 *The impact of changing climate on erosion rates*

It is useful to understand independently the influence of streamflow mean and variability on the longterm erosion rate as we have done above. However, the relationship between streamflow mean and variability that emerges from the theory presented in

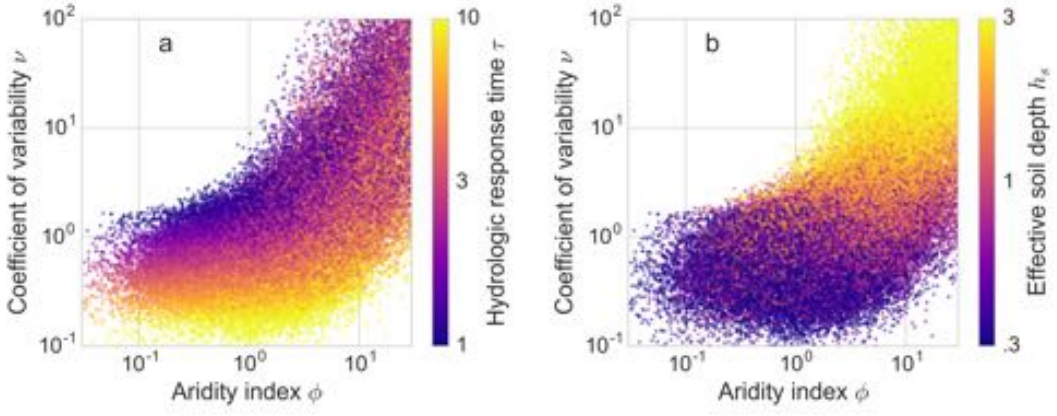

Figure 21: Monte Carlo simulations of the coefficient of streamflow variability for a wide range of hydrological and climatic boundary conditions (for more information see chapter 4). Panel (a) for a wide rang of conditions, hydrological response time is an important control on variability in humid basins ($\phi < 1$). Panel (b) Effective soil depth is another important control on variability, but for arid basins rather than humid ones ($\phi > 1$). Overall, the aridity index is an important control variability, with humid basins tending to be less variable than wet basins.

this study suggests that the two should be considered together. This is supported by the widespread empirical observation of an anticorrelation between streamflow mean and variability (Molnar et al., 2006; Lague, 2014; Rossi, Whipple, and Vivoni, 2016), which led to efforts to consider the influence of covarying mean and variability on longterm erosion rates (Molnar et al., 2006; DiBiase and Whipple, 2011). However, previous work was based on empirical relationships. With our theoretical framework relating streamflow mean and variability to climate and ecohydrology we are ideally suited to explore the effect of covarying, anticorrelated mean and variability as a result of changing climate.

W do this by changing the underlying climatic and ecohydrological parameters, which causes the mean and variability to change accordingly. We can calculate the trajectory a river basin will chart in μ-ν parameter space in response to changing climatic and hydrological boundary conditions (22a). These trajectories tend to follow the negative correlation between mean and variability, i.e. to trend from high variability, low mean discharge to high mean discharge, low variability. This dominant trend results in portions of μ-ν space that are unlikely to be occupied by a river basin, because it requires extreme climatic and ecohydrological conditions. These regions consist of the upper right and lower left corners of the parameter space in figure 22, which is useful for directing our analysis to the realistic parameter space.

We use equation 27 to calculate the longterm erosion rate as a function of the streamflow mean and variability (shown as contours in figure 22a, where $b = 2$, $q_{c*} = 10$, $\gamma = 1$). We compare the response of the erosion rate to increases in rainfall intensity or frequency using the hydrological model to models where erosion rate is a simple function of mean discharge, e.g. $\langle E \rangle = K \langle Q \rangle^m S^n$, or rainfall, e.g. $\langle E \rangle = K \langle P \rangle^m S^n$ (figure 22b and c). The reduction in variability as mean discharge increases reduces the impact of a higher mean discharge. As a result, erosion is less efficient for high mean discharge than predicted by simpler stream power models. However, this is not true for the entire parameter space. In particular, if $\gamma > 1$, the erosion rate predicted by the cou-

pled hydrological model can exceed that predicted directly by mean rainfall or mean streamflow rates. In general, rivers with a slower response time are more dramatically affected by the trade off of the mean and variability of streamflow.

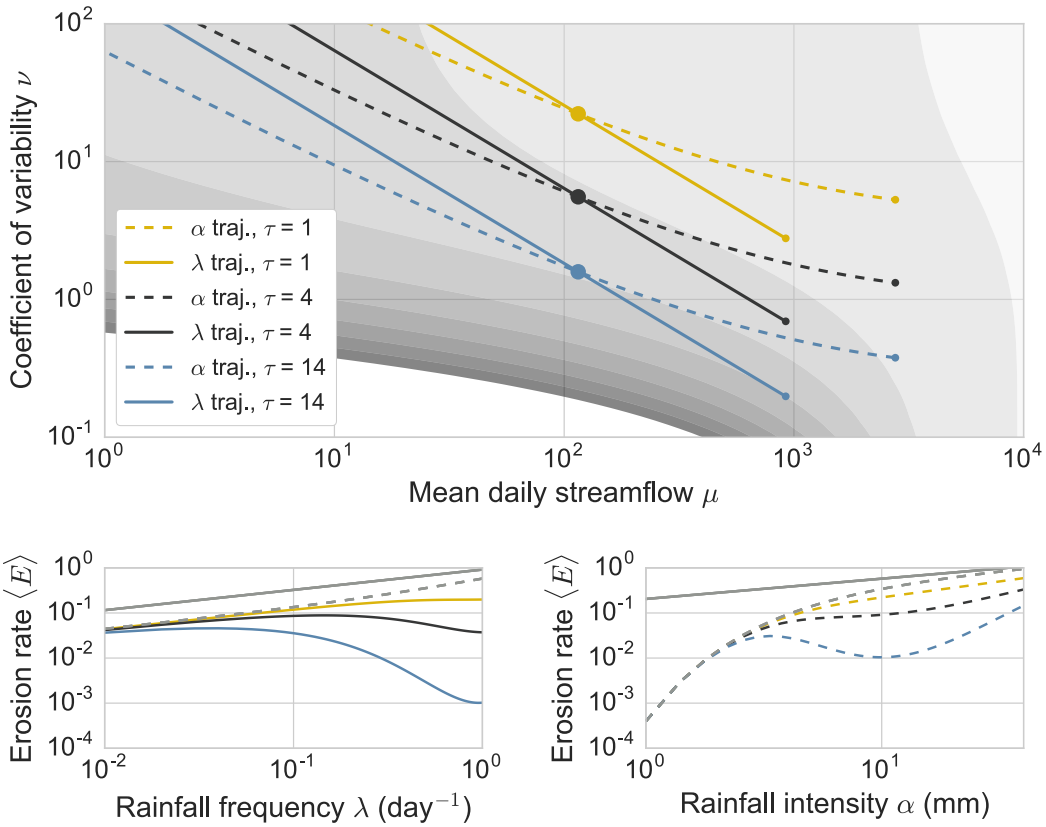

Figure 22: In panel (a) hypothetical river basins with the same ecohydrological conditions, but different hydrological response times, are shown as circles in the streamflow mean-variability parameter space on top of the longterm erosion rate (grey contours - each contour represents an order of magnitude change in erosion rate with lower erosion rates represented by darker colors). The trajectories that these basins follow with changing mean storm frequency (solid lines) and mean storm depth (dashed lines) are also plotted. Panels (b) and (c) show the longterm erosion rate along the trajectories with the corresponding line color and style in panel (a). Also shown is the erosion rate as a function of rainfall intensity or frequency using the model $\langle E \rangle \propto \langle P \rangle^m$ (dashed gray lines) and using the model $\langle E \rangle \propto \langle Q \rangle^m$ (solid gray lines). The erosion threshold is set at 10x the mean discharge ($q_{c*} = 10$). As a consequence, the absolute magnitude of the threshold increases with increasing mean streamflow.

Figure 22 illustrates why the changes in longterm erosion rate depend so heavily on both the climatic and ecohydrological conditions of the river basin. While we can guess that the trajectory a basin will follow with changing climatic forcing will trend from the lower right corner to the upper left corner of μ-ν space, we cannot know how this will effect the erosion rate until we know its position in μ-ν space. This requires knowledge of both the climatic and ecohydrological conditions in that basin. Therefore, understanding what ecohydroclimatic regime a particular basin is in is key to understanding how the longterm erosion rate will respond to changes in climatic

forcing. Another key to understanding how the erosion rate will evolve with changing climate is the response of the erosion threshold.

3.5.3.2 *Steepness index and the long stream profile*

To provide some tangible examples of the magnitude of influence of climatic and hydrological boundary conditions on the stream power model, we model the steady state long stream profile for several sets of different boundary conditions. Lague, (2014) provide evidence suggesting that it is more common for bedrock rivers to be in a 'stochastic-threshold' domain (Lague, 2014, figure 6), which corresponds approximately to $q_{c*} > 1$. For all the following simulations the relative erosion threshold, q_{c*}, is between 1 and 10. As a result, streamflow variability always plays a significant role. For computational efficiency, we take advantage of analytical solutions ($b = 2$). Unless otherwise noted, we use moderate values for all climatic and hydrological parameters: s_o = 3-30 mm, ET_{max} = 10 mm/day, α = 10 mm/day, λ = 0.25 or 0.6 day^{-1}, $\bar{p}$ = 2 or 6 mm/day, τ = 3-6 days. In the context of the stream power model, modifications to the climatic and hydrologic boundary conditions are effectively changes in the erodibility rate constant K, which are already understood (e.g. Lague, Hovius, and Davy, 2005; DiBiase and Whipple, 2011; Lague, 2014). However, we attempt to show with the numerical experiments that reasonable changes in climatic and hydrological boundary conditions can result in significant changes in the steady state stream profile relief and steepness index.

In this model, the hydrological response time, τ, is the sole parameter that influences the streamflow variability independent of the mean daily streamflow. Therefore, it's impact may be over-exaggerated here. However, the impact the response time has on the steady state long river profile is significant, suggesting that the response time should be an important control on streamflow variability and fluvial erosion rates. Rivers with shorter response times will be characterized by rapid streamflow responses to rainfall that have higher peak discharges than rivers with longer response times. In the model, this translates to a higher coefficient of variability, which usually leads to more efficient fluvial erosion. River basins at steady state with short response times should have lower relief and smaller steepness indices than similar river basins with longer response times, all else equal. This is borne out in the first numerical experiment, in which two river basins, identical except for the response time, are evolved to steady state (figure 23).

The river basin with a shorter response time has lower relief and steepness indices, as anticipated (figure 23a and b). It also exhibits a different scaling relationship between the steepness index and erosion rate (figure 23c). This is because the relative erosion threshold is greater than one, which puts the rivers in regime 3 as described by Lague, Hovius, and Davy, (2005) and DiBiase and Whipple, (2011). In this regime the coefficient of variability controls the scaling between steepness index and erosion rate. An interesting consequences of the two different scalings is that for the right set of conditions, the river with the largest steepness index for a given erosion rate could switch. This means that one river would be steeper at low erosion rates, and the other would be steeper at high erosion rates.

Changing the response time from 3 to 6 days, which is well within the observed range (figure 24), results in a factor 3 change in relief (figure 23a). The conditions of the numerical experiment are ideally suited to be influenced by the response time, i.e. the threshold is larger than the mean. However, there is evidence that this is not

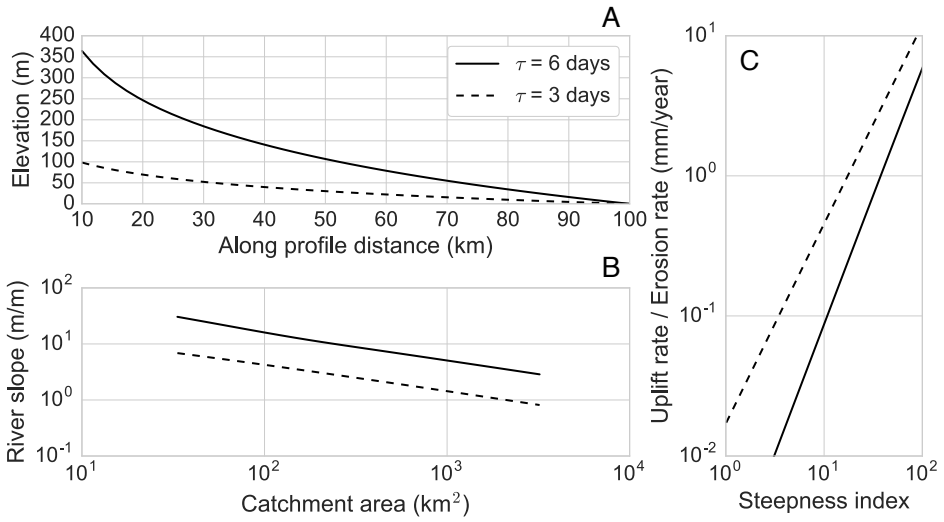

Figure 23: Panel (a) steady state river long profile for short response time (3 days - dashed line) and long response time (6 days - solid line) for an uplift rate of 0.5 mm/year. Panel (b) slope-area relationship associated with long river profiles in panel (a). The concavity is the same for both rivers, but the steepness index is greater for river with longer response time. Panel (c) the relationship between steepness index and erosion rate is nonlinear and different in both cases due to influence of hydrological response time.

uncommon (e.g. Lague, 2014). Thus we conclude that the hydrologic response time, which can be an expression of tectonic history (i.e. fracturing), lithology or basin size, may be an important control on streamflow variability, and by extension, the steady state profile of rivers.

Differences in the aridity index, ϕ, or the effective soil depth, h_s, between basins will have a similar effect as the response time. These nondimensional numbers control the runoff ratio, which influences both the mean and variability of streamflow. We explore this effect here by modifying the soil moisture storage capacity, s_o. However, differences in other controls on the aridity index or effective soil depth, such as the intensity or frequency of rainfall, or the mean evapotranspiration rate should have similar effects. In this numerical experiment, we model three identical river basins, with the exception of s_o, which is 3, 10 and 30 mm. For the chosen conditions this equates to effective soil depths of 0.3, 1 and 3 respectively. The aridity index, $\phi = 4.3$, is the same for all three basins. As a result the difference in soil storage capacity means that the basin with $s_o = 3$ is in the thin, dry soil regime, while the basin with $s_o = 30$ is in the thick, dry soil regime. This has significant consequences for the runoff ratio, resulting in different streamflow means and coefficients of variability between the three basins, and different steady state river profiles (figure 25a). As before, the difference is in the steepness index only, and all rivers have the same concavity index, set by

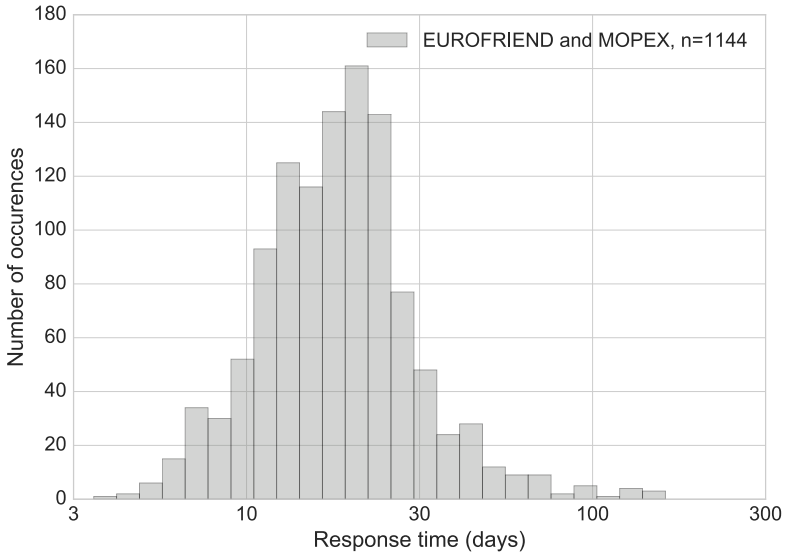

Figure 24: Observed distribution of τ from 1144 rivers, 725 in Europe (Berghuijs, Hartmann, and Woods, 2016) and 419 in the US [Berghuijs, personal communication]. This distribution does not control for river setting, steepness, catchment size, or fraction of snowfall. Regardless, it is clear that the range of the nonlinear hydrological response time, τ, is large.

the ratio of the stream power exponents m and n (figure 25b). Similarly, the scaling of steepness index and erosion rate is also different between the basins, for the same reasons as with the response time experiment (figure 25c).

In the final experiment, we change hydrologic response time progressively along the length of a river as a function of the catchment area. We calibrate the magnitude of the change in the hydrological response time using a data set from the Thur river in Switzerland (Basso, Schirmer, and Botter, 2015), see figure 26a. When the resulting steady state profile is compared to the steady state profile of a river with a constant response time of 5 days, the relief between the two is significantly different, similar to previous experiments. However, in this case, the concavity of the two rivers is also significantly different. This is because the increase in the response time downstream increases the steepness index downstream, resulting in a lower concavity. A similar response is expected when the other climatic and hydrological boundary conditions such as the soil storage capacity or evapotranspiration rate are spatially variable.

3.5.3.3 *The failure to find trends between rainfall rates and erosion rates*

Regional comparisons of mean rainfall rates to longterm erosion rates rarely find significant correlation between the two (e.g. Riebe et al., 2001b; Burbank et al., 2003; Blanckenburg, 2005; Bermudez, van der Beek, and Bernet, 2012; Godard et al., 2014; Acosta et al., 2015). This is perhaps not surprising as there are several confounding factors such as river slope, catchment area, and spatially varying lithology and uplift rate. However, even when controlling for these factors, there is reason to think that rainfall will not be a good predictor of erosion rate. Different ecohydrological conditions can give rise to different fluvial responses to the same climatic forcing, and therefore different longterm erosion rates.

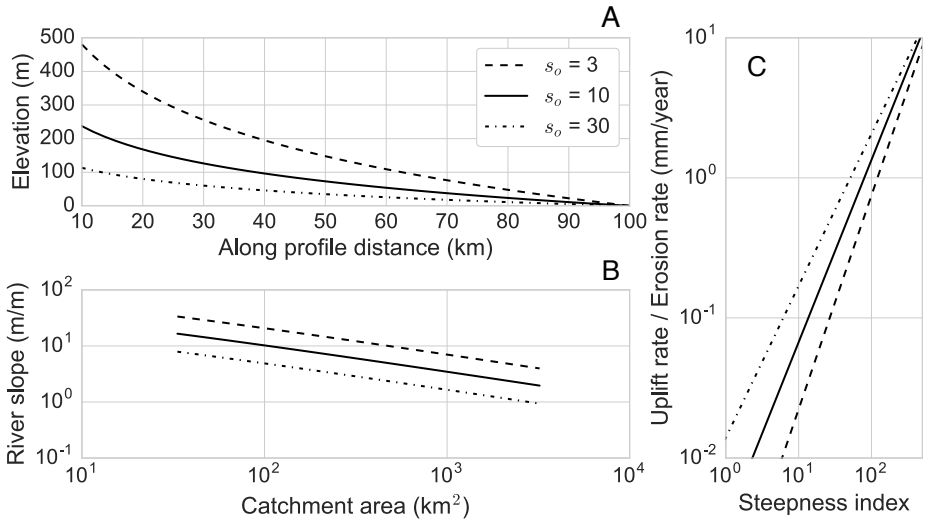

Figure 25: For constant climatic conditions, changes in soil storage capacity, s_o lead to long river profiles of different relief (panel (a)), as well as different steepness indices, (panel (b)), and different scaling relationships between steepness index and erosion rate (panel (c)). This is because the storage capacity influences both the mean and variability of streamflow, which drive erosion efficiency. Here we have changed the storage capacity, but changes in rainfall intensity and frequency or evapotranspiration rates would have a similar effect.

This is demonstrated in figure 27a, which plots the result 2 million Monte Carlo simulations of the longterm erosion rate for a wide range of ecohydrological and climatic conditions. We have shown a small sub-sample of the simulations as black dots. The contours represent the probability distribution of the full two million simulations as a function of rainfall rate and longterm erosion rate. For each simulation, longterm erosion rate is calculated using equation 27 from a random set of values of the climatic and ecohydrological parameters chosen from normal distributions spanning a wide range of reasonable values. The river slope S, catchment area A, erodibility coefficient K, and the exponents n and m were held constant. The longterm erosion rate can be seen to vary significantly (2-6 orders of magnitude) for a given rainfall rate. This is mostly due to variations in streamflow ratio, ω, the streamflow variability (parameterized by b and ν), the erosion threshold, q_{c*}, and the erosion nonlinearity, γ. Figure 27 illustrates how spatially and temporally varying ecohydrological, climatic and channel conditions can obfuscate the relationship between mean rainfall rate and the longterm erosion rate. However, a trend between mean annual rainfall rate and the erosion rate emerges from the Monte Carlo simulations when these important controls are taken into consideration. To show this we selected a set of values for b, ν, ω, q_{c*} and γ. The predicted trend between mean rainfall rate and longterm erosion rate for this set of val-

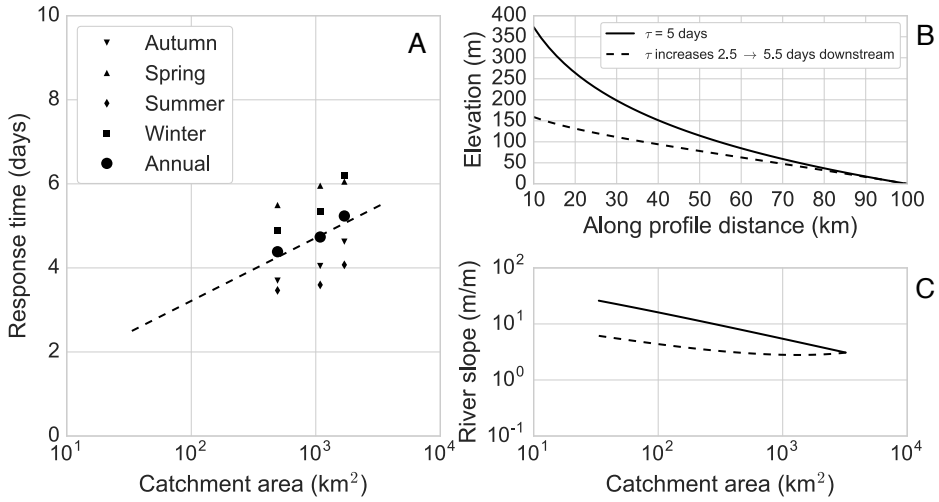

Figure 26: Panel (a) proposed increase of hydrological response time as a function of catchment area from 2.5 days to 5.5 days agrees well with data from Thur river (data from Basso, Schirmer, and Botter, (2015)). Panel (b) long river profile for river with response time of 5 days (solid line) compared to long river profile of river with response time that increase from 2.5 days to 5.5. days downstream (dashed line). Panel (c) slope-area relationships associated with long river profiles in panel (b). The change in response time along the river length as a function of catchment area causes the steepness index to change continuously, leading to a different channel concavity than river with constant response time.

ues is shown as a black line. The river basins that have values for these key parameters within 10% of the selected values are shown as blue points.

Although the predicted trend between mean rainfall rate and longterm erosion rate is as expected (increasing the rainfall rate increases the erosion rate), the general trend of the Monte Carlo simulations is opposite this, with higher probability of lower erosion rates as the mean rainfall rate increases. While it is tempting to conclude that this unexpected trend is robust, i.e. something that would also be observed in nature, that would be premature. The shape of the distribution of Monte Carlo simulations is a function of the chosen distributions of the governing parameters. Here we used normal distributions spanning reasonable ranges, ignoring any correlation between parameters. Our goal was simply to show the significant spread in erosion rates possible for a given rainfall rate. A proper assessment of appropriate distributions for the governing parameters, correlations between them, and the resulting shape of the distribution Monte Carlo simulations, though fascinating, is beyond the scope of this work. We leave it to a future study.

An important caveat to any comparison of mean rainfall rates to longterm erosion rates is that in a steady state landscape - a landscape where the erosion rate approximately balances the uplift rate everywhere - the erosion rate must necessarily be deter-

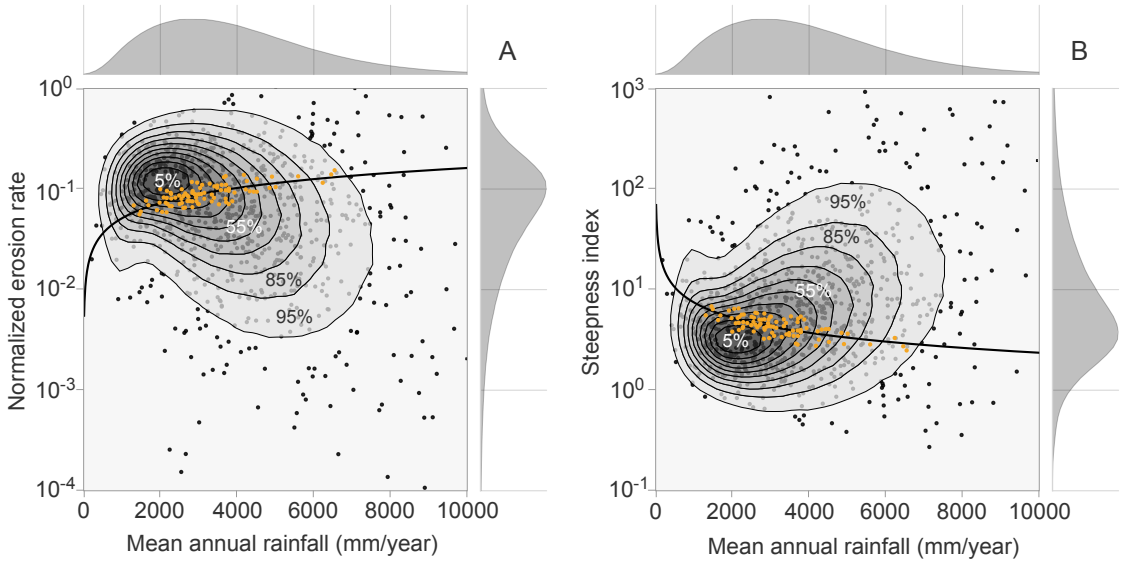

Figure 27: The distribution of two million Monte Carlo simulations of the long-term erosion rate for a wide range of ecohydrological and climatic conditions plotted against (a) normalized erosion rate and (b) steepness index required to achieve an erosion rate of 1 mm/year. Contours encompass given percentage of all simulations, in 10% steps. Additionally, we have shown a small sub-sample of the simulations as black dots. The trend of the normalized erosion rate or steepness index for a selected set of ecohydroclimatic parameters according to equation 27 is shown as black lines in (a) and (b), the simulations with parameters falling with $\pm 10\%$ of the selected set are shown as yellow points.

mined by the uplift rate (i.e. tectonics). This decouples mean rainfall rates and mean erosion rates in a landscape. However, the influence of climate should still manifest itself in the shape of the landscape, with higher uplift rates or weaker climatic forcing giving rise to generally steeper landscapes, all else equal. The channel steepness index takes this the landscape form into account, and can be used as a measure of erosional efficiency even in steady state landscapes. The erosional efficiency is in part determined by lithology, but must also contain information about the strength of the climatic forcing.

In general, comparisons of the steepness index against longterm erosion rates yield much clearer trends than rainfall rates (Wobus et al., 2006; DiBiase et al., 2010; DiBiase and Whipple, 2011). However, they still exhibit considerable spread. Spatially varying lithologies can be responsible for this spread, but, similar to figure 27a, 27b shows how spatial variation of b, ν, ω, q_{c*} and γ can also cause this spread. Figure 27b shows the steepness index required to erode one mm/year based on the erosional efficiency of the river basins in the Monte Carlo simution. As the erosional efficiency is determined by streamflow mean and variability and the erosion threshold, etc. (the erodibility coefficient K is held constant) we see a similar story as with the mean erosion rate. For a given mean annual rainfall rate, ecohydrology and erosion thresholds intervene to produce a wide range (upwards of four orders of magnitude) of steepness indices. The probability of a low steepness index is higher for moderate to low mean annual rainfall rates, as with 27a, and we urge the same caution in interpreting this trend.

Figure 27 suggests that it should be expected that comparisons of mean rainfall rate, specific stream power or channel steepness index against the longterm erosion rate over large regions of the Earth do not yield a clear relationship, even when the

landscape is expected to be at steady state and the spatial distribution of uplift rate is known and accounted for. The implication is that the failure of many studies to find regional trends in erosion rate correlated to mean rainfall rate or stream power does not necessarily point to a dominance of tectonics over climate. It may simply reflect the fact that not nearly all of the important factors determining how rainfall drives erosion in a fluvially dominated landscape have been taken into account.

3.5.4 *Outstanding issues and limitations*

3.5.4.1 *The erosion threshold*

In this study we have parameterized the erosion threshold using q_{c*}, and treated it as an independent parameter. However, the concept of a simple erosion threshold for fluvial erosion hides a much more complex relationship between sediment transport dynamics, river streamflow, and fluvial bedrock erosion. Adding this complexity by including a model for q_{c*} that depends on slope, grain size and channel hydraulics or by replacing equation 17 with one that accounts more explicitly for channel hydraulics and sediment transport is an important step to understand the influence of climate on fluvial erosion across a range of timescales. Also important are empirical investigations into what determines the erosion threshold in bedrock mountainous rivers, and how it evolves with changing climate and landscape. As suggested by Phillips and Jerolmack, (2016), the behavior of q_{c*} might be quite different than has been expected.

3.5.4.2 *Climate nonstationarity*

In this study we have chosen daily rainfall to represent the variability in climate and study how it affects mean erosion rate which evolves over much longer timescales. The difference in timescales between the forcing (rainfall) and the response (erosion) is very large. While a stochastic approach is useful to upscale these daily processes to landscape evolution timescales, it assumes that the climatic and ecohydrological conditions are stationary - that they do not change over long periods of time. However, it is clear that climate does in general change consistently over periods as short as decades to centuries. Some of the key parameters, such as the streamflow ratio ω, streamflow variability ν and recession exponent b are relatively straightforward to measure in present day basins, but it raises the important question of whether or not these values have any meaning over geological time.

3.5.4.3 *Catchment-scale parameters*

The model presented here is purposely minimalistic. It reflects an effort to simply capture the key behaviors of complex nonlinear systems while retaining low dimensionality. A result of this is that the presented framework makes use of spatially integrated catchment-scale parameters, with the implicit assumption that that a single value can be used to represent spatially heterogeneous local, or point-scale, parameters. This produces a challenge. It is not always clear how the behavior at the point-scale relates to a catchment-scale parameter. For example, although the mean rainfall rate at the catchment-scale is simply the arithmetic mean of the point-scale mean rainfall rates, the same is not true for the mean storm depth or the mean storm frequency. An understanding of how the point-scale parameters relate to the catchment-scale parameters,

either empirical or theoretical, is needed to extend this work to 2D or 3D landscape evolution models.

[It is worth noting, however, that the specific storm depth, α, is not necessarily the same as the mean storm depth that would be measured at a point. There are often scaling effects that can cause the point-scale value and the catchment-scale specific value to differ. In the case of rainfall, for α to be equal to the point-scale storm depth requires uniform rainfall across the catchment, which is usually not the case. Thus, in general, and for the majority of parameters discussed in this work, the point-scale value and the catchment-scale specific value will differ.]

3.5.4.4 *Heavy tailed rainfall*

There are three important statistical characteristics of daily rainfall in the context of fluvial erosion rates. The mean storm depth, the mean storm frequency and the heaviness of the tail of the distribution of rainfall. In this work, we use an exponential distribution for daily rainfall that prohibits exploring the effects of a heavier tail. The exponential distribution is known to be imperfect for modelling daily distributions of storm depths, because it is often lighter tailed than empirical rainfall distributions. However, the stochastic nature of rainfall is still captured, with the exponential distribution approximating the strongly right skewed magnitude-frequency structure observed in nature while exhibiting the key memoryless property that makes it analytically tractable. It has been shown that there are no true analytical solutions for the probability distribution of soil moisture, and therefore for the probability distributions of daily streamflow and erosion for other functions commonly used to represent daily rainfall, such as the gamma distribution (Verma, Yeates, and Daly, 2011).

Müller, Dralle, and Thompson, (2014) tested numerically the error in the estimated distribution of daily streamflow produced by using an exponential distribution to represent rainfall, and found it to be a poor assumption only in the case of heavy tailed storm depth distributions (gamma shape parameter < 0.5) . While there is some evidence that the heaviness of the tail of rainfall is important in arid regions (Daly and Porporato, 2010; Müller, Dralle, and Thompson, 2014), Rossi, Whipple, and Vivoni, (2016) presented an empirical analysis that suggests it is only a secondary control on the distribution of daily streamflow. We feel that the uncertainties in other parts of the derivation, mainly the streamflow-erosion relation preclude the need to focus on the details of rainfall. The fact that the exponential model of storm depths captures the highly right skewed nature of rainfall distributions is sufficient. Additionally we find the benefits of analytical solutions make the exponential distribution a worthwhile choice for daily storm depth.

3.5.4.5 *Limitations of the stream power approach*

The stream power approach used in this study is limited in that it does not allow for sediment transport dynamics to be modelled at all, and does not work well on short timescales (Beer and Turowski, 2015). The hydrological model outlined above could be integrated with a more sophisticated model of fluvial erosion. However the stream power approach remains popular because it successfully predicts many aspects of the steady state long river profile (Lague, 2014). Further, as pointed out by DiBiase and Whipple, (2011) at steady state it is not possible to distinguish between the stream power model and sediment transport driven models. We have chosen to use the stream

power approach because its simplicity enhances clarity in an already complex analysis, which is useful for a first step. It also allows us to compare our results with previous results and provides a standard for future analysis using a more sophisticated erosion model.

3.5.5 *Significance and Future work*

A very early example of the application of stochastic concepts to the problems of fluvial erosion appears in Wolman and Miller, (1960) wherein they discuss the relative importance of moderate versus extreme events. Free from the constraints of a quantitative approach, they offer a sophisticated qualitative analysis of the roles of erosion thresholds and stochastic forcing in setting the pace and style of landscape evolution. Among their conclusions is the realization that the relative importance of extreme events will be heavily influenced by the nature and magnitude of the erosion threshold. More than 50 years later, we reach the same conclusion.

With the application of the latest stochastic hydrology model, we find that to understand the importance of variability and the role of extreme events we must know more about the threshold streamflow and how it evolves with the landscape. This leads to two paths of future research. The first is to apply the stochastic streamflow distributions to a more physically realistic model of fluvial erosion than the stream power law in order to estimate the erosion threshold based on measurable channel properties. The second is an empirical investigation into what controls the erosion threshold and how it evolves with changing boundary conditions.

One of the main strengths of integrating hydrology into the stream power model is to reveal the dependence of both streamflow mean and variability on the climatic forcing and ecohydrological response. The anticorrelation of the mean and variability vastly restricts the likely responses of a river basin to changing climate and must therefore guide our understanding. The ecohydrological aspect of this relationship (parameterized by ω) has a heavy biotic influence which is partly determined by the landscape setting and climate and will respond to changes in both. Furthermore the hydrologic response timescale τ and recession exponent b have been shown to be influenced to some degree by catchment vegetation and soil type (Berghuijs et al., 2014). This framework can be used as a foundation for a holistic landscape evolution model exploring the coevolution of climate, ecology, hydrology and geomorphology as called for by Istanbulluoglu, (2009). The inclusion of climate, ecology and hydrology into landscape evolution models may at first seem like a dauntingly large and complex parameter space, however it is possible that the interdependence of the different processes on one another may yield a relatively restricted realistic parameter space similar to what we demonstrated between streamflow mean and variability.

3.6 CONCLUSIONS

We have developed a theoretical framework for the longterm erosion rate based on a stochastic-mechanistic model of hydrology in the context of the stream power incision model. This theory points to seven important controls: 1) the statistics of rainfall, described by the mean storm depth α and frequency λ, 2) soil and vegetation dynamics which interact with rainfall to drive streamflow, described here by aridity index ϕ, the effective soil storage capacity h_s and the streamflow ratio ω, 3) basin response to input

described by the hydrological response time τ and the nonlinearity of the response b to forcing, 4) the maximum streamflow ever seen by the system, q_{m*}, 5) the erosion threshold, q_{c*}, 6) the nonlinearity of the daily streamflow-erosion relationship, γ, and 7) the stream power parameters (the exponents m and n, the erodibility coefficient K, and the river slope S). The first four controls determine the distribution of daily streamflow (essentially by setting μ, ν and b), and the last three controls determine how that distribution of streamflow relates to the distribution of daily erosion and the mean longterm erosion rate. This highlights the two necessary aspects of any climate driven fluvial erosion model, a model for how rainfall translates into streamflow, and a model for how streamflow drives fluvial erosion. The framework presented here allows for a large range of daily streamflow regimes and makes use of a general daily streamflow-erosion law (a power law with a threshold and an exponent that can be less than or greater than one). Therefore, we expect that the main conclusions laid out here will generally apply, even when compared to models with more sophisticated hydrological or streamflow-erosion laws.

We defined a coefficient of daily streamflow variability that it is applicable to a wide range of hydrological regimes and established that it has a solid physical basis. We also provided a theoretical basis for how it is anticorrelated with the mean daily streamflow, a long observed relationship which is useful for determining the erosional response to changing climate in a threshold-stochastic stream power context. Furthermore, by using the hydrological model to relate both the mean and variability of streamflow to the climatic and ecohydrological boundary conditions we show how fluvial erosion responds to realistic climatic forcing. This allows for direct comparison to meteorological, hydrological and geomorphological observations.

The erosion threshold, parameterized as q_{c*} emerged as a major unknown with an influence on how the longterm erosion rate responds to climate. In particular it is vital in determining the sensitivity of the longterm erosion rate to the mean streamflow magnitude, which may not be as important as previously thought.

Finally we demonstrated that the ecohydrological conditions in a river basin and the stochastic-threshold nature of the streamflow-erosion relationship can cause the longterm erosion rate to vary over several orders of magnitude for a given mean annual rainfall or streamflow rate. Since these effects have generally not been taken into account in studies comparing measured rainfall or streamflow rates with measured erosion rates, the failure to find a dependence of the erosion rate on rainfall rates does not necessarily imply that climate is not an important control on erosion rates and landscape evolution.

3.7 APPENDIX A: DISTRIBUTION OF DAILY STREAMFLOW WHEN $b = 2$

Botter et al., (2009) showed that the pdf of q is,

$$f_Q(q) = C\frac{dr(q)/dq}{q}\exp\left[-\frac{r(q)}{\alpha} + \omega\lambda\int g(r(q))^{-1}dr(q)\right] + p_o\delta(q), \tag{28}$$

where C is a normalising constant, $p_o\delta(q)$ is an atom of probability that $q = 0$, $g(x)$ is the storage loss function $q = g(W)$ and $r(q)$ is its inverse,

$$W = g^{-1}(q) = r(q). \tag{29}$$

To find $r(q)$ in the case $b = 2$, we start with,

$$\frac{dq}{dt} = -aq^2. \tag{30}$$

We also note that due to conservation of mass, the storage term W will change over time as,

$$\frac{dW}{dt} = -q. \tag{31}$$

Integrating both 30 and 31, it is straightforward to show that (with the assumption that $q(0) = 0$),

$$q(t) = (at)^{-1} \tag{32}$$

and,

$$W(t) = -\frac{1}{a}\ln(t) + c. \tag{33}$$

Inverting 32 and substituting it into 33 leads to,

$$r(q) = \frac{1}{a}\ln(cq), \tag{34}$$

where c is some constant. Putting $r(q)$ into the general solution for the pdf of daily stream flow (equation 28) we find that for $b = 2$,

$$f_Q(q) = \frac{(\omega\lambda/a)^{1/\alpha a+1}}{\Gamma(1/\alpha a + 1)}\, q^{-1/\alpha a-2} \exp\left[-\omega\lambda/aq\right], \tag{35}$$

which is an inverse gamma function equivalent to equation 13 when the substitution $a = \mu^{1-b}/\tau$ is made.

3.8 APPENDIX B: ANALYTICAL APPROXIMATIONS FOR C

We can rewrite the general distribution of daily streamflow (equation 14) as,

$$f_{Q_*}(q_*) = Cq_*^{-b}\, e^{-k_1 q_*^{1-b}} e^{k_2 q_*^{2-b}} \tag{36}$$

where $k_1 = k/(b-1)$ and $k_2 = k/(b-2)$. To find C, we need to integrate from o to ∞,

$$C = \left[\int_0^\infty q_*^{-b}\, e^{-k_1 q_*^{1-b}} e^{k_2 q_*^{2-b}} dq_*\right]^{-1} \tag{37}$$

If we make the substitution $t = x^{1-b}$ and $dt = (1-b)x^{-b}dx$,

$$C = \frac{(1-b)}{\int_0^\infty e^{k_2 t^\phi} e^{-k_1 t} dt} \tag{38}$$

where $\phi = -k_1/k_2 = (2-b)/(1-b)$. This is equivalent to the laplace transform of the first term of the integrand,

$$C = \frac{(1-b)}{\mathcal{L}\{e^{k_2 t^\phi}\}(k_1)}. \tag{39}$$

This is the laplace transform of a stretched exponential, and it is known that there is no analytical solution, though some approximations and fast numerical algorithms exist. We offer one approximation, valid only for $1 < b < 2$, arrived at by noting the similarity between equations 12, 13 and 14, and by taking advantage of the known normalizing factors from equations 12 and 13,

$$C = \left(\frac{2\pi(2-b)(b-1)}{\mu^2 k}\right)^{1/2} \frac{(k/(2-b))^{k/(2-b)}}{\Gamma(k/(2-b))} \frac{k/(b-1)^{k/(b-1)}}{\Gamma(k/(b-1))} \tag{40}$$

This approximation has very low error when $k > 1$. When $k < 1$, the error is low when b is close to 1 or 2, and reaches a maximum when $b = 1.5$. The error reaches about 50% for $b = 1.5$ when $k = 0.01$.

3.9 APPENDIX C: CHANNEL HYDRAULICS

A common starting point for derivations of the stream power model is (Tucker, 2004; Lague, Hovius, and Davy, 2005),

$$\varepsilon = k_e(\tau_s^c - \tau_c^c), \quad \tau_s > \tau_c, \tag{41}$$

which relates the daily fluvial incision rate ε to the excess shear stress on the riverbed. In order to make use of the distribution of daily streamflow, it is necessary to relate the streamflow to the shear stress it exerts. To do this we use the derivation of Lague, Hovius, and Davy, (2005) to relate the shear stress exerted on the riverbed to the flow depth (approximated by the streamflow q divided by the river width) and the riverbed slope using a formulation equivilant to the Manning or Darcy-Weisbach equation, depending on the values for α_t and β_t,

$$\tau_s = k_t \left(\frac{q}{w}\right)^{\alpha_t} S^{\beta_t} \tag{42}$$

where w is the channel width, S is the riverbed slope, and k_t is a factor accounting for acceleration of gravity, density of water and a friction factor. This implies that what we need to know in order to estimate the shear stress τ_s from the distribution of streamflow is the relationship between stage (the height of water surface) and streamflow. Lague, Hovius, and Davy, (2005) accomplish this with two empirical relations. First they describe how the width of the river at one location on the river changes relative to a benchmark width - e.g. bankfull width or mean streamflow width - with daily variations in streamflow,

$$\frac{w}{w_a} = \left(\frac{q}{\mu}\right)^{\omega_s} \tag{43}$$

where w_a is the benchmark width. This amounts to describing the cross sectional profile of the channel. Different shapes can be described by changing the value of ω_s. Lague, Hovius, and Davy, (2005) then describe how the benchmark width of the river increases with increasing $\langle Q \rangle$ downstream as a power law,

$$w_a = k_w \langle Q \rangle^{\omega_a} \tag{44}$$

where k_w and ω_a are empirically derived constants.

Substituting equations 42, 43 and 44 into 41 leads to equation 18 which describes the daily erosion rate in terms of daily streamflow and river slope.

$$\varepsilon = K\langle Q\rangle^{m} S^{n} q_*^{\gamma} - \Psi, \quad q > q_c \tag{45}$$

where $K = k_e k_t^c k_w^{c\alpha_t}$, $m = c\alpha_t(1-\omega_a)$, $n = c\beta_t$, $\gamma = c\alpha_s(1-\omega_s)$, and $\Psi = k_e \tau_c^c$ (Lague, Hovius, and Davy, 2005).

3.10 APPENDIX D: LONG-TERM EROSION RATE

3.10.1 *pdf of daily erosion*

We start with the distributions of streamflow for $b = 1$,

$$f_{Q_*}(q_*) = \frac{k^k}{\Gamma(k)} q_*^{k-1} \exp[-kq_*] \tag{46}$$

$b = 2$,

$$f_{Q_*}(q_*) = \frac{k^k}{\Gamma(k)} q_*^{-k-2} \exp\left[-kq_*^{-1}\right] \tag{47}$$

and $b \neq 1, 2$,

$$f_{Q_*}(q_*) = C\, q_*^{-b} \exp\left[-k\left(\frac{q_*^{2-b}}{2-b} - \frac{q_*^{1-b}}{1-b}\right)\right] \tag{48}$$

Imposing a maximum observed daily streamflow q_{m*} and a erosion threshold q_{c*} truncates the pdf above q_{m*} and below q_{c*} and requires that the pdf be renormalized such that $\int_{q_{c*}}^{q_{m*}} f_{Q_*}(q_*)dq_* = 1$. This leads to a new distribution $f^t_{Q_*}(q_*)$,

$$f^t_{Q_*}(q_*) = \begin{cases} 0 & q_* < q_{c*} \\ C f_{Q_*}(q_*) & q_{c*} \leqslant q_* \leqslant q_{m*} \\ 0 & q_* > q_{m*} \end{cases}, \tag{49}$$

where C is a normalising constant. We can find this constant by integrating $f^t_{Q_*}(q_*)$:

$$\int_0^\infty f^t_{Q_*}(q_*)dq_* = \int_0^{q_{c*}} 0\, dq_* + C\int_{q_{c*}}^{q_*} f_{Q_*}(q_*)dq_* + \int_{q_{m*}}^\infty 0\, dq_* = 1 \tag{50}$$

which leads to in the case $b = 1$,

$$C = [\Gamma(k,\, kq_{c*}) - \Gamma(k,\, kq_{m*})]^{-1} \tag{51}$$

and in the case $b = 2$,

$$C = [\Gamma(k+1,\, k/q_{m*}) - \Gamma(k+1,\, k/q_{c*})]^{-1} \tag{52}$$

where $\Gamma(a, x)$ is the regularised upper incomplete gamma function.

The effect of a threshold at $q_* = q_{c*}$ is different than truncating the pdf because we gather the probability of $q_* < q_{c*}$ into an atom of probability in the pdf of ε at $\varepsilon = 0$. This atom of probability is equal to $\Pr[q_* < q_{c*}]$. We define this atom of probability as $1 - \lambda_\varepsilon$. The probability that an erosion event occurs then is λ_ε, defined in the text.

If we assume a relationship between daily incision ε and daily streamflow q of the form $\varepsilon = g(q)$, then we can calculate the pdf of daily incision as a simple change of variable,

$$f_E(\varepsilon) = f_Q(g^{-1}(\varepsilon))\frac{dq}{d\varepsilon} \tag{53}$$

So then the overall pdf of ε is composed of three parts. First the atom of probability at $\varepsilon = 0$, second the truncated probability distribution of $q > q_c$ as a function of ε, and finally 0 for all values of ε corresponding to $q > q_m$ because the probability of $q > q_m$ is also 0:

$$f_E(\varepsilon) = \begin{cases} 1-\lambda_\varepsilon & \varepsilon = 0 \\ \lambda_\varepsilon f_Q^t(g^{-1}(\varepsilon)) & 0 < \varepsilon \leqslant \varepsilon_m \\ 0 & \varepsilon > \varepsilon_m \end{cases}, \tag{54}$$

where $\varepsilon_m = \varepsilon(q_m)$. If we want to use the pdf of daily incision to calculate the long-term erosion rate, we simply calculate the mean incision rate:

$$\langle E \rangle = \int_0^\infty \varepsilon\, f_E(\varepsilon) d\varepsilon \tag{55}$$

Which, using the definition of $f_E(\varepsilon)$ breaks down into:

$$\langle E \rangle = \varepsilon(q_c)\,(1-\lambda_\varepsilon) + \int_0^{\varepsilon_m} \varepsilon\, \lambda_\varepsilon f_E^t(\varepsilon) d\varepsilon + \int_{\varepsilon_m}^\infty \varepsilon\, 0\, d\varepsilon \tag{56}$$

Where $\varepsilon(q_c) = 0$. This reduces to:

$$\langle E \rangle = \lambda_\varepsilon \int_0^{\varepsilon_m} \varepsilon\, f_Q^t(g^{-1}(\varepsilon))\frac{dq}{d\varepsilon} d\varepsilon \tag{57}$$

This is functionally equivalent to the approach of Tucker and Bras, (2000), Lague, Hovius, and Davy, (2005), Huang and Niemann, (2006a), and DiBiase and Whipple, (2011). We integrate over the magnitude of daily incision as a function of streamflow prorated by the probability of observing a particular streamflow magnitude,

$$\langle E \rangle = \int_{q_c}^{q_m} \varepsilon(q)\, f_Q^t(q) dq \tag{58}$$

except we keep explicit track of the effects of the erosion threshold and streamflow distribution on the frequency of erosion (λ_ε) and the magnitude of daily erosion (expressed by the pdf of ε).

The function $g^{-1}(\varepsilon)$ can be found from daily incision as a function of daily streamflow as derived by Lague, Hovius, and Davy, (2005),

$$\varepsilon = K\langle Q \rangle^m S^n q_*^\gamma - \Psi \tag{59}$$

where K is a complex erodibility coefficient, m, n, and γ exponents defined in Lague, Hovius, and Davy, (2005) and Ψ is the threshold of erosion. It can easily be shown $\Psi = K\langle Q \rangle^m S^n q_{c*}^\gamma$, which, if we set $\varepsilon_o = K\langle Q \rangle^m S^n$ (a constant w.r.t. q) reduces daily incision to:

$$\varepsilon = g(q) = \varepsilon_o q_*^\gamma - \Psi_c = \varepsilon_o(q_*^\gamma - q_{c*}^\gamma), \tag{60}$$

where $q_* = q/\mu$. The inverse is then,

$$g^{-1}(\varepsilon) = \left(\frac{\varepsilon + \Psi}{\varepsilon_o \mu^{-\gamma}}\right)^{1/\gamma} \tag{61}$$

and then

$$\frac{dq}{d\varepsilon} = \frac{(\varepsilon + \Psi)^{1/\gamma - 1}}{\gamma \varepsilon_o^{1/\gamma} \mu^{-1}} \tag{62}$$

Recalling,

$$f_E(\varepsilon) = f_Q^t\left(g^{-1}(\varepsilon)\right) \frac{dq}{d\varepsilon} \tag{63}$$

We arrive at the pdf of daily erosion by substituting equations 61 and 62 into 63, choosing the appropriate form of $f_Q^t(q)$ (equations 46-48). In the case $b = 1$,

$$f_E(\varepsilon) = \frac{(\varepsilon + \Psi)^{k/\gamma - 1}}{\Gamma_\varepsilon \gamma (\varepsilon_o k^{-\gamma})^{k/\gamma}} \exp\left[-\left(\frac{\varepsilon + \Psi}{\varepsilon_o k^{-\gamma}}\right)^{1/\gamma}\right] \tag{64}$$

where $\Gamma_\varepsilon = \Gamma(k)[\Gamma(k, kq_{c*}) - \Gamma(k, kq_{m*})]$.

In the case $b = 2$,

$$f_E(\varepsilon) = \frac{(\varepsilon + \Psi)^{-(k+1)/\gamma - 1}}{\Gamma_\varepsilon \gamma (\varepsilon_o k^{\gamma})^{-(k+1)/\gamma}} \exp\left[-\left(\frac{\varepsilon + \Psi}{\varepsilon_o k^{\gamma}}\right)^{-1/\gamma}\right] \tag{65}$$

where $\Gamma_\varepsilon = \Gamma(k+1)[\Gamma(k+1, k/q_{m*}) - \Gamma(k+1, k/q_{c*})]$.

In the case $b \neq 1, 2$,

$$\begin{aligned} f_E(\varepsilon) = C_\varepsilon & \frac{(\varepsilon + \Psi)^{(1-b)/\gamma - 1}}{\varepsilon_o^{(1-b)/\gamma}} \times \\ & \exp\left[-k\left(\frac{(\varepsilon + \Psi)^{(2-b)/\gamma}}{(2-b)\varepsilon_o^{(2-b)/\gamma}} - \frac{(\varepsilon + \Psi)^{(1-b)/\gamma}}{(1-b)\varepsilon_o^{(1-b)/\gamma}}\right)\right] \end{aligned} \tag{66}$$

3.10.2 *long-term erosion rate*

Before we solve the mean erosion intensity, it is useful to show two identities. First we define a new variable ε_*.

$$\varepsilon_* = \frac{\varepsilon + \Psi}{\varepsilon_o}. \tag{67}$$

If we substitute x into the pdf of daily erosion, where, in the case $b = 1$,

$$x = k\varepsilon_*^{1/\gamma}, \tag{68}$$

it can be shown that,

$$f_E(\varepsilon) = \frac{-x^{k-1}}{\Gamma_\varepsilon} e^{-x}, \tag{69}$$

and

$$k^\gamma \varepsilon_* f_E(\varepsilon) = \frac{-x^{k+\gamma-1}}{\Gamma_\varepsilon} e^{-x}. \tag{70}$$

Similarly, in the case $b = 2$ if,

$$x = k\varepsilon_*^{-1/\gamma}, \tag{71}$$

then,

$$f_E(\varepsilon) = \frac{-x^k}{\Gamma_\varepsilon} e^{-x}, \tag{72}$$

and

$$k^{-\gamma}\varepsilon_* f_E(\varepsilon) = \frac{-x^{k-\gamma}}{\Gamma_\varepsilon} e^{-x}. \tag{73}$$

To solve for the mean erosion intensity in the case $b = 1$,

$$\bar{E} = \int_0^{\varepsilon_m} \varepsilon\, f_E^t(\varepsilon) d\varepsilon \tag{74}$$

we multiply by $\varepsilon_o k^{-\gamma}/\varepsilon_o k^{-\gamma}$ and add and subtract the same term,

$$\begin{aligned} \bar{E} = {} & \varepsilon_o k^{-\gamma} \int_0^{\varepsilon_m} \frac{\varepsilon}{\varepsilon_o k^{-\gamma}} f_E^t(\varepsilon) d\varepsilon \\ & + \varepsilon_o k^{-\gamma} \int_0^{\varepsilon_m} \frac{\Psi}{\varepsilon_o k^{-\gamma}} f_E^t(\varepsilon) d\varepsilon \\ & - \varepsilon_o k^{-\gamma} \int_0^{\varepsilon_m} \frac{\Psi}{\varepsilon_o k^{-\gamma}} f_E^t(\varepsilon) d\varepsilon \end{aligned} \tag{75}$$

Which becomes,

$$\bar{E} = \varepsilon_o k^{-\gamma} \int_0^{\varepsilon_m} k^\gamma \varepsilon_*\, f_E^t(\varepsilon) d\varepsilon - \Psi \int_0^{\varepsilon_m} f_E^t(\varepsilon) d\varepsilon. \tag{76}$$

Making use of our identities we can write:

$$\bar{E} = \frac{-\varepsilon_o k^{-\gamma}}{\Gamma_\varepsilon} \int_{x_c}^{x_m} x^{k+\gamma-1} e^{-x} dx - \frac{-\Psi}{\Gamma_\varepsilon} \int_{x_c}^{x_m} x^{k-1} e^{-x} dx \tag{77}$$

Where $x_c = kq_{c*}$, and $x_m = kq_{m*}$. We complete the solution using the following relationship derived from the definition of the incomplete gamma function:

$$\begin{aligned} \int_\alpha^\beta x^{s-1} e^{-x} dx &= \int_0^\beta x^{s-1} e^{-x} dx - \int_0^\alpha x^{s-1} e^{-x} dx \\ &= \Gamma(s)\left[\Gamma(s,\alpha) - \Gamma(s,\beta)\right] \end{aligned} \tag{78}$$

Therefore the analytical solution for the mean erosion intensity is,

$$\begin{aligned} \bar{E} = {} & \frac{\varepsilon_o k^{-\gamma}\Gamma(k+\gamma)}{\Gamma_\varepsilon}\left[\Gamma(k+\gamma, kq_{c*}) - \Gamma(k+\gamma, kq_{m*})\right] \\ & - \frac{\Psi\Gamma(k)}{\Gamma_\varepsilon}\left[\Gamma(k, kq_{c*}) - \Gamma(k, kq_{m*})\right] \end{aligned} \tag{79}$$

Recalling that $\Gamma_\varepsilon = \Gamma(k)[\Gamma(k, kq_{c*}) - \Gamma(k, kq_{m*})]$ 79 can be rewritten as,

$$\begin{aligned} \bar{E} &= \varepsilon_o \left[\frac{\Gamma(k+\gamma)}{\Gamma(k)k^\gamma}\left(\frac{\Gamma(k+\gamma, kq_{c*}) - \Gamma(k+\gamma, kq_{m*})}{\Gamma(k, kq_{c*}) - \Gamma(k, kq_{m*})}\right) - q_{c*}^\gamma\right] \\ &= \varepsilon_o \psi \end{aligned} \tag{80}$$

In the case the $b = 2$ we follow the same steps to find that,

$$\begin{aligned}\bar{E} = &\frac{\varepsilon_o k^\gamma \Gamma(k+1-\gamma)}{\Gamma_\varepsilon}\left[\Gamma(k+1-\gamma, k/q_{m*}) - \Gamma(k+1-\gamma, k/q_{c*})\right] \\ &-\frac{\Psi\Gamma(k+1)}{\Gamma_\varepsilon}\left[\Gamma(k+1, k/q_{m*}) - \Gamma(k+1, k/q_{c*})\right]\end{aligned} \tag{81}$$

Recalling again that here $\Gamma_\varepsilon = \Gamma(k+1)[\Gamma(k+1, k/q_{m*}) - \Gamma(k+1, k/q_{c*}]$ 81 can be rewritten as,

$$\begin{aligned}\bar{E} &= \varepsilon_o\left[\frac{\Gamma(k+1-\gamma)}{\Gamma(k)k^{1-\gamma}}\left(\frac{\Gamma(k+1-\gamma, k/q_{m*}) - \Gamma(k+1-\gamma, k/q_{c*})}{\Gamma(k+1, k/q_{m*}) - \Gamma(k+1, k/q_{c*})}\right) - q_{c*}^\gamma\right] \\ &= \varepsilon_o\psi\end{aligned} \tag{82}$$

The mean long-term erosion rate is,

$$\langle E\rangle = \lambda_\varepsilon \bar{E} = \lambda_\varepsilon \psi \varepsilon_o \tag{83}$$

3.11 APPENDIX E: IMPORTANCE OF LARGE FLOODS

In order to calculate the frequency of occurrence of the largest erosion events responsible for some fraction x of the total erosion rate, we must find a streamflow q_x such that:

$$\int_{q_x}^{q_m} f_E(\varepsilon)d\varepsilon = x\int_{q_c}^{q_m} f_E(\varepsilon)d\varepsilon \tag{84}$$

where x is the fraction of total erosion taking place above the streamflow magnitude q_x This is equal to

$$\frac{\int_{q_c}^{q_x} f_E(\varepsilon)d\varepsilon}{\bar{E}} = 1 - x \tag{85}$$

Which becomes

$$x = 1 - \frac{\psi_x}{\psi} \tag{86}$$

where

$$\psi_x = \begin{cases} \frac{\Gamma(k+\gamma)}{\Gamma(k)k^\gamma}\left(\frac{\Gamma(k+\gamma, kq_{c*}) - \Gamma(k+\gamma, kq_{x*})}{\Gamma(k, kq_{c*}) - \Gamma(k, kq_{x*})}\right) - q_{c*}^\gamma & ; b = 1 \\ \frac{\Gamma(k+1-\gamma)}{\Gamma(k)k^{1-\gamma}}\left(\frac{\Gamma(k+1-\gamma, k/q_{x*}) - \Gamma(k+1-\gamma, k/q_{c*})}{\Gamma(k+1, k/q_{x*}) - \Gamma(k+1, k/q_{c*})}\right) - q_{c*}^\gamma & ; b = 2 \end{cases} \tag{87}$$

We find numerically the value for q_{x*} that satisfies equation 86. The frequency of the largest erosion events responsible for the fraction x of the total erosion rate is then simply the probability of daily streamflow to be above q_{x*},

$$\begin{aligned}\Pr[q_* \geqslant q_{x*}] &= \int_{q_{x*}}^{\infty} f_{Q_*}^t(q_*)dq_* \\ &= \begin{cases} \frac{\Gamma(k, kq_{x*}) - \Gamma(k, kq_{m*})}{1 - \Gamma(k, kq_{m*})} & ; b = 1 \\ \frac{\Gamma(k+1, k/q_{m*}) - \Gamma(k+1, k/q_{x*})}{\Gamma(k+1, k/q_{m*})} & ; b = 2 \end{cases}\end{aligned} \tag{88}$$

4

NEGATIVE CORRELATION BETWEEN MEAN AND VARIABILITY OF DISCHARGE

4.1 ABSTRACT

Hydrology will always be ruled by local conditions, making it difficult to make global predictions of the impact of climate change on the behavior of streams and rivers. Despite this, some general patterns can be observed everywhere, such as the observation that river discharge increases after a rainstorm, and rivers get larger as their catchments get larger. Another pattern commonly observed is that fluctuations in streamflow are more dramatic when the average streamflow is less. The first two truisms have well established explanations, the third less so. Here we demonstrate that an understanding of how certain aspects of the hydrograph determine the long-term statistical features of streamflow explains how mean streamflow is negatively correlated with its variance.

4.2 INTRODUCTION

It has long been observed that rivers with high runoff exhibit lower variability in daily flows than rivers with low runoff (Wolman and Miller, 1960; Molnar et al., 2006; Lague, 2014; Rossi, Whipple, and Vivoni, 2016). This is in part due to the fact that larger catchments, which tend to have higher mean specific runoff, react more slowly to rainfall, smearing out the effect of storm impulses and reducing the runoff variability. However, the inverse relationship between mean runoff and daily variability persists even when catchment area is controlled for (Molnar et al., 2006, figure 4). We introduce here a stochastic hydrology model that predicts this observed inverse relationship between mean and variability without appealing to catchment area. The model predicts several other observed features of the mean runoff and variability relationship. It also predicts a global upper limit on runoff variability as a simple function of mean runoff, mean rainfall intensity and basin response time. The existence of a global limit on daily runoff variability as a function of the mean runoff is useful to understand the range of behaviours that could be expected, in particular for high mean runoff rivers, where the limit is particularly restrictive.

Here we consider a simplified river hydrograph that consists of a series of rapid peaks in river streamflow resulting from rainfall, each followed by a slow decline in streamflow until the next peak. This decline is called a recession, and its shape is a reflection of many hydrological processes operating inside the river basin. Botter et al., (2007) and Botter et al., (2009) showed that if a hydrograph can be approximated as a marked poisson arrival process that resembles the simplified hydrograph described above, then the long-term distribution of streamflow is only a function of a small set of parameters controlling the recession shape, magnitude and frequency. These parameters are the mean magnitude and mean arrival frequency of storm discharge impulses, and the shape and speed of the resulting recessions. The long-term mean streamflow is the product of the mean magnitude and mean frequency of impulses. The variance is a function of the speed of the recessions and the mean period between peaks, which

is the reciprocal of the mean frequency of peaks. It is this mutual dependence of the mean and variance on the mean frequency of peaks and the reciprocal of the mean frequency of peaks, respectively, that leads to the negative correlation between them.

This theory requires only the assumptions that the hydrograph can be approximated by a marked poisson arrival process and the recessions can be modeled as a power law function of streamflow. Any river meeting these simple requirements will exhibit a relationship between mean and variance that can be understood in this framework. However, a better understanding of the relationship between streamflow mean and variance can be reached by adding a model for how rainfall drives the peaks in streamflow. Doing so implies that the mean properties of these peaks are a function of the mean intensity and frequency of rainfall events modulated by ecohydrological conditions in a river basin. This extension allows us to predict the impact of changes to the climatic or ecohydrological regimes on the mean and variability of streamflow.

The mean intensity of rainstorms will modulate the negative correlation between the mean and variance of streamflow. For a given intensity of storms, there will be an upper limit on the variance for streamflow with a certain magnitude. This limit decreases rapidly with increasing streamflow mean, implying that rivers with significant streamflow are limited in the variance they will exhibit. However, increasing the intensity of storms increases this upper limit on variance. Rivers that experience more intense storms will have large variances relative to the mean. Climate change is predicted to increase the intensity of rainfall (e.g. Trenberth et al., 2003; Berg, Moseley, and Haerter, 2013; O'Gorman, 2015) globally. As a result, the variance of streamflow may, in general, increase alongside an increase in mean streamflow where rainfall becomes more intense, despite the usual negative correlation between them.

The theory discussed here is simple and approximate. Therefore predictions using more sophisticated models tailored to a particular location will always be more specific and accurate. However, its power lies in the simplicity of its application, and the ability to use it in regions where the information needed for more sophisticated models is not available. A field that has these requirements is that of long-term landscape evolution, which requires simple, yet accurate models of how climate and hydrology influence the streamflow regime over long periods of time. It also useful to understand the general response to changing climate in places that are not be carefully monitored. Finally, simple models like ours are useful to develop intuition, interpret data and can help validate more sophisticated models.

4.3 SECTION 1: ESTIMATING DISTRIBUTIONS OF DISCHARGE FROM HYDROGRAPHS

We use a probabilistic hydrology model to estimate the distribution of daily runoff (Botter et al., 2007, 2009). Runoff derives from catchment-wide storage in a deterministic manner, where storage recharge is modelled as a Poisson point process that has exponentially distributed waiting periods between recharge events with mean $1/\omega\lambda$ and exponentially distributed recharge magnitudes with mean α, where α is the mean rainfall intensity, λ is the mean rainfall frequency and ω is the ratio of mean annual runoff to mean annual precipitation (MAR/MAP). The recharge Poisson process derives from a stochastic state dependent soil moisture model driven by rainfall modelled by a Poisson process of its own, where soil moisture is decreased by evapotranspiration and recharge of catchment-wide storage, and increased by random rainfall events. Recharge events are considered to occur when the soil moisture reaches a critical sat-

uration value. Both the soil moisture model (e.g. Milly, 1993; Rodriguez-Iturbe et al., 1999; Laio et al., 2001; Porporato, Daly, and Rodriguez-Iturbe, 2004; Settin et al., 2007) and the runoff model (e.g. Botter et al., 2010; Ceola et al., 2010; Müller, Dralle, and Thompson, 2014; Basso et al., 2015; Doulatyari et al., 2015) have demonstrated considerable predictive ability when tested against empirical distributions of daily soil moisture and runoff respectively.

The daily runoff is related to catchment wide water storage monotonically, such that there is a unique daily runoff for each possible storage amount, and runoff always decreases with decreasing storage. This leads to

$$\frac{dq}{dt} = -aq^b \tag{89}$$

Where q is the (specific) daily discharge, a is the recession coefficient and b the recession exponent (e.g. Brutsaert and Nieber, 1977; Botter et al., 2009; Kirchner, 2009). The parameter a is a function of the mean length of time that water is retained in the catchment after a storm (Botter et al., 2013). The mean water retention time defines a characteristic timescale of the catchment's hydrologic response to a storm, which depends on important catchment wide hydrological features (catchment morphology and aspect ratio, average hydrological pathway length and conductivity, etc.) (Botter et al., 2013). The timescale of the hydrologic response is in fact a function of the catchment wide storage, leading to faster response times for higher water storage (and by extension river runoff). This implicitly captures the fact that different hydrological processes are dominant at different levels of catchment saturation, such as surface runoff (quick) at high levels of saturation, and subsurface flow (slow) at low levels of saturation (Basso, Schirmer, and Botter, 2015). However, we can still define a mean response time τ by using the mean daily runoff μ such that $\tau = \mu^{1-b}/a$ with the caveat that the mean response time may not be accurate for values of q far from the mean daily runoff.

Botter et al., (2007) and Botter et al., (2009) showed that we can use equation 89 and knowledge about the arrival frequency and magnitude of storm impulses to the hydrological system to calculate the steady state probability distribution of daily discharge. This work also shows how the arrival frequency and magnitude of storm impulses can be related to ecohydroclimatic boundary conditions, which is valuable as it allows us to relate climatic boundary conditions directly to discharge distributions. Though powerful, this minimalistic statistical model necessarily makes strong assumptions and approximations that may weaken its accuracy and general acceptance. In order to address this we split the model into two components. The first component, at the core of the model, is a mathematical relationship between the hydrograph and the probability distribution of discharge. The second component consists of ecohydrological models that predict how the frequency and magnitude of storm impulses are driven by climatic and ecohydrological conditions. In the following work, we outline the assumptions demanded by the first component of the model, and investigate how well they are met using a data set of river discharge data. We do not test the second component of the model here, as it has already been tested extensively (e.g. Milly, 1993; Rodriguez-Iturbe et al., 1999; Laio et al., 2001; Porporato, Daly, and Rodriguez-Iturbe, 2004; Settin et al., 2007).

4.3.1 *Theory*

Botter et al., (2007) and Botter et al., (2009) showed that there is a mathematical relationship between the hydrograph and the probability distribution of daily discharge if the hydrograph can be approximated as a marked Poisson arrival process, which requires three assumptions be met:

1. Recessions can be well approximated using equation 89
2. Interarrival periods between storm impulses are exponentially distributed
3. Magnitudes of recharge events to catchment wide storage are exponentially distributed

Here we show how these assumptions can be tested by using a time series of daily discharge data.

4.3.1.1 *Approximation of recessions*

We test the first assumption by calculating values for the recession coefficient a and exponent b from equation 89 from the hydrograph and comparing the resulting synthetic recession using measured values of a and b to the measured recessions.

4.3.1.2 *Interarrival periods*

The second assumption is easily tested by finding all of the storm impulses in a hydrograph and measuring the length of the periods between them. The assumption requires that they be exponentially distributed,

$$f_T(t) = \frac{1}{\tau_s} \exp^{-t/\tau_s} \tag{90}$$

where τ_s is the mean of the interarrival period distribution.

4.3.1.3 *Recharge magnitudes*

The final assumption is not as straightforward to test assuming we only have a time series of daily discharge data to test it. We must observe the magnitudes of catchment wide storage recharge from discharge data. We can indirectly observe this using equation 89, which is consistent with a storage-discharge model,

$$S = c_s q^d, \tag{91}$$

where S is catchment-wide storage above a base storage, $c_s = [a(2-b)]^d$ and $d = 1/(2-b)$ (Clark et al., 2009; Bogaart, Lyon, and Dekker, 2016). Using this, the magnitude of storage recharge can be related to changes in discharge over storm impulses. If S_1 and q_1 are the storage and discharge right before a storm impulse and S_2 and q_2 those right after, then the magnitude of storage recharge $\Delta S = S_2 - S_1$ can be rewritten in terms of q_1 and q_2, which can easily be measured,

$$\Delta S = S(q_2) - S(q_1) = c_s(q_2^d - q_1^d). \tag{92}$$

We can rewrite this using the relationships between a, b, c_s and d,

$$\Delta S = \frac{q_2^{2-b} - q_1^{2-b}}{a(2-b)}, \tag{93}$$

where a, b, q_1 and q_2 can all be measured from a daily discharge time series. The distribution of storage recharge magnitudes should also be exponentially distributed,

$$f_{\Delta S}(\Delta S) = \frac{1}{\alpha_s} \exp^{-\Delta S/\alpha_s}, \tag{94}$$

with a mean of α_s.

4.3.1.4 *Time series processing*

In order to test the assumptions of the model, we need to find the start and the end of each recession. We can then obtain the recessions and recession parameters a and b, storm impulse magnitudes, and interarrival periods. We find the recessions by finding all increases in discharge that are sufficiently rapid. The rate of increase in river discharge was found by taking the derivative of the daily discharge where it was positive. The criterion for rapid increase was chosen to be at least $1/200^{th}$ of the maximum rate of increase in the time series. This threshold was chosen because we observed it to perform well in selecting storm impulses for a wide range of time series (for example, see figure 28 where recession starts and endings are shown with red points and green points respectively). The recession parameters a and b were found by fitting the solution to equation 89 to every recession in a time series and taking the median values for a and b, where the solution is,

$$q(t) = [q_o^{1-b} - a(1-b)t]^{1/(1-b)}, \tag{95}$$

and q_o is the discharge at the beginning of the recession.

4.3.2 *Results and discussion*

We test the assumptions required for the Poisson arrival process using a data set of time series of daily discharge, all spanning at least 30 years, from 177 rivers in the US taken from Newman et al., (2015). In the following section we show the results obtained from a specific station (station ID 9081600) for reference, as well as the overall results from the entire data set.

4.3.2.1 *Approximation of recessions*

We calculate values for a and b from each discharge time series by fitting each recession in the time series, and taking the median values of a and b. We then compare each measured recession in a discharge time series to a synthetic one constructed using the median of a and b. To asses the quality of the fits, we compute the root mean square error (RMSE) of each recession, normalized by the mean discharge magnitude over the recession. A RMSE of 0.1 implies that the average misfit between the measured and synthetic recessions is 10% of the mean discharge. An example recession with associated RMSE is given for reference (figure 29a), as well as the distribution of the mean RMSE from each river (figure 29b).

4.3.2.2 *Interarrival periods*

We compared the distribution of interarrival periods of storm impulses to an exponential distribution characterized by the mean interarrival period from each time series.

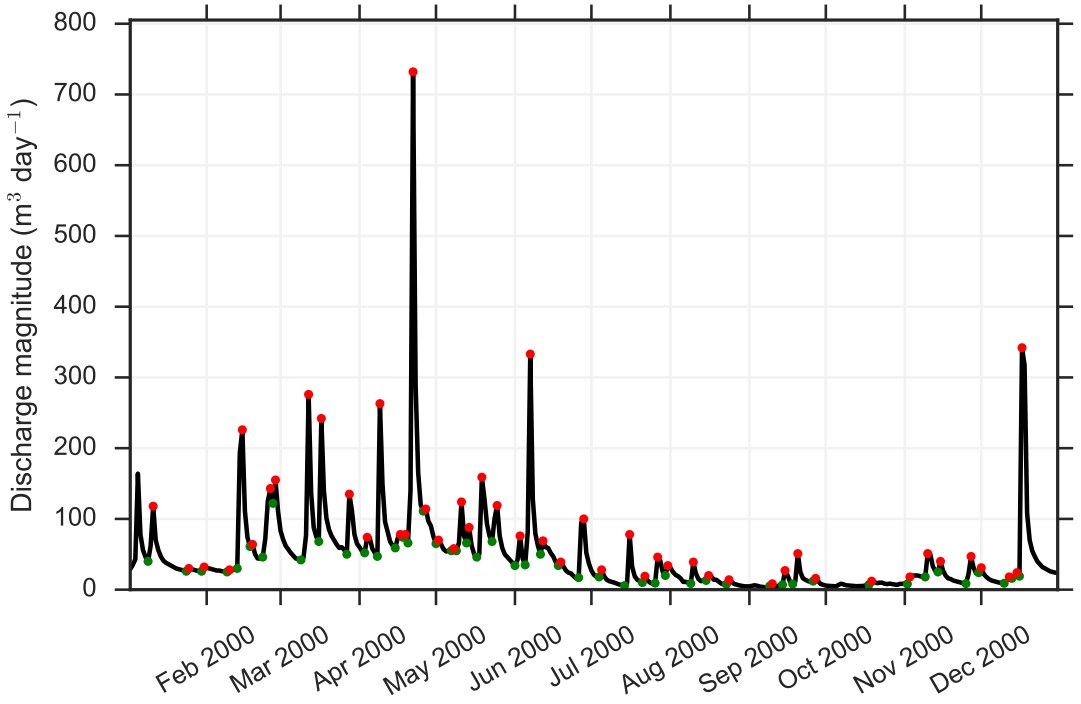

Figure 28: A year of discharge data with recession starts marked in red and recession ends marked in green.

The exponential distribution (figure 30a) is not fit or optimized to the observed estimation, we simply calculate the mean interarrival period from the time series. The quality of the fit was measured by the coefficient of determination, r^2, of the match between the observed quantiles and the theoretical quantiles of the exponential distribution (figure 30a). The higher the coefficient of determination, up to a maximum value of one, the better the fit. The values of r^2 for the interarrival distribution range from 0.1 to 1, with the bulk of the values above 0.6 (figure 30b). An r^2 value above 0.9 implies a good fit, 0.6 implies an acceptable to poor fit. We can conclude from this that for a representative data set of 177 rivers in the US, the assumption of exponentially distributed interarrival periods is often an acceptable to good assumption, with a small, but non-negligible chance of being a poor assumption.

4.3.2.3 *Recharge magnitudes*

We conduct the same tests on the distribution of recharge magnitudes to catchment-wide storage (figure 31). Overall the quality of the fit is better than with the distribution of interarrival periods, with the majority of fits above 0.9, and many above 0.95. We conclude that the assumption of exponentially distributed recharge magnitudes is often a good one for the 177 rivers in the US data set.

4.3.2.4 *Implications for relationship between mean and variability*

The joint distribution of the quality of the assumptions of exponentially distributed interarrival periods and recharge magnitudes shows that most rivers fall in the upper right quadrant of the parameter space, implying that both assumptions are generally met together in this data set (figure 32). As we discussed earlier, Botter et al., (2007)

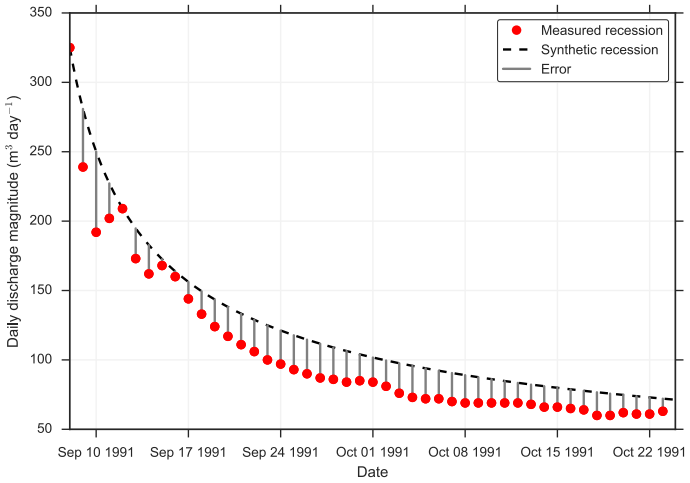

(a)

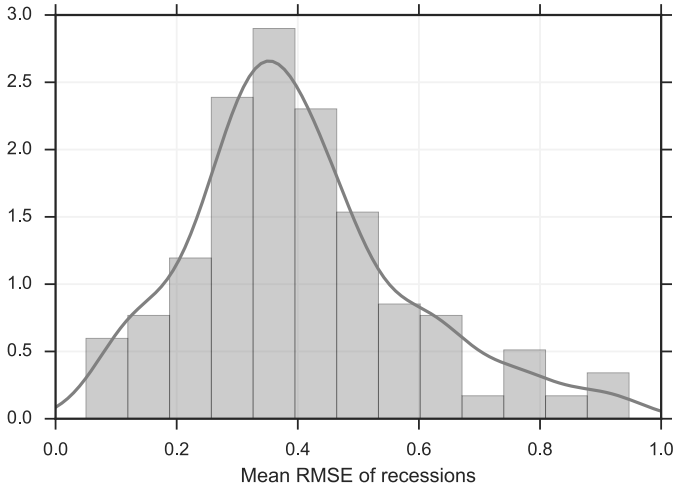

(b)

Figure 29: (a) A long recession from our example station with its associated synthetic recession and error. The RMSE of this recession is 0.17. (b) Distribution of the mean RMSE of each of the 177 discharge time series.

and Botter et al., (2009) showed that when these conditions are met, the steady-state distribution of daily discharge will be determined by the mean magnitude of recharge events, α_s, the mean interarrival period, τ_s, and the recession coefficient a and exponent b. These parameters can be measured directly from the hydrograph, and do not need to be related to climatic or ecohydrological boundary conditions in order to be useful.

For example, these parameters can be used to estimate the long-term distribution of discharge from short time series. Botter (personal communication) recently presented work showing that the error in predicting the magnitude of rare events (e.g. 100 and 1000 year floods) using this method does not increase when the magnitude of progressively rarer floods is estimated. In contrast, for traditional statistical methods, the error associated with the prediction of the magnitude of rare events increases with the infrequency of the flood in question - e.g. prediction of the 1000 year flood magnitude is worse than that of the 100 year flood magnitude.

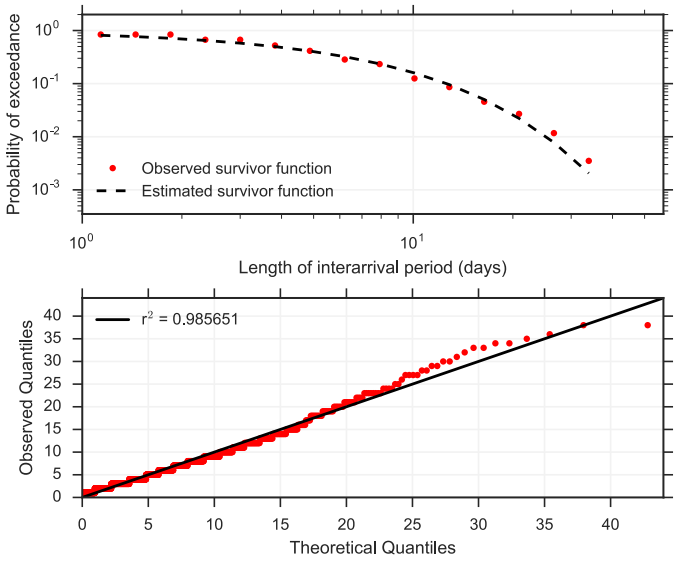

(a)

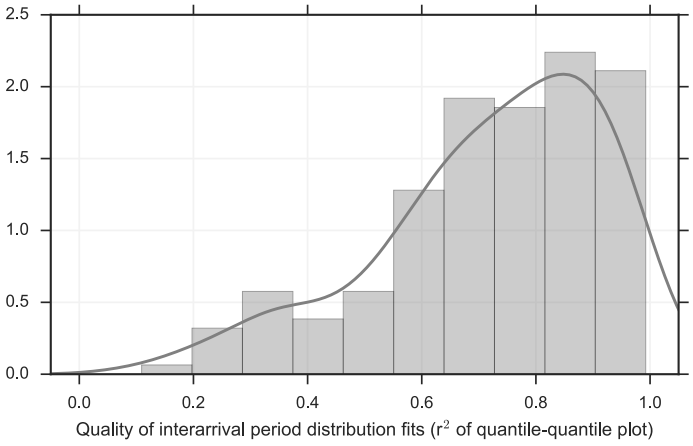

(b)

Figure 30: (a) Top panel: comparison of observed distribution of interarrival periods from example station to the exponential distribution required to meet assumption 2. Bottom panel: quantile-quantile plot with 1:1 line shown for reference. (b) Distribution of r^2 values assessing quality of fit between observed interarrival distribution and exponential distribution from 177 rivers in the US.

These parameters can also be used to understand the nature of the relationship between the mean and variability of daily discharge, which we discuss in the following section. We also relate the parameters α_s, τ_s, a and b to ecohydrological and climatic parameters. This provides more insight into the relationship between rainfall, hydrology and distributions of discharge, but potentially at the cost of more approximations and simplifications because of the added layer of ecohydrological models. Therefore, we wish to point out that as long as the three assumptions are met, the relationship between the mean and variability of discharge that we discuss arises from the frequency and magnitude of discharge impulses, whatever the cause behind them.

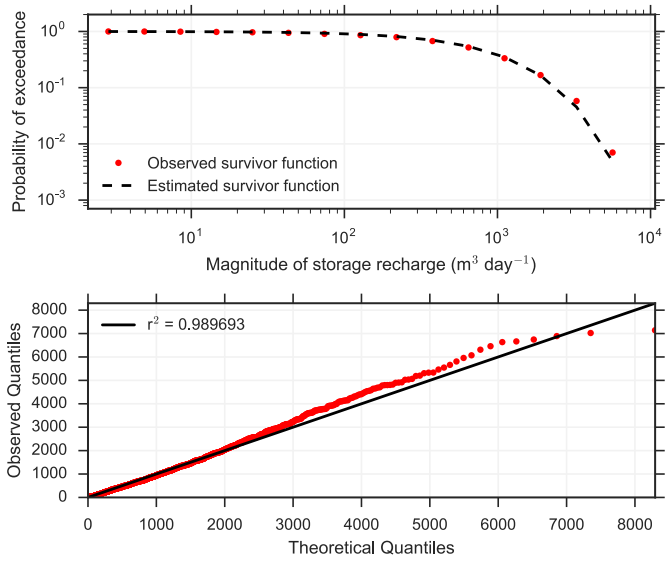

(a)

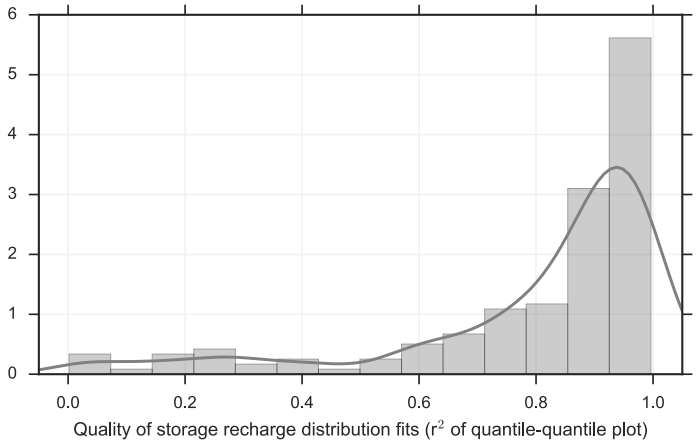

(b)

Figure 31: (a) Top panel: comparison of observed distribution of recharge magnitudes from example station to the exponential distribution required to meet assumption 3. Bottom panel: quantile-quantile plot with 1:1 line shown for reference. (b) Distribution of r^2 values assessing quality of fit between observed recharge distribution and exponential distribution from 177 rivers in the US.

4.4 SECTION 2: NEGATIVE CORRELATION OF MEAN AND VARIABILITY

4.4.1 *Coefficient of variability*

In chapter 3, we showed that the shape parameter of the distribution of daily discharge is $1/\nu$, regardless of the value of b. This is the inverse of the coefficient of variability,

$$\nu = \omega\lambda\tau, \tag{96}$$

where ω is the runoff ratio, λ is the mean storm frequency, and τ is the response time of the river basin. When ν is small, the likelihood of very large magnitude floods is very low and the runoff variability is also low. When ν is large, the likelihood of large floods can be orders of magnitude higher, leading to high variability runoff.

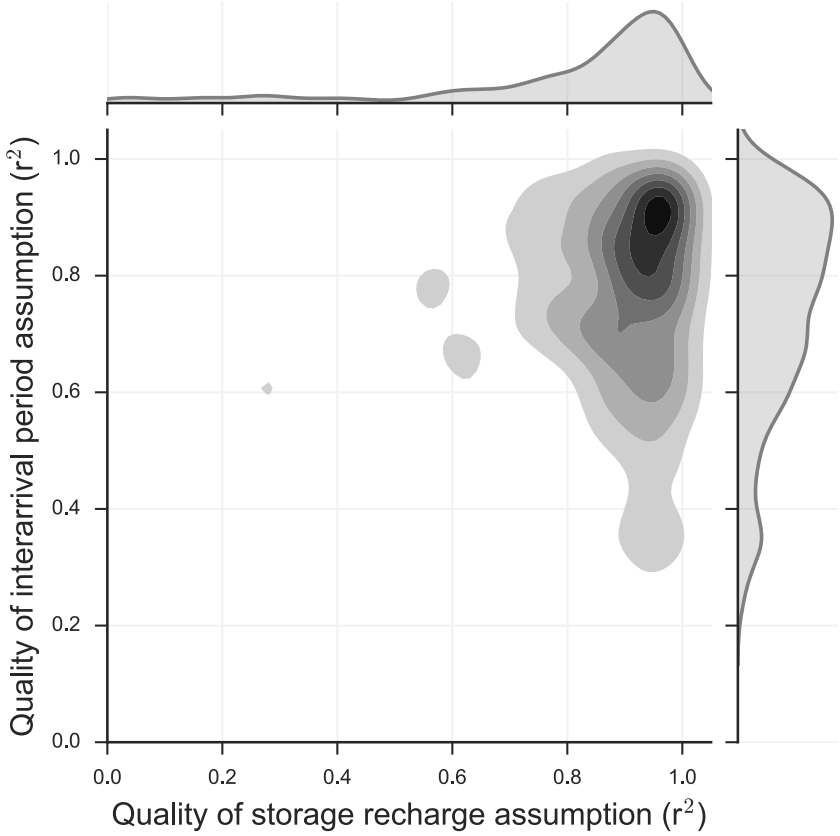

Figure 32: Joint distribution of coefficient of determination for fit to exponential distribution for both interarrival periods and recharge magnitudes.

Also known as the erraticity index (Botter et al., 2013), the coefficient of variability, ν, is a nondimensional ratio of the timescale of the catchment-scale hydrologic response to an average storm (τ), to the mean interarrival period of runoff producing storms ($\tau_s = 1/\omega\lambda$). If the mean time τ_s between runoff producing storms is small compared to the time τ for a storm pulse to completely leave the basin, the supply of water to the river will be relatively consistent, and the daily discharge will stay close to the mean daily discharge (as in figure 33b). This will yield a discharge regime with low variability. On the other hand if the time it takes for the river basin to drain a storm pulse is small relative to the interstorm period τ_s then the river discharge will often be well below the mean, with infrequent but significant deviations well above the mean (as in figure 33a). This would be considered a flashy basin, and will yield a discharge regime with high variability. The response time of the basin is determined by the mean daily discharge, and the recession coefficient and exponent ($\tau = a^{-1}\mu^{1-b}$).

The coefficient of variability can also be understood in terms of damped and undamped oscillating systems, where the basin response time is a measure of the degree of damping. The longer the response time, the higher the degree of damping, and the more steady the long-term behaviour as a result. However, whether the response time of the river is long (damped) or short (undamped) can only be understood relative to the frequency of the forcing $\omega\lambda$. So it is logical that the variability of river discharge is the ratio of the interarrival period of runoff producing storms to the basin response time ($\nu = \tau_s/\tau = 1/\omega\lambda\tau$).

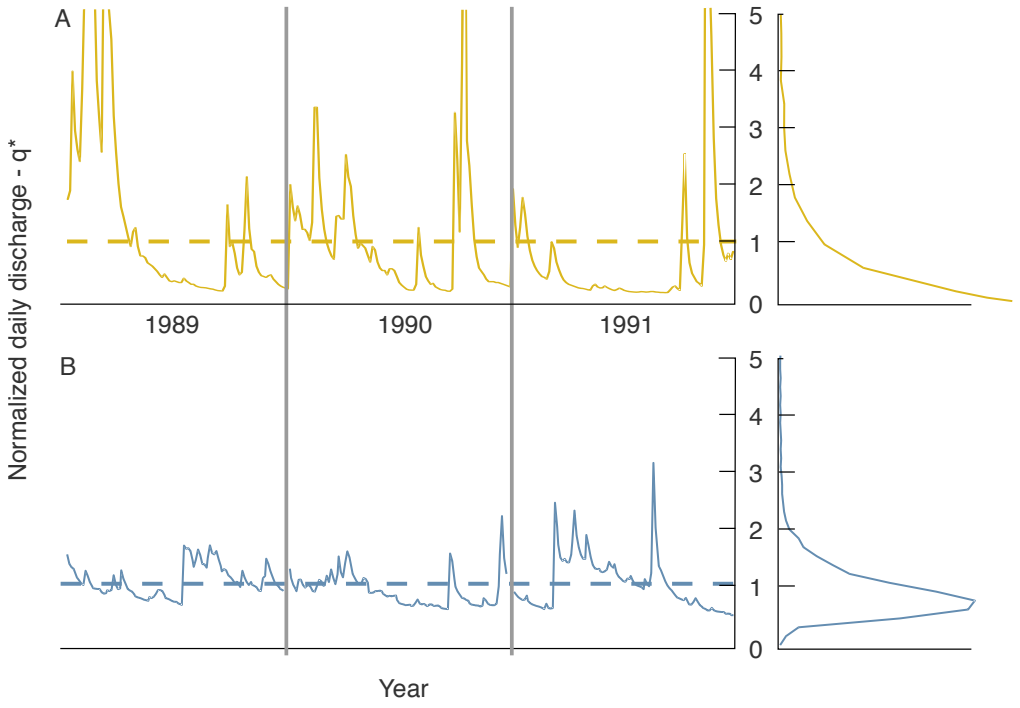

Figure 33: Figure adapted from Botter et al. 2013, discharge time series from rivers in the erratic regime (A) and persistent regime (B) are shown along with the associated distributions. It can easily be seen that the erratic river has a much higher probability of significantly exceeding the mean discharge, which has implications for its ability to erode its bed.

As stated above, this measure of variability is independent of the choice of b. The value of b will modify the tail heaviness, and therefore the overall variability, which is important when absolute values of storm frequency and magnitude are sought. However, for a given value of b, changing ν has a proportional effect in terms of the change in frequency of high magnitude, low frequency events. For example, doubling the coefficient of variability from 1 to 2 increases the frequency of high magnitude events by about an order of magnitude across all values of b (figure 34). Using the set of equations from chapter 3 (equations 12, 13, and 14), the distribution of discharge is fully defined by b, ν, and the mean daily discharge μ. The mean discharge is the fraction of precipitation that ends up in the river, making it the product of the mean precipitation rate and the runoff ratio,

$$\mu = \omega\alpha\lambda, \tag{97}$$

where the mean precipitation rate is the product of the mean storm depth α and the mean storm frequency λ. This definition of μ is also independent of the value of b. Therefore, μ and ν are consistent for all values of b.

Historically, in work that addresses the variability of discharge in context of fluvial erosion, a pdf is chosen to represent discharge distributions, and fit to data to estimate the shape parameter as a measure of variability (Lague, Hovius, and Davy, 2005; Molnar et al., 2006; DiBiase and Whipple, 2011; Rossi, Whipple, and Vivoni, 2016). This is equivalent to setting b beforehand, and investigating only variations in ν. In the following sections, we don't concern ourselves with the value of b, measured or theoretical, but instead only variations in ν and μ. This is supported by the proportional effect of variations in ν for all values of b, and allows comparison with earlier work.

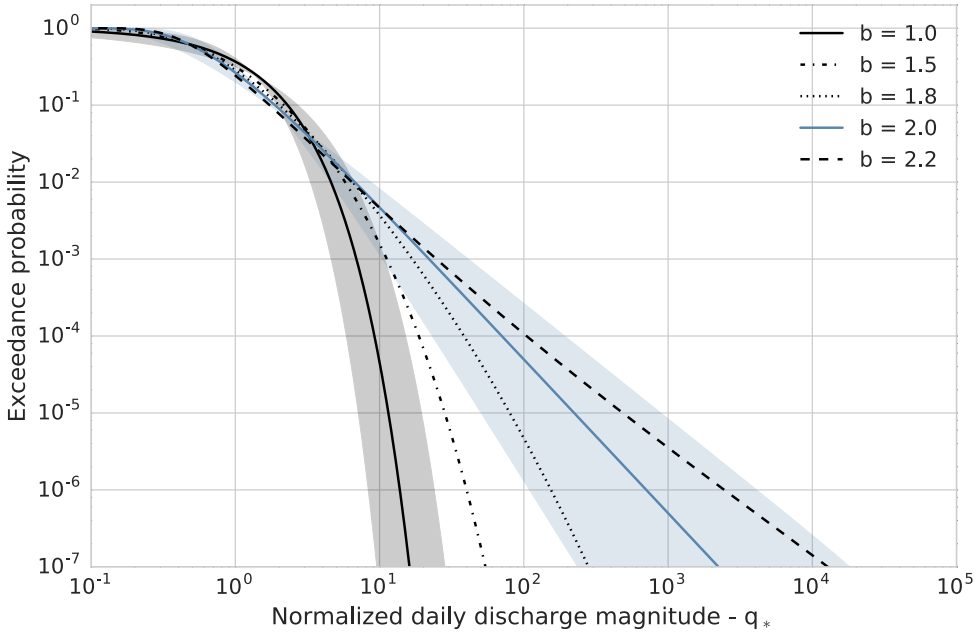

Figure 34: Runoff distributions for $b = 1.0$, 1.5, 1.8, 2.0 and 2.2. For all distributions, $\mu = 1$ and $\nu = 1$. The shaded regions correspond to the range of ν from 0.5 to 2 for $b = 1$ and $b = 2$. Note that the predicted frequency of moderate events is similar for all distributions, but the frequency of large events depends strongly on the value of b.

4.4.2 *Covariation of daily runoff variability and mean*

The mean and variability share an important term, the frequency of effective, or runoff-producing, storms, $\omega\lambda$. We can use this to establish an analytical relationship between μ and ν,

$$\nu = \frac{\alpha}{\tau\mu} \tag{98}$$

This relationship is simple; it predicts that variability is a power law function of the specific daily discharge with an exponent of -1, providing a negative correlation between μ and ν. Several studies have found an inverse relationship of the form $\nu \propto \mu^{-\eta}$ (Molnar et al., 2006; Lague, 2014; Rossi, Whipple, and Vivoni, 2016). However, these studies typically find that $\eta \approx 0.3$ (35a). We also find that in general, using Monte Carlo simulations, $\eta < 1$ because ν and μ both depend on the same parameters, and changing ν usually results in a change to μ, and vice versa. This is made particularly complex by the runoff ratio ω, which appears in both ν and μ and is a nonlinear function of rainfall intensity α, rainfall frequency λ as well as the maximum potential evapotranspiration rate ET_{max} and the soil water storage capacity w_o,

$$\omega = \frac{\phi\, h_s^{h_s/\phi} e^{-h_s}}{h_s \Gamma(h_s/\phi, h_s)}, \tag{99}$$

where ϕ is the Budyko aridity index ($\phi = ET_{max}/\alpha\lambda$), h_s is the effective soil capacity ($h_s = w_o/\alpha$), and the $\Gamma(\cdot,\cdot)$ is the lower incomplete gamma function. The predicted linear relationship between μ and ν, along with an understanding of how the underlying climatic and ecohydrologic parameters control both simultaneously allows the

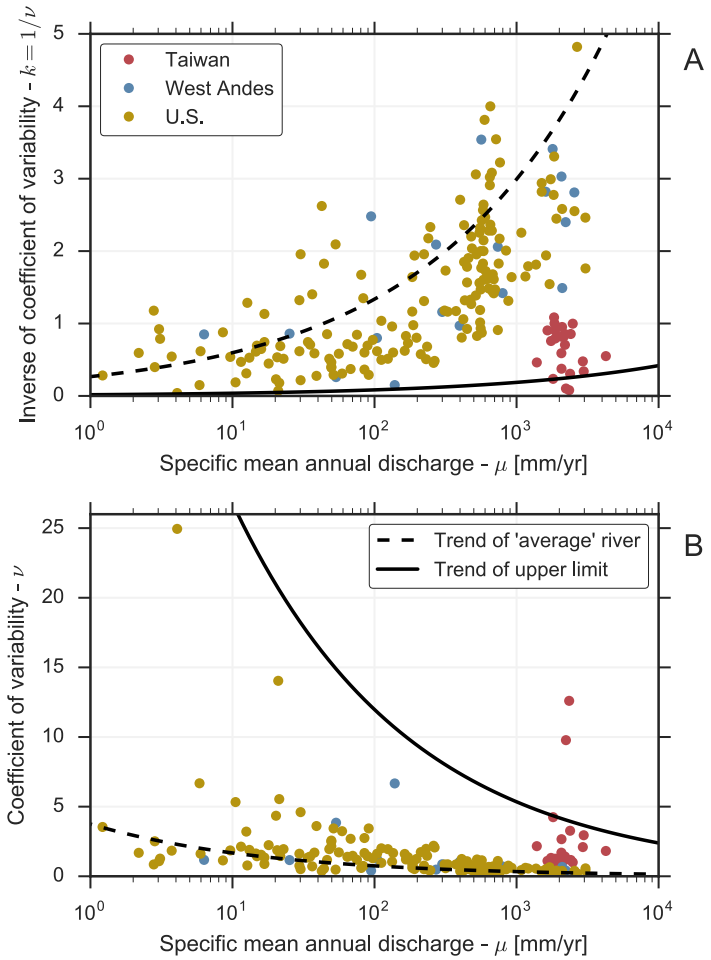

Figure 35: Measured variability for rivers from Taiwan, the West Andes and the US from (Lague, 2014, and references therein). (a) We use variability parameter $k = 1/\nu$, assuming $b = 2$ (Lague, 2014). The trend of an 'average' river is shown as dashed line, the upper limit is shown as solid line. Upper limit and 'average' are defined by response time and mean rainfall intensity ($\tau_{avg} = 4\,\text{days}$, $\alpha_{avg} = 15\,\text{mm/day}$, $\tau_{min} = 1/2\,\text{day}$, $\alpha_{max} = 30\,\text{mm/day}$. (b) Upper limit is seen as more restrictive when the ν is plotted directly, and does not capture the two most extreme rivers from Taiwan.

observed relationships between μ and ν on earth to be well explained. Even if equation 98 does not capture the proper value for η, it is still useful for providing upper bounds on the trend of variability with the mean by recognizing that this bound is modulated by the maximum rainfall intensity expected and the shortest response time expected, α_{max}/τ_{min}, (solid line in figure 35).

4.5 RESULTS AND DISCUSSION

4.5.1 *Monte Carlo simulations*

To further probe the controls on discharge variability, we conducted a series of Monte Carlo simulation for a wide range of ecohydroclimatic conditions, similar to the ranges found on Earth. The parameter space is as follows: $ET_{max} = [0.2 - 20\,\text{mm/day}]$, $\alpha =$

$[0.25 - 25\,\mathrm{mm/day}]$, $\lambda = [0.01 - 1.0\,\mathrm{day}^{-1}]]$, $s_o = [0.5 - 10\,\mathrm{mm}]$, $\tau = [1 - 10\,\mathrm{days}]$. The parameters are chosen randomly from either uniform distributions or uniform distributions in logarithmic space over the above ranges. Uniform-logarithmic distributions are sometimes used to provide a more uniform distribution of simulations when logarithmic axes are used for plotting.

These simulations reproduce one of the main features of empirical data, which is an inverse relationship between ν and μ. The theory predicts that the maximum variability for a given mean runoff will be determined by the maximum average storm intensity that can produce that mean runoff (α_{max}) and the minimum expected response time (τ_{min}). Because a basin could potentially have perfect transmission of rainfall to discharge (no soil and/or no evapotranspiration), the α_{max} that applies for any μ will simply be the regional or global maximum average storm intensity.

On Earth, α_{max} is in the range of tens of mm/day. Here we take a value of 25 mm/day. Similarly, we choose a reasonable value of one day as the fastest basin response time, assuming a basin size larger than a few tens of km^2. This leads to an upper limit on variability as a function of mean discharge ($\nu_{max} = (\alpha_{max}/\tau_{min})\mu^{-1}$). This limit is quite restrictive for high specific mean daily discharge (black solid line in figure 36), and has important implications for long-term threshold fluvial erosion rates as a function of rainfall. The upper limit will vary from region to region and through time as a function of α_{max} and τ_{min}.

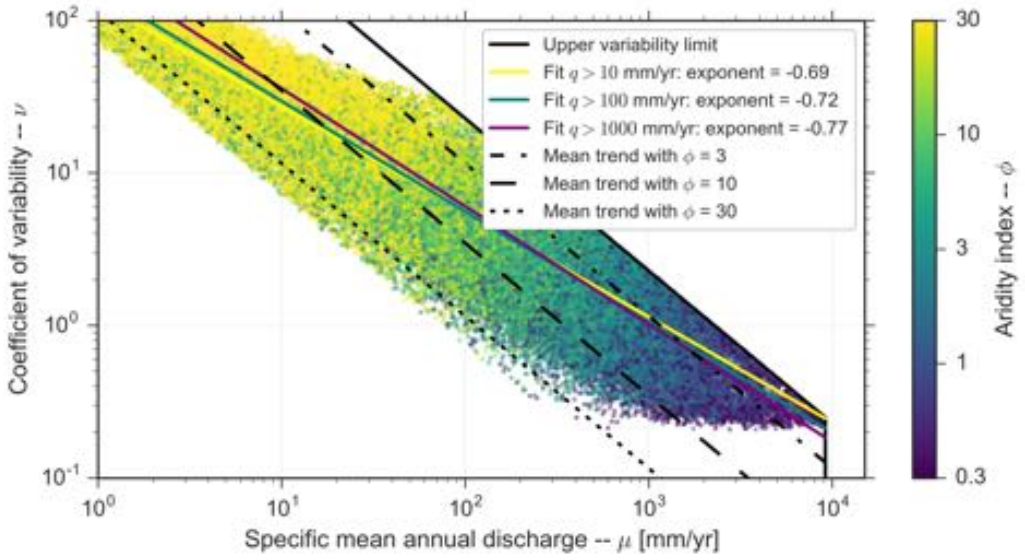

Figure 36: Monte Carlo simulations of mean and variability using parameter space described in text, with response time between 4 and 5 days. No correlation between rainfall intensity, α and rainfall frequency λ. Dashed-dotted, dashed and dotted line show trends of mean and variability for different aridity levels with average conditions; drier conditions lead to overall trend between mean and variability with exponent less than one.

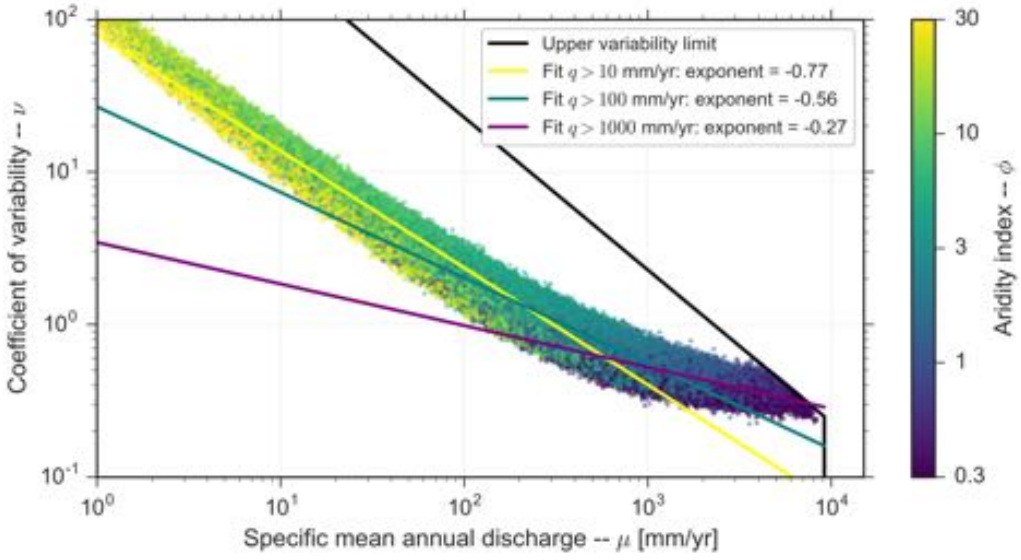

Figure 37: Monte Carlo simulations of mean and variability using parameter space described in text, with response time between 4 and 5 days. In contrast to figure 36, there is a positive correlation between rainfall intensity and frequency weakens correlation between mean and variability further, leading to smaller exponents.

4.5.2 *Empirical nonlinear dependence of variability on mean runoff*

The analytical relationship between ν and μ is linear. However, a nonlinear relationship naturally arises in this theoretical framework using Monte Carlo simulations (figure 36). When we conduct simulations with completely uncorrelated parameters, we find a exponent $\eta \approx 0.7$ instead of $\eta = 1$. This can be understood through ecohydrological controls on both μ and ν. For mean conditions, the higher the aridity index, the lower the coefficient of variability for a given mean (dashed, dotted and dashed-dotted lines in figure 36). Most basins do not have mean conditions, and therefore do not fall on this trend, however, as the mean discharge becomes much lower, basins become much drier basins on average, and move towards the trend of higher aridity and lower variability. This is visible in figure 36, where the basins from the Monte Carlo simulation cluster around the dry basin trend ($\phi = 10$) at low mean runoff and transition to the wet basin trend ($\phi = 1$) at high mean runoff. This trend only manifests itself on the scale of the entire parameter space. For a given mean discharge, more arid basins tend to have higher variability, because most basins do not have mean parameter values, and locally the relationship between aridity and variability is controlled by other factors.

In the previous set of simulations, the governing parameters were assumed to be uncorrelated, however, we observed that rainfall intensity and frequency are positively correlated in the Himalaya (chapter 2) an observation that can be made in other data sets (Rossi, Whipple, and Vivoni, 2016). The relationship we find is $\alpha = (1-\lambda)^{-c_2}$; $c_2 \approx 1$. If we use this relationship in our simulations, we find it weakens the negative correlation between the mean and variability of discharge, leading to values for the exponent, η, more in line with observations (figure 37).

The trend of mean and variability in our simulations can be understood as a combinations of the response of the variability to changes in the mean rainfall frequency and mean rainfall intensity (figure 44). The variability decreases in response to increasing

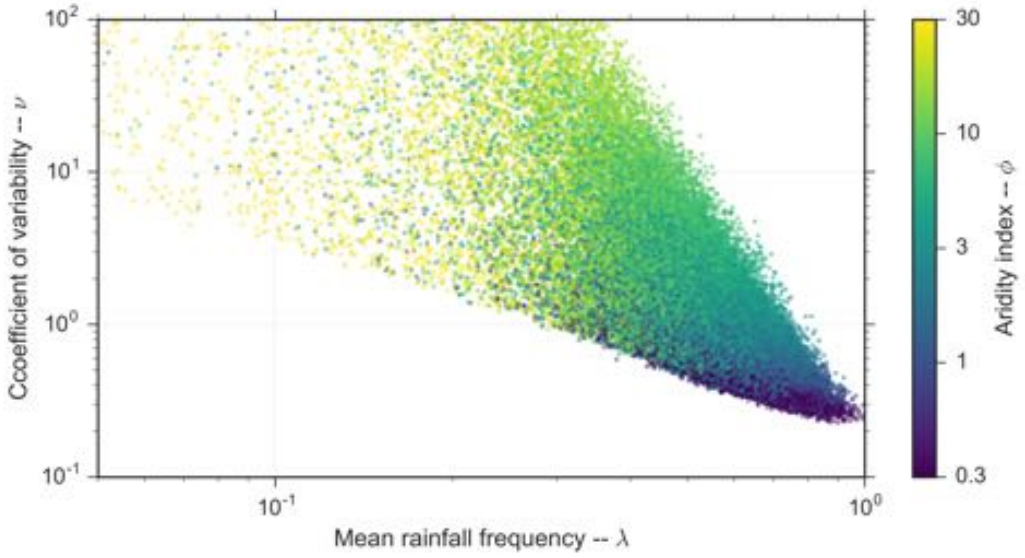

Figure 38: Monte Carlo simulations of variability as a function of rainfall frequency and intensity using parameter space described in text, with response time between 4 and 5 days. Response of variability to changes in rainfall frequency is a power law with higher variability at low rainfall frequencies.

rainfall frequency and intensity. However, the manner of the response is quite different for the two controlling rainfall parameters. The changes in variability are essentially power law trends (linear in log-log space) as a function of rainfall frequency, with de-

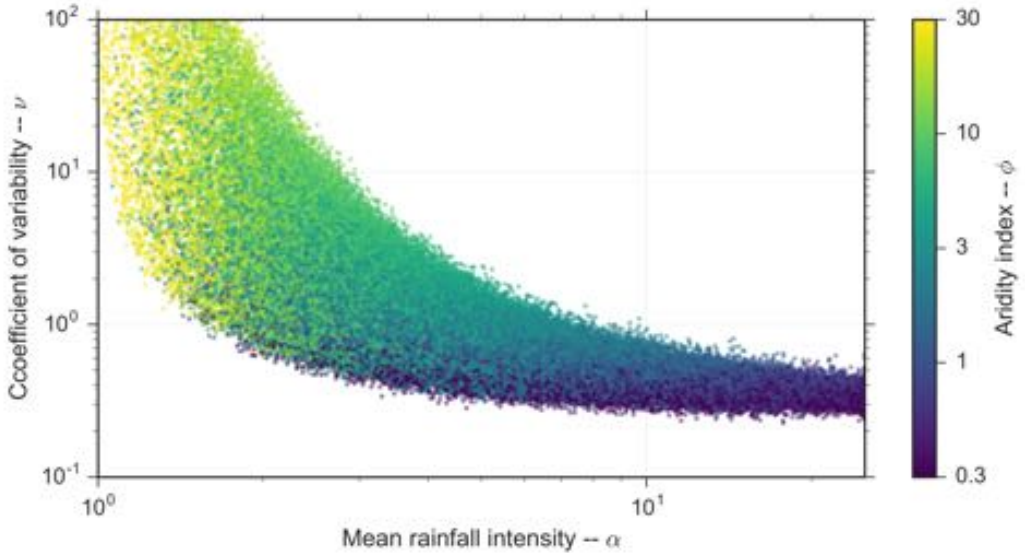

Figure 39: Monte Carlo simulations of variability as a function of rainfall frequency and intensity using parameter space described in text, with response time between 4 and 5 days. Response of variability to changes in rainfall intensity is notably different than the response to changes in the rainfall frequency. The variability does not decrease for increases in rainfall intensity above a certain point.

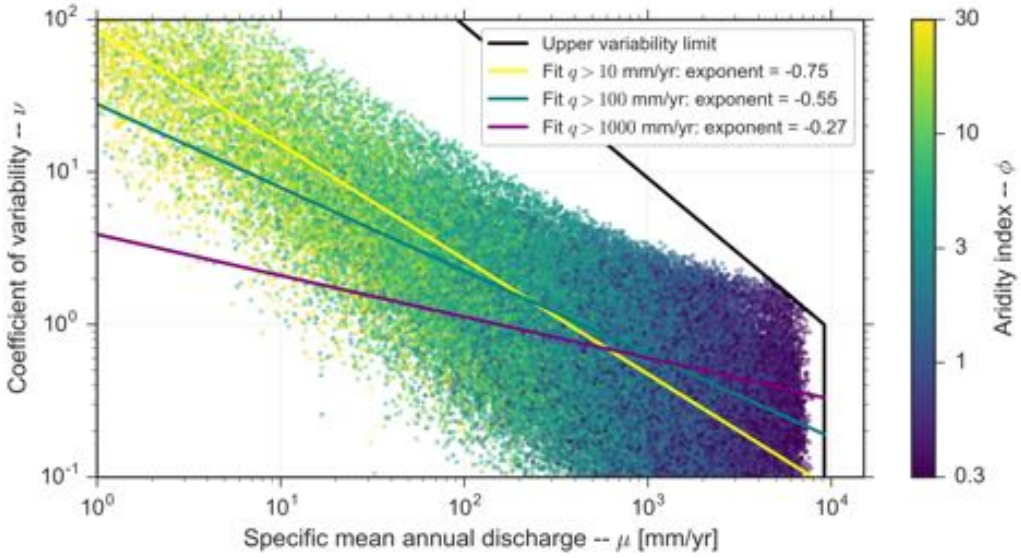

Figure 40: Monte Carlo simulations of mean and variability using parameter space described in text, with response time between 1 and 30 days and positive correlation between rainfall intensity and frequency. Trends observed with narrow range of response times still have the same exponents with wider range of response times.

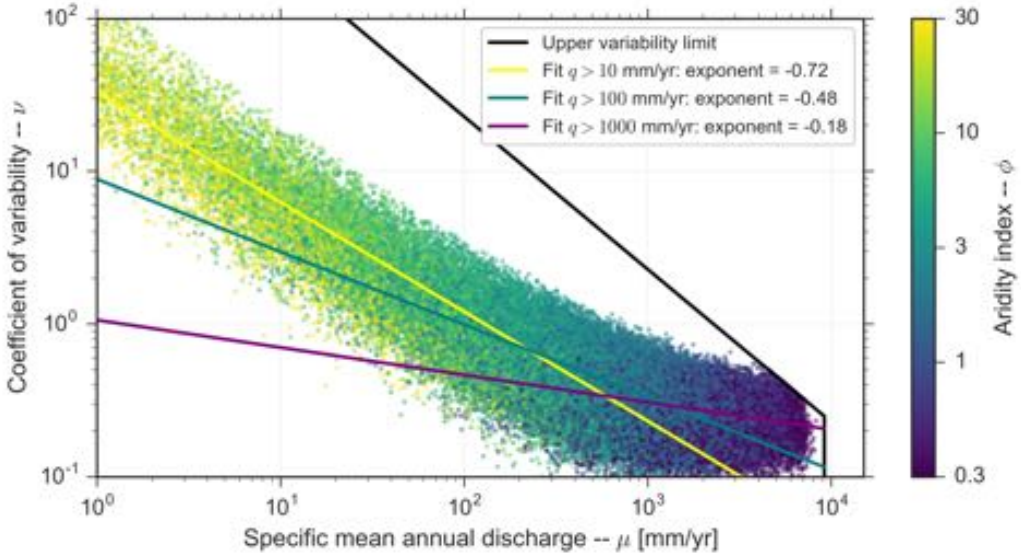

Figure 41: Monte Carlo simulations of mean and variability using parameter space described in text, with response time between 1 and 30 days and positive correlation between rainfall intensity and frequency. Further correlation between maximum response time and mean daily discharge has been included as described in text. The result is a further weakened correlation between mean and variability, and yet smaller exponents.

creasing variance for higher rainfall frequencies. In contrast, the variability responds sensitively to changes in rainfall frequency for low rainfall intensities, but is insensitive when the rainfall intensity is high. When the intensity and frequency of rainfall

are correlated, the insensitivity of variability to high rainfall intensities is more clearly expressed, leading to lower values of the exponent η when mean discharge is high.

Up to this point we have restricted the hydrologic response time, τ, to a narrow range of 4-5 days. When we allow it to vary over a larger range, 1-30 days, we observe a larger range of variability for a given mean discharge. However, the exponents of power law fits to the simulation results remain essentially unchanged (figure 40).

We find that accounting for the correlation between rainfall mean and intensity changes the aggregate result of our simulations, bringing them more in line with observations. We imagine that in general there are often other important correlations between governing climatic and ecohydrological parameters that may vary from region to region. We test briefly another correlation between the mean annual discharge and the maximum response time, τ_{max}. The basis for this is the observation that in the data set of variability and mean discharge from Rossi, Whipple, and Vivoni, (2016), the basins with the longest response time tend to have low mean discharges. This may only be a sampling bias, but we find that this correlation further weakens the correlation between the mean and variability of discharge, bringing the simulations closer to observations across a wider range of discharges (figure 41). For the following simulations, we retain the correlation between mean rainfall intensity and frequency, but not between maximum response time and mean annual discharge.

4.5.3 *The effect of the basin response time*

The only controlling variable that effects just one of μ or ν is the basin response time τ. The response time changes only the daily variability, with longer response times resulting in lower variability. Changing τ changes the scaling of of ν with μ. Therefore, we would expect that regions with different average response times should exhibit different ν-μ scaling. If we plot the 'classic' variability parameter $k = 1/\nu$ (Lague, Hovius, and Davy, 2005), we see that the simulations capture the general features of the observed variability and mean discharge from Lague, (2014) (figure 42). It is striking that this theory can capture the first order features of empirical ν-μ scalings even with simplistic parameter ranges (independent, uniformly distributed parameters). One important caveat is that the simulations tend to have higher variability at low mean annual discharges than observations. This may be due to sampling bias or important correlations between governing parameters that we have not taken into account.

The importance of the response time τ in organizing the scaling of variability with mean annual discharge is clear (figure 43). There are several effects that can systematically change the basin response time. One example would be the lithology of the basin, which can control the response time with different groundwater permeabilities and conductivities. Basin response time is also known to scale with basin area, because water must travel further to exit the basin, which takes longer. Another influence on the basin response time is the temperature of the basin during the winter season. A basin that gathers snowpack during the winter will retain that water until spring or summer. This can be roughly parameterised with a longer response time for winter precipitation. In this way, snowmelt dominated catchments can be taken into account in an approximate way in our framework. By accounting for the winter delay in snowmelt such that the hydrological response time is $\tau_w = \tau + \tau_d$, where τ_d is the delay between snowfall and snowmelt, Schaefli, Rinaldo, and Botter, (2013) showed that this yields a winter

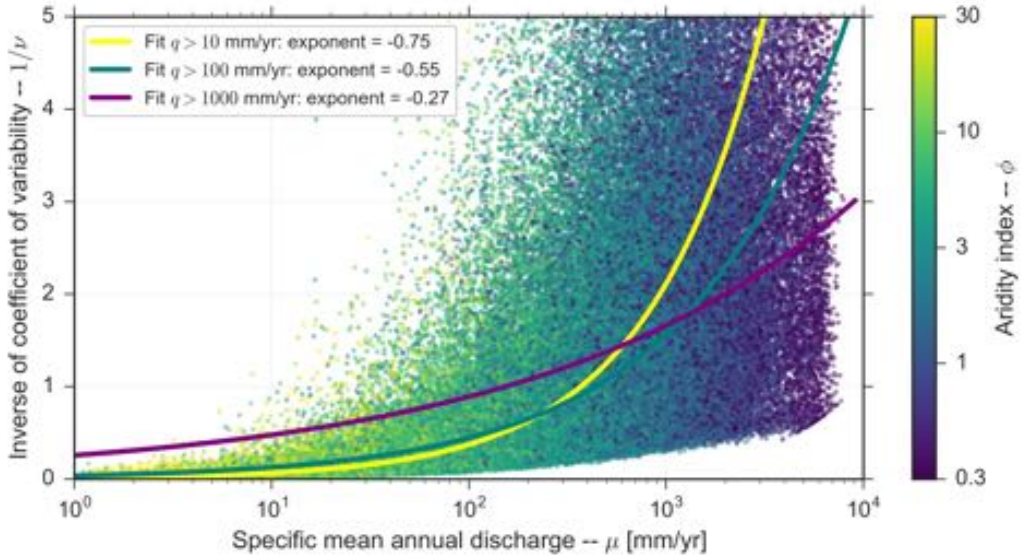

Figure 42: Monte Carlo simulations of mean and variability using parameter space described in text, with response time between 1 and 30 days and positive correlation between rainfall intensity and frequency. Results replotted in the parameter space of Lague, Hovius, and Davy, (2005) for comparison to previous results.

variability $\nu_w = (\omega\lambda\tau_w)^{-1}$ that is systematically lower in catchments with solid phase precipitation, matching general observations.

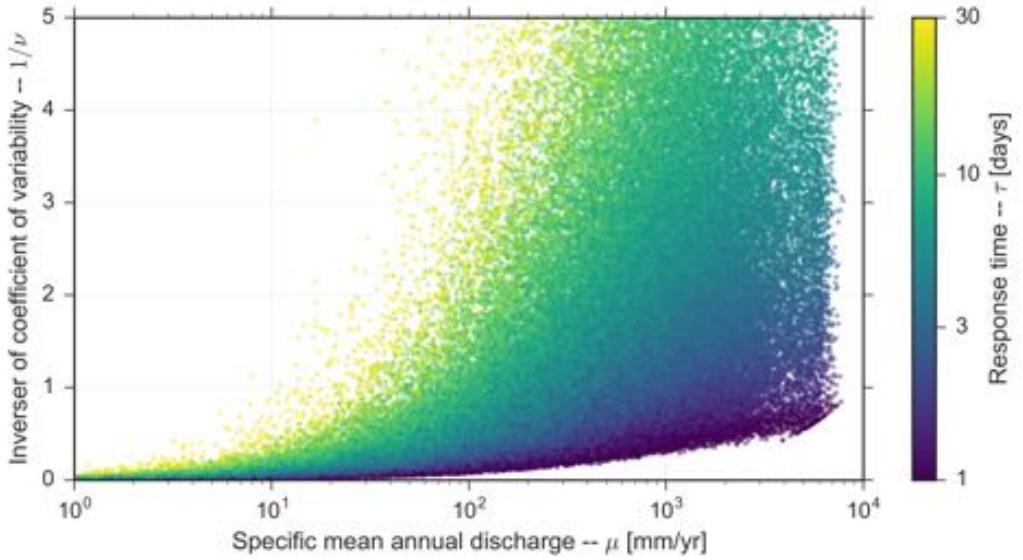

Figure 43: Monte Carlo simulations of mean and variability using parameter space described in text, with response time between 1 and 30 days and positive correlation between rainfall intensity and frequency. Same plot as figure 42, but colored by response time instead of aridity index. The importance of the response time as a control on variability is clear.

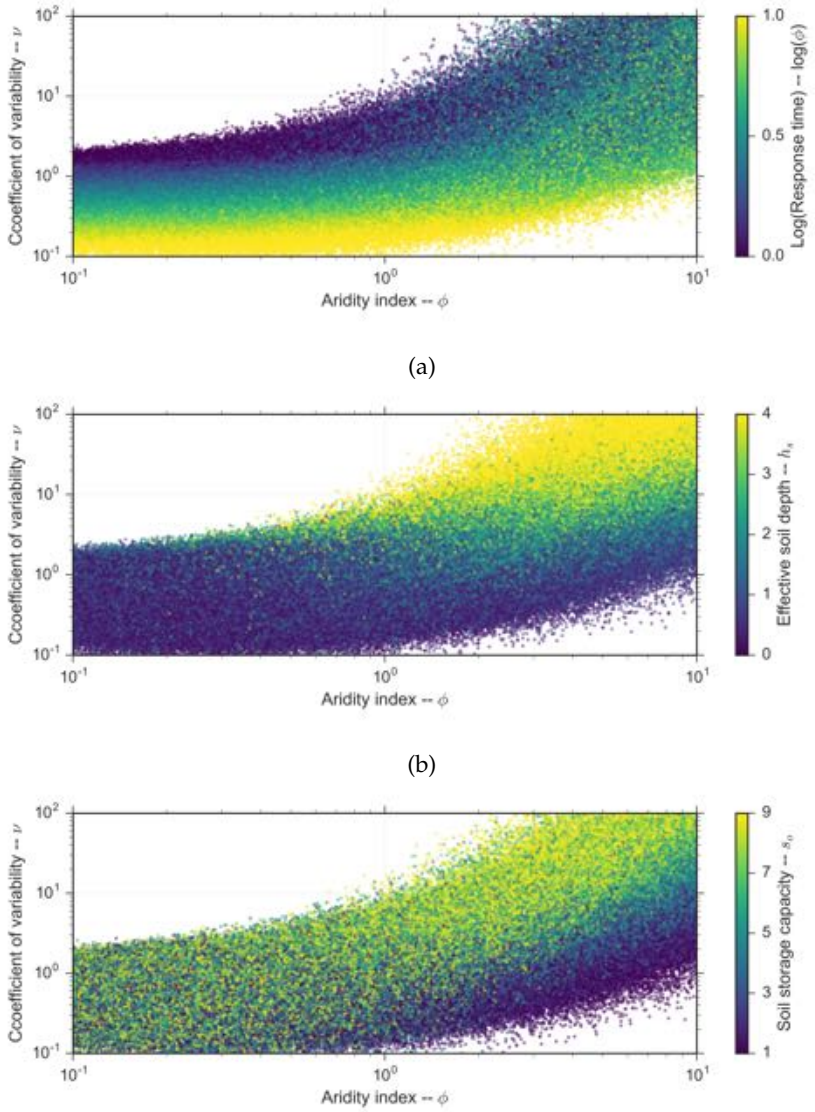

(a)

(b)

(c)

Figure 44: Monte Carlo simulations of variability as a function of aridity index ($1 \leqslant \tau \leqslant 10$). (a) When $\phi < 1$, response time is the main control on variability. (b) When $\phi > 1$, the effective soil depth, h_s, is the main control on variability. (c) The effective soil depth is mainly controlled by the soil capacity, s_o, which is therefore a key control on variability when $\phi > 1$.

4.5.4 *Understanding controls on discharge variability*

We can understand the controls on variability in the Monte Carlo simulations by referring to the ecohydroclimatic parameters that describe variability, $\nu = 1/\omega\lambda\tau$. Clearly, from this equation, as well as the results of the simulations, aridity is an important control. Aridity is expressed in ν through the runoff ratio ω. This is supported by Rossi, Whipple, and Vivoni, (2016), which find aridity to be an important control of variability. Plotting the results of the simulations as a function of variability and aridity, we find that more arid basins lead to higher variability (figure 44).

However, there is a lot of spread in this trend, which is explained by the dependence on other parameters. When the aridity is less than one (wet basins), the response time, τ, is the main control on discharge variability, with faster response times leading to higher variability (figure 44a). This is not surprising given the form of ν. However, as the aridity increases, the importance of the response time in determining variability decreases. Instead, the effective soil depth, $h_s = s_o/\alpha$ becomes the dominant determinant of variability (figure 44b). When the effective soil depth increases, it causes an increase in variability. In chapter 3, we showed that the runoff ratio can be explained in terms of the aridity index and the effective soil depth. When $\phi > 1$, we see the expression of the effective soil depth through the runoff ratio, and its effect on the variability. Because the aridity is closely related to the rainfall intensity, it is the soil storage capacity, s_o, that controls the effective soil depth for a given aridity. Therefore, the soil storage capacity is the dominant control on variability when $\phi > 1$. Even though the rainfall frequency is part of the definition of ν, we don't see its effects here because it is closely linked to the aridity index. However, insofar as rainfall frequency drives the basin aridity, it also drives discharge variability.

4.5.5 *Comparison to data*

The data set of Rossi, Whipple, and Vivoni, (2016) shows the ν-μ scaling for a large sample of basins from around the United States, as well as a smaller sample from Puerto Rico. The basins from the US have an interquartile range of 118 to 796 km^2, while the basins in Puerto Rico range from 3 to 48 km^2. We performed a Monte Carlo simulation with uniformly distributed, ecohydroclimatic parameters, all independent except for the previously discussed correlation between rainfall frequency and intensity, and assume that catchments with greater than 10% snow have a response time of 15-60 days, that those with less than 10% have a mean response time of 5-8 days (a common response time for moderate sized basins) and that the small basins of Puerto Rico have a response time of 2-4 days.

The theory presented here captures the first order features of empirical ν-μ scalings even with simplistic parameter ranges (uniformly distributed parameters) and simple estimates of the response time behaviour (figure 45) .

Similar to the mean runoff, the scaling of ν with the ratio of wet days to dry days ($f = \lambda/(1-\lambda)$) can also be simulated. First, the patterns observed by Rossi, Whipple, and Vivoni, (2016), that the variability decreases (c_r increases) with higher rainfall frequency (figure 47b), matches general theoretical expectations (figure 44a). Further, we find that the scaling found with our simulation matches the empirical data well (figure 47). The assumed difference in the basin response time between the US sample and the Puerto Rico sample due to basin size can potentially explain the observed differences in the scaling of ν with $\lambda/(1-\lambda)$ between the two regions.

The final comparison we make to this data set is the scaling of daily variability with the aridity index (ϕ). The general trend of increasing variability (decreasing c_r) with aridity observed by Rossi, Whipple, and Vivoni, (2016) (figure 48b) is again in line with theoretical predictions (figure 44). Again, as before, we can replicate the observations with our Monte Carlo simulation (figure 48a).

The effect of increasing the basin size on the μ-ν scaling can be approximated if it is assumed that the basin response time increases with increasing basin area. In addition to an increasing response time (due to longer travel paths for the water), it is also likely

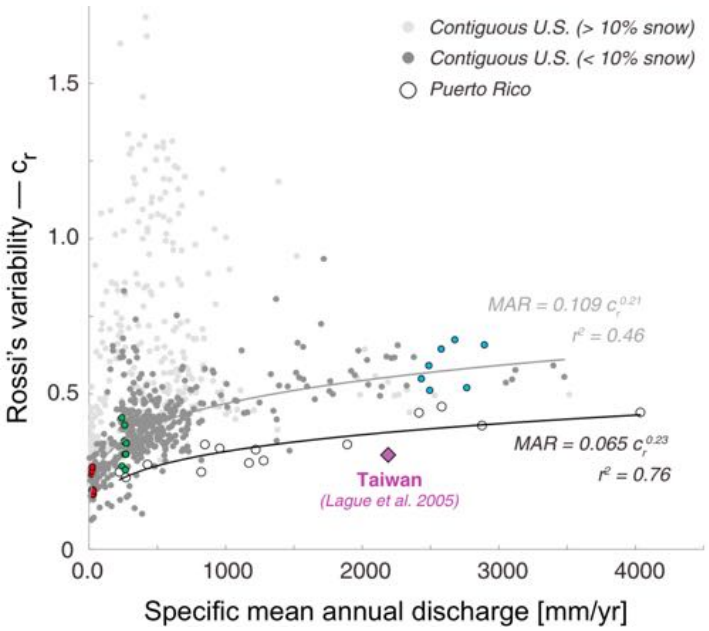

Figure 45: Figure from Rossi, Whipple, and Vivoni, (2016) showing observed relationship between μ and ν for rivers from the US with >10% contribution from snow (light grey points), <10% contribution from snow(dark grey points), and rivers from Puerto Rico. I believe the relationship between MAR and c_r in the figure is written backwards, and should be $c_r \propto MAR^{0.2}$, which means $\eta \approx 0.2$ in this data set.

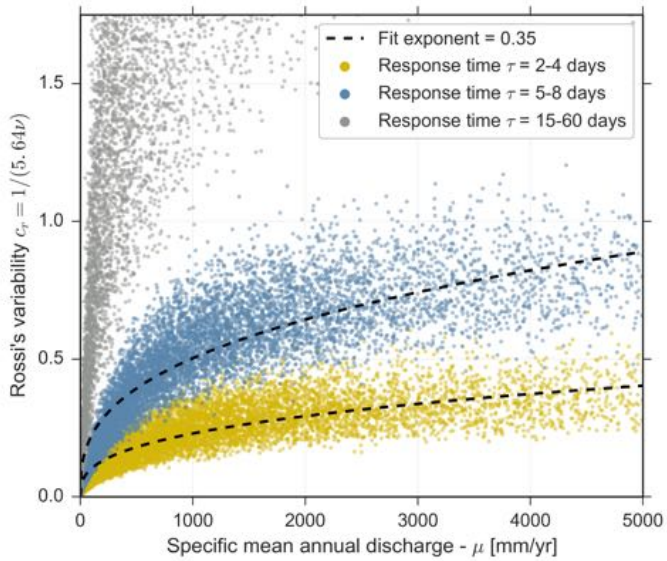

Figure 46: Results of the Monte Carlo simulation. The blue points correspond the moderate sized US catchments with $<$ 10% snow (dark grey points in figure 45), the grey points to the US catchments with $>$ 10% (light grey points in figure 45) and the yellow points to small Puerto Rico catchments (white points in figure 45). c_r is a measure of daily variability linearly related to $1/\nu$ used by Rossi, Whipple, and Vivoni, (2016) to describe variability.

that the storm intensity will decrease. This is because the storm intensity is averaged over the entire basin, and as the basin increases in size, the likelihood that a storm only

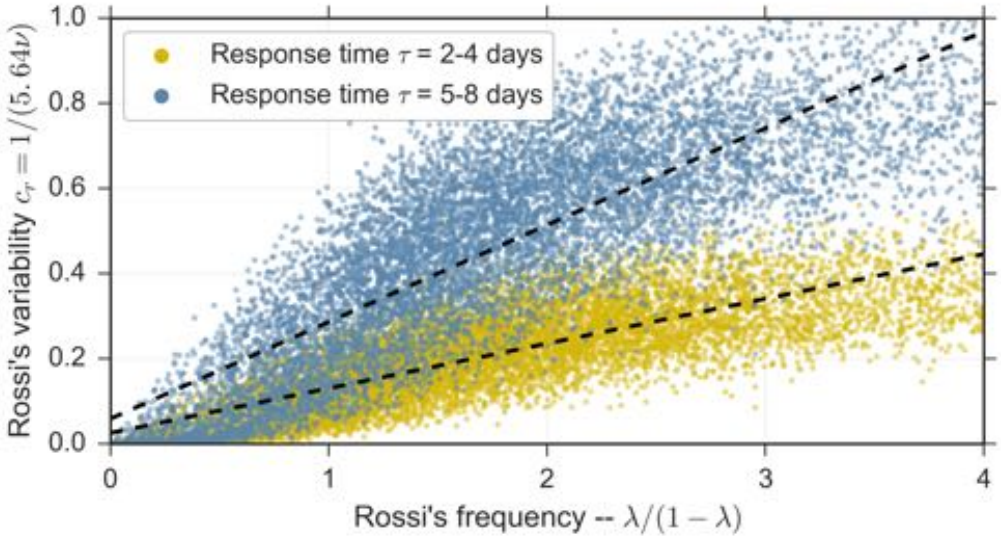

(a)

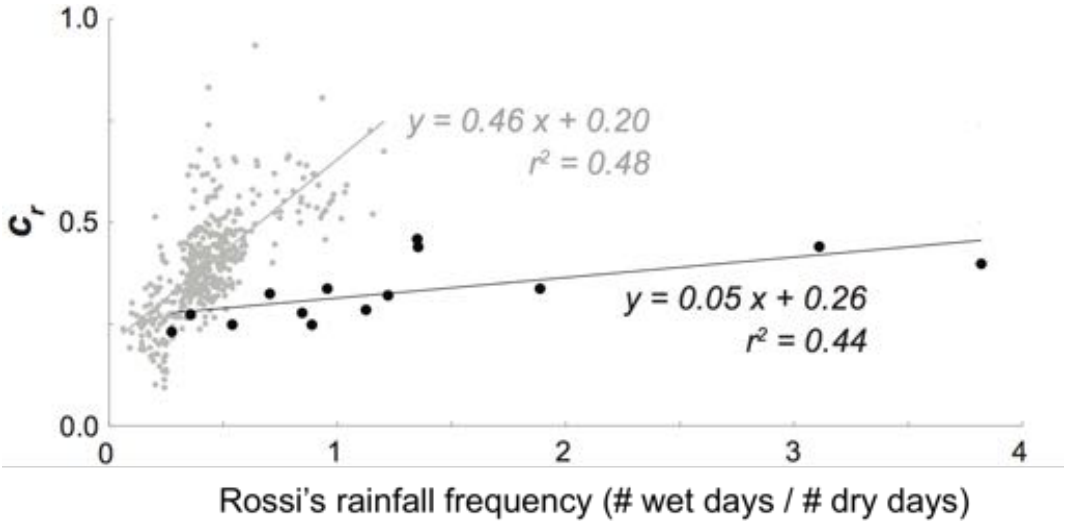

(b)

Figure 47: (a) Results of the Monte Carlo simulation. The blue points correspond the moderate sized US catchments with $<$ 10% snow (grey points in panel b) and the yellow points to the small Puerto Rico catchments (black points in panel b) from Rossi, Whipple, and Vivoni, (2016). (b) Figure from Rossi, Whipple, and Vivoni, (2016) showing observed relationship between rainfall frequency and variability for rivers in the US (gray points) and Puerto Rico (black points).

effects a portion of the basin increases. These 'partial' storms are then averaged over the entire area of the basin, with the effect of decreasing the observed storm intensity. We compare the results of a Monte Carlo simulation to a different data set from Molnar et al., (2006). Figure 49 compares the model results to the data set. The fact that larger basins are shifted to the right relative to smaller basins is well reproduced by the simulations. Increasing the response time and decreasing the storm intensity have the same effect on the μ-ν scaling, so either one is sufficient to replicate the observations, but together they have a stronger effect.

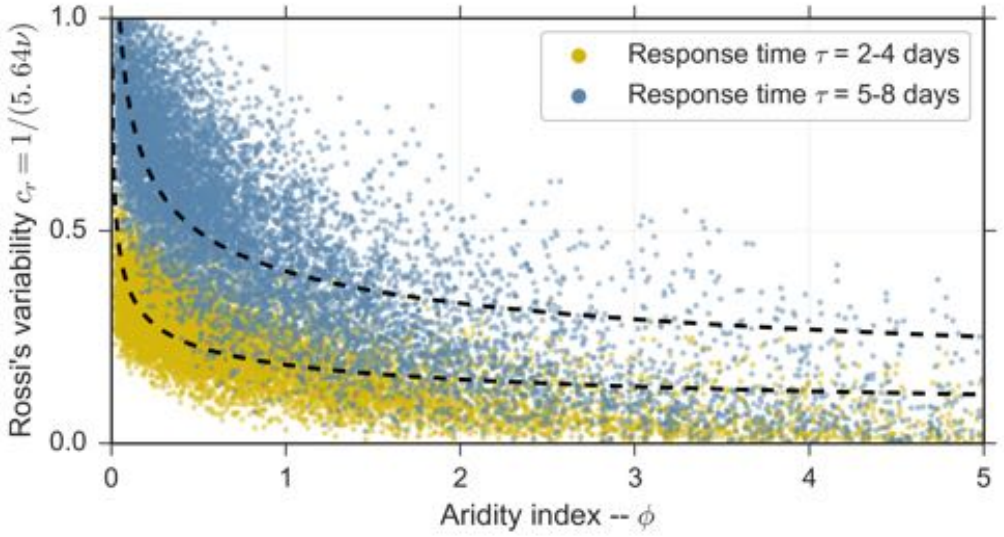

(a)

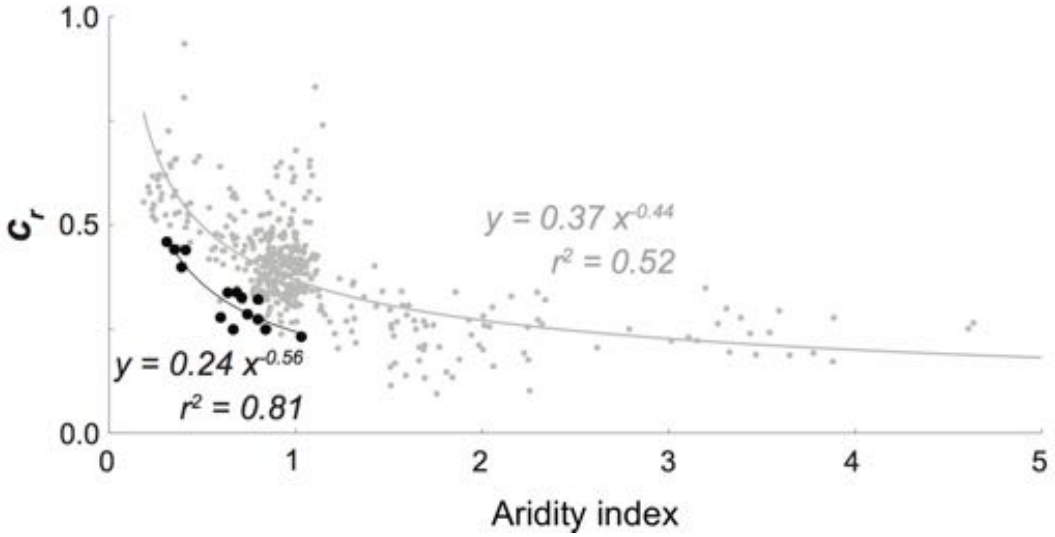

(b)

Figure 48: (a) Results of the Monte Carlo simulation. The blue points correspond the moderate sized US catchments with $<$ 10% snow (grey points in panel b) and the yellow points to the small Puerto Rico catchments (black points in panel b) from Rossi, Whipple, and Vivoni, (2016). (b) Figure from Rossi, Whipple, and Vivoni, (2016) showing observed relationship between aridity and variability for rivers in the US (gray points) and Puerto Rico (black points).

4.6 CONCLUSION

We have demonstrated that there exists a global limit on variability as a function of mean runoff that depends on a few easily measured parameters. Because it is the combined knowledge of the mean runoff and the runoff variability that yields information about the frequency and magnitude of flood events, this scaling allows for the estimation of the upper limit of flood distributions with limited information. By combining this upper limit with an estimate of the shape of the runoff distribution, concrete esti-

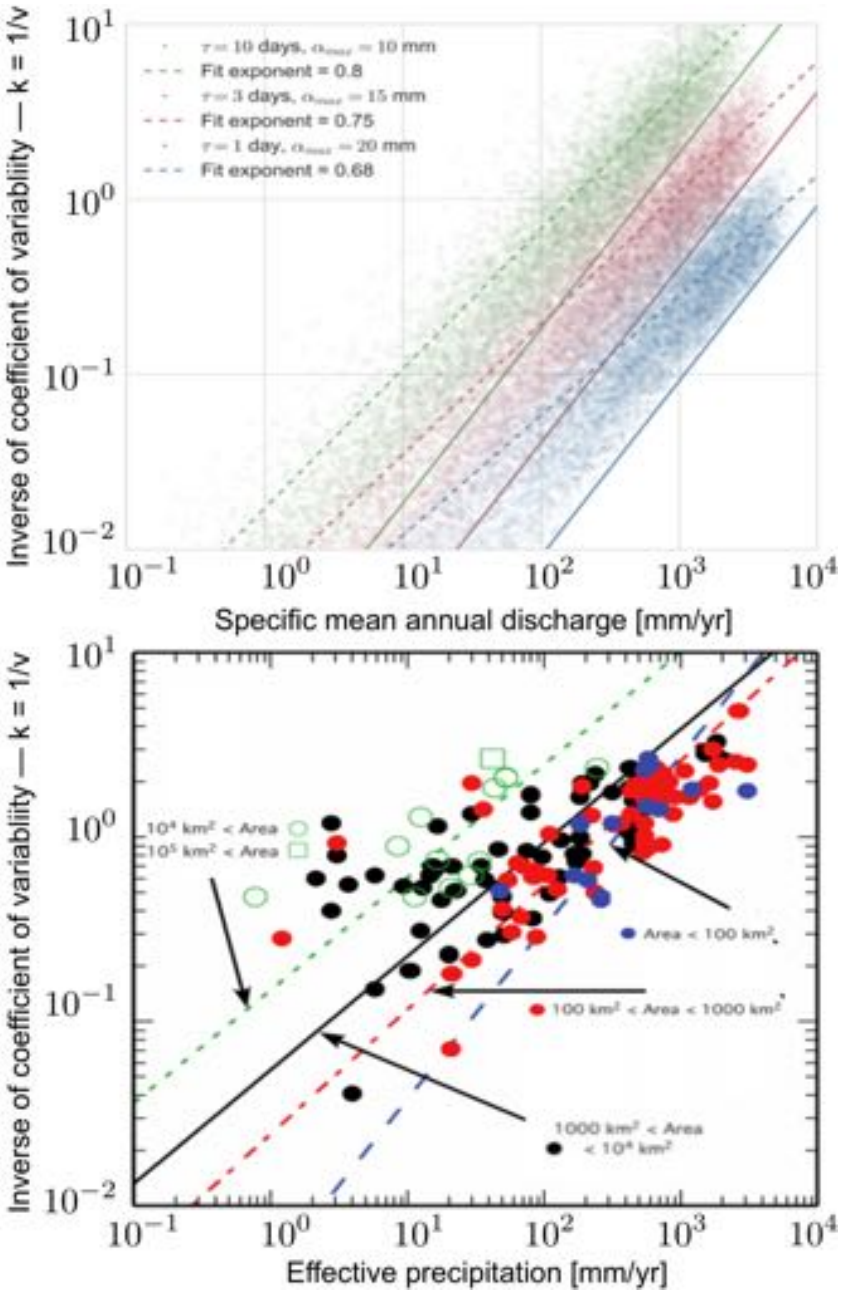

Figure 49: (a) Coloured points represent changes in the μ-ν scaling as a result of increasing the basin response time and decreasing the storm intensity as a surrogate for increasing catchment area. Solid lines show the upper variability limit, dashed lines show fit trend. (b) Figure from Molnar et al., (2006) showing data set of discharge variability and mean separated by basin size. Lines represent fit trends.

mates of the upper limit on flood distribution can be made. The close match between the theory and the observations with very limited knowledge about the individual river basins implies a generality to the controls on discharge variability.

The theoretical scaling of daily variability with several ecohydroclimatic parameters, and especially the mean runoff, provides a simple framework to interpret the observed range of daily runoff variability and its controls. We find that the aridity index, ϕ, the basin response time, τ, and the effective soil depth, h_s, are the most important controls on the coefficient of variability; a result that emerges from theoretical considerations

and the Monte Carlo simulations. This conclusion is further supported by the data set of Rossi, Whipple, and Vivoni, (2016). Finally, a power law relationship between the mean and variability of discharge with a negative exponent emerges naturally from the theory, and the value of the exponent matches observations when correlation between governing ecohydroclimatic parameters is taken into account.

5

PROCESS INDEPENDENT INFLUENCE OF CLIMATIC VARIABILITY

5.1 ABSTRACT

How climate and short-term climate variability (i.e. meteorology) modulate erosional processes and, on the longer term, control the shape of the Earth's surface is a much debated issue. Here we demonstrate that the way the Earth's surface responds to short-term climatic forcing variability is primarily determined by the existence and magnitude of erosional thresholds. We show that, irrespective of the nature of the erosional process, it is the ratio between the threshold magnitude and the mean magnitude of climatic forcing that determines whether variability matters or not and in which way. Among many other implications, our findings help provide a general framework to understand and predict the response of the Earth's surface to changes in mean and variability of, in particular, rainfall, associated with the anthropogenic release of greenhouse gases into the atmosphere.

5.2 INTRODUCTION

Climatic forcing undoubtedly plays an important role in shaping the Earth's surface. However, precisely how climate affects erosion rates, landscape morphology and the sedimentary record is highly debated (e.g. Burbank et al., 2003; Dadson et al., 2003; Reiners et al., 2003a; Tucker and Hancock, 2010a; Finnegan, Schumer, and Finnegan, 2014; Godard et al., 2014; Willenbring and Jerolmack, 2015; Herman and Champagnac, 2016). Much attention is paid to how erosion responds to changes in climate (e.g. Molnar and England, 1990; Molnar, 2004). However, even stable climatic conditions are intrinsically variable over short timescales, as rainfall rate and temperature change from hour to hour and month to month. An important question that arises is to determine how this 'meteorological variability' influences erosion rates. This is essential to predict not only the long-term evolution of Earth's landforms but also how the warming climate of the Anthropocene and the associated changes in the distribution of extreme climatic events are likely to affect the frequency of landslides, rockfalls and mudslides. It is now well established that the intensity of rainfall increases with air temperature (Trenberth et al., 2003; Berg, Moseley, and Haerter, 2013; O'Gorman, 2015), changing the probability distribution of both stratiform and convective rainfall, which will increase rainfall variability without substantially increasing the mean amount of rainfall (figure 50a).

Previous studies have shown that the cumulative erosional effect of rain storms and floods of different magnitudes cannot be understood in terms of their mean tendencies alone (Tucker and Bras, 2000; Snyder et al., 2003; Tucker, 2004; Lague, Hovius, and Davy, 2005; Lague, 2014). This is attributable in large part to the existence of erosion thresholds that inhibit erosion during small to moderate meteorological events. This can be understood intuitively following, for example Leopold, (1951), who argued that because sediment is only mobilized by storms with rainfall intense enough to

produce surface runoff, the maximum rainfall intensity might be a better measure of the erosivity of a given climate than mean annual rainfall.

Erosional thresholds have been demonstrated or hypothesised to exist for many processes, including erosion and channel head initiation due to overland flow (e.g. Horton, 1945; Montgomery and Dietrich, 1992; Prosser and Dietrich, 1995), fluvial transport of bed-load sediment (e.g. Shields, 1936; Bagnold, 1980), fluvial erosion of bedrock channels (e.g. Howard, 1994; Baker and Kale, 1998), debris flows and shallow land sliding (e.g. Gabet et al., 2004; Guzzetti et al., 2008), as well as solifluction and soil creep (e.g. Matsuoka, 2001). Throughout the history of quantitative geomorphology, they have been invoked to describe the complexity of the relationship between climate and erosion, as well as the relative importance of moderate vs. extreme climatic events (Wolman and Miller, 1960; Schumm, 1979; Blum and Valastro, 1989; Tucker and Bras, 1998; Lague, 2014).

Although previous studies have demonstrated the important role of erosion thresholds and meteorological variability in erosional systems, they have exclusively dealt with fluvial sediment transport and erosion, and have made use of process laws where erosion is a monotonically increasing function of meteorological forcing, such as the stream power model. Such simple process laws are known to dramatically oversimplify the process of fluvial erosion and transport, and the wisdom of their application in modelling fluvial erosion, particularly over short timescales, is debated (e.g. Beer and Turowski, 2015) (c.f. Ferrier, Huppert, and Perron, 2013). In particular, these laws ignore the effect of sediment supply entirely, which is known to be important (**others**; Sklar and Dietrich, 2004), especially when variable climatic forcing is taken into account (Lague, 2010).

Here we demonstrate that the influence of erosion thresholds and the relative importance of extreme events to the mean magnitude of forcing (i.e. variability) are fundamental in nature, and do not depend on any given process law. We show how this general conclusion arises mostly from the nature of the probability distribution of meteorological forcing. We demonstrate that even without a functional description of a process law, these results hold true, further supporting the process independence of the dynamics of variability and erosion thresholds.

5.3 RESULTS AND DISCUSSION

The most important factor determining the influence of meteorological variability and erosion thresholds on long-term erosion rates is the erosion frequency (the fraction of time erosion is occurring). How the frequency of erosion responds to changes in variability depends on the magnitude of the erosion threshold. When erosion thresholds are low, they are exceeded often and erosion frequency is high. This is true for both low and high variability forcing. When thresholds are high, low variability systems suffer a major reduction in erosion frequency because large magnitude events that can exceed the erosion threshold are rare (solid lines in figure 50b and c). The result is a significant decrease in the erosion efficiency (erosion rate divided by mean climatic forcing). In contrast, the erosion efficiency of high variability streamflow is relatively immune to high erosion thresholds (dashed lines in figure 50b and c).

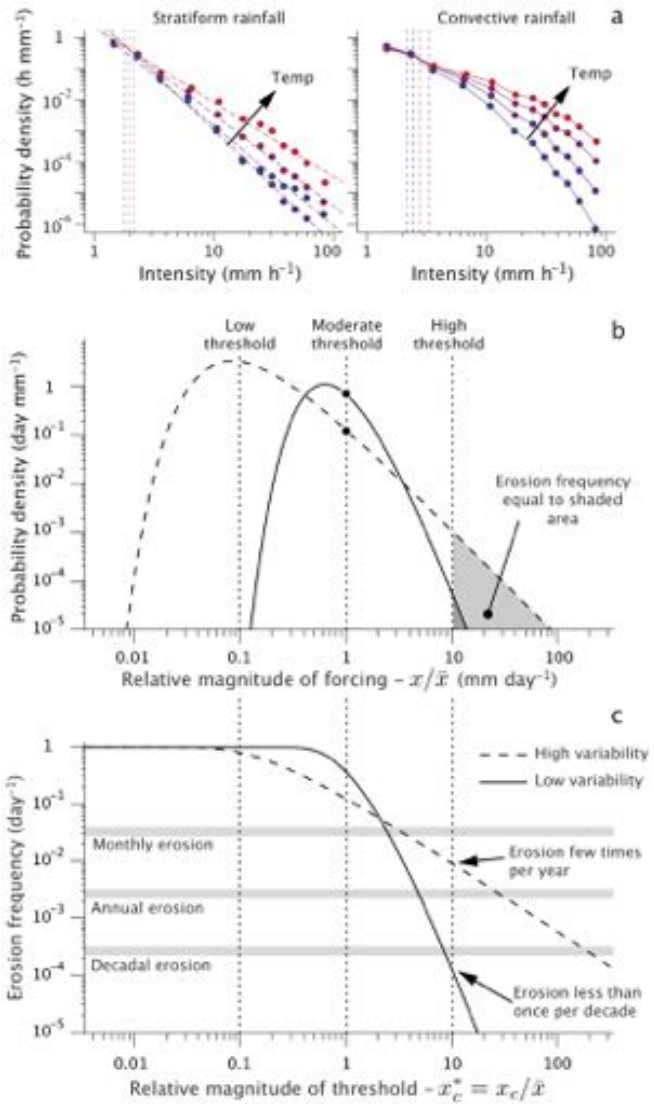

Figure 50: (a) Observed changes in distributions of hourly rainfall intensity as a function of temperature over Germany (adapted from Berg, Moseley, and Haerter, (2013)). There is less than a factor of 2 change in mean hourly rainfall rate, but greater than factor 5 increase for maximum annual hourly rainfall rate. (b) Comparison of low variability and high variability distributions (shown is inverse gamma distribution commonly used to model daily river discharge). Black circles show mean. (c) Erosion frequency as a function of relative erosion threshold magnitude for distributions in (b). When $x_c^* > 1$, the frequency of erosion for high and low variability distributions quickly deviates.

Erosion frequency is the probability of exceeding the erosion threshold (figure 50c), which can be calculated from the probability distribution of meteorological forcing $f_X(x)$ (figure 50b),

$$\Pr[x > x_c] = \int_{x_c}^{\infty} f_X(x)\, dx. \tag{100}$$

where x_c is the critical meteorological forcing magnitude required to exceed the erosion threshold. For simplicity, we will call x_c the climatic threshold. Equation 100 implies that erosion frequency is independent of the erosion process law used, depend-

ing solely on the probability distribution of meteorological forcing and the magnitude of the erosion threshold.

By definition, low variability distributions are more tightly clustered around the mean (figure 50b). As a result, the erosion efficiency of systems under low variability meteorological forcing begins to decrease rapidly when the erosion threshold is large enough that the climatic threshold, x_c, becomes larger than the mean climatic forcing, $\bar{x}$. In contrast, the erosion efficiency of systems under high variability forcing is dominated by extreme events that are only impacted by very large erosion thresholds. Therefore the erosion efficiency of climatic regimes with high and low variability begins to diverge when the climatic threshold, x_c, approaches the mean magnitude of climatic forcing (equivalently when $x_c^* = x_c/\bar{x} \approx 1$). This critical erosion threshold value is a fundamental property of probability distributions, and not related to any particular meteorological probability distribution or erosion process law.

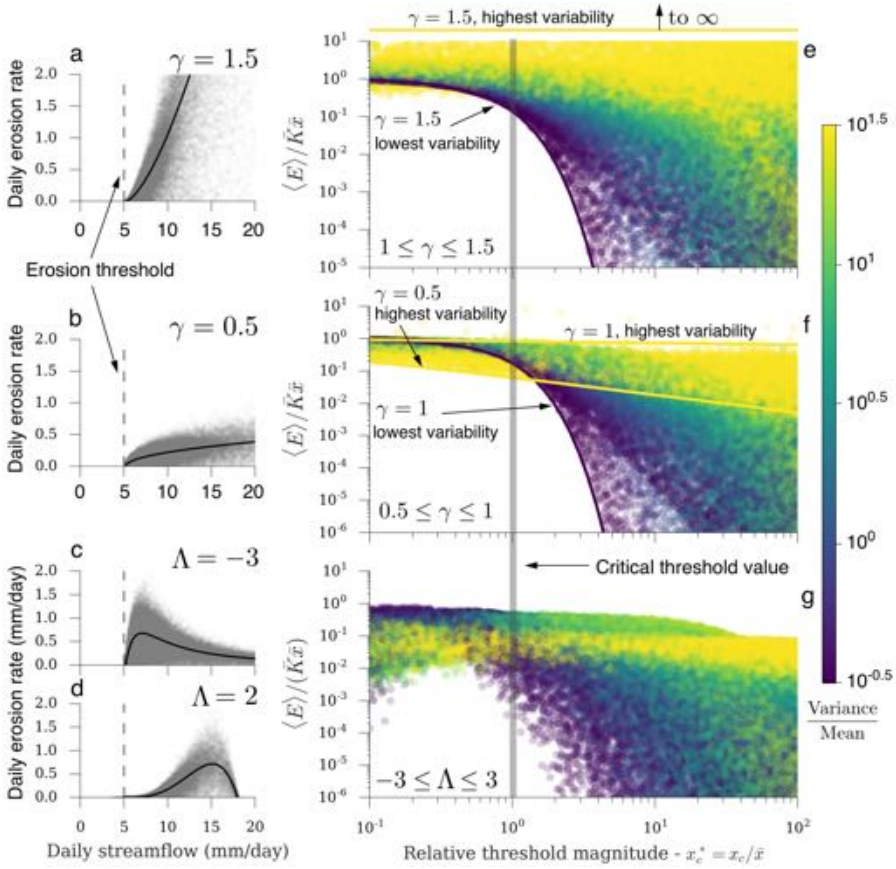

Figure 51: Monte Carlo simulations were conducted for super-liner stream power like laws (a), sub-linear stream power like laws (b), and tool and cover like laws with sediment supply characterized as flood cleaning (c) and flood depositing (d). Noise was introduced into each law (gray points in a-d). (e) shows the result of 50,000 simulations for super-linear laws ($1 \leqslant \gamma \leqslant 1.5$). Each point represents a simulation, the color shows the variance of the meteorological forcing distribution. Theoretical bounds are shown as colored lines. (f) shows the result of 50,000 simulations for sub-linear laws ($1 \leqslant \gamma \leqslant 1.5$). (g) shows the result of 100,000 simulations for decreasing, tools and cover laws ($-3 \leqslant \Lambda \leqslant 3$).

We tested our theoretical predictions by investigating the impact of meteorological variability on erosional efficiency using a variety of erosion process laws. We considered laws where erosion rate increases monotonically with climatic forcing (similar

to the stream power model) and the relationship between erosion efficiency and climatic forcing can be sub-linear or super-linear, parameterized by $\gamma < 1$ and $\gamma > 1$ respectively (figure 51a and b). We also considered laws were erosion rate can decrease with increasing climatic forcing (similar to the tool-and-cover effect (Sklar and Dietrich, 2004)) where we parameterize the relationship between fluvial transport capacity and sediment supply in a manner that allows for a flood-cleaning regime ($\Lambda < 0$ - big floods expose riverbed to erosion, figure 51c) and a flood-depositing regime ($\Lambda > 0$ - big floods cover riverbed, protecting it from erosion,, figure 51d) (Turowski et al., 2013). These are all fluvial erosion laws, but they also represent a wide range of functional forms that could parameterize many other processes. To further emphasise the process independence and simulate multiple controls on erosion (e.g. river discharge and sediment supply for fluvial erosion), we introduce a significant random element by making the rate constant in each process law a random variable that is normally distributed with standard deviation equal to half the mean value of the rate constant ($\sigma = \bar{K}/2$). For each law we explored the impact of variability with 50,000 Monte Carlo simulations, each averaging 50,000 individual erosion events (figure 51e-g). To describe the forcing, we used both heavy tailed and light tailed gamma distributions with randomly chosen shape parameters. This provided a range of variability similar to that seen in natural systems (Lague, 2014; Rossi, Whipple, and Vivoni, 2016). We further randomly selected the erosion threshold and calculated the resulting long-term erosion efficiency (for more details on the model setup see appendix).

Despite random noise, the Monte Carlo simulations match the theory (figure 51e and f). In addition, the Monte Carlo simulations of tools and cover laws yield similar results (figure 51g). We stress how striking it is that the results are so similar, despite the use of very different functions for erosion as well as both heavy- (inverse gamma) and light-tailed (gamma) distributions simulating meteorological forcing. Even the introduction of significant random noise into the process laws does not change the influence of thresholds and variability on the erosion efficiency: when the climatic threshold is much smaller than the mean magnitude of climatic forcing ($x_c^* < 1$ - left-hand side of figure 51e-g), variability in forcing has little to no influence on erosional efficiency. If it does, whether high variability systems are more or less erosive than low variability ones depends on the nonlinearity of the relationship between meteorological forcing and erosion. Sub-linear or decreasing process laws (figure 51b-d) lead to high variability systems having less efficient erosion than low variability systems. When the climatic threshold is larger than the mean magnitude of climatic forcing ($x_c^* > 1$ - right-hand side of 51e-g) variability dominates and erosion systems driven by higher variability are always more erosive. One marked difference is that decreasing and sub-linear process laws cannot exceed an erosion efficiency of 1 (figure 51e and g), in contrast to the super-linear laws, which are unbounded (figure 51e).

Table 1: The efficiency of erosion driven by high variability meteorological forcing relative to low variability meteorological forcing

	Low threshold: $x_c/\bar{x} < 1$	High threshold: $x_c/\bar{x} > 1$
$\gamma < 1$	erosion moderately **less** efficient	erosion more efficient
$\gamma = 1$	Variability doesn't matter	erosion more efficient
$\gamma > 1$	erosion moderately more efficient	erosion more efficient

Our calculation, summarized in table 1, reproduces the main results of previous studies on the role of variability in determining long-term erosion efficiency in predominantly fluvial systems. We can also confirm more specific results concerning critical erosion threhold values, for example, that of Tucker, (2004) which stated that rainfall variability begins to become significant when more than half of all rainfall events are filtered out by the threshold. Also confirmed is the critical return time of 1 to 7 days determined in Lague, Hovius, and Davy, (2005), which is associated with an x_c approximately equal to the mean daily discharge. Finally, also shown to match are the regimes defined by Lague, Hovius, and Davy, (2005) and DiBiase and Whipple, (2011) that stated that variability influences the scaling of river channel steepness with erosion rate when the long-term erosion rate is smaller than the normalized erosion threshold, and has little to no influence when the erosion rate is greater than the threshold. However, we can now demonstrate that this behaviour (table 1) is not limited to a specific process, nor is the critical threshold.

To illustrate our point, consider an erosion process driven by rainfall such as soil erosion by surface runoff. If erosion thresholds are small relative to the mean rainfall rate, most storms will cause enough surface runoff to trigger erosion, and the erosion rate will be proportional to mean rainfall rate. The erosion rate will increase during wetter periods and decrease during drier ones. In contrast, when the erosion threshold is large relative to the mean rainfall rate, only storms with high rainfall intensity will trigger erosion. In this case, changes in the intensity of large storms will have a significant impact.

The absolute magnitude of erosional thresholds is likely defined by a combination of external conditions, such as the fracture density of bedrock and the chemical weathering rate on hill slopes which partly determine the average grain size and the degree to which the landscape is vegetated (Sklar et al., 2016). The relative magnitude of the climatic threshold x_c^*, i.e. - the ratio of the absolute threshold magnitude x_c to the mean climatic forcing $\bar{x}$ - does, however, vary when the magnitude of climatic forcing changes through time. This tends to reduce the influence of variability. Returning to the soil erosion example, if climate changes such that the mean rainfall rate increases significantly, the relative magnitude of the erosion threshold decreases, turning high threshold processes into low threshold processes, and rendering variability less important. On the other hand, if the mean rainfall rate decreases significantly, the relative threshold can become so large that nearly no storms can cause surface runoff sufficient to drive soil erosion. As a result erosion rate decreases despite high variability and high thresholds. Therefore, we expect that changes in mean magnitude of meteorological forcing alone influences both high and low threshold processes through the associated change in the relative threshold magnitude (figure 52b).

Note that the situation described above is more likely to occur when the distribution of meteorological forcing is light tailed (dashed line in figure 52a and b). For light-tailed distributions there is a small range of relative threshold magnitudes that are large enough for variability to be important, but small enough to be exceeded on a regular basis. Thresholds larger than this are exceeded so rarely that erosion efficiency is very low. High threshold processes driven by heavy tailed distributions, such a river discharge, respond more consistently to changes in variability across a wider range of relative threshold magnitudes. Because rainfall tends to be light tailed, this implies that erosion processes driven directly by rainfall (such as land sliding) will respond

to changes in the mean rainfall more than changes in the intensity as mean climatic forcing changes through time, regardless of the magnitude of the threshold.

Our findings have important implications for the response of erosional processes to changes in Earth's mean surface temperature. It is well known that the intensity of rainstorms, a major factor in determining rainfall variability, increases in response to increases in the temperature of the atmosphere (Trenberth et al., 2003; Berg, Moseley, and Haerter, 2013). Therefore, high threshold, rainfall driven processes will increase systematically with temperature, while low threshold processes will respond to changes in mean annual rainfall rates, which will vary from location to location (figure 52c).

Our findings leads to even more interesting implications if one considers that the mean magnitude and variability of climatic forcing are often negatively correlated. Regions with high mean rainfall or river discharge tend to exhibit low variability and vice versa chapter 2 as well as (Tucker, 2004; Lague, Hovius, and Davy, 2005; Molnar et al., 2006; Rossi, Whipple, and Vivoni, 2016). This implies that changes in erosion rates of high threshold processes can be negatively correlated with changes in the mean magnitude of climatic forcing through time, as well as negatively correlated with changes in erosion rates of low threshold processes in the same landscape (figure 52d). In agreement with Molnar et al., (2006), we find that the range of conditions over which this is possible is relatively narrow, though it is broader for heavier tailed distributions of meteorological forcing. The negative correlation of mean and variability also has the effect of tempering the response of high threshold processes to changes in either. We expect that the sensitivity of high threshold processes will be largest when meteorological variability changes independent of the mean - e.g. changes in air temperature, or when the relative magnitude of the threshold changes due to external controls on the absolute magnitude - e.g. changes in grain size on hillslopes or in rivers.

There is field evidence to support the idea that the response of erosion processes to climate change is governed by the magnitude of the erosion threshold. In the region encompassing Owen's and Death valleys in the US, it is known that during glacial maxima, when temperatures were lower, the mean annual rainfall rate was higher due to changes in global atmospheric circulation (D'Arcy, Whittaker, and Roda-Boluda, 2016, and references therein). In addition, the Clausius-Clapyron relation, which is the physical basis for the prediction that rainfall intensity will increase with air temperature (Berg, Moseley, and Haerter, 2013; O'Gorman, 2015), implies that these cold, wet periods had low intensity rainfall. Interglacials, on the other hand, were warmer and drier, yet associated with more intense storms. (D'Arcy, Whittaker, and Roda-Boluda, 2016) found evidence in Death Valley that the fluvial transport of sand and gravels increased during cold, wet periods and decreased during warm, dry periods. This makes sense given that transport of these fines is a relatively low threshold process. On the other hand (D'Arcy, 2015) found evidence that in nearby Owen's Valley, the grain size distribution of debris flows decreased during cold, wet glacial maxima and increased again during warmer, drier interglacials. Debris flows are a higher threshold process than the transport of sand and gravel observed in Death Valley, and taking the grain size distribution as a marker of the magnitude of the debris flows, they appear to have responded to increases in rainfall intensity even while the mean annual rainfall rate decreased.

Finally, there are implications for how meteorological variability and erosion thresholds influences the equilibrium form of landscapes. There is a general expectation for many erosion processes that climatic thresholds decrease as slope steepness increases.

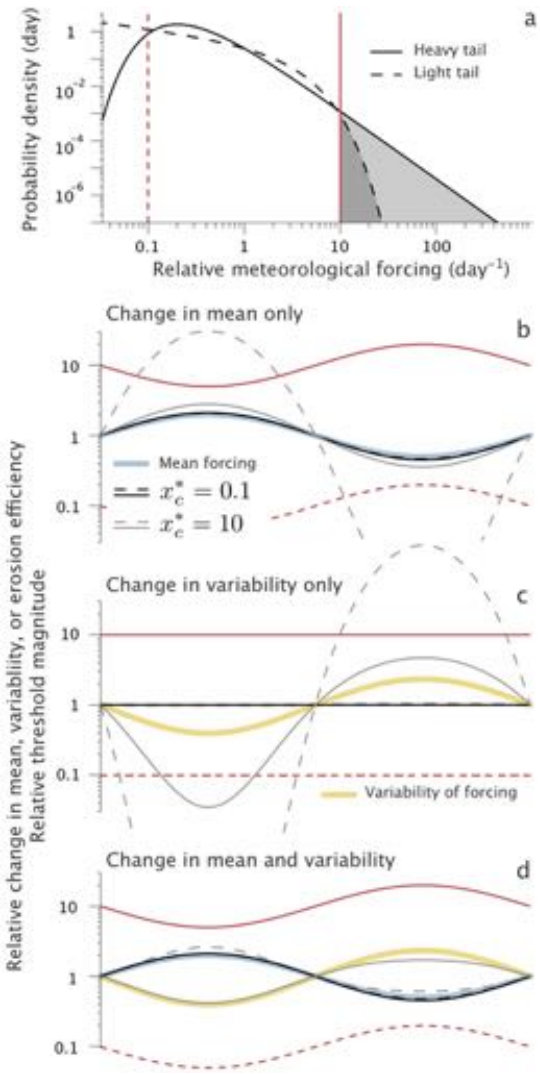

Figure 52: (a) Comparison of the heavy-tailed distribution to the light tailed distribution used in the calculation of (a)-(c). (b) Relative changes in the erosion efficiency due to doubling the mean meteorological forcing and then halving it. Shown are high threshold processes (gray lines) and low threshold processes (black lines) driven by light-tailed distributions of meteorological forcing (dashed lines) or heavy-tailed ones (solid lines). The relative magnitude of the high and low erosion thresholds are shown in solid and dashed red lines, respectively. (c) Same as (b), but halving and then doubling variability of meteorological forcing while holding the mean constant. (d) Same as (b) and (c), but variability and mean vary simultaneously and in the opposite sense.

In the case of fluvial erosion, for example, the streamflow required to exceed the erosion threshold decreases as the riverbed becomes steeper. This implies that steep landscapes (or the steeper parts of a given landscape) are less sensitive to meteorological variability than their less steep counterparts. For fluvial erosion, it has also been demonstrated that the scaling between erosion rate and channel steepness index (a measure of river channel steepness normalized by catchment area) should be a power law (channel steepness $\sim$ (erosion rate)$^{\varphi}$) (Lague, Hovius, and Davy, 2005). When thresholds are high, the exponent, φ, is expected to be less than one. Bolstered by the results of this study that these results are process independent, the frequent observations of scal-

ing between channel steepness index and erosion rate with exponents less than one (Ouimet, Whipple, and Granger, 2009; DiBiase and Whipple, 2011; Lague, 2014) is evidence that fluvial erosion thresholds are commonly larger than the mean streamflow (regardless of fluvial erosion law).

This work provides a basis for the intuition that high variability increases erosion efficiency - with the important qualifier "when thresholds are high". It further provides a metric to assess whether thresholds are high or low. Knowledge of the specifics of a particular place in space and time will be important to understand in detail the erosional response to climatic change. But the generality of these results suggest that previous work on variability and erosion thresholds can be more widely applied. This will be useful as a rule of thumb for making first order approximations for places and processes about which little is known and helps us understand the impact of rapid climate change on the frequency of extreme erosional events.

5.4 APPENDIX A: THRESHOLD STREAM POWER MODEL

Tucker and Bras, (2000) derived equations to describe the impact of stochastic rainfall on sediment transport (using divergence of sediment transport capacity) and erosion in a detachment limited case (using threshold stream power model). These equations can be cast in the general form,

$$\varepsilon = K(x - x_c)^{\gamma}, \tag{101}$$

where ε is the instantaneous erosion rate, K is a rate constant, x is the meteorological forcing (in the case of Tucker and Bras, (2000), it is surface runoff), x_c is the climatic threshold and γ is the nonlinearity between erosion and meteorological forcing.

5.5 APPENDIX B: DERIVATION OF TOOL AND COVER TRANSPORT LAW

We start with an approximate form of the cover and tool law, ignoring effects from the suspension of sediment,

$$\varepsilon(x) \sim \frac{Q_s}{(\tau - \tau_c)^{1/2}} \left(1 - \frac{Q_s}{Q_{cap}}\right), \tag{102}$$

Q_s is the mass sediment supply rate, Q_{cap} is the transport capacity, τ and τ_c are the shear stress and critical shear stress for transport respectively (Sklar and Dietrich, 2006, eq. 1). Relating transport capacity to excess shear stress as $Q_{cap} \sim (\tau - \tau_c)^{3/2}$ (Sklar and Dietrich, 2006), we can simplify equation 102,

$$\varepsilon(x) \sim Q_{cap}^{2/3} \frac{Q_s}{Q_{cap}} \left(1 - \frac{Q_s}{Q_{cap}}\right), \tag{103}$$

Finally, we the relationship between transport capacity, sediment supply, and river discharge from Turowski et al., (2013),

$$\left(\frac{x - x_c}{x_b}\right)^{\wedge} = \frac{Q_s}{Q_{cap}}, \tag{104}$$

where x is daily streamflow, x_c is a critical streamflow to move sediment and x_b is a reference streamflow. We make the further assumption that the transport capacity is

approximately proportional to daily streamflow ($x \sim Q_{cap}$). This allows us to reach an approximate erosion rate as a function of daily streamflow, as well as represent both flood cleaning and flood depositing regimes,

$$\varepsilon(x) = Kx^{2/3} \left(\frac{x - x_c}{x_b} \right)^{\Lambda} \left(1 - \left(\frac{x - x_c}{x_b} \right)^{\Lambda} \right), \tag{105}$$

where K is a rate constant to provide equality.

5.6 APPENDIX C: MONTE CARLO SIMULATION SETUP

To provide an even spread of simulations in the logarithmic space of figure 51, half of the erosion threshold x_c values are selected randomly from a uniform distribution ($0.1 \leqslant x_c^* \leqslant 100$) and half are selected randomly from a uniform distribution of the log of the threshold ($-1 \leqslant \log_{10}(x_c^*) \leqslant 2$). The probability distribution used is either a light tailed gamma distribution,

$$f_X(x) = \frac{k^k}{\Gamma(k)} \left(\frac{x}{\mu} \right)^{k-1} e^{-kx/\mu}, \tag{106}$$

or a heavy tailed inverse gamma distribution,

$$f_X(x) = \frac{k^{k+1}}{\Gamma(k+1)} \left(\frac{x}{\mu} \right)^{-k-2} e^{-k\mu/x} \tag{107}$$

where k is the shape parameter that controls the variability for both distributions. There is a 50% chance of selecting one or the other distribution. The natural log of the shape parameter is chosen from a uniform distribution for $-3 \leqslant \log(k) \leqslant 1.5$, which covers most of the natural range of shape parameters observed on Earth (Rossi, Whipple, and Vivoni, 2016). We chose from a distribution of $\log(k)$ to ensure that high variable regimes ($k < 1$) are properly sampled.

Each simulation consists of 20,000 daily erosion events. The daily erosion rate $\varepsilon(x)$ is calculated using either equation 101 or 105. The exponents γ and Λ, which dictates the behavior of the process law, were randomly selected from a uniform distribution ($0.5 \leqslant \gamma \leqslant 1.5$ or $-3 \leqslant \Lambda \leqslant 3$), and are held constant for all 20,000 events in a single simulation. The erosion threshold x_c, meteorological probability distribution function $f_X(x)$ and shape parameter k are also held constant over each simulation. Noise is introduced into the process laws by substituting the rate constant K with a random variable K_{rand} normally distributed around the value of K, with a standard deviation equal to K/2. For each daily erosion event, a value of K_{rand} is selected randomly. The rare values of K_{rand} that would be negative are reflected back into the positive domain. The long-term erosion rate is calculated by taking the mean of the 20,000 erosion events, and is normalized with the mean of K_{rand}. Referred to as $\bar{K}$, the mean value is approximately equal to K, which in these simulations is set to one.

NOMENCLATURE

Ecohydrology Symbols

α_s	Mean magnitude of storage recharge
ΔS	Catchment-wide storage change
η	Exponent of power law relationship between discharge mean and variability
$\hat{a}$	Decorrelated recession coefficient
$\langle ET \rangle$	Long-term average daily rate of evapotranspiration
μ	Specific long-term average daily rate of discharge
ν	Coefficient of variability
ν_w	Coefficient of variability for winter season in catchments affected by winter snowfall
ν_{max}	Maximum coefficient expected in a region for a given mean daily discharge
ω	Runoff ratio
ϕ	Aridity index
τ	Average catchment-scale hydrologic response time
τ_d	Delay between snow fall and snow melting [days]
τ_w	Winter catchment-scale hydrologic response time in basins with significant snowfall [days]
τ_{max}	Maximum catchment-scale hydrologic response time in a region [days]
τ_{min}	Minimum catchment-scale hydrologic response time in a region
τ_{storm}	Average time between discharge producing rainstorms
ξ_r	Stochastic catchment-wide recharge events
a	Recession coefficient
b	Recession exponent
C	Normalization constant of pdf of daily discharge when $b \neq 1, 2$
c_r	Shape parameter of stretched exponential distribution, used in Rossi, Whipple, and Vivoni, (2016) to describe variability. Related to ν as $c_r = 0.177/\nu$
c_s	Coefficient of catchment-wide storage-discharge relationship
d	Exponent of catchment-wide storage-discharge relationship

ET_{max} Maximum or potential evapotranspiration rate [mm day^{-1}]

$f_Q^t(q)$ pdf of daily discharge truncated at $q = q_m$ and renormalized so integral over pdf equals one

$f_T(t)$ pdf of rainstorm interarrival periods

$f_{\Delta S}(\Delta S)$ pdf of catchment-wide storage recharge magnitudes

h_s Effective soil depth

k Shape parameter of pdf of daily discharge

n_s Soil layer porosity

p_o Atom of probability that $q = 0$

q Random variable representing daily discharge magnitude

q_* Daily discharge magnitude normalized by mean daily discharge

q_o Daily discharge magnitude at beginning of recession

S Catchment-wide storage

s Random variable representing soil layer moisture fraction

s_1 Soil moisture saturation threshold

s_o Dynamic soil moisture capacity [mm]

s_w Wilting point at which evapotranspiration stops - soil moisture does not decrease below this threshold

Z_r Active soil layer depth [mm]

Stream Power Symbols

$\bar{E}$ Mean long-term daily erosion intensity [mm]

$\bar{K}$ Mean magnitude of noisy erodibility constant used in chapter 5

γ At-a-station stream power discharge-erosion exponent

λ_ε Mean frequency of stream power erosion events [day^{-1}]

$\langle Q \rangle$ Long-term average daily rate of river discharge

Ψ Normalized erosion threshold

ψ Stochastic term describing impact of threshold on discharge events that exceed that threshold

τ_c Critical shear stress for erosion to begin

τ_s Shear stress applied by flowing water

ε Instantaneous stream power erosion rate

ε_m Daily stream power erosion magnitude associated with maximum discharge q_m

ε_o Reference constant-discharge threshold-free stream power erosion rate

A Contributing catchment area

c Exponent of shear stress erosion law

C_ε Normalizing constant for pdf of daily erosion when $b \neq 1, 2$

$f_E(\varepsilon)$ pdf of daily stream power erosion intensity

K Erodibility coefficient

k_e Shear stress erosion law rate constant

m Exponent on A in stream power model

n Exponent on S in stream power model

q_c Critical daily discharge magnitude that exceeds shear stress erosion threshold τ_c

q_m Maximum daily discharge magnitude observed over period of observation

q_{c*} Critical daily discharge magnitude that exceeds erosion threshold normalized by mean daily discharge

q_{m*} Maximum daily discharge magnitude normalized by mean daily discharge

S River channel slope

OTHER SYMBOLS

$\bar{x}$ Mean magnitude of general daily meteorological forcing

$\delta(\cdot)$ Dirac delta function

$\Gamma(\cdot)$ Gamma function

$\Gamma(\cdot, \cdot)$ Regularized upper incomplete gamma function

$\gamma(\cdot, \cdot)$ Regularized lower incomplete gamma function

$\langle E \rangle$ Long-term average erosion rate

$\mathbb{E}[\cdot]$ Expected value

σ Standard deviation of normal distribution used for noise generation in chapter 5

$f_X(x)$ pdf of general meteorological forcing

Q_s Sediment supply rate

Q_{cap} Sediment transport capacity

r^2 Coefficient of determination - used as a measure of quality of fit

x Random variable representing general daily meteorological forcing magnitude of an erosional system

x_b Reference streamflow, such as bankfull

x_c Critical meteorological forcing magnitude required to exceed erosion threshold

x_c^* Critical meteorological forcing magnitude required to exceed erosion threshold normalized by mean magnitude of meteorological forcing

Rainfall Symbols

α Mean daily rainfall intensity [mm] (mean rainfall on days with rainfall)

α_d Dry season mean rainfall intensity

α_w Monsoon season mean rainfall intensity

α_{max} Maximum mean daily rainfall intensity in a region

$\bar{p}$ Specific long-term average daily rate of rainfall

β Scale parameter of gamma distribution

β_d Scale parameter of dry season gamma distribution

β_w Scale parameter of monsoon season gamma distribution

κ Shape parameter of gamma distribution

κ_d Shape parameter of dry season gamma distribution

κ_w Shape parameter of monsoon season gamma distribution

λ Mean daily rainfall frequency

λ_d Dry season mean rainfall frequency

λ_w Monsoon season mean rainfall frequency

$\langle P \rangle$ Long-term average daily rate of rainfall

c_1 Exponent of power law relationship between gamma shape parameter and rainfall frequency

c_1 Exponent of power law relationship between rainfall frequency and intensity

c_2 Exponent of power law relationship between gamma shape parameter and rainfall intensity

$f_d(p)$ Dry season pdf of daily rainfall intensity

$f_w(p)$ Monsoon season pdf of daily rainfall intensity

$f_{max}(p)$ pdf of maximum annual daily rainfall intensity

$F_P(p)$ Annual cdf of daily rainfall intensity

$f_P(p)$ Annual pdf of daily rainfall intensity

n_a Number of rainy days per year

n_w Number of rainy days per monsoon season

p Random variable representing daily rainfall rate

P_{max} Mean maximum annual daily rainfall intensity

T_w Length of monsoon season [days]

BIBLIOGRAPHY

Acosta, V et al. (2015). "Effect of vegetation cover on millennial-scale landscape denudation rates in East Africa." In: *Lithosphere*. DOI: 10.1130/L402.1.

Andermann, C., S. Bonnet, and R. Gloaguen (2011). "Evaluation of precipitation data sets along the Himalayan front." In: *Geochemistry, Geophysics, Geosystems* 12.7.

Anders, Alison M et al. (2006). "Spatial patterns of precipitation and topography in the Himalaya." In: *Geological Society of America Special Papers* 398, pp. 39–53.

Anderson, Malcolm G and Ann Calver (1977). "On the persistence of landscape features formed by a large flood." In: *Transactions of the Institute of British Geographers*, pp. 243–254.

Andrews, Edmund D (1980). "Effective and bankfull discharges of streams in the Yampa River basin, Colorado and Wyoming." In: *Journal of Hydrology* 46.3-4, pp. 311–330. ISSN: 0022-1694. DOI: 10.1016/0022-1694(80)90084-0.

Armitage, John J et al. (2011). "Transformation of tectonic and climatic signals from source to sedimentary archive." In: *Nature Geoscience* 4.4, pp. 231–235.

Armitage, John J et al. (2013). "Temporal buffering of climate-driven sediment flux cycles by transient catchment response." In: 369, pp. 1–11.

Bagnold, RA (1980). "An empirical correlation of bedload transport rates in flumes and natural rivers." In: *Proceedings of the Royal Society of London A: Mathematical, Physical and Engineering Sciences*. Vol. 372. 1751. The Royal Society, pp. 453–473.

Baker, Victor R and Vishwas S Kale (1998). "The role of extreme floods in shaping bedrock channels." In: *Rivers over rock: Fluvial processes in bedrock channels*, pp. 153–165.

Balen, Ronald T van, Freek S Busschers, and Gregory E Tucker (2010a). "Modeling the response of the Rhine–Meuse fluvial system to Late Pleistocene climate change." In: *Geomorphology* 114.3, pp. 440–452.

— (2010b). "Modeling the response of the Rhine–Meuse fluvial system to Late Pleistocene climate change." In: 114.3, pp. 440–452.

Banwart, Steven A, Astrid Berg, and David J Beerling (2009). "Process-based modeling of silicate mineral weathering responses to increasing atmospheric CO2 and climate change." In: *Global Biogeochemical Cycles* 23.4.

Basso, S., M. Schirmer, and G. Botter (2015). "On the emergence of heavy-tailed streamflow distributions." In: *Advances in Water Resources* 82, pp. 98–9105. DOI: 10.1016/j.advwatres.2015.04.013.

Basso, S. et al. (2015). "Climatic and landscape controls on effective discharge." In: *Geophysical Research Letters* 42.20, pp. 8441–8447. DOI: 10.1002/2015GL066014.

Beaty Chester, B. (1963). "Origin of Alluvial Fans, White Mountains, California and Nevada." In: *Annals of the Association of American Geographers* 53.4, pp. 516–535. ISSN: 1467-8306. DOI: 10.1111/j.1467-8306.1963.tb00464.x.

Beaumont, Christopher, Philippe Fullsack, and Juliet Hamilton (1992). "Erosional control of active compressional orogens." In: *Thrust tectonics*. Springer, pp. 1–18.

Beer, Alexander R and JM Turowski (2015). "Bedload transport controls bedrock erosion under sediment-starved conditions." In: *Earth Surface Dynamics* 3.3, p. 291.

Benda, Lee and Thomas Dunne (1997a). "Stochastic forcing of sediment routing and storage in channel networks." In: *Water Resources Research* 33.12, pp. 2865–2880.

Benda, Lee and Thomas Dunne (1997b). "Stochastic forcing of sediment supply to channel networks from landsliding and debris flow." In: *Water Resources Research* 33.12, pp. 2849–2863.

Berg, Peter, Christopher Moseley, and Jan O. Haerter (2013). "Strong increase in convective precipitation in response to higher temperatures." In: *Nature Geoscience*. DOI: 10.1038/ngeo1731.

Berghuijs, Wouter R et al. (2014). "Patterns of similarity of seasonal water balances: A window into streamflow variability over a range of time scales." In: *Water Resources Research* 50.7, pp. 5638–5661.

Berghuijs, Wouter, Andreas Hartmann, and Ross Woods (2016). "Streamflow sensitivity to water storage changes across Europe." In: *Geophysical Research Letters* 43.5, pp. 1980–1987. ISSN: 1944-8007. DOI: 10.1002/2016GL067927.

Bermudez, M, P van der Beek, and M Bernet (2012). "Strong tectonic and weak climatic control on exhumation rates in the Venezuelan Andes." In: *Lithosphere* 5.1, pp. 3–16. ISSN: 1941-8264. DOI: 10.1130/L212.1.

Bharti, Vidhi et al. (2016). "Spatiotemporal characteristics of extreme rainfall events over the Northwest Himalaya using satellite data." In: *International Journal of Climatology*.

Biswal, B. and M. Marani (2010). "Geomorphological origin of recession curves." In: *Geophysical Research Letters* 37.24. DOI: 10.1029/2010GL045415.

Blanckenburg, Friedhelm (2005). "The control mechanisms of erosion and weathering at basin scale from cosmogenic nuclides in river sediment." In: *Earth and Planetary Science Letters* 237.3-4, pp. 462–479. ISSN: 0012-821X. DOI: 10.1016/j.epsl.2005.06.030.

Blum, Michael D and Torbjörn E Törnqvist (2000). "Fluvial responses to climate and sea-level change: a review and look forward." In: *Sedimentology* 47.s1, pp. 2–48.

Blum, Michael D and Salvatore Valastro (1989). "Response of the Pedernales River of Central Texas to Late Holocene Climatic Change." In: *Annals of the Association of American Geographers* 79.3, pp. 435–456. ISSN: 1467-8306. DOI: 10.1111/j.1467-8306.1989.tb00271.x.

Bogaart, Patrick W, Steve W Lyon, and Stefan C Dekker (2016). "Streamflow recession patterns can help unravel the role of climate and humans in landscape coevolution." In: *Hydrology and Earth System Sciences* 20.4, p. 1413.

Bogaart, Patrick W et al. (2003). "Process-based modelling of fluvial system response to rapid climate change I: model formulation and generic applications." In: *Quaternary Science Reviews* 22.20, pp. 2077–2095.

Bookhagen, Bodo (2010). "Appearance of extreme monsoonal rainfall events and their impact on erosion in the Himalaya." In: *Geomatics, Natural Hazards and Risk* 1.1, pp. 37–50.

Bookhagen, Bodo and Douglas Burbank (2006). "Topography, relief, and TRMM-derived rainfall variations along the Himalaya." In: *Geophysical Research Letters* 33.8.

— (2010). "Toward a complete Himalayan hydrological budget: Spatiotemporal distribution of snowmelt and rainfall and their impact on river discharge." In: *Journal of Geophysical Research: Earth Surface (2003-2012)* 115.F3.

Bookhagen, Bodo and Manfred R Strecker (2012). "Spatiotemporal trends in erosion rates across a pronounced rainfall gradient: Examples from the southern Central Andes." In: *Earth and Planetary Science Letters* 327-328.C, pp. 97–110.

Botter, Gianluca et al. (2007). "Basin-scale soil moisture dynamics and the probabilistic characterization of carrier hydrologic flows: Slow, leaching-prone components of the hydrologic response." In: *Water Resources Research* 43.2, n/a–n/a. DOI: 10.1029/2006WR005043.

Botter, Gianluca et al. (2009). "Nonlinear storage-discharge relations and catchment streamflow regimes." In: *Water Resources Research* 45.10, n/a–n/a. DOI: 10.1029/2008WR007658.

Botter, Gianluca et al. (2010). "Natural streamflow regime alterations: Damming of the Piave river basin (Italy)." In: *Water Resources Research* 46.6, n/a–n/a. DOI: 10.1029/2009WR008523.

Botter, Gianluca et al. (2013). "Resilience of river flow regimes." In: *Proceedings of the National Academy of Sciences* 110.32, pp. 12925–12930. DOI: 10.1073/pnas.1311920110.

Bovy, Benoît, Jean Braun, and Alain Demoulin (2016). "A new numerical framework for simulating the control of weather and climate on the evolution of soil-mantled hillslopes." In: 263, pp. 99–112.

Brakenridge, G Robert (1980). "Widespread episodes of stream erosion during the Holocene and their climatic cause." In:

Brutsaert, Wilfried and John L. Nieber (1977). "Regionalized drought flow hydrographs from a mature glaciated plateau." In: *Water Resources Research* 13.3, pp. 637–643. ISSN: 1944-7973. DOI: 10.1029/WR013i003p00637.

Budyko, MI (1974). *Climate and Life, 508 pp*.

Burbank, D. W. et al. (2003). "Decoupling of erosion and precipitation in the Himalayas." In: *Nature* 426.6967, pp. 652–655.

Burgueño, August et al. (2010). "Statistical distributions of daily rainfall regime in Europe for the period 1951–2000." In: *Theoretical and applied climatology* 102.1-2, pp. 213–226.

Caloiero, Tommaso (2014). "Analysis of daily rainfall concentration in New Zealand." In: *Natural hazards* 72.2, pp. 389–404.

Carretier, S et al. (2015). "Erosion in the Chilean Andes between 27° S and 39° S: tectonic, climatic and geomorphic control." In: *Geological Society, London, Special Publications* 399.1, pp. 401–418.

Carretier, Sébastien et al. (2013). "Slope and climate variability control of erosion in the Andes of central Chile." In: *Geology* 41.2, pp. 195–198.

Ceola, Serena et al. (2010). "Comparative study of ecohydrological streamflow probability distributions." In: *Water Resources Research* 46.9. DOI: 10.1029/2010WR009102.

Chen, Bo and Witold Krajewski (2016). "Analysing individual recession events: sensitivity of parameter determination to the calculation procedure." In: *Hydrological Sciences Journal* just-accepted.

Chorley, Richard J and MA Morgan (1962). "Comparison of morphometric features, Unaka Mountains, Tennessee and North Carolina, and Dartmoor, England." In: *Geological Society of America Bulletin* 73.1, pp. 17–34.

Clark, M. P. et al. (2009). "Consistency between hydrological models and field observations: linking processes at the hillslope scale to hydrological responses at the watershed scale." In: *Hydrological Processes* 23.2, pp. 311–319. ISSN: 1099-1085. DOI: 10.1002/hyp.7154.

Collins, D., R. Bras, and Gregory E. Tucker (2004). "Modeling the effects of vegetation-erosion coupling on landscape evolution." In: *Journal of Geophysical Research: Earth Surface (2003-2012)* 109.F3. ISSN: 2156-2202. DOI: 10.1029/2003JF000028.

Coulthard, TJ and MG Macklin (2001). "How sensitive are river systems to climate and land-use changes? A model-based evaluation." In: *Journal of Quaternary Science* 16.4, pp. 347–351.

Craddock, William H. et al. (2007). "Bedrock channel geometry along an orographic rainfall gradient in the upper Marsyandi River valley in central Nepal." In: *Journal of Geophysical Research: Earth Surface (2003-2012)* 112.F3.

Crave, A. and P. Davy (2001). "A stochastic precipiton model for simulating erosion/sedimentation dynamics." In: *Computers & Geosciences* 27.7, pp. 815–827.

D'Arcy, Mitch (2015). "Glacial-Interglacial Climate Changes Recorded by Debris Flow Grain Size, Eastern Sierra Nevada, California." In: *2015 AGU Fall Meeting*. Agu.

D'Arcy, Mitch, Alexander C Whittaker, and Duna C Roda-Boluda (2016). "Measuring alluvial fan sensitivity to past climate changes using a self-similarity approach to grain-size fining, Death Valley, California." In: *Sedimentology*.

Dadson, Simon J et al. (2003). "Links between erosion, runoff variability and seismicity in the Taiwan orogen." In: *Nature* 426.6967, pp. 648–651.

Dahlen, FA and John Suppe (1988). "Mechanics, growth, and erosion of mountain belts." In: *Geological Society of America Special Papers* 218, pp. 161–178.

Daly, Edoardo and Amilcare Porporato (2010). "Effect of different jump distributions on the dynamics of jump processes." In: *Physical Review E* 81.6. ISSN: 1539-3755. DOI: 10.1103/PhysRevE.81.061133.

Del Jesus, Manuel, Andrea Rinaldo, and Ignacio Rodríguez-Iturbe (2015). "Point rainfall statistics for ecohydrological analyses derived from satellite integrated rainfall measurements." In: *Water Resources Research* 51.4, pp. 2974–2985.

Densmore, Alexander L, Philip A Allen, and Guy Simpson (2007). "Development and response of a coupled catchment fan system under changing tectonic and climatic forcing." In: *Journal of Geophysical Research: Earth Surface* 112.F1.

DiBiase, Roman A and Kelin X Whipple (2011). "The influence of erosion thresholds and runoff variability on the relationships among topography, climate, and erosion rate." In: *Journal of Geophysical Research: Earth Surface (2003-2012)* 116.F4. DOI: 10.1029/2011JF002095.

DiBiase, Roman A et al. (2010). "Landscape form and millennial erosion rates in the San Gabriel Mountains, CA." In: *Earth and Planetary Science Letters* 289.1, pp. 134–144.

Dietrich, William E et al. (1993). "Analysis of erosion thresholds, channel networks, and landscape morphology using a digital terrain model." In: *The Journal of Geology*, pp. 259–278.

Doulatyari, Behnam et al. (2015). "Predicting streamflow distributions and flow duration curves from landscape and climate." In: *Advances in Water Resources* 83, pp. 285–298. DOI: 10.1016/j.advwatres.2015.06.013.

Dralle, David, Nathaniel Karst, and Sally Thompson (2015). "a, b careful: The challenge of scale invariance for comparative analyses in power law models of the streamflow recession." In: *Geophysical Research Letters* 42.21, pp. 9285–9293. ISSN: 1944-8007. DOI: 10.1002/2015GL066007.

Eagleson, Peter S. (1978). "Climate, soil, and vegetation: 2. The distribution of annual precipitation derived from observed storm sequences." In: *Water Resources Research* 14.5, pp. 713–721.

Feng, Xue, Amilcare Porporato, and Ignacio Rodriguez-Iturbe (2015). "Stochastic soil water balance under seasonal climates." In: *Proc. R. Soc. A* 471.2174, p. 20140623. DOI: 10.1098/rspa.2014.0623.

Fernandes, Nelson F and William E Dietrich (1997). "Hillslope evolution by diffusive processes: The timescale for equilibrium adjustments." In: *Water Resources Research* 33.6, pp. 1307–1318.

Ferrier, Ken, Kimberly Huppert, and Taylor Perron (2013). "Climatic control of bedrock river incision." In: *Nature* 496.7444, pp. 206–9. ISSN: 0028-0836. DOI: 10.1038/nature11982.

Finnegan, Noah J, Rina Schumer, and Seth Finnegan (2014). "A signature of transience in bedrock river incision rates over timescales of 104-107 years." In: *Nature* 505.7483, pp. 391–394.

Gabet, Emmanuel J. et al. (2004). "Rainfall thresholds for landsliding in the Himalayas of Nepal." In: *Geomorphology* 63.3-4, pp. 131–143. ISSN: 0169-555X. DOI: 10.1016/j.geomorph.2004.03.011.

Gallen, Sean F et al. (2015). "The dynamic reference frame of rivers and apparent transience in incision rates." In: *Geology* 43.7, pp. 623–626. ISSN: 0091-7613. DOI: 10.1130/g36692.1.

Galy, Valier et al. (2007). "Efficient organic carbon burial in the Bengal fan sustained by the Himalayan erosional system." In: *Nature* 450.7168, pp. 407–410.

Ganti, Vamsi et al. (2016). "Time scale bias in erosion rates of glaciated landscapes." In: 2.10, e1600204. DOI: 10.1126/sciadv.1600204.

Gilbert, Grove Karl (1877). *Report on the Geology of the Henry Mountains*. US Government Printing Office.

Godard, Vincent et al. (2013). "Frequency-dependent landscape response to climatic forcing." In: *Geophysical Research Letters* 40, pp. 1–5.

Godard, Vincent et al. (2014). "Dominance of tectonics over climate in Himalayan denudation." In: *Geology* 42.3, pp. 243–246.

Guzzetti, Fausto et al. (2008). "The rainfall intensity-duration control of shallow landslides and debris flows: an update." In: *Landslides* 5.1, pp. 3–17. ISSN: 1612-510X. DOI: 10.1007/s10346-007-0112-1.

Hancock, Gregory S and Robert S Anderson (2002). "Numerical modeling of fluvial strath-terrace formation in response to oscillating climate." In: *Geological Society of America Bulletin* 114.9, pp. 1131–1142.

Harman, C J, M Sivapalan, and P Kumar (2009). "Power law catchment-scale recessions arising from heterogeneous linear small-scale dynamics." In: *Water Resources Research* 45.9. DOI: 10.1029/2008WR007392.

Herman, Frédéric and Jean-Daniel Champagnac (2016). "Plio-Pleistocene increase of erosion rates in mountain belts in response to climate change." In: *Terra Nova* 28.1, pp. 2–10.

Hodges, KV, JM Hurtado, and KX Whipple (2001). "Southward extrusion of Tibetan crust and its effect on Himalayan tectonics." In: *Tectonics* 20.6, pp. 799–809.

Horton, RE (1945). "Erosional development of streams and their drainage basins; hydrophysical approach to quantitative morphology." In: *Geological society of America bulletin*.

Howard, Alan D (1994). "A detachment-limited model of drainage basin evolution." In: *Water Resources Research* 30.7, pp. 2261–2285.

Huang, Xiangjiang and Jeffrey Niemann (2006a). "An evaluation of the geomorphically effective event for fluvial processes over long periods." In: *Journal of Geophysical Research: Earth Surface (2003-2012)* 111.F3. ISSN: 2156-2202. DOI: 10.1029/2006jf000477.

— (2006b). "Modelling the potential impacts of groundwater hydrology on long-term drainage basin evolution." In: *Earth Surface Processes and Landforms* 31.14, pp. 1802–1823. ISSN: 1096-9837. DOI: 10.1002/esp.1369.

— (2008). "How do streamflow generation mechanisms affect watershed hypsometry?" In: *Earth Surface Processes and Landforms* 33.5, pp. 751–772.

Huffman, George et al. (2007). "The TRMM Multisatellite Precipitation Analysis (TMPA): Quasi-Global, Multiyear, Combined-Sensor Precipitation Estimates at Fine Scales." In: *Journal of Hydrometeorology* 8.1, p. 3855.

Ijjász-Vásquez, Ede J, Rafael L Bras, and Glenn E Moglen (1992). "Sensitivity of a basin evolution model to the nature of runoff production and to initial conditions." In: *Water Resources Research* 28.10, pp. 2733–2741.

Istanbulluoglu, Erkan (2009). "An Eco-hydro-geomorphic Perspective to Modeling the Role of Climate in Catchment Evolution." In: *Geography Compass* 3.3, pp. 1151–1175.

Istanbulluoglu, Erkan and Rafael L. Bras (2006a). "On the dynamics of soil moisture, vegetation, and erosion: Implications of climate variability and change." In: *Water Resources Research*. DOI: 10.1029/2005WR004113.

Istanbulluoglu, Erkan and Rafael Bras (2005). "Vegetation-modulated landscape evolution: Effects of vegetation on landscape processes, drainage density, and topography." In: *Journal of Geophysical Research: Earth Surface (2003-2012)* 110.F2. ISSN: 2156-2202. DOI: 10.1029/2004jf000249.

— (2006b). "On the dynamics of soil moisture, vegetation, and erosion: Implications of climate variability and change." In: *Water Resources Research* 42.6. ISSN: 1944-7973. DOI: 10.1029/2005wr004113.

Jiang, Peng, Dagang Wang, and Yongqiang Cao (2016). "Spatiotemporal characteristics of precipitation concentration and their possible links to urban extent in China." In: *Theoretical and Applied Climatology* 123.3-4, pp. 757–768.

Joshi, Sneh et al. (2014). "Rainfall variability and indices of extreme rainfall-analysis and perception study for two stations over Central Himalaya, India." In: *Natural Hazards* 72.2, pp. 361–374.

Kirby, Eric and Kelin X Whipple (2012). "Expression of active tectonics in erosional landscapes." In: *Journal of Structural Geology* 44, pp. 54–75.

Kirchner, James W. (1993). "Statistical inevitability of Horton's laws and the apparent randomness of stream channel networks." In: *Geology* 21.7, pp. 591–594. ISSN: 0091-7613. DOI: 10.1130/0091-7613(1993)021<0591:siohsl>2.3.co;2.

Kirchner, James W et al. (2001). "Mountain erosion over 10 yr, 10 ky, and 10 My time scales." In: *Geology* 29.7, pp. 591–594.

Kirchner, James (2009). "Catchments as simple dynamical systems: Catchment characterization, rainfall-runoff modeling, and doing hydrology backward." In: *Water Resources Research* 45.2. ISSN: 1944-7973. DOI: 10.1029/2008WR006912.

Lague, Dimitri (2010). "Reduction of long-term bedrock incision efficiency by short-term alluvial cover intermittency." In: *Journal of Geophysical Research: Earth Surface* 115.F2.

— (2014). "The stream power river incision model: evidence, theory and beyond." In: *Earth Surface Processes and Landforms* 39.1, pp. 38–61. DOI: 10.1002/esp.3462.

Lague, Dimitri, Niels Hovius, and Philippe Davy (2005). "Discharge, discharge variability, and the bedrock channel profile." In: *Journal of Geophysical Research: Earth Surface (2003-2012)* 110.F4. DOI: 10.1029/2004JF000259.

Laio, Francesco et al. (2001). "Plants in water-controlled ecosystems: active role in hydrologic processes and response to water stress: II. Probabilistic soil moisture dynamics." In: *Advances in Water Resources* 24.7, pp. 707–723.

Langbein, W. B. and S. A. Schumm (1958). "Yield of sediment in relation to mean annual precipitation." In: *Eos, Transactions American Geophysical Union*. DOI: 10.1029/TR039i006p01076.

Leopold, Luna B (1951). "Rainfall Frequency: An aspect of climatic variation." In: *Eos, Transactions American Geophysical Union* 32.3, pp. 347–357. ISSN: 2324-9250. DOI: 10.1029/tr032i003p00347.

Malik, Nishant, Bodo Bookhagen, and Peter J Mucha (2016). "Spatiotemporal patterns and trends of Indian monsoonal rainfall extremes." In: *Geophysical Research Letters* 43.4, pp. 1710–1717.

Martin-Vide, Javier (2004). "Spatial distribution of a daily precipitation concentration index in peninsular Spain." In: *International Journal of Climatology* 24.8, pp. 959–971.

Matsuoka, Norikazu (2001). "Solifluction rates, processes and landforms: a global review." In: *Earth-Science Reviews* 55.1, pp. 107–134.

May, W (2004a). "Simulation of the variability and extremes of daily rainfall during the Indian summer monsoon for present and future times in a global time-slice experiment." In: *Climate Dynamics* 22.2-3, pp. 183–204.

May, Wilhelm (2004b). "Variability and extremes of daily rainfall during the Indian summer monsoon in the period 1901-1989." In: *Global and Planetary Change* 44.1, pp. 83–105.

Milly, PCD (1993). "An analytic solution of the stochastic storage problem applicable to soil water." In: *Water Resources Research* 29.11, pp. 3755–3758. DOI: 10.1029/93wr01934.

Molnar, P. and P. England (1990). "Late Cenozoic uplift of mountain ranges and global climate change: chicken and egg?" In: *Nature* 346, pp. 29–34.

Molnar, Peter (2001). "Climate change, flooding in arid environments, and erosion rates." In: *Geology* 29.12, pp. 1071–1074.

— (2004). "Late Cenozoic increase in accumulation rates of terrestrial sediment: How might climate change have affected erosion rates?" In: *Annu. Rev. Earth Planet. Sci.* 32, pp. 67–89.

Molnar, Peter et al. (2006). "Relationships among probability distributions of stream discharges in floods, climate, bed load transport, and river incision." In: *Journal of Geophysical Research: Earth Surface (2003-2012)* 111.F2. DOI: 10.1029/2005JF000310.

Montgomery, David R and William E Dietrich (1992). "Channel initiation and the problem of landscape scale." In: *Science* 255.5046, p. 826.

Mooley, Diwakar A (1973). "Gamma distribution probability model for Asian summer monsoon monthly rainfall." In: *Monthly Weather Review* 101.2, pp. 160–176.

Moon, Seulgi et al. (2011). "Climatic control of denudation in the deglaciated landscape of the Washington Cascades." In: *Nature Geoscience* 4.7, pp. 469–473. ISSN: 1752-0894. DOI: 10.1038/ngeo1159.

Mueller, Marc F. and Sally E. Thompson (2013). "Bias adjustment of satellite rainfall data through stochastic modeling: Methods development and application to

Nepal." In: *Advances in Water Resources* 60, pp. 121–134. ISSN: 0309-1708. DOI: 10.1016/j.advwatres.2013.08.004.

Müller, Marc F, David N Dralle, and Sally E Thompson (2014). "Analytical model for flow duration curves in seasonally dry climates." In: *Water Resources Research* 50.7, pp. 5510–5531.

Newman, A. J. et al. (2015). "Development of a large-sample watershed-scale hydrometeorological data set for the contiguous USA: data set characteristics and assessment of regional variability in hydrologic model performance." In: *Hydrology and Earth System Sciences* 19.1, pp. 209–223. ISSN: 1027-5606. DOI: 10.5194/hess-19-209-2015.

Newson, Malcolm (1980). "The geomorphological effectiveness of floods - a contribution stimulated by two recent events in mid-wales." In: *Earth Surface Processes* 5.1, pp. 1–16.

O'Gorman, Paul A. (2015). "Precipitation Extremes Under Climate Change." In: *Current Climate Change Reports*. ISSN: 2198-6061. DOI: 10.1007/s40641-015-0009-3.

Olen, Stephanie M, Bodo Bookhagen, and Manfred R Strecker (2016). "Role of climate and vegetation density in modulating denudation rates in the Himalaya." In: *Earth and Planetary Science Letters* 445, pp. 57–67.

Ouimet, William B, Kelin X Whipple, and Darryl E Granger (2009). "Beyond threshold hillslopes: Channel adjustment to base-level fall in tectonically active mountain ranges." In: *Geology* 37.7, pp. 579–582.

Park, Jeryang et al. (2014). "Stochastic modeling of hydrologic variability of geographically isolated wetlands: Effects of hydro-climatic forcing and wetland bathymetry." In: *Advances in Water Resources* 69, pp. 38–48. ISSN: 0309-1708. DOI: 10.1016/j.advwatres.2014.03.007.

Pearson, Karl (1896). "Mathematical Contributions to the Theory of Evolution. On a Form of Spurious Correlation Which May Arise When Indices Are Used in the Measurement of Organs." In: *Proceedings of the Royal society of London* 60.359-367, pp. 489–498.

Pedersen, Vivi and David Egholm (2014). "Glaciations in response to climate variations preconditioned by evolving topography." In: *Nature* 493.7431, pp. 206–210.

Phillips, Colin B and Douglas J Jerolmack (2016). "Self-organization of river channels as a critical filter on climate signals." In: *Science* 352.6286, pp. 694–697.

Porporato, A et al. (2002). "Ecohydrology of water-controlled ecosystems." In: *Advances in Water Resources* 25.8, pp. 1335–1348.

Porporato, Amilcare, Edoardo Daly, and Ignacio Rodriguez-Iturbe (2004). "Soil water balance and ecosystem response to climate change." In: *The American Naturalist* 164.5, pp. 625–632.

Prakash, Satya, Ashis K Mitra, and DS Pai (2015). "Comparing two high-resolution gauge-adjusted multisatellite rainfall products over India for the southwest monsoon period." In: *Meteorological Applications* 22.3, pp. 679–688.

Prakash, Satya et al. (2014). "An evaluation of high-resolution multisatellite rainfall products over the Indian monsoon region." In: *International Journal of Remote Sensing* 35.9, pp. 3018–3035.

Prakash, Satya et al. (2015). "Error characterization of TRMM Multisatellite Precipitation Analysis (TMPA-3B42) products over India for different seasons." In: *Journal of Hydrology* 529, pp. 1302–1312.

Prosser, Ian P and William E Dietrich (1995). "Field experiments on erosion by overland flow and their implication for a digital terrain model of channel initiation." In: *Water Resources Research* 31.11, pp. 2867–2876.

Raymo, ME and William F Ruddiman (1992). "Tectonic forcing of late Cenozoic climate." In: *Nature* 359.6391, pp. 117–122.

Reiners, P.W. et al. (2003a). "Coupled spatial variations in precipitation and long-term erosion rates across the Washington Cascades." In: *Nature* 426, pp. 645–647.

Reiners, Peter W et al. (2003b). "Post-orogenic evolution of the Dabie Shan, eastern China, from (U-Th)/He and fission-track thermochronology." In: *American Journal of Science* 303.6, pp. 489–518.

Riebe, C S et al. (2001a). "Strong tectonic and weak climatic control of long-term chemical weathering rates." In: *Geology* 29, pp. 511–514.

Riebe, Clifford S et al. (2001b). "Minimal climatic control on erosion rates in the Sierra Nevada, California." In: *Geology* 29.5, pp. 447–450.

Rinaldo, A et al. (1995). "Geomorphological signatures of varying climate." In: *Nature* 374.6523, pp. 632–635.

Rodriguez-Iturbe, I., D.R. Cox, and V. Isham (1987). "Some Models for Rainfall Based on Stochastic Point Processes." In: *Proceedings of the Royal Society A: Mathematical, Physical and Engineering Sciences* 410.1839, pp. 269–288. ISSN: 1364-5021. DOI: 10.1098/rspa.1987.0039.

Rodríguez-Iturbe, I. et al. (2006). "Space-time modeling of soil moisture: Stochastic rainfall forcing with heterogeneous vegetation." In: *Water Resources Research* 42.6. DOI: 10.1029/2005WR004497.

Rodriguez-Iturbe, Ignacio (2000). "Ecohydrology: A hydrologic perspective of climate-soil-vegetation dynamies." In: *Water Resources Research* 36.1, pp. 3–9.

Rodriguez-Iturbe, Ignacio et al. (1999). "Probabilistic modelling of water balance at a point: the role of climate, soil and vegetation." In: *The Royal Society* 455.1990, pp. 3789–3805.

Roe, Gerard H, David R Montgomery, and Bernard Hallet (2002). "Effects of orographic precipitation variations on the concavity of steady-state river profiles." In: *Geology* 30.2, pp. 143–146.

Roering, Joshua J et al. (2004). "Constraining climatic controls on hillslope dynamics using a coupled model for the transport of soil and tracers: Application to loess-mantled hillslopes, South Island, New Zealand." In: *Journal of Geophysical Research* 109.F1.

Rossi, Matthew W., Kelin X. Whipple, and Enrique R. Vivoni (2016). "Precipitation and evapotranspiration controls on daily runoff variability in the contiguous United States and Puerto Rico." In: *Journal of Geophysical Research: Earth Surface*. DOI: 10.1002/2015JF003446.

Rupp, David E. and John S. Selker (2006). "On the use of the Boussinesq equation for interpreting recession hydrographs from sloping aquifers." In: *Water Resources Research* 42.12. W12421. ISSN: 1944-7973. DOI: 10.1029/2006WR005080.

Schaefli, Rinaldo, and Botter (2013). "Analytic probability distributions for snow-dominated streamflow." In: *Water Resources Research* 49.5, pp. 2701–2713. ISSN: 1944-7973. DOI: 10.1002/wrcr.20234.

Schorghofer, Norbert and Daniel H Rothman (2002). "Acausal relations between topographic slope and drainage area." In: *Geophysical Research Letters* 29.13.

Schumer, Rina and Douglas J Jerolmack (2009). "Real and apparent changes in sediment deposition rates through time." In: *Journal of Geophysical Research: Earth Surface* 114.F3.

Schumm, S. A. (1973). "Geomorphic thresholds and complex response of drainage systems." In: *Fluvial geomorphology* 6, pp. 69–85.

— (1979). "Geomorphic Thresholds: The Concept and Its Applications." In: *Transactions of the Institute of British Geographers* 4.4, p. 485. ISSN: 0020-2754. DOI: 10.2307/622211.

Schumm, Stanley Alfred (1977). "The fluvial system." In:

Settin, T et al. (2007). "Numerical studies on soil moisture distributions in heterogeneous catchments." In: *Water Resources Research* 43.5. DOI: 10.1029/2006WR005737.

Shields, Albert (1936). *Application of similarity principles and turbulence research to bed-load movement*. Tech. rep. Soil Conservation Service.

Simpson, G and S Castelltort (2012). "Model shows that rivers transmit high-frequency climate cycles to the sedimentary record." In: *Geology* 40.12, pp. 1131–1134.

Singh, Arvind, Liam Reinhardt, and Efi Foufoula-Georgiou (2015). "Landscape reorganization under changing climatic forcing: Results from an experimental landscape." In: *Water Resources Research* 51.6, pp. 4320–4337. ISSN: 1944-7973. DOI: 10.1002/2015WR017161.

Sklar, Leonard S. and William E. Dietrich (2004). "A mechanistic model for river incision into bedrock by saltating bed load." In: *Water Resources Research* 40.6, n/a–n/a. ISSN: 1944-7973. DOI: 10.1029/2003WR002496.

— (2006). "The role of sediment in controlling steady-state bedrock channel slope: Implications of the saltation-abrasion incision model." In: *Geomorphology* 82.1-2, p. 5883. ISSN: 0169-555X. DOI: 10.1016/j.geomorph.2005.08.019.

Sklar, Leonard S. et al. (2016). "The problem of predicting the size distribution of sediment supplied by hillslopes to rivers." In: *Geomorphology*. ISSN: 0169-555X. DOI: 10.1016/j.geomorph.2016.05.005.

Snyder, Noah P. et al. (2003). "Importance of a stochastic distribution of floods and erosion thresholds in the bedrock river incision problem." In: *Journal of Geophysical Research: Solid Earth (1978-2012)* 108.B2. DOI: 10.1029/2001JB001655.

Srikanthan, R. and T. A. McMahon (2001). "Stochastic generation of annual, monthly and daily climate data: A review." In: *Hydrology and Earth System Sciences Discussions* 5.4, pp. 653–670.

Stephenson, DB et al. (1999). "Extreme daily rainfall events and their impact on ensemble forecasts of the Indian monsoon." In: *Monthly Weather Review* 127.9, pp. 1954–1966.

Sugai, Toshihiko (1993). "River terrace development by concurrent fluvial processes and climatic changes." In: *Geomorphology* 6.3, pp. 243–252. ISSN: 0169-555X. DOI: 10.1016/0169-555X(93)90049-8.

Suhaila, Jamaludin et al. (2011). "Introducing the mixed distribution in fitting rainfall data." In: *Open Journal of Modern Hydrology* 1.02, p. 11.

Szilagyi, Jozsef, Zoltan Gribovszki, and Peter Kalicz (2007). "Estimation of catchment-scale evapotranspiration from baseflow recession data: Numerical model and practical application results." In: *Journal of Hydrology* 336.1-2, pp. 206–217. DOI: 10.1016/j.jhydrol.2007.01.004.

Tague, C. and G. E. Grant (2004). "A geological framework for interpreting the low-flow regimes of Cascade streams, Willamette River Basin, Oregon." In: *Water Resources Research* 40.4. DOI: 10.1029/2003WR002629.

Tamea, Stefania et al. (2010). "Stochastic description of water table fluctuations in wetlands." In: *Geophysical Research Letters* 37.6, n/a–n/a. ISSN: 1944-8007. DOI: 10.1029/2009GL041633.

Thayyen, Renoj J et al. (2013). "Study of cloudburst and flash floods around Leh, India, during August 4–6, 2010." In: *Natural hazards* 65.3, pp. 2175–2204.

Thiede, R.C. et al. (2004). "Climatic control on rapid exhumation along the Southern Himalayan Front." In: *Earth and Planetary Science Letters* 222, pp. 791–806.

Thiede, Rasmus C and Todd A Ehlers (2013). "Large spatial and temporal variations in Himalayan denudation." In: *Earth and Planetary Science Letters* 371, pp. 278–293.

Trenberth, Kevin E. et al. (2003). "The Changing Character of Precipitation." In: *Bulletin of the American Meteorological Society*. DOI: 10.1175/BAMS-84-9-1205.

Tucker, Gregory E. (2004). "Drainage basin sensitivity to tectonic and climatic forcing: implications of a stochastic model for the role of entrainment and erosion thresholds." In: *Earth Surf. Process. Landforms* 29.2, pp. 185–205.

Tucker, Gregory E. and RL Bras (1998). "Hillslope processes, drainage density, and landscape morphology." In: *Water Resources Research* 34.10, pp. 2751–2764.

Tucker, Gregory E. and Rafael L. Bras (2000). "A stochastic approach to modeling the role of rainfall variability in drainage basin evolution." In: *Water Resources Research* 36.7, pp. 1953–1964.

Tucker, Gregory E. and G.R. Hancock (2010a). "State of Science: Modelling landscape evolution." In: *Earth Surface Processes and Landforms* 35, pp. 28–50.

Tucker, Gregory E. and Gregory R. Hancock (2010b). "Modelling landscape evolution." In: *Earth Surface Processes and Landforms* 35.1, pp. 28–50. DOI: 10.1002/esp.1952.

Tucker, Gregory E and Rudy L Slingerland (1994). "Erosional dynamics, flexural isostasy, and long-lived escarpments: A numerical modeling study." In: *Journal of Geophysical Research: Solid Earth* 99.B6, pp. 12229–12243.

Tucker, Gregory E. and Rudy Slingerland (1997). "Drainage basin responses to climate change." In: *Water Resources Research* 33.8, pp. 2031–2047.

Turowski, Jens M. (2010). "Probability distributions of bed load transport rates: A new derivation and comparison with field data." In: *Water Resources Research* 46.8, n/a–n/a. ISSN: 1944-7973. DOI: 10.1029/2009wr008488.

Turowski, Jens M (2012). "Semi-alluvial channels and sediment-flux-driven bedrock erosion." In: *Gravel-bed Rivers: Processes, Tools, Environments, edited by: Church, M., Biron, PM, and Roy, AG, John Wiley & Sons*, pp. 401–418.

Turowski, Jens M. et al. (2013). "Large floods, alluvial overprint, and bedrock erosion." In: *Earth Surface Processes and Landforms* 38.9, pp. 947–958. ISSN: 1096-9837. DOI: 10.1002/esp.3341.

Verma, Parikshit, James Yeates, and Edoardo Daly (2011). "A stochastic model describing the impact of daily rainfall depth distribution on the soil water balance." In: *Advances in Water Resources* 34.8, pp. 1039–1048. ISSN: 0309-1708. DOI: 10.1016/j.advwatres.2011.05.013.

Wang, Bin (2002). "Rainy season of the asian-pacific summer monsoon." In: *Journal of Climate* 15.4, pp. 386–398.

Webb, B.W. and D.E. Walling (1982). "The magnitude and frequency characteristics of fluvial transport in a devon drainage basin and some geomorphological im-

plications." In: *CATENA* 9.1-2, pp. 9–23. ISSN: 0341-8162. DOI: 10.1016/S0341-8162(82)80002-7.

Whipple, Kelin X. (2004). "BEDROCK RIVERS AND THE GEOMORPHOLOGY OF ACTIVE OROGENS." In: *Earth and Planetary Sciences* 32.1, pp. 151–185. DOI: 10.1146/annurev.earth.32.101802.120356.

Whipple, Kelin X (2009). "The influence of climate on the tectonic evolution of mountain belts." In: *Nature Geoscience* 2.2, pp. 97–9104. DOI: 10.1038/ngeo413.

Whipple, Kelin X., Gregory S. Hancock, and Robert S. Anderson (2000). "River incision into bedrock: Mechanics and relative efficacy of plucking, abrasion, and cavitation." In: *Geological Society of America Bulletin* 112.3, pp. 490–503. DOI: 10.1130/0016-7606(2000)112<490:riibma>2.0.co;2.

Whipple, Kelin X, Eric Kirby, and Simon H Brocklehurst (1999). "Geomorphic limits to climate-induced increases in topographic relief." In: *Nature* 401.6748, pp. 39–43.

Whipple, Kelin X and Brendan J Meade (2006). "Orogen response to changes in climatic and tectonic forcing." In: *Earth and Planetary Science Letters* 243.1, pp. 218–228.

Whipple, Kelin X and Gregory E Tucker (1999). "Dynamics of the stream-power river incision model: Implications for height limits of mountain ranges, landscape response timescales, and research needs." In: *Journal of Geophysical Research: Solid Earth (1978-2012)* 104.B8, pp. 17661–17674. DOI: 10.1029/1999JB900120.

Willenbring, Jane K and Douglas J Jerolmack (2015). "The null hypothesis: globally steady rates of erosion, weathering fluxes and shelf sediment accumulation during Late Cenozoic mountain uplift and glaciation." In: *Terra Nova* 28.1, pp. 11–18.

Willett, Sean D (1999). "Orogeny and orography: The effects of erosion on the structure of mountain belts." In: *Journal of Geophysical Research: Solid Earth* 104.B12, pp. 28957–28981.

Willett, Sean D et al. (2014). "Dynamic Reorganization of River Basins." In: *Science* 343.6175, p. 1248765. ISSN: 0036-8075. DOI: 10.1126/science.1248765.

Wobus, Cameron et al. (2006). "Tectonics from topography: Procedures, promise, and pitfalls." In: *Geological Society of America Special Papers* 398, pp. 55–74. DOI: 10.1130/2006.2398(04.

Wolman, Gordon M and Ran Gerson (1978). "Relative scales of time and effectiveness of climate in watershed geomorphology." In: *Earth Surface Processes* 3.2, pp. 189–208. ISSN: 1931-8065. DOI: 10.1002/esp.3290030207.

Wolman, Gordon M and John P Miller (1960). "Magnitude and frequency of forces in geomorphic processes." In: *The Journal of Geology*, pp. 54–74.

Wulf, H., B. Bookhagen, and D. Scherler (2012). "Climatic and geologic controls on suspended sediment flux in the Sutlej River Valley, western Himalaya." In: *Hydrology and Earth System Sciences* 16.7, pp. 2193–2217.

Wulf, Hendrik, Bodo Bookhagen, and Dirk Scherler (2010). "Seasonal precipitation gradients and their impact on fluvial sediment flux in the Northwest Himalaya." In: *Geomorphology* 118.1-2, p. 1321.

— (2016). "Differentiating between rain, snow, and glacier contributions to river discharge in the western Himalaya using remote-sensing data and distributed hydrological modeling." In: *Advances in Water Resources* 88, pp. 152–169.

Yatagai, Akiyo et al. (2012). "APHRODITE: Constructing a Long-Term Daily Gridded Precipitation Dataset for Asia Based on a Dense Network of Rain Gauges." In: *Bulletin of the American Meteorological Society*.

Ye, Sheng et al. (2014). "Regionalization of subsurface stormflow parameters of hydrologic models: Derivation from regional analysis of streamflow recession curves." In: *Journal of Hydrology* 519, pp. 670–682.

Zhisheng, An et al. (2001). "Evolution of Asian monsoons and phased uplift of the Himalaya–Tibetan plateau since Late Miocene times." In: *Nature* 411.6833, pp. 62–66.